JAERI-M
82-125

PIPE RUPTURE TEST RESULTS: 4-INCH PIPE WHIP TESTS UNDER PWR LOCA CONDITIONS

(RUN No. 5506, 5507, 5508, 5604)

September 1982

Noriyuki MIYAZAKI, Shuzo UEDA, Toshikuni ISOZAKI, Rokuro KATO, Ryoichi KURIHARA, Toshikazu YANO and Shohachiro MIYAZONO

日本原子力研究所
Japan Atomic Energy Research Institute

JAERI-M レポートは，日本原子力研究所が不定期に公刊している研究報告書です。
入手の問合わせは，日本原子力研究所技術情報部情報資料課（〒319—11 茨城県那珂郡東海村）あて，お申しこしください。なお，このほかに財団法人原子力弘済会資料センター（〒319—11 茨城県那珂郡東海村日本原子力研究所内）で複写による実費頒布をおこなっております。

JAERI-M reports are issued irregularly.
Inquiries about availability of the reports should be addressed to Information Section, Division of Technical Information, Japan Atomic Energy Research Institute, Tokai-mura, Naka-gun, Ibaraki-ken 319—11, Japan.

編集兼発行　日本原子力研究所
印　　刷　日立高速印刷株式会社

JAERI-M 82-125

Pipe Rupture Test Results: 4-inch Pipe Whip Tests under PWR LOCA Conditions (RUN No. 5506, 5507, 5508, 5604)

Noriyuki MIYAZAKI, Shuzo UEDA, Toshikuni ISOZAKI, Rokuro KATO, Ryoichi KURIHARA, Toshikazu YANO and Shohachiro MIYAZONO

Division of Nuclear Safety Research
Tokai Research Establishment, JAERI

(Received August 12, 1982)

This report summarizes the results of 4-inch pipe whip tests (RUN No. 5506, 5507, 5508 and 5604) under the PWR LOCA conditions. The dynamic behaviors of the test pipe and restraints were studied in the tests. In the tests, the gap between the test pipe and the restraints was kept at the constant value of 8.85 mm and the overhang length was varied from 250 mm to 650 mm.

The dynamic behaviors of the test pipe and the restraint were made clear by the outputs of strain gages and the measurements of residual deformations. The data of water hammer in subcooled water were also obtained by the pressure transducers mounted on the test pipe.

The main conclusions obtained from the tests are as follows. (1) The whipping of pipe can be prevented more effectively as the overhang length becomes shorter. (2) The load acting on the restraint-support structure becomes larger as the overhang length becomes shorter. (3) The restraint farther from the break location does not limit the pipe movement except for the first impact when the overhang length is long. (4) The ultimate moment M_u of the pipe at the restraint location can be used to predict the plastic collapse of the whipping pipe. (5) The restraints slide along the pipe axis and are subjected to bending moment, when the overhang length is long.

Keywords: Pipe Whip Test, PWR LOCA Conditions, Dynamic Behavior, Test Pipe, Restraints, Strain, Residual Deformation

---

This work was performed under the contract between the science and Technology Agency of Japan and JAERI to demonstrate the safety for pipe rupture of the primary coolant circuits in nuclear power plants.

JAERI－M 82－125

配管破断試験・ＰＷＲ４インチ口径パイプホイップ試験結果
（RUN No. 5506，5507，5508，5604）

日本原子力研究所東海研究所安全工学部
宮崎　則幸・植田　脩三・磯崎　敏邦・加藤　六郎
栗原　良一・矢野　歳和・宮園昭八郎

（1982年8月12日受理）

本報は４インチ口径試験配管を用いてPWR－LOCA条件で実施した４回のパイプホイップ試験（RUN No. 5506，5507，5508，5604）についてまとめたものである。これらの試験では，パイプホイップ時の試験配管，及びレストレントの動的挙動について調べた。試験配管とレストレントとの間のギャップは8.85mm一定とし，オーバハング長さを250 mm から650 mm の間で変えた。

ひずみゲージ出力，及び残留変形計測の結果より，試験配管，及びレストレントの動的挙動を明らかにした。また，試験配管に取付けた圧力変換器出力からサブクール水中での水撃データが得られた。

本試験から得られた主要な結論は次の通りである。(1) オーバハングが短いほど，配管のパイプホイップ運動は効果的に抑制される。(2) レストレント支持構造物に加わる荷重は，オーバハングが短いほど大きくなる。(3) オーバハングが長くなるとレストレントと配管との第１撃時を除いて，２本のレストレントのうち，破断口より遠いレストレントが有効に働かなくなる。(4) 配管のレストレント設置位置での極限モーメント M_u を用いることにより，配管が塑性崩壊を起こす条件を定めることができる。(5) オーバハングが長くなると，レストレントが配管の管軸方向にすべり，レストレントには曲げモーメントも加わるようになる。

この報告書は，電源開発促進対策特別会計施行令に基づき，科学技術庁から日本原子力研究所への委託研究，昭和54年度，及び昭和56年度配管信頼性実証試験のうち，４インチ口径試験配管を用い，ＰＷＲ・ＬＯＣＡ条件で実施したパイプホイップ試験結果についてまとめたものである。

CONTENTS

目　　次

1. INTRODUCTION

The loss-of-coolant accident, LOCA, must be taken into account in designing nuclear power plants. The accident is assumed to be triggered by instantaneous pipe rupture. The dynamic motion of pipe called pipe whip will be caused by the blowdown thrust force acting on the ruptured pipe, if the intantaneous pipe rupture occurs. In LWR nuclear power plants, pipe whip restraints are installed to limit the movement of whipping pipe and to protect such surrounding structures as piping and containment against pipe whipping.

The pipe rupture tests are being performed at Mechanical Strength and Structure Laboratory at JAERI to demonstrote the safety for pipe rupture of the primary coolant circuits in LWR nuclear power plants by using Facility for Reliability Study of Pressure Boundary Components, FRPC-II. In the pipe rupture tests, pipe whip tests are being carried out using 4-, 6- and 8-inch test pipes under both the BWR and PWR LOCA conditions.[1][2]

This report summarizes the results of four pipe whip tests, RUN No. 5506, 5507, 5508 and 5604, performed under the PWR LOCA conditions using 4-inch test pipes. Various types of restraints are used in PWR nuclear power plants. The restraints used in the tests are U-type one which is almost the same ones used in the pressurizer spray line (3-inch piping) and the delyge line (6-inch piping). In the tests, the gap between the test pipe and the restraints was hept at the constant valve of 8.85 mm and the overhang lengths were varied from 250 mm to 650 mm. The main purpose of the tests was to study the effects of the overhange length on the pipe whip behaviors by means of measuring the residual deformations and dynamic strains of the test pipe and the restraints.

2. TEST PROCEDURE

2.1 Test Apparatus

Figure 2.1 shows the schematic figure of the pipe whip test. The pressurizer was used to make subcooled water in the pressure vessel. An auxiliary connecting pipe was attached to the nozzle of the pressure vessel. A test pipe was connected to the end of the auxiliary connecting pipe. The test pipe was 114.3 mm in outer diameter, 13.5 mm in thickness and 5500 mm in length. Its material was SUS304 stainless steel. Table 2.1 shows the chemical compositions and the mechanical properties of the test pipe. The tensile test data of the test pipe are given in APPENDIX B. The test pipe was supported by the pipe support at the distance of 3000 mm from the break locations. The rupture disk assembly shown in Fig. 2.2 was welded to the end of the test pipe. This was developed for the pipe whip test. An additional mass was not added to the test pipe by using this rupture disk assembly. An instantaneous pipe break was simulated by breaking the rupture disk with an electric arc method. A flexible tube was used as a part of warming-up line to reduce its resistance against the pipe whip motion.

Two pipe whip restraints were fixed on the restraint support by double nuts. The overhang length defined as the distance between the break location of the test pipe and the restraint location was varied by moving the restraint support along the T-shaped groove of the test bed. Figure 2.3 shows the shape of U-type restraint made from SS41 mild steel whose chemical compositions and mechanical properties are given in Table 2.2. The tensile test data of the restraint material are given in APPENDIX B. The dead weight support and the pipe stopper were installed to keep the gap between the test pipe and the restraints constant during heating-up. There are following differences between the U-type restraint for the BWR plant and that for the PWR plant used in the present tests.

(1) The U-type restraint for the BWR plant is based on the plastic design concept considering the energy abosrption of the kinematic energy of pipe due to the plastic deformation of restraints, while the U-type restraint for the PWR plant is based on the elastic design concept. Thus, the former is made from ductile material such as SUS304 stainless steel, while the latter is made from SS41 mild steel. Furthermore, the rod diameter of the latter is much larger than that the

former.

(2) The gap between pipe and restraints is about 100 mm for the U-type restraint for the BWR plant to allow unrestricted normal pipe thermal movements and potential externally induced movements due to seismic and other transient loading. On the other hand, a relatively small gap such as the value of 10 mm is taken for the U-type restraint for the PWR plant to decrease the dynamic loading acting on the restraint.

(3) A bearing plate is attached to the U-type restraint for the BWR plant to wrap around the pipe and to minimize pipe rebound, whereas there is no bearing plate for the U-type restraint for the PWR plant.

(4) The U-type restraint for the BWR plant is held to a restraint support with pins, so that bending moment is zero at the support point. On the other hand for the U-type restraint for the PWR plant bending momnet is generated at the fixed point where the restraint is completely fixed on restraint support with nuts.

Photographs 2.1 and 2.2 show the overall view of the pipe whip test apparatus and the view of the restraint installed on the restraint support, respectively.

2.2 Test Conditions

Table 2.3 shows the test conditions of four pipe whip tests. The test pressure and test temperature were alsomst the same as ones in PWR operational conditions. The gap between the test pipe and the restraints were set at the value of 8.85 mm before heating up the system. The overhang length was varied from 250 mm to 650 mm as shown in the table. The break area ratio was obtained through measuring the open area of the rupture disk by means of the photograph of the break location of the test pipe. As can be seen from the table, the tests of RUN No. 5508 and 5604 have the same test parameters except for the break area ratio. The test of RUN No. 5604 was performed to attain the full open of the rupture disk, since the rupture disk did not completely open in the test of RUN No. 5508. Photograph 2.3 shows the view of the rupture disk after test.

Table 2.4 shows the initial tempertures at various locations measured by a digital thermometer. The temperatures in the test pipe were not so much different from those in the pressure vessel, because hot water

was circulated through the warming-up line.

2.3 Measuring Items and Methods

Following three types of measurements were performed in the tests.

(1) Electrical measurements

(2) Residual deformation measurements

(3) Observation of pipe whip phenomenon by high speed cameras

Measurement locations and their objectives are given in the following.

(1) Electrical measurements

Table 2.5 shows the list of measuring items for electrical measurements. The main items of the electrical measurements were strain, pressure, temperature, displacement, acceleration, load and water level.

Figure 2.4 shows the locations of the high temperature strain gages of XU111 through XU126 mounted on the surface of the test pipe. These strain gages were mounted in the axial direction of the test pipe except for XU127 and XU128 in the test of RUN No. 5604.

Figure 2.5 shows the locations of the strain gages for large strain of XU131 through XU146 and XU151 through XU166 mounted on the restraints in the axial direction. The restraints were named R1 and R2, respectively, in order of the distance from the break location of the test pipe. As can be seen from the figure, couples of the strain gages were mounted at the same height of the straight parts of restraints to measure the bending strains generating in the restraints. These strain gages were also used to obtain the residual strain distributions of the restraints.

As shown in the Fig. 2.5, four couples of bi-axial strain gages were mounted on the parts of each restraint of 27 mm in diameter to make load transducers, WU131 to WU134 and W141 to WU144. These load transducers were used to measure the reaction forces of the restraints.

The strain gage XU169 was mounted on the pipe stopper in the test of RUN No. 5506 to examine whether or not the test pipe clashed against pipe stopper after rebounding from restraints. In the test of RUN No. 5507, the strain gage XU 170 was mounted on the restraint support where little mechanical strain was caused. The aim of this strain gage was to examine how much the outputs of the strain gages for large strain increase with temperature after pipe break.

The pressure transducers, PU101, PU103, PU105 and PU110 to PU114,

were attached to the pressure vessel and piping. Among those, the pressure transducers, PU101, PU103 and PU105, were mounted at the ends of cooling pipes whose length were about 30 cm. On the other hand, PU110 to PU116 were the pressure transducers of water-cooled type. In order to measure such high speed phenomenon as water hammer, the pressure transducers PU110 to PU114 used in the tests of RUN No. 5506 to 5508 were so mounted on the pipe that the transducer-diaphram surfaces corresponded with the inner surface of the pipe. The data obtained from these pressure transducers were, however, greater than the expected values because of the thermal deformations of the transducer-diaphram surfaces. Therefore, the pressure transducers PU110 to PU116 used in the test of RUN No.5604 were used together with the water-cooled mounts shown in Photo. 2.4 to prevent the thermal deformations of the transducer-diahpram surfaces. The pressure transducer PU107 was used to measure the pressure variation in the test pit after pipe break.

The fluid temperatures in the pressure vessel were measured with the C-A sheathed thermocouples TU101 and TU102. The C-A sheathed thermocouples TU106 and TU111 were used for measurement of metal temperatures of the pressure vessel. Five C-A sheathed thermocouples were spaced in the pipe to measure fluid temperature. The thermocouple TU126 was used for measuring the temperature in the test pit. The thermocouple TU134 was attached to the R2 restraint in the test of RUN No. 5506 to monitor temperature increase due to radiation from the test pipe which had ill effect on the strain gages mounted on the restraints.

The eddy current displacement transducers XU200 and XU201 were used to measure pipe displacement. The dial gages XU202 and XU203 were installed near the restraints to monitor pipe movement during heathng up.

The piezoelectric accelerometers XU300 and XU301 were mounted on the test pipe.

WU115 and WU116 denote the level transmitters of the pressure vessel and the pressurizer, respectively.

Almost all transducer outputs were recorded on the five analog data-recorders at the speed of 60 in/sec. The record was able to be reproduced at the minimum sampling period of 12.5 μsec. Other transducer outputs were recorded either on a temporal digital memory at the sampling period of 10 msec or on XY-recorders for monitor.

(2) Residual deformation measurements

The following residual deformations were obtained from the variation of the distance between two markings before and after test.

① Residual strains of the test pipe: The axial distances between marking on the surface of the test pipe were measured with slide calipers before and after test.

② Residual cross-sectional deformations of the test pipe: The variations of outer diameters before and after test were measured with outside calipers.

③ Residual deformations of the test pipe: The heights of the test pipe from the base level were measured with a transit before and after test.

④ Residual strains of the restraints: The distances between markings on the restraints were measured with slide calipers before and after test.

⑤ Residual deformations of the restraints: The variations of heights of the restraints before and after test were measured with a transit.

The outputs of the strain gages mounted on the restraint were also used to obtain the residual strains of the restraints, since the diameter of the restraint was thought to be too large to obtain the residual strains accurately by the mechanical measurement mentioned above. In this case, the residual strain was defined as the strain at the time of 100 sec after pipe break.

(3) Obserbation of the pipe whip phenomenon by high speed cameras

Two high speed cameras were used in each test. One was used for the overall view of the test section and another was used for the view near the restraints. In all cases, photographs were taken at the speed of 3000 frames/sec.

Table 2.1 Chemical Compositions and Mechanical Properties of Test Pipe ----- SUS304TP

Chemical Composition

ELEMENT	C	Si	Mn	P	S	Np	Cr
RESULT (%)	0.05	0.49	1.48	0.028	0.003	9.30	18.40

Mechanical Properties

ITEM	Yield Strength MPa	Tensile Strength MPa	Elongation %
RESULT	279	608	67

Table 2.2 Chemical Compositions and Mechanical Properties of Restraint ----- SS41

Chemical Composition

ELEMENT	C	Si	Mn	P	S
RESULT (%)	0.21	0.19	0.47	0.031	0.02

Mechanical Properties

ITEM	Yield Strength MPa	Tensile Strength MPa	Elongation %
RESULT	289	476	37.5

Table 2.3 Test Conditions

RUN No.		5506	5507	5508	5604
Pressure		15.58MPa	15.55MPa	15.55MPa	15.68MPa
Temperature	Pressure Vessel	319.7°C	320.2°C	319.6°C	321°C
	Test Section	313.1°C	314.8°C	313.4°C	313°C
Diameter & Thickness of Test Pipe		4B, sch160	4B, sch160	4B, sch160	4B, sch160
Length of Test Section		3000mm	3000mm	3000mm	3000mm
Break Area Ratio		79.4%	78.1%	38.9%	77.5%
Restraint	Type	U-bar	U-bar	U-bar	U-bar
	Overhang	250mm	400mm	650mm	650mm
	Gap	8.85mm	8.85mm	8.85mm	8.85mm
	Diameter	18mm	18mm	18mm	18mm
	Number	2	2	2	2

Table 2.4 Initial Temperatures at Various Locations

(Unit: °C)

RUN No. / Tag No.	5506	5507	5508	5604
TU101	319.7	320.2	319.6	320.0
TU102	289.2	291.8	289.4	320.0
TU104	319.1		319.4	
TU106				
TU111		318.4	318.0	
TU130	313.1	314.8	313.4	313.1
TU131	319.4	319.2	320.9	316.0
TU132	318.0	319.0	318.3	316.9
TU133	316.1	315.2	317.4	

(Note) • These temperatures except TU106 were recorded by the degital thermometer.
• The thermocople TU102 is supposed to be out of order.

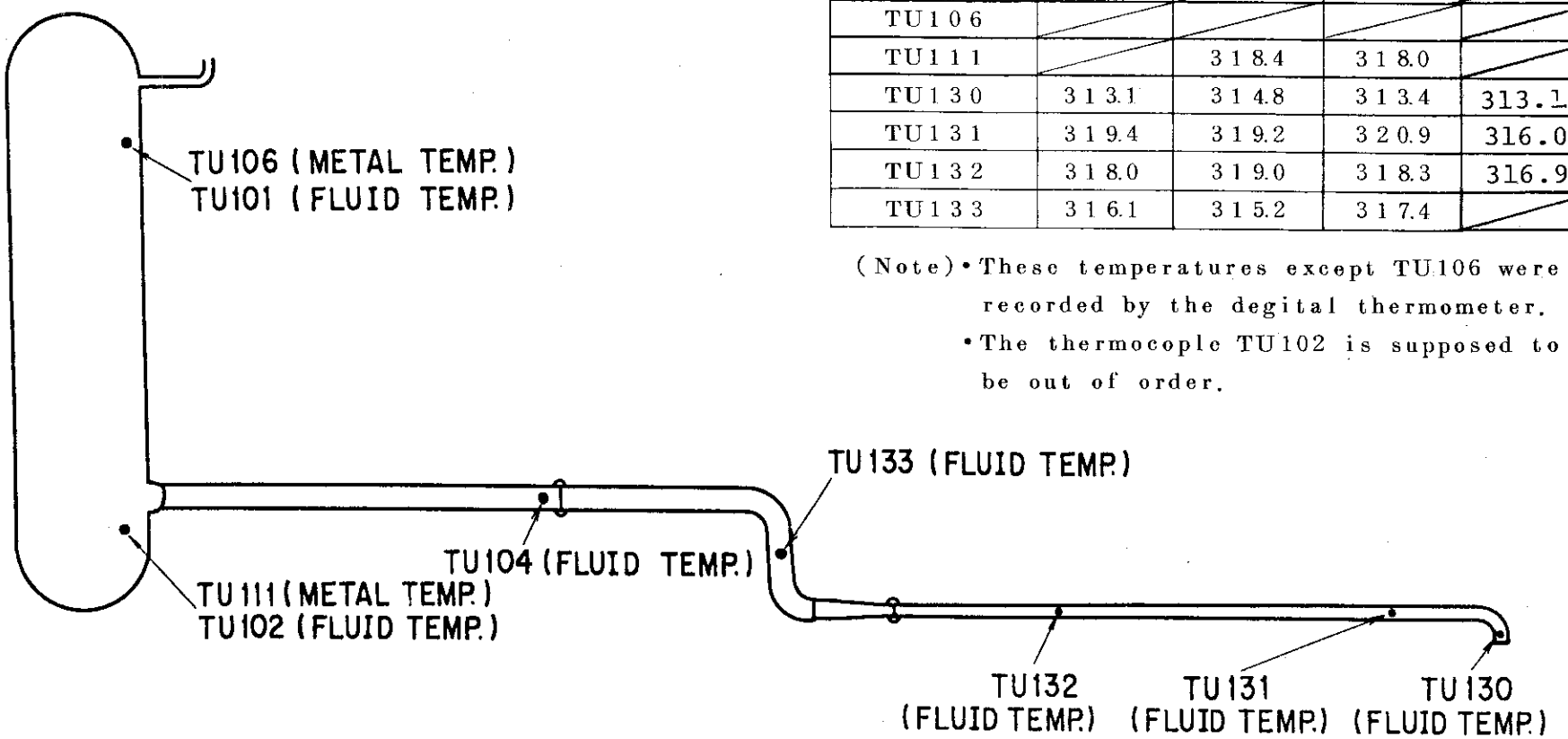

Table 2.5 List of Measuring Items (1)

TAG No.	LOCATION	SPECIFICATION	MANUFACTURER TYPE	RECORD DEVICE 5506	5507	5508	5604
STRAIN GAGE – PIPE							
XU 111	See Fig. 2.4	High Temp. Spot Welded Plastic	AILTECH SG–125–01F–10	L DR	M DR	M DR	M DR
112				M	M	M	L DR
113				L	L	L	L
114				L	L	L	L
115				L	L	L	L
116				L	L	L	L
117				M	L	L	L
118				M	M	L	L
119				M	M	L	L
120				M	M	M	M
121				M	M	M	M
122				M	M	M	M DR
123				M DR	M DR	M DR	M DR
124				M DR	M DR	M DR	M DR
125				M DR	M DR	M DR	M DR
126				M DR	M DR	M DR	M DR
127				M DR	M DR	M DR	M DR
128				M DR	M DR	M DR	M DR
STRAIN GAGE – R1 RESTRAINT							
XU 131	R1 RESTRAINT See Fig. 2.5	Plastic	TOKYO SOKKI YL–5	M DR	M DR	M DR	M DR
141				M	M	M	M
142				L	L DR	L DR	L DR
143				H			
144				H DR			
145					L DR	L DR	L DR
146					L DR	L DR	L DR

Table 2.5 List of Measuring Items (2)

TAG No.	LOCATION	SPECIFICATION	MANUFACTURER TYPE	RECORD DEVICE 5506	5507	5508	5604
STRAIN GAGE - R2 RESTRAINT							
XU 151 ↕ 161	R 2 Restraint See Fig. 2.5	Plastic	Tokyo SOKKI YL-5	M ↕ M	DR ↕ DR	M ↕ M	DR ↕ DR	M ↕ M	DR ↕ DR	M ↕ M	DR ↕ DR
162				L		L	DR	L	DR	L	DR
163				H							
164				H	DR						
165						L	DR	L	DR	L	DR
166						L	DR	L	DR	L	DR
ADDITIONAL STRAIN GAGE							
WU 169	Pipe Stopper	Plastic	Tokyo SOKKI YL-5	L	ON						
170	Restraint Support					L	ON				
WU 131 ↕ 134	R 1 Restraint See Fig. 2.5	Each transducer was composed of four elstic strain gages	The strain gage used was : KYOWA KFD-2-D16-11	M ↕ M	DR ↕ DR	M ↕ M	DR ↕ DR	M ↕ M	DR ↕ DR	M ↕ M	DR ↕ DR
WU 141 ↕ 144	R 2 Restraint See Fig. 2.5			M ↕ M	DR ↕ DR	M ↕ M	DR ↕ DR	M ↕ M	DR ↕ DR	M ↕ M	DR ↕ DR
PRESSURE							
PU 101 103 105	See Fig. 2.1	Strain Gage Type	BLH GP-H	H ↕ H	DR ↕ DR	H ↕ H	DR ↕ DR	H ↕ H	DR ↕ DR	H ↕ H	DR ↕ DR
PU 107	Test Pit	Strain Gage Type	KYOWA, PD500GA			L	ON	L	ON		

Table 2.5 List of Measuring Items (3)

TAG No.	LOCATION	SPECIFICATION	MANUFACTURER TYPE	RECORD DEVICE 5506	5507	5508	5604
PRESSURE							
PU 110 ↕ 114	See Fig. 2.1	Strain Gage Type	SHINKOH MP-200	H DR / H DR	H DR / H DR	H DR / H DR	H DR / H DR
PU 115	See Fig. 2.1	Semi-Conductor Type	TOYODA KOKI PMS-10KTMN-200H	S DR			
116				S DR			
PU 200	Pressurizer	Semi-Conductor Type	FUJI FAC23WD3-110Y	XY			
TEMPERATURE							
TU 101	See Fig. 2.1	C-A Sheath Type 0.5 φ	OKAZAKI	B ON / B ON	B ON / B ON	B ON / B ON	B ON / B ON
102							
104							
106		C-A Sheath Type 1.6 φ					
111							
TU 126	Test Pit	C-A Sheath Type	1.6 φ HANAWA	B ON	B ON	B ON	
TU 130 ↕ 133	See Fig. 2.1	C-A Sheath Type 3.2 φ	SUKEGAWA	B ON / B ON	B ON / B ON	B ON / B ON	B ON / B ON
TU 134	R2 Restraint	C-A Sheath Type	SUKEGAWA	B ON			
TU 200	Pressurizer	C-A Sheath Type	FUJI PRA1E003-1	B ON			
DISPLACEMENT							
XU 200	See Fig. 2.1	Eddy Current Type	SHIN NIPPON SOKKI NP-1000	DR			
201			SHIN NIPPON SOKKI FP-400	ON			
XU 202	See Fig. 2.1	Dial Gage Type	TOKYO SOKKI	L XY	L ON	L ON	L XY
203				L XY			
ACCELERATION							
XU 300	See Fig. 2.1	Piezoelectric Type	ENDEVCO 2273A	C DR	C DR	C DR	C DR
301				C DR			

Table 2.5 List of Measuring Items (4)

TAG No.	LOCATION	SPECIFICATION	MANUFACTURER TYPE	RECORD DEVICE							
				5506		5507		5508		5604	
LOAD											
WU 101	See Fig. 2.1	Strain Gage Type	BLH T2G-1	L	DR	L	DR	L	DR		
WATER LEVEL											
WU 115	Pressure Vessel	Press. Diff. Type	FUJI FEC34WD3-160Y		DR		DR		DR		
WU 116	Pressurizer				DR		DR		DR		

H : High Freq. Amp. (50kHz) ····· SHINKOH DA-4007-F

M : Medium Freq. Amp. (10kHz) ····· SHINKOH DA-4006-F

L : Low Freq. Amp. (2kHz) ····· SHINKOH DA-6005-F

B : DC Amp. ····· BLH BLH-5300

S : Multi Purpose Amp. ····· SAN-EI 6M72V

C : Charge Amp. ····· ENDEVCO MODEL 2735

DR : Analog Data Recorder (Off-Line) ····· AMPEX PR2200

ON : Temporally Digital Memory (ON-Line)

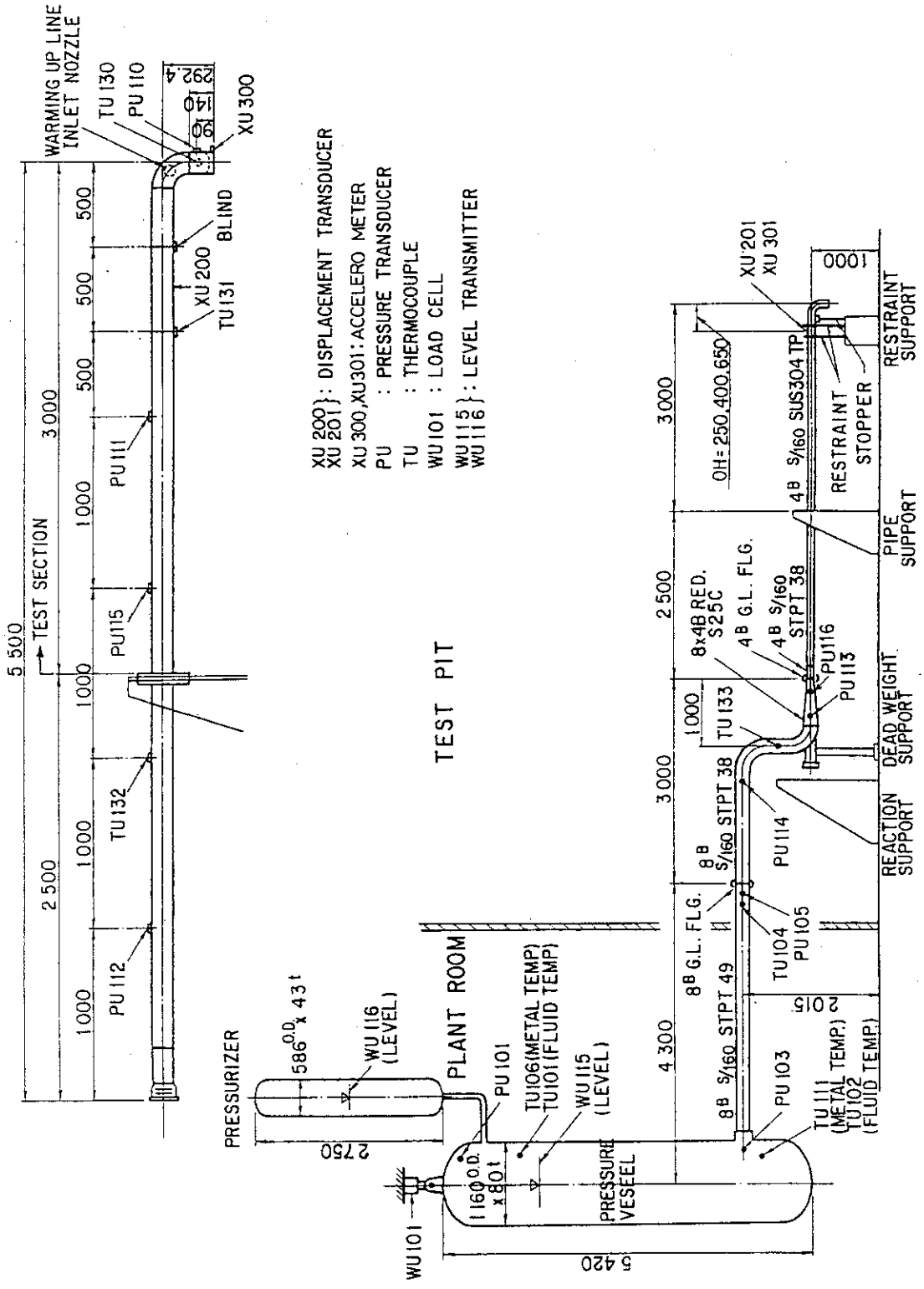

Fig. 2.1 Schematic Figure of Pipe Whip Test

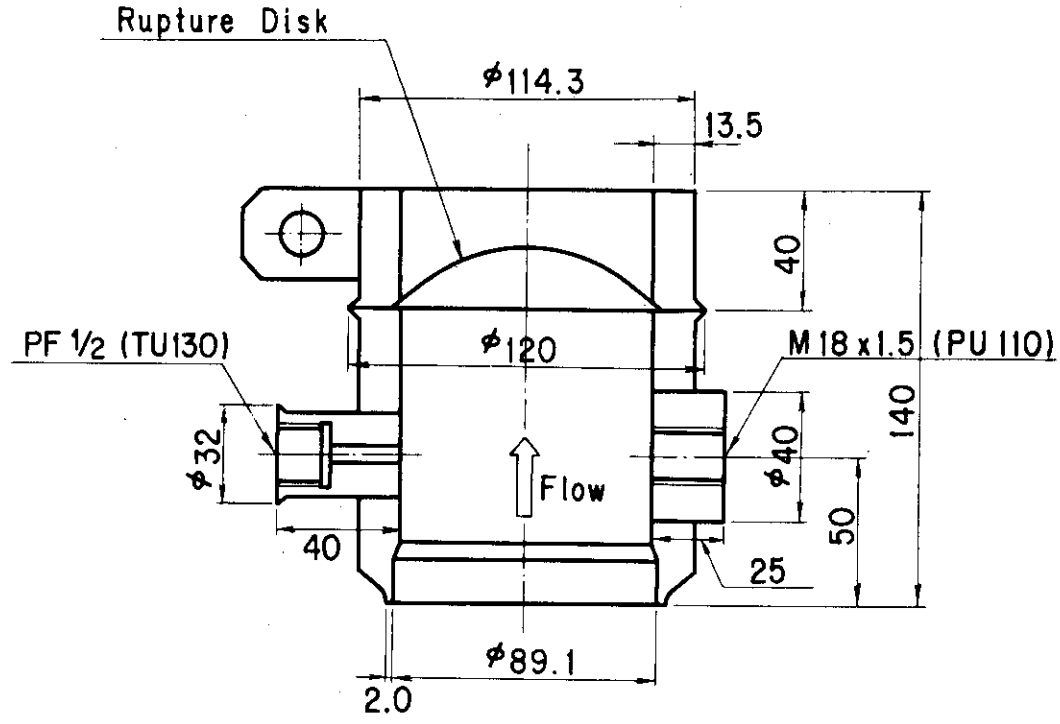

Fig. 2.2 Details of Welded Rupture Disk

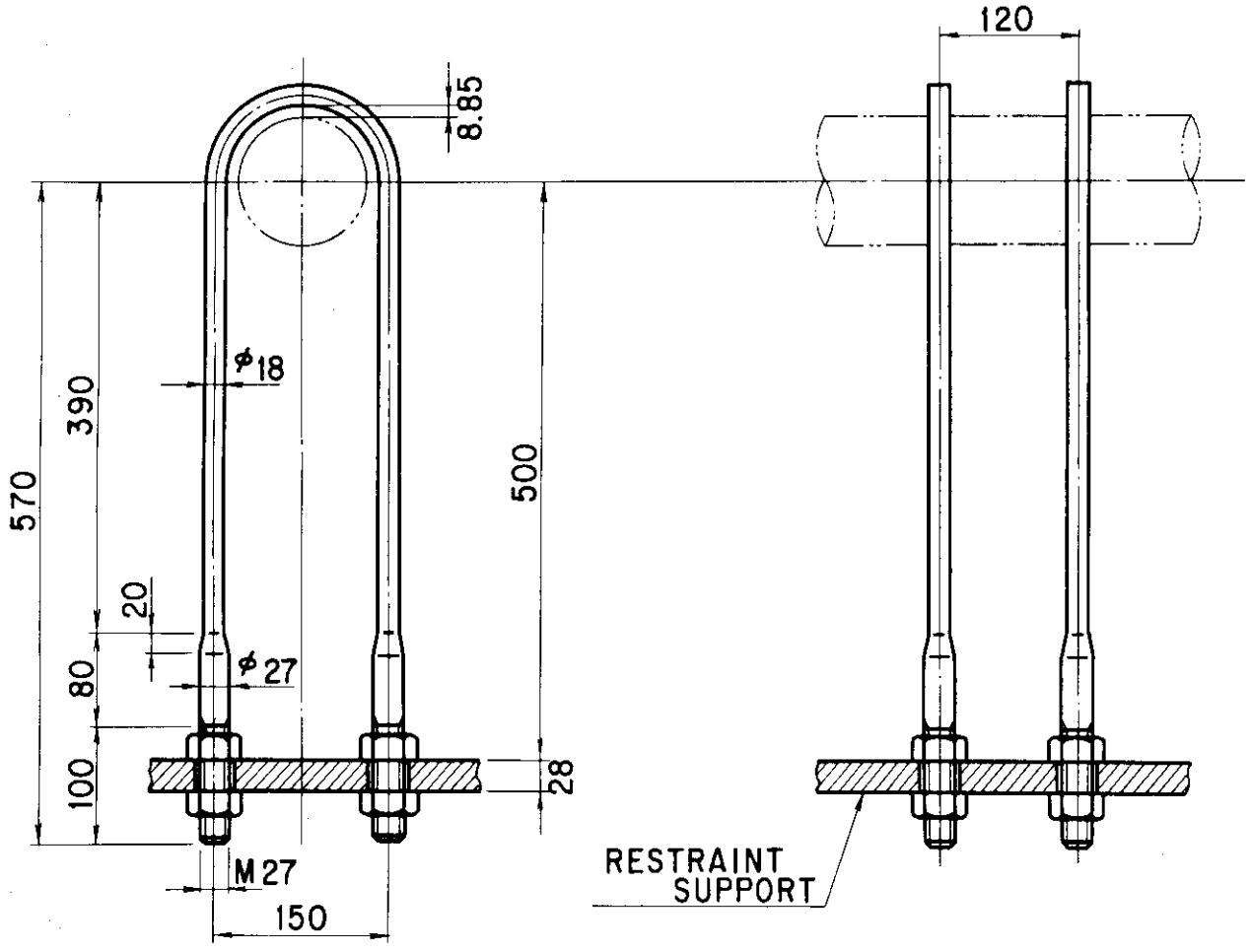

Fig. 2.3 Dimensions of Restraint

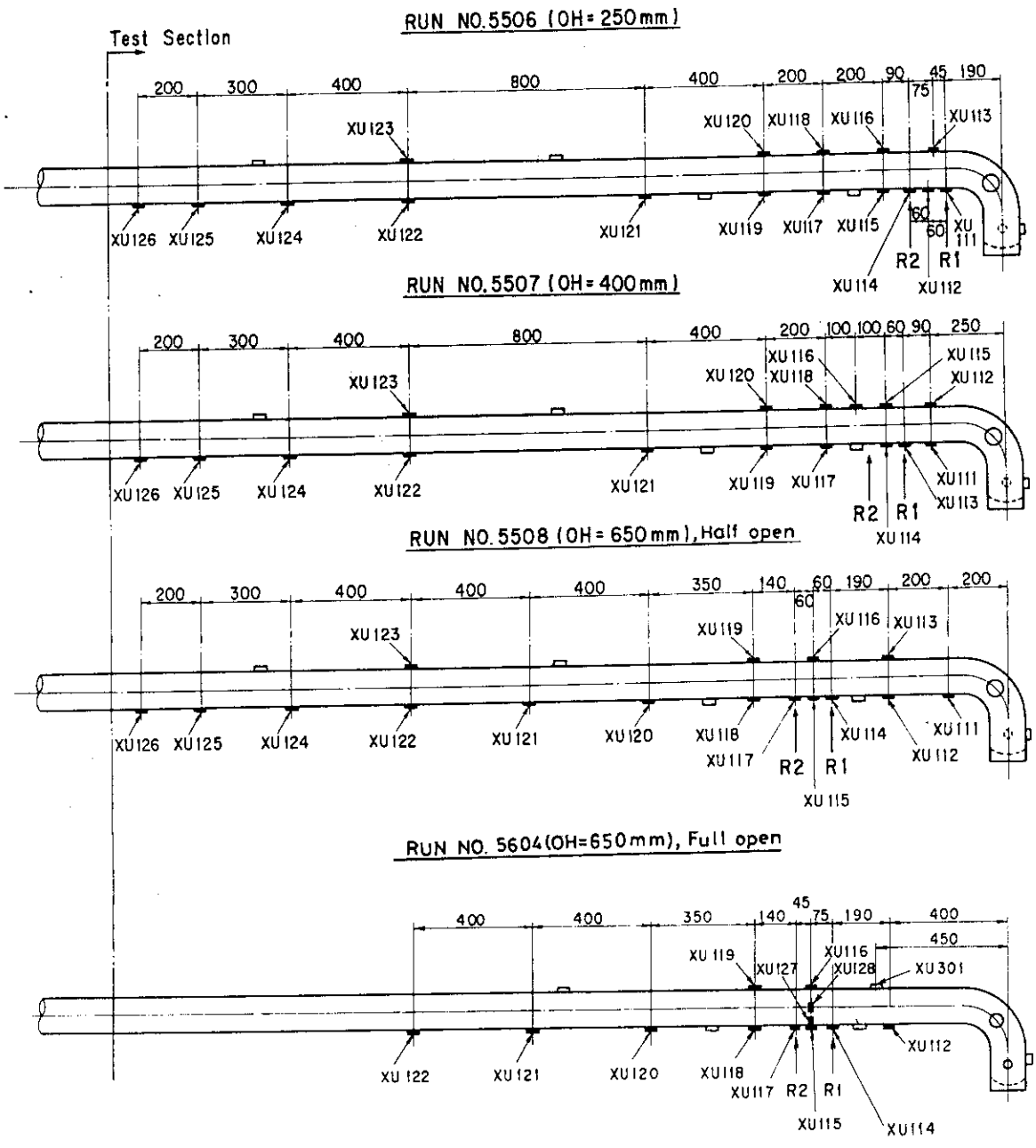

Fig. 2.4 Locations of Strain Gages Mounted on Test Pipe

LOCATION	TAG NO. Restraint R1	TAG NO. Restraint R2
①	XU 131	XU 151
②	132	152
③	133	153
④	134	154
⑤	135	155
⑥	136	156
⑦	137	157
⑧	138	158
⑨	139	159
⑩	140	160
⑪	141	161
⑫	142	162
⑬	143	163
⑭	144	164
⑮	145	165
⑯	146	166
⑰	WU 131	WU 141
⑱	132	142
⑲	133	143
⑳	134	144

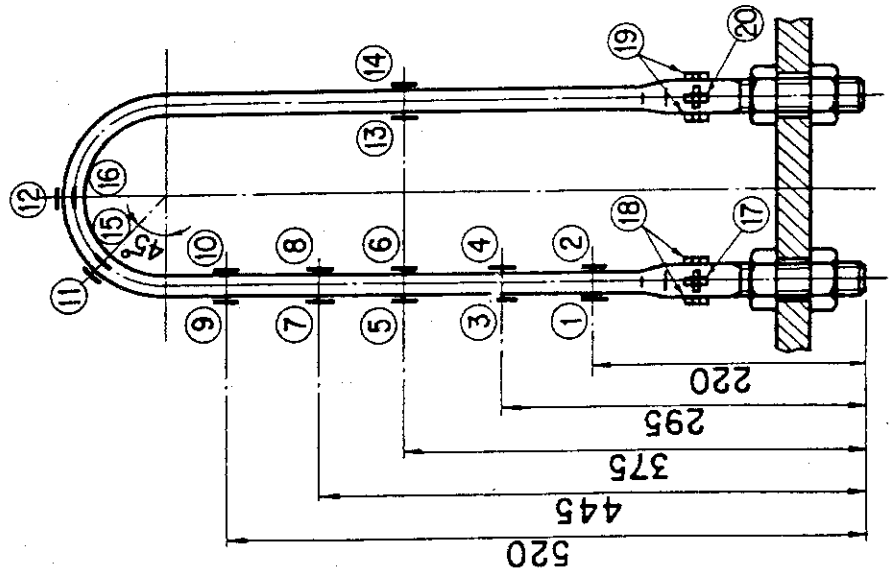

Fig. 2.5 Locations of Strain Gages Mounted on Restraints

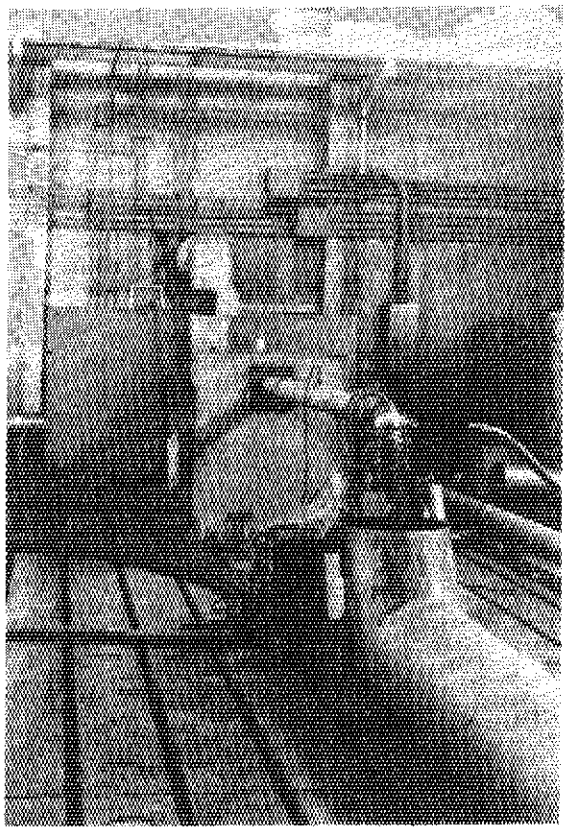

Photo. 2.1 Overall View of the Pipe Whip Test Apparatus (RUN No.5507)

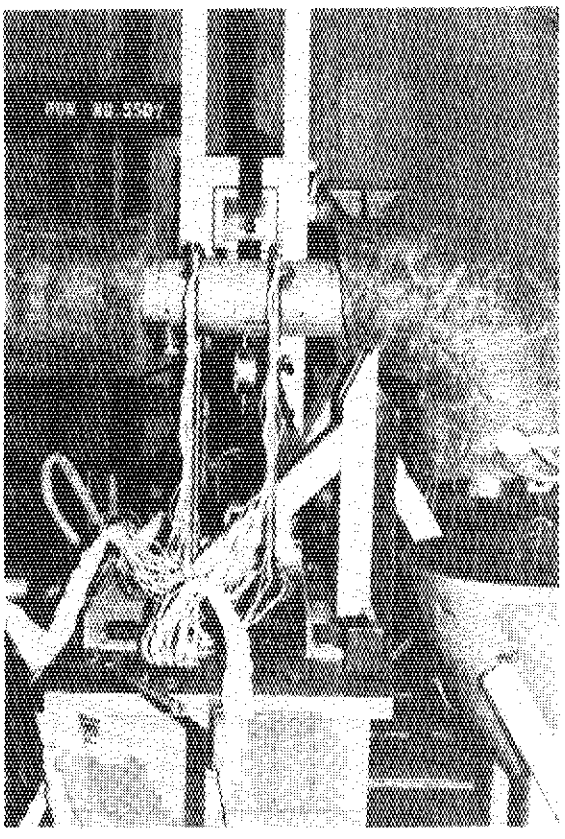

Photo. 2.2 View of the Restraint Installed on the Restraint Support

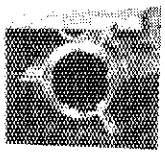

(a) RUN No. 5506

(b) RUN No. 5507

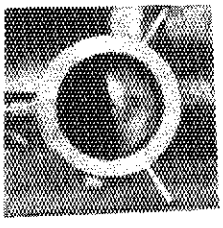

(c) RUN No. 5508

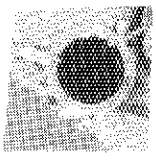

(d) RUN No. 5604

Photo. 2.3 View of the Rupture Disk after Test

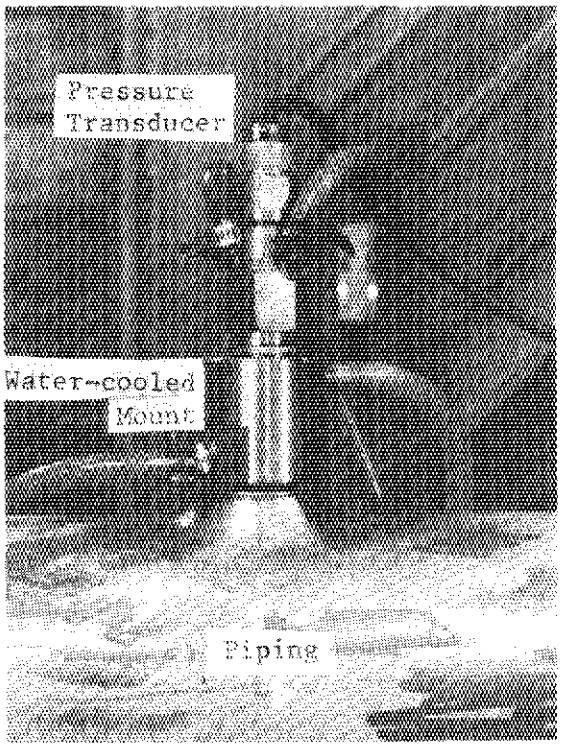

Photo. 2.4 Pressure transducer with watercooled moent

3. TEST RESULTS

3.1 Results of Electrical Measurements

The results of electrical measurements are given in APPENDIX A. A discription "ONLINE" written in the figure means that this datum was recorded with the temporal digital memory. Others were recorded with the data-recorders. The time-origin of the data recorded with the data-recorders was not the time origin of the pipe whip phemomenon, but the time when current began to flow into a electrode.

(a) Pressures in the pressure vessel

A.1 to A.16 show the time histories of pressures in the pressure vessel. Pressure drops rapidly from subcooled state to saturated one just after pipe break. Then, pressure decreases in saturated relation with water temperature. The slope of the pressure-time curve changes suddenly during saturated decompression owing to transition from low quality discharge to high quality one.

(b) Pressures in the piping

A.17 to A.87 show the time histories of pressures in the piping. Good data could not be obtained in the test of RUN No. 5507, because the temperature of the pressure transducers increased due to the leak of steam from the piping. The oscillation with relatively high frequency observed in PU105 was due to the effect of the pressure vibration in the cooling pipe which was installed to lower the temperature of the diaphram of the pressure transducer.

(c) Fluid temperatures in the pressure vessel and piping

A.88 to A.106 show the fluid temperatures in the pressure vessel and piping. The response time of the thermocouples attached to the piping was about 2 sec. Thus, the transient variation of the temperature could not be discussed by using these data.

(d) Strains of the test pipe

A.107 to A.218 show the strains of the test pipe. In the tests of RUN No.5508 and 5604, large strain was caused near the restraint location. Thus, the outputs of the strain gages mounted near the restraint location were intermitted because of exceeding the scales of the graphs.

The following can be seen from the figures. ① The strains near the restraint location are larger than those of other locations.

② The tensile strain is caused on the upper surface of the test pipe, while the compressive strain is caused on the lower surface of the test pipe. ③ The strains near the restraint location reach maximum late after the first impact of the test pipe on the restraints.

(e) Strains of the restraints

A.219 to A.436 show the strains of the restraints. The following can be found from the figures. ① The strains of the R1 restraint are larger than those of the R2 restraint. ② The tensile strain is caused on the outer side of the restraint, whereas the compressive strain is caused on the inner side of the restraint. ③ The large peak strain appears at the first impact of the test pipe on the restraints. ④ The strains of the restraint reach steady state within 0.1 sec after pipe break.

(f) Reaction forces of the restraints

A.437 to A.500 show the reaction forces of the restraints. The following can be seen from the figures. ① The reaction force of the R1 restraint is larger than that of the R2 restraint. ② The large peak reaction force appears at the first impact of the test pipe on the restraints. ③ The reaction force of the R2 restraint becomes equal to zero at the steady state for RUN No. 5507 and 5508.

(g) Accelerations of the test pipe

A.501 to A.510 show the accelerations of the test pipe. The acceleration of the value of about 500G is induced in the test pipe.

(h) Strains of the strain gages XU169 and XU170

A.511 and A.512 shows the results of the strain gages XU169 and XU170, respectively. The strain gage XU169 was mounted on the pipe stopper to examine whether or not the test pipe clashed against the pipe stopper after rebounding from the restraints. If the test pipe clashes against the pipe stopper, the compressive strain will appear in XU169. The strain of XU169 shows the tensile strain, so that it can be concluded that the test pipe did not clash against the pipe stopper.

The strain gages XU170 was mounted on the restraint support where little mechanical strain was caused in order to examine how much the outputs of the strain gages for large strain mounted on the restraints increase with temperature after pipe break. It is found from the figure that the strain of 200×10^{-6} was induced in the strain gage due to temperature increase.

3.2 Results of Residual Deformation Measurements

(1) Residual strains of the test pipe

Table 3.1 summarizes the results of measuring the axial distences between markings on the upper and lower surfaces of the test pipe. Figure 3.1 shows the axial distributions of the residual strains of the test pipe obtained from the above measurement.

(2) Residual cross-sectional deformations of the test pipe

Table 3.2 summarizes the results of measuring the horizontal and vertical outer diameters of the test pipe. Figure 3.2 shows the axial distributions of the residual cross-sectional deformations of the test pipe.

(3) Residual deformations of the test pipe

Table 3.3 summarizes the results of measuring the hights of the test pipe from the base level. Figure 3.3 shows the axial distributions of the residual deformations of the test pipe.

(4) Residual strains of the restraints

Table 3.4.1 through Table 3.4.3 show the results of measuring the distance between markings on the restraints. The errors of the residual strains obtained from the above measurements were about $\pm 700 \times 10^{-6}$ in the straight section of the restraint and about $\pm 1500 \times 10^{-6}$ in the circular section of the restraint, respectively. On the other hand, the errors of the residual strains obtained from the outputs of the strain gages mounted on the restraints were about 200×10^{-6}, judging from the result of XU170 in the test of RUN No. 5507 shown in A.512 which represents the apparent strain caused by temperature increase. Thus, the latter method was more accurate than the former one. Figure 3.4 shows the residual strains of the restraints obtained from the latter method.

(5) Residual deformations of the restraints

The results are shown in Table 3.5.

Table 3.1 Results of Dimensional Measurements of Test Pipe along Axial Direction

(a) RUN No.5506

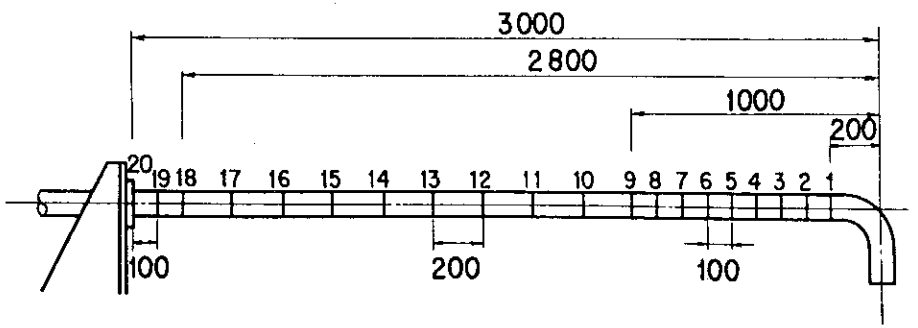

(Unit : mm)

	Location	1 – 2	2 – 3	3 – 4	4 – 5	5 – 6	6 – 7	7 – 8
Upper Side	Before Test	99.85	100.10	100.10	99.80	99.80	99.70	99.70
	After Test	99.65	100.00	100.00	99.90	99.75	99.70	99.75
Lower Side	Before Test	99.70	99.90	200.00		99.70	99.90	99.80
	After Test	99.90	100.00	200.05		99.85	100.00	99.90

	Location	8 – 9	9 – 10	10 – 11	11 – 12	12 –13	13 – 14	14 – 15
Upper Side	Before Test	99.70	199.80	199.85	200.00	200.00	199.95	199.85
	After Test	99.75	199.85	199.80	200.00	199.95	199.90	199.80
Lower Side	Before Test	300.00		199.90	200.10	199.45	199.90	199.80
	After Test	300.00		199.90	200.05	199.40	199.95	199.80

	Location	15 – 16	16 – 17	17 – 18	18 – 19	19 – 20
Upper Side	Before Test	200.00	200.05	200.25	100.00	100.00
	After Test	200.00	200.00	200.20	100.00	99.90
Lower Side	Before Test	199.80	199.70	200.20	99.75	99.85
	After Test	199.80	199.65	200.20	99.65	99.75

(d) RUN No.5604

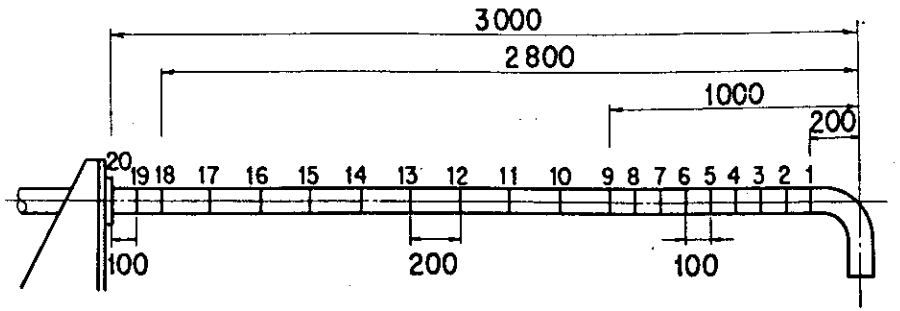

(Unit : mm)

	Location	1 – 2	2 – 3	3 – 4	4 – 5	5 – 6	6 – 7	7 – 8
Lower Side	Before Test	99.90	100.00	100.10	100.10	100.00	100.00	99.95
	After Test	99.80	99.65	99.75	99.95	99.95	99.95	99.90
Lower Side	Before Test	99.80	99.80	200.00		100.00	100.00	100.00
	After Test	99.95	100.35	200.70		100.25	100.20	100.05

	Location	8 – 9	9 – 10	10 – 11	11 – 12	12 – 13	13 – 14	14 – 15
Upper Side	Before Test	100.15	200.00	200.10	200.00	200.20	200.00	200.10
	After Test	100.15	200.10	200.10	200.05	200.20	200.10	200.10
Lower Side	Before Test	300.30		200.00	199.80	200.00	200.05	200.00
	After Test	300.40		200.10	200.00	200.10	200.10	200.00

	Location	15 – 16	16 – 17	17 – 18	18 – 19	19 – 20
Upper Side	Before Test	200.00	200.10	200.10	100.05	99.95
	After Test	200.05	200.15	200.10	100.10	99.95
Lower Side	Before Test	200.05	200.00	200.00	99.90	99.90
	After Test	200.10	199.90	200.00	99.95	99.90

Table 3.1 (Continued)

(c) RUN No.5508

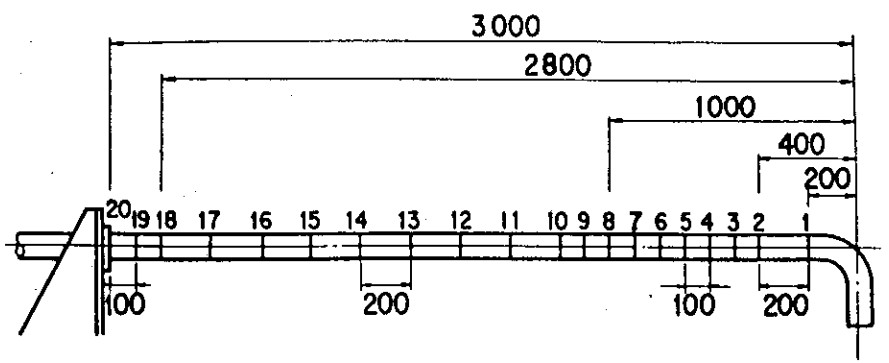

(Unit : mm)

	Location	1 – 2	2 – 3	3 – 4	4 – 5	5 – 6	6 – 7
Upper Side	Before Test	200.00	100.10	99.95	100.00	100.10	99.95
	After Test	199.80	99.20	97.00	99.85	96.00	96.95
Lower Side	Before Test	200.05	200.10		100.00	100.00	100.00
	After Test	200.25	204.55		105.00	104.25	103.05

	Location	7 – 8	8 – 9	9 – 10	10 – 11	11 – 12	12 – 13	13 – 14
Upper Side	Before Test	99.80	100.10	100.05	200.10	200.05	200.20	200.10
	After Test	98.40	99.55	99.80	199.85	200.05	200.25	200.20
Lower Side	Before Test	200.10		100.20	200.00	200.30	200.25	200.30
	After Test	200.35		100.55	200.30	200.45	200.25	200.35

	Location	14 – 15	15 – 16	16 – 17	17 – 18	18 – 19	19 – 20
Upper Side	Before Test	200.15	200.20	200.10	200.20	100.00	100.00
	After Test	200.10	200.20	200.10	200.20	100.05	100.00
Lower Side	Before Test	200.45	200.45	200.20	200.30	100.00	99.95
	After Test	200.45	200.55	200.25	200.40	100.00	99.95

(b) RUN No.5507

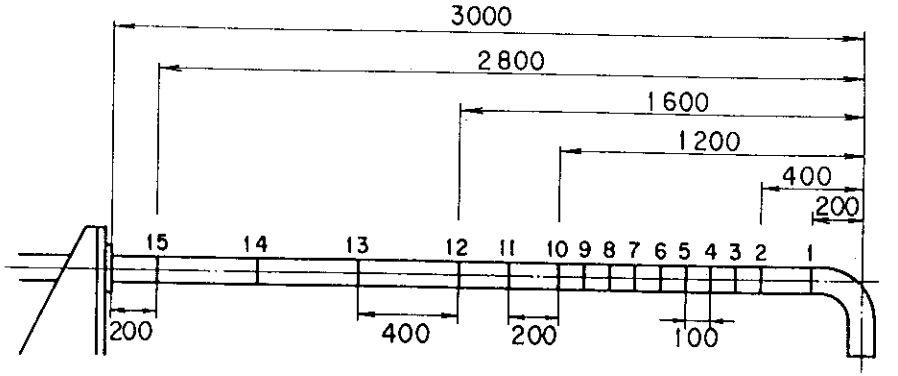

(Unit:mm)

	Location	1–2	2–3	3–4	4–5	5–6	6–7
Upper Side	Before Test	200.00	99.70	100.20	99.60	99.90	99.85
	After Test	199.30	97.75	94.85	89.2	85.0	64.0
Lower Side	Before Test	200.10			100.00	99.90	99.80
	After Test	200.90			114.2	122.4	129.2

	Location	7–8	8–9	9–10	10–11	11–12	12–13	13–14
Upper Side	Before Test	100.00	99.65	100.00	200.00	200.00	400.20	400.30
	After Test	79.2	87.5	90.90	188.20	197.00	393.00	400.50
Lower Side	Before Test			99.80	200.00	200.20	400.30	400.20
	After Test			110.00	202.80	204.00	408.10	400.10

	Location	14–15	15–16
Upper Side	Before Test	400.45	200.00
	After Test	409.70	216.4
Lower Side	Before Test	400.30	200.00
	After Test	392.50	182.90

Table 3.2 Results of Dimensional Measurements in Cross Section of Test Pipe

(a) RUN No.5506

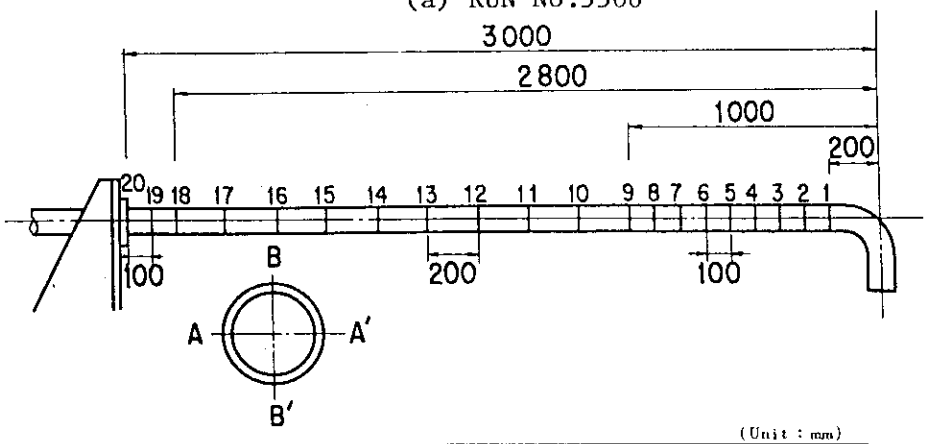

(Unit : mm)

	Location	1	2	3	4	5	6	7
A-A′	Before Test	114.13	114.08	114.10	114.38	114.07	114.12	114.15
	After Test	114.07	114.15	114.07	114.37	114.08	114.20	114.15
B-B′	Before Test	114.24	114.33	114.27		114.25	114.26	114.25
	After Test	114.22	114.33	114.28		114.27	114.28	114.27

	Location	8	9	10	11	12	13	14
A-A′	Before Test	114.18	114.40	114.15	114.18	114.18	114.17	114.27
	After Test	114.18	114.39	114.16	114.20	114.19	114.18	114.28
B-B′	Before Test	114.19		114.23	114.20	114.21	114.22	114.02
	After Test	114.19		114.23	114.19	114.20	114.20	114.05

	Location	15	16	17	18	19	20
A-A′	Before Test	114.17	114.15	114.12	114.15	114.26	114.25
	After Test	114.18	114.16	114.13	114.16	114.27	114.26
B-B′	Before Test	114.20	114.24	114.24	114.19	114.06	114.06
	After Test	114.20	114.24	114.24	114.20	114.06	114.06

(b) RUN No.5507

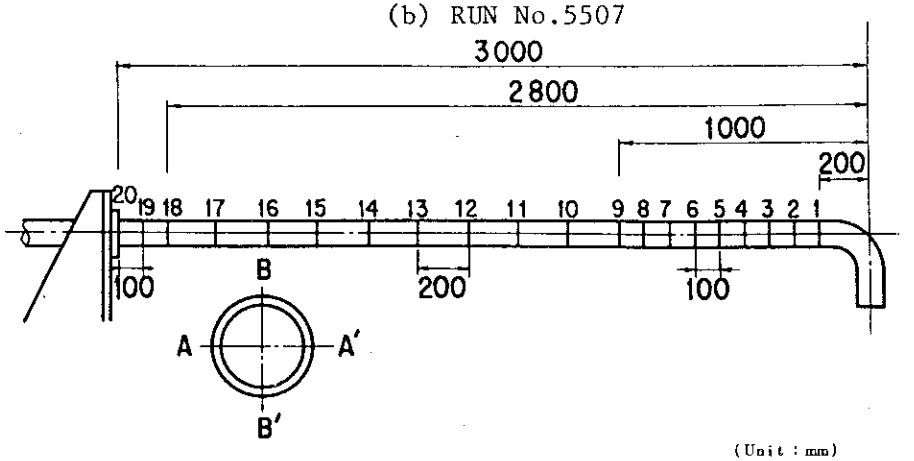

(Unit : mm)

	Location	1	2	3	4	5	6	7
A-A′	Before Test	114.14	114.19	114.15	114.51	114.13	114.10	114.15
	After Test	114.13	114.20	114.16	114.49	114.05	114.13	114.10
B-B′	Before Test	114.28	114.28	114.27		114.30	114.26	114.30
	After Test	114.29	114.27	114.34		114.40	114.30	114.43

	Location	8	9	10	11	12	13	14
A-A′	Before Test	114.14	114.45	114.14	114.17	114.14	114.17	114.18
	After Test	114.15	114.42	114.14	114.18	114.13	114.16	114.17
B-B′	Before Test	114.29		114.31	114.28	114.23	114.27	114.25
	After Test	114.31		114.33	114.30	114.24	114.28	114.25

	Location	15	16	17	18	19	20
A-A′	Before Test	114.17	114.15	114.15	114.18	114.20	114.19
	After Test	114.16	114.13	114.13	114.15	114.18	114.22
B-B′	Before Test	114.25	114.29	114.30	114.25	114.26	114.26
	After Test	114.25	114.29	114.30	114.25	114.24	114.24

Table 3.2 (Continued)

(c) RUN No.5508

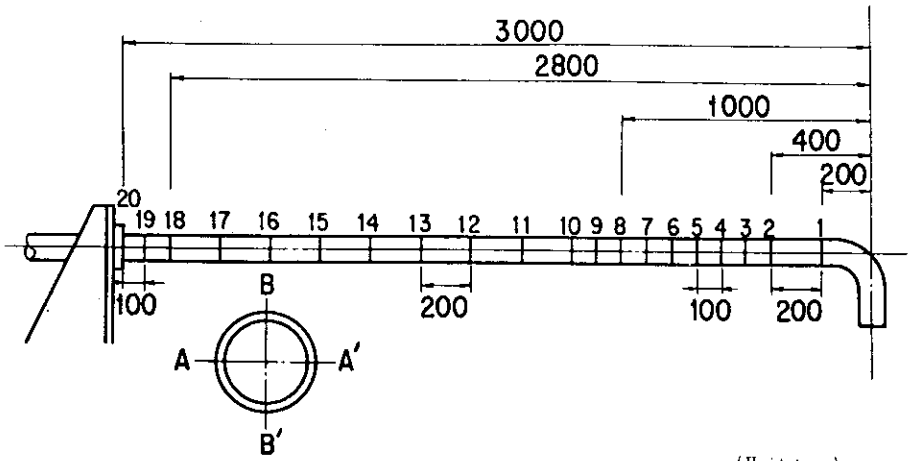

(Unit : mm)

	Location	1	2	3	4	5	6	7
A–A'	Before Test	114.14	114.13	114.36	114.14	114.15	114.13	114.15
	After Test	114.14	114.14	113.93	115.58	115.61	115.04	114.50
B–B'	Before Test	114.17	114.23		114.23	114.24	114.21	114.21
	After Test	114.21	114.25		113.01	113.57	113.95	114.30

	Location	8	9	10	11	12	13	14
A–A'	Before Test	114.43	114.15	114.19	114.15	114.21	114.17	114.18
	After Test	114.60	114.16	114.20	114.19	114.20	114.16	114.18
B–B'	Before Test		114.22	114.21	114.17	114.05	114.18	114.17
	After Test		114.31	114.25	114.18	114.05	114.17	114.15

	Location	15	16	17	18	19	20
A–A'	Before Test	114.19	114.14	114.13	114.14	114.16	114.14
	After Test	114.18	114.15	114.12	114.13	114.16	114.16
B–B'	Before Test	114.16	114.23	114.23	114.19	114.20	114.18
	After Test	114.15	114.23	114.23	114.20	114.23	114.17

(d) RUN No.5604

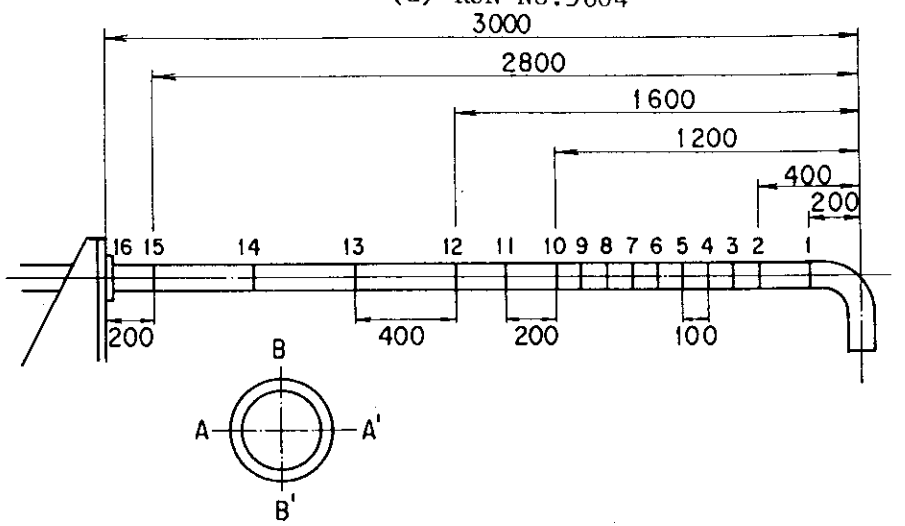

(Unit:mm)

	Location	1	2	3	4	5	6	7
A–A'	Before Test	114.210	114.200	114.490	114.100	114.190	114.200	114.190
	After Test	114.200	114.240	115.670	117.850	122.890	136.60	151.90
B–B'	Before Test	114.120	114.150		114.120	114.110	114.180	114.70
	After Test	114.130	114.150		109.380	103.890	81.55	

	Location	8	9	10	11	12	13	14
A–A'	Before Test	114.510	114.180	114.190	114.140	114.170	114.220	114.200
	After Test	126.90	126.90	117.110	115.265	114.625	114.320	114.125
B–B'	Before Test		114.130	114.150	114.200	114.210	114.150	114.190
	After Test		109.050	111.835	113.760	113.960	114.155	114.255

	Location	15	16
A–A'	Before Test	114.230	114.230
	After Test	115.770	116.840
B–B'	Before Test	114.140	114.140
	After Test	113.105	109.800

Table 3.3 Results of Residual Deformation of Test Pipe

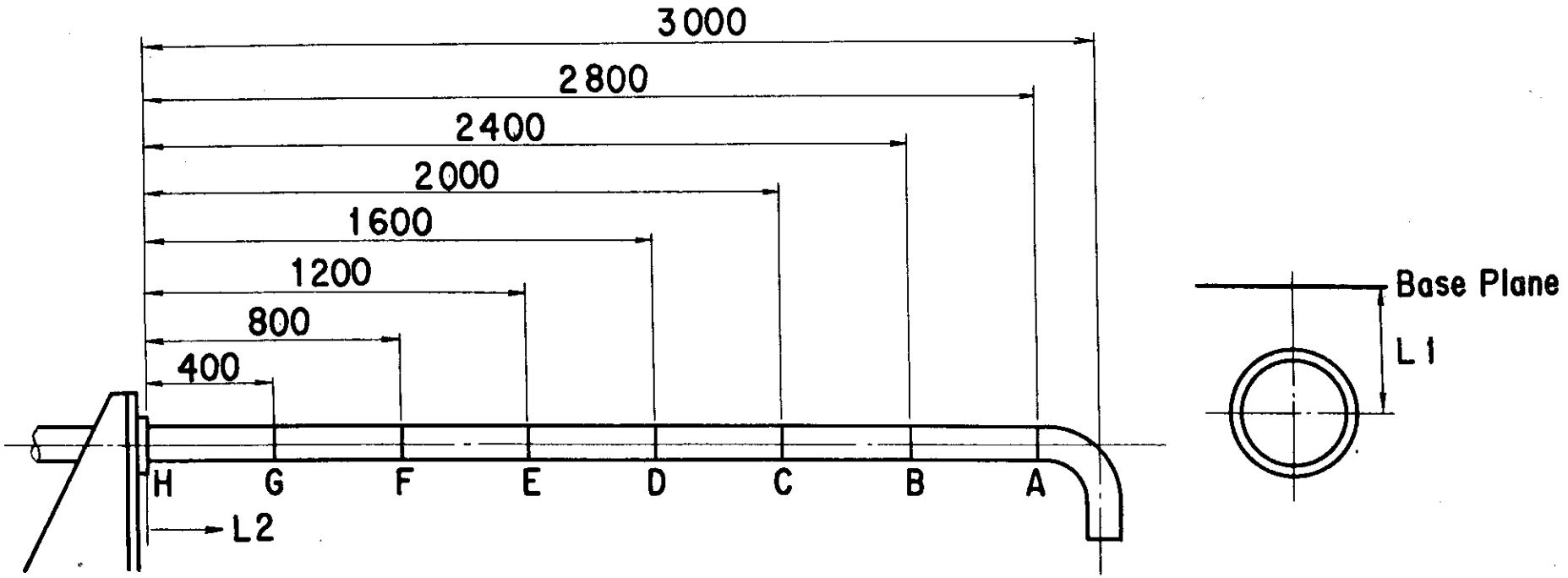

(Unit : mm)

	RUN №. 5506				RUN №. 5507				RUN №. 5508			
	L 1		L 2		L 1		L 2		L 1		L 2	
	Before Test	After Test	Before Test	After Test	Before Test	After Test	Before Test	After Test	Before Test	After Test	Before Test	After Test
A	248.0	250.0	2800.0	2798.7	247.0	241.8	2799.8	2799.8	250.7	116.8	2800.0	2780.5
B	247.5	250.0	2400.0	2398.9	247.3	249.5	2399.5	2399.5	250.7	238.3	2400.0	2398.5
C	247.2	249.2	1999.5	1999.2	247.0	250.1	1999.5	1999.7	250.5	275.3	2000.0	1999.5
D	247.5	248.5	1600.2	1599.9	247.4	250.5	1599.8	1600.0	250.5	271.2	1600.0	1599.8
E	247.5	248.2	1200.0	1199.8	247.4	249.5	1200.0	1200.0	250.5	265.0	1200.0	1200.0
F	248.0	248.2	800.0	800.0	247.5	248.5	800.0	800.0	250.7	259.3	800.0	800.0
G	248.0	247.5	399.8	400.0	247.0	247.8	400.0	400.0	250.7	255.3	400.0	400.0
H	247.0	247.0	0.0	0.0	247.0	247.0	0.0	0.0	251.0	251.9	0.0	0.0

Table 3.4.1 Results of Dimensional Measurements of Restraints

----- RUN No.5506

(a) R1 Restraint

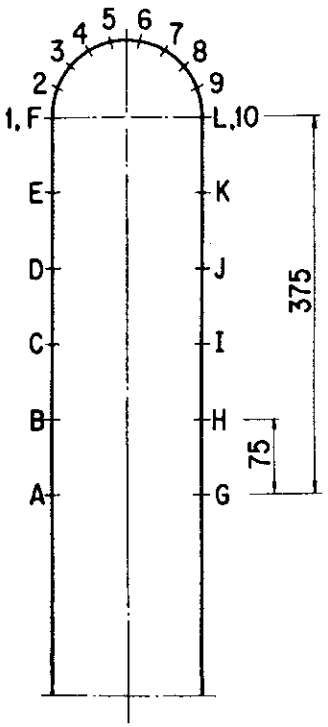

Straight Section

Outside (Unit : mm)

Location	A－B	B－C	C－D	D－E	E－F
Before Test	75.00	74.70	75.00	75.00	74.90
After Test	74.95	74.55	74.85	74.85	74.65

Location	A－C	C－E	D－F	B－E	A－F
Before Test	149.90	150.00	149.90	224.90	375.90
After Test	149.50	149.80	149.60	224.70	375.00

Location	G－H	H－I	I－J	J－K	K－L
Before Test	74.90	74.70	75.00	74.90	74.95
After Test	74.80	74.60	74.90	74.70	74.60

Circular Section

Outside (Unit : mm)

Location	1－2	2－3	3－4	4－5	5－6	6－7	7－8	8－9	9－10
Before Test	28.50	28.85	29.00	29.20	29.25	28.70	29.30	29.25	29.15
After Test	28.45	28.75	28.95	29.50	29.45	29.05	29.45	28.95	28.90

Inside

Location	1－2	2－3	3－4	4－5	5－6	6－7	7－8	8－9	9－10
Before Test	23.05	22.70	22.65	22.90	22.65	22.90	22.60	22.70	22.65
After Test	23.15	22.70	22.60	22.45	22.40	22.45	22.45	22.65	23.00

Lateral Side

Location	1－2	2－3	3－4	4－5	5－6	6－7	7－8	8－9	9－10
Before Test	25.55	25.60	25.75	26.15	26.00	26.00	25.85	25.75	26.20
After Test	25.65	25.50	25.70	26.15	26.05	25.70	25.80	25.70	26.15

(b) R2 Restraint

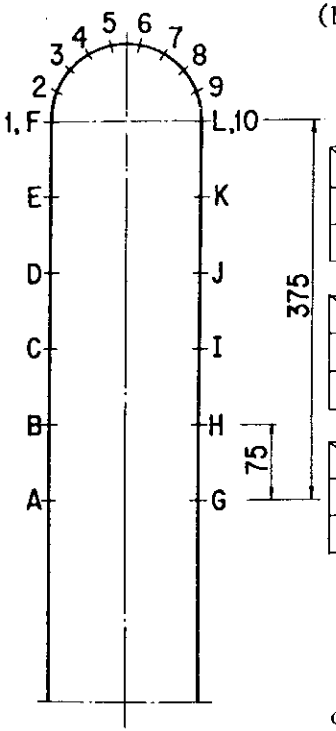

Straight Section

Outside (Unit : mm)

Location	A－B	B－C	C－D	D－E	E－F
Before Test	74.90	74.65	74.75	74.80	75.00
After Test	74.85	74.60	74.60	74.65	74.85

Location	A－C	C－E	D－F	B－E	A－F
Before Test	149.75	149.70	149.90	224.50	374.55
Afuer Test	149.70	149.65	149.85	224.35	375.00

Location	G－H	H－I	I－J	J－K	K－L
Before Test	74.65	74.65	74.90	74.65	75.00
After Test	74.60	74.60	74.85	74.60	74.90

Circular Section

Outside (Unit : mm)

Location	1－2	2－3	3－4	4－5	5－6	6－7	7－8	8－9	9－10
Before Test	28.60	28.60	28.65	29.05	29.05	28.75	29.00	28.85	29.20
After Test	28.65	28.45	28.60	29.10	29.35	28.90	28.90	28.75	29.15

Inside

Location	1－2	2－3	3－4	4－5	5－6	6－7	7－8	8－9	9－10
Before Test	22.70	23.00	23.00	22.60	22.40	22.35	22.50	22.15	22.45
After Test	22.95	23.00	23.05	22.50	22.35	22.25	22.50	22.10	22.35

Lateral Side

Location	1－2	2－3	3－4	4－5	5－6	6－7	7－8	8－9	9－10
Before Test	26.00	25.70	25.70	26.00	25.60	25.60	26.30	26.00	25.90
After Test	26.00	25.70	25.70	25.90	25.55	25.60	26.25	26.00	25.90

JAERI-M 82-125

Table 3.4.2 Results of Dimensional Measurements of Restraints

----- RUN No.5507

(a) R1 Restraint

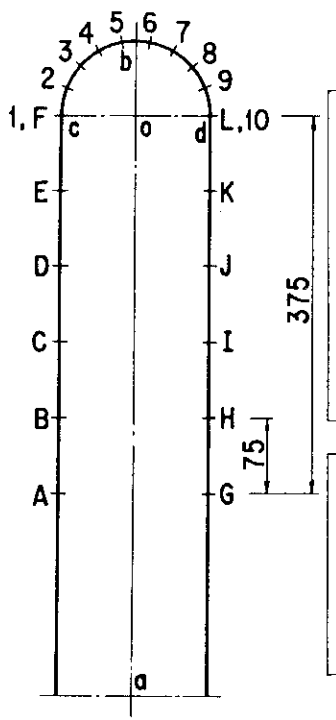

Straight Section

(Unit : mm)

	Location	A－B	B－C	C－D	D－E	E－F
Outside	Before Test	74.75	74.70	75.00	75.00	74.50
	After Test	74.85	74.60	75.00	75.00	74.30
	Location	A－C	C－E	D－F	B－E	A－F
	Before Test	149.60	150.20	149.60	225.00	374.50
	After Test	149.65	150.15	149.45	224.95	374.30
	Location	G－H	H－I	I－J	J－K	K－L
	Before Test	75.00	74.60	74.95	74.65	75.10
	After Test	75.00	74.55	74.95	74.60	74.80

	Location	A－B	B－C	C－D	D－E	E－F
Inside	Before Test	74.75	74.75	74.75	74.95	74.90
	After Test	74.70	74.70	74.80	74.85	75.00
	Location	A－C	C－E	D－F	B－E	E－F
	Before Test	149.70	150.00	150.00	224.90	374.80
	After Test	149.65	150.00	150.15	224.95	374.80

Circular Section

(Unit : mm)

	Location	1－2	2－3	3－4	4－5	5－6	6－7	7－8	8－9	9－10
Outside	Before Test	28.75	28.90	28.75	29.00	28.90	29.10	28.70	29.20	28.60
	After Test	28.50	28.90	28.90	29.30	29.25	29.45	28.85	29.10	28.40
	Location	1－2	2－3	3－4	4－5	5－6	6－7	7－8	8－9	9－10
Inside	Before Test	22.90	22.70	22.55	22.50	22.60	22.55	22.60	22.60	22.60
	After Test	23.55	22.85	22.45	22.05	22.30	22.40	22.60	22.70	23.10

(Unit : mm)

Location	a－b	a－o	c－d
Before Test	648.00	573.20	149.65
After Test	651.50	573.70	142.80

(b) R2 Restraint

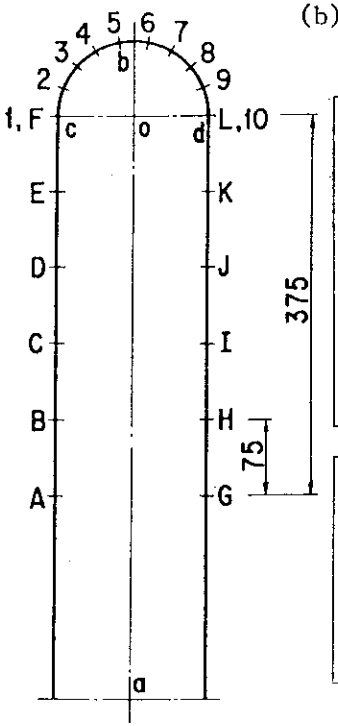

Straight Section

(Unit : mm)

	Location	A－B	B－C	C－D	D－E	E－F
Outside	Before Test	74.60	74.40	75.00	74.80	74.60
	After Test	74.60	74.40	75.00	74.70	74.60
	Location	A－C	C－E	D－F	B－E	A－F
	Before Test	149.30	150.00	149.70	224.60	374.00
	After Test	149.20	149.95	149.65	224.60	374.00
	Location	G－H	H－I	I－J	J－K	K－L
	Before Test	74.80	74.60	74.80	74.65	74.95
	After Test	74.85	74.65	74.80	74.65	74.95

	Location	A－B	B－C	C－D	D－E	E－F
Inside	Before Test	74.65	75.05	74.50	75.00	74.75
	After Test	74.65	75.05	74.45	75.00	74.75
	Location	A－C	C－E	D－F	B－E	A－F
	Before Test	150.00	149.75	150.00	225.00	374.65
	After Test	150.00	149.75	150.00	225.00	374.65

Circular Section

(Unit : mm)

	Location	1－2	2－3	3－4	4－5	5－6	6－7	7－8	8－9	9－10
Outside	Before Test	29.25	29.00	29.00	29.05	29.05	28.80	29.15	28.95	28.85
	After Test	29.40	29.00	29.30	29.05	29.10	28.80	29.15	28.95	28.90
	Location	1－2	2－3	3－4	4－5	5－6	6－7	7－8	8－9	9－10
Inside	Before Test	23.40	22.45	22.70	22.75	22.70	22.50	22.80	22.70	22.70
	After Test	23.45	22.55	22.65	22.80	22.70	22.55	22.85	22.70	22.70

(Unit : mm)

Location	a－b	a－o	c－d
Before Test	648.50	573.50	149.85
After Test	649.00	573.50	149.20

Table 3.4.3 Results of Dimensional Measurements of Restraints

----- RUN No.5508

(a) R1 Restraint

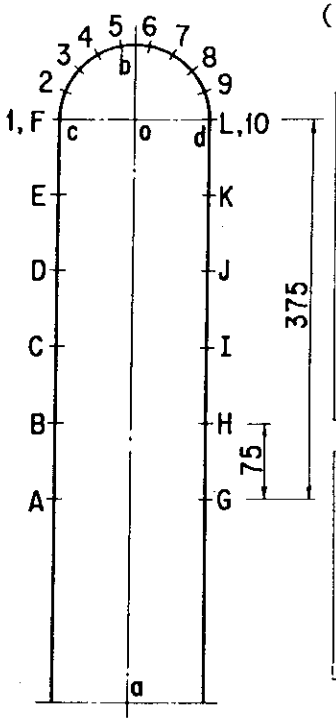

Straight Section

(Unit : mm)

Outside	Location	A－B	B－C	C－D	D－E	E－F
	Before Test	75.00	74.40	74.80	75.00	74.60
	After Test	75.00	74.40	74.80	75.00	74.50
	Location	A－C	C－E	D－F	B－E	A－F
	Before Test	149.60	150.00	149.75	224.70	374.40
	After Test	149.60	150.00	149.70	224.60	374.30
	Location	G－H	H－I	I－J	J－K	K－L
	Before Test	74.90	74.60	74.70	74.85	74.65
	After Test	74.90	74.55	74.75	74.85	74.55

Inside	Location	A－B	B－C	C－D	D－E	E－F
	Before Test	74.75	74.65	75.00	74.65	74.80
	After Test	74.75	74.60	75.00	74.70	74.90
	Location	A－C	C－E	D－F	B－E	A－F
	Before Test	149.60	149.95	149.70	224.80	374.60
	After Test	149.60	150.00	149.80	224.80	374.70

Circular Section

(Unit : mm)

	Location	1－2	2－3	3－4	4－5	5－6	6－7	7－8	8－9	9－10
Outside	Before Test	28.60	28.80	28.80	28.80	29.10	28.90	28.75	29.00	28.80
	After Test	27.50	28.70	28.75	29.00	29.40	29.10	28.80	29.00	28.65
Inside	Location	1－2	2－3	3－4	4－5	5－6	6－7	7－8	8－9	9－10
	Before Test	22.45	22.65	22.45	22.70	22.55	22.15	22.35	22.65	22.95
	After Test	22.50	22.65	22.45	22.50	22.25	21.85	22.30	22.70	22.95

(Unit : mm)

Location	a－b	a－o	c－d
Before Test	648.70	574.30	148.30
After Test	651.00	574.50	144.20

(b) R2 Restraint

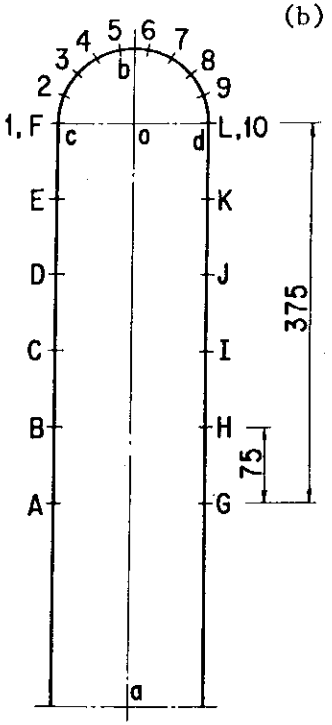

Straight Section

(Unit : mm)

Outside	Location	A－B	B－C	C－D	D－E	E－F
	Before Test	74.95	74.60	74.75	74.75	74.85
	After Test	74.95	74.55	74.70	74.75	74.90
	Location	A－C	C－E	D－F	B－E	A－F
	Before Test	149.85	149.65	149.80	224.55	374.60
	After Test	149.75	149.65	149.80	224.50	374.60
	Location	G－H	H－I	I－J	J－K	K－L
	Before Test	75.00	74.75	74.80	74.80	74.65
	After Test	74.90	74.65	74.85	74.70	74.70

Inside	Location	A－B	B－C	C－D	D－E	E－F
	Before Test	74.90	74.75	74.90	74.80	74.70
	After Test	74.90	74.75	74.90	84.80	74.70
	Location	A－C	C－E	D－F	B－E	A－F
	Before Test	149.85	149.90	149.65	224.90	374.70
	After Test	149.85	149.90	149.65	224.90	374.70

Circular Section

(Unit : mm)

	Location	1－2	2－3	3－4	4－5	5－6	6－7	7－8	8－9	9－10
Outside	Before Test	28.90	28.90	28.70	28.75	29.30	29.05	28.95	28.65	28.75
	After Test	28.90	28.90	28.70	28.75	29.30	29.10	29.00	28.65	28.75
Inside	Location	1－2	2－3	3－4	4－5	5－6	6－7	7－8	8－9	9－10
	Before Test	23.15	22.40	22.25	22.35	22.65	22.45	22.75	22.85	22.50
	After Test	23.10	22.55	22.25	22.35	22.55	22.30	22.70	22.95	22.55

(Unit : mm)

Location	a－b	a－o	c－d
Before Test	647.70	573.80	148.05
After Test	647.70	573.80	148.00

Table 3.5 Residual Deformation of Restraints

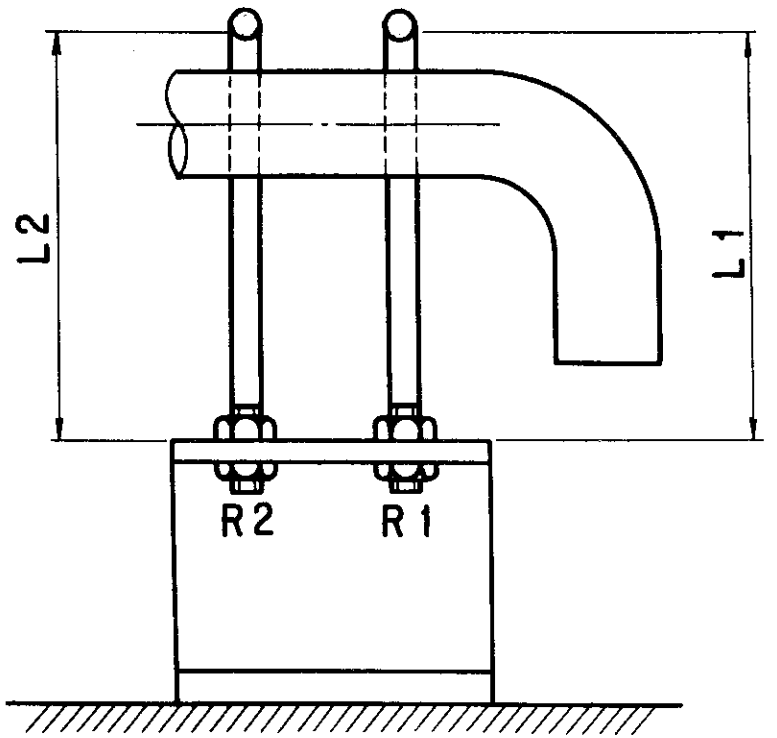

(Unit : mm)

	RUN №. 5506		RUN №. 5507		RUN №. 5508	
	L1	L2	L1	L2	L1	L2
Before Test	561.35	561.35	566.65	565.85	564.8	564.9
After Test	569.47	567.13	569.60	566.50	566.3	564.8
Elongation	8.12	5.76	2.95	0.65	1.5	−0.1

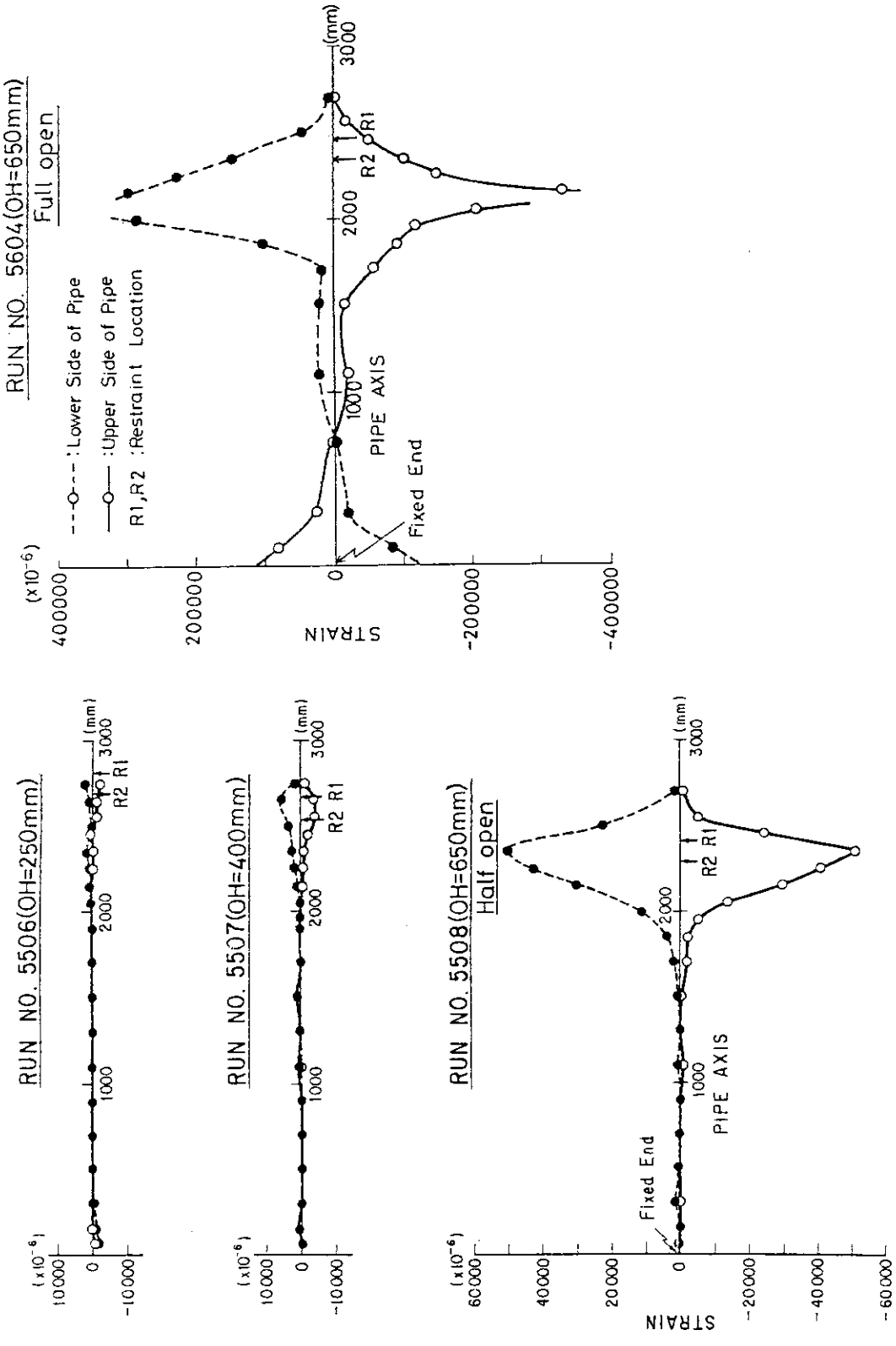

Fig. 3.1 Residual Strain of Test Pipe

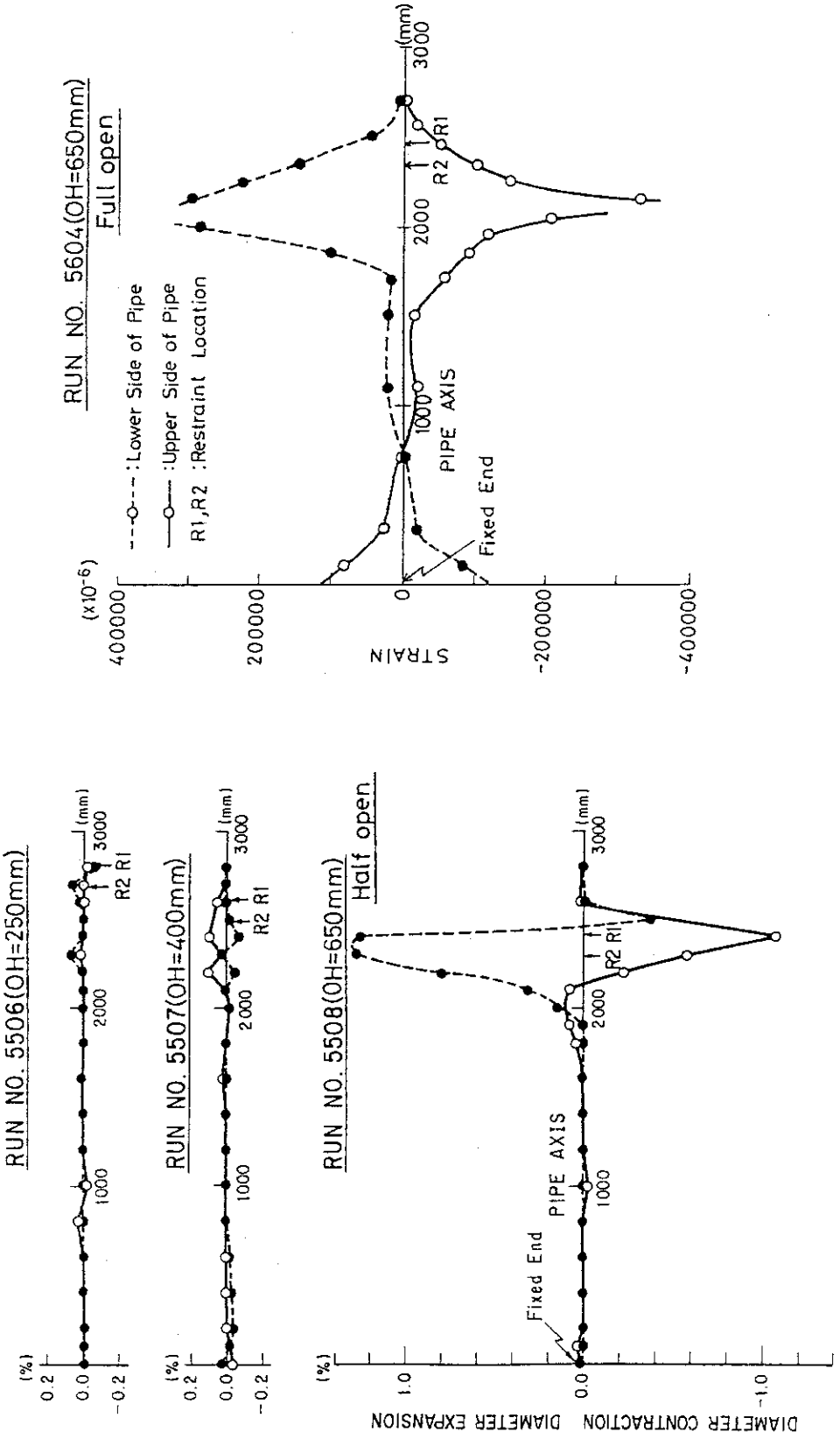

Fig. 3.2 Residual Cross-Sectional Deformation of Test Pipe

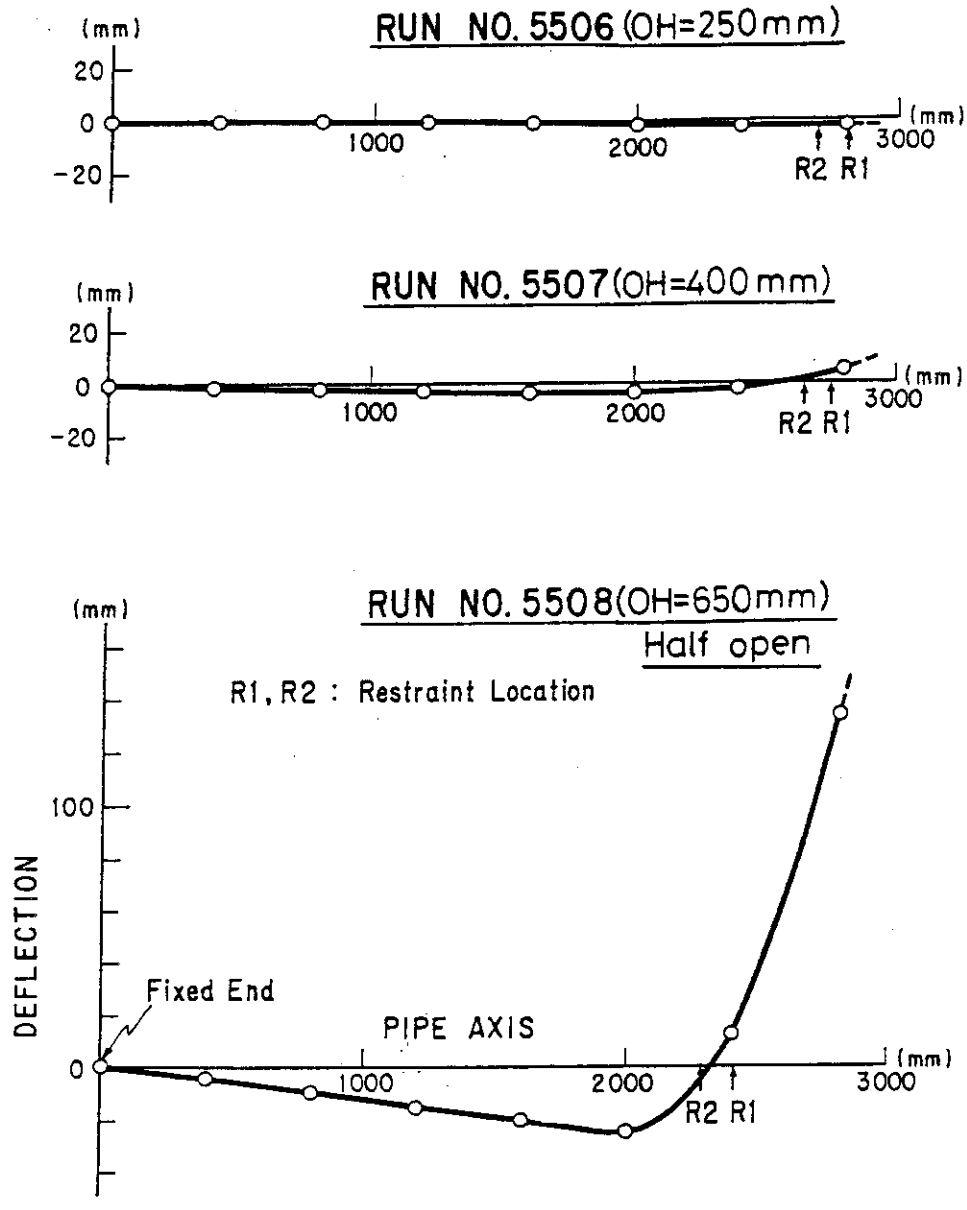

Fig. 3.3 Residual Deformation of Test Pipe

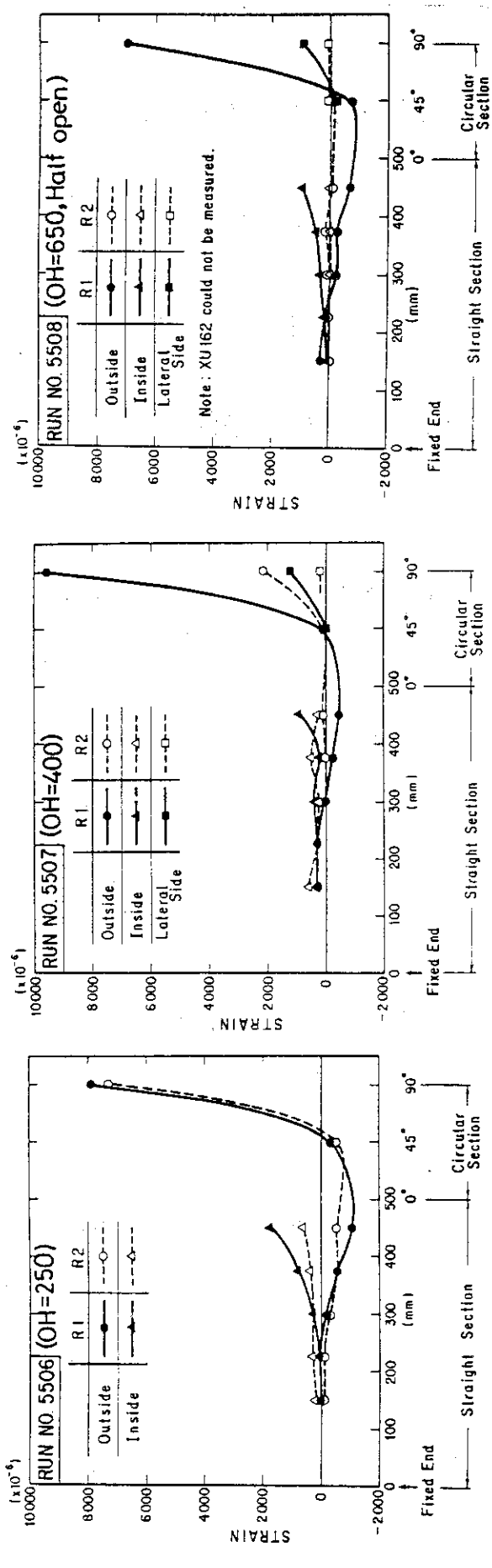

Fig. 3.4 Residual Strain of Restraint

4. DISCUSSION

4.1 Time Sequence of Events in Pipe Whip Phenomenon

As stated in Section 3.1, the time origins of the data recorded with the data-recorders do not correspond to those of the pipe whip phenomenon. The time sequence of the major events is given in Fig. 4.1, where PU110, XU300, XU142, and XU162 denote the pressure near the break location of the test pipe, the accelerometer mounted on the test pipe, the strain gage mounted on the top of the R1 restraint and the strain gage mouted on the top of the R2 restraint, respectively. The outputs of PU110 and XU300 appear earliest, so that the time origin of the pipe whip phenomenon can be defined as the starting time of these events. The impact time of the test pipe on each restraint is also given in the figure.

Figure 4.2 shows the selected data, which represent the fluid pressures, PU101, PU110 and PU105, the dynamic behavior of the test pipe, XU300, and the dyanmic behavior of the restraint, WU131. It can be seen from the figures that all phenomena reach the steady state at the time of 0.2 sec or 0.3 sec.

4.2 Pressures in the pressure vessel and piping

The pressure-time history of subcooled water blowdown is characterized by the following two processes.

(i) Subcooled decompression process

Rapid pressure drop occurs at the break location of the pipe and pressure wave propagates towards the upstream side. Pressure decreases to the saturated pressure corresponding to the initial temperature after repeating the wave propagation and reflection.

(ii) Saturated decompression process

After the subcooled decompression process, pressure decreases in saturated relation with water temperature. During the transition from the subcooled decompression to the saturated decompression, pressure decreases below the saturated pressure because of retardation of the bubble generation. This is called a transition regime.

A detailed discussion is given to the test data in accordance with the discremination between the subcooled decompression process and the saturated decompression process.

4.2.1 Subcooled decompression process

Figure 4.3 shows the pressure-time histories in the pressure vessel and the piping for RUN No. 5506. The figures represent the pressure decrease, so that the origin of the pressure corresponds to the value of the initial pressure. In the present system, the following three types can be found in the subcooled decompression process.

① Type 1: Pressure drops suddenly to the pressure $P_{min}^{(*)}$ which is much lower than the saturated pressure corresponding to the initial temperature. Then, after recovering to the higher pressure than P_{sat}, pressure decreases gradually to the pressure P_{min} which represents the minimum pressure in the transition regime. The pressures in the piping near the break location show the Type 1.

② Type 2: Pressure decreases to P_{min} with the pressure oscillation due to the propagation and reflection of pressure wave. The pressures in the piping relatively far from the break location show the Type 2.

③ Type 3: Pressure decreases smoothly to P_{min} without pressure oscillation. The pressures in the pressure vessel show the Type 3.

The time delay in the first decompression is found in the pressure-time histories shown in Fig. 4.3. This is due to the propagation of the pressure wave generated at the break location toward the pressure vessel. The average velocity of pressure wave, v_{ave}, is calculated at about 830 m/sec for all the tests, using the above test data. On the other hand, the sonic velocity in the fluid, a, is expressed as follows, under the assumption that the stiffness of piping is infinite:

$$a = (Kg/\gamma)^{1/2} = (Kvg)^{1/2}$$
$$K = -dP/(dv/v) \quad , \tag{1}$$

in which K, g, γ and v denote volumetric elastic modulus, gravitational acceleration, specific weight and specific volume, respectively. Using the above equation, the sonic velocity in subcooled water whose temperature and pressure are 320°C and 15.5 MPa, respectively, is calculated at 854 m/sec. This velocity is almost coincident with v_{ave}. Therefore, it is confirmed from the test data that pressure wave propagates at the sonic velocity. The pressure oscillation with a period of 33 msec indicates the propagation and reflection of pressure wave between the break location and the junction of the pressure vessel and the piping. The period of pressure oscillation is identical with the value calculated from the equation $v_{ave}/2\ell$, where v_{ave} and ℓ denote the average

velocity of pressure wave, 830 m/sec, and the pipe length between the break location and the pressure vessel, 13.6 m. The piping was thought to be filled up with subcooled water during the appearance of the pressure oscillation, because the sonic velocity of two-phase flow is much less than that of single-phase flow. Considering the whipping phenomenon of the test pipe settled down at 0.2 through 0.3 sec after pipe break, it is concluded that the pipe whip tests could be performed under the LOCA conditions of subcooled water.

4.2.2 Saturated decompression process

Figure 4.4 shows the pressure-time history in the pressure vessel. The saturated pressures obtained from the measured temperatures are also dipcted in the figure. After the subcooled decompression, pressure is found to decrease in saturated relation with water temperature. In the satureated decompression, the great change of pressure decrease rate is observed at the time of 20 sec for RUN No. 5506 and 30 sec for RUN No. 5508 and 5604 because of the change from low quality discharge to high quality one. It can be seen from Fig. 4.4 that the curve of RUN No. 5604 is almost the same as that of RUN No. 5508. In the test of RUN No. 5604, the flow area of the test pipe was contracted to 36.9% of the cross-sectional area of the test pipe because of plastic collapse as shown in Photo. 4.1. This value is the same as the break area ratio of rupture disk in the test of RUN no. 5508. Thus, the pressure-time curves are almost coincident for RUN No. 5508 and 5604.

4.3 Deformation of Test Pipe

4.3.1 Residual deformation of test pipe

Photograph 4.1 shows the deformation of the test pipe after test. The large deformation cannot be found in the tests of RUN No. 5506 (OH = 250 mm) and RUN No. 5507 (OH=400 mm). On the other hand, in the test of RUN No. 5604 where the ovehang length was 650 mm and the rupture disk opened completely, plastic hinge was formed at the distance of 900 mm from the break location, on which the free end of the test pipe rotated and hit against the pipe itself. The following are found from Fig. 3.1 which shows the residual strain of the test pipe. Large

residual strain cannot be found in the test of RUN No. 5506 (OH=250 mm), while relatively large residual strain can be observed near the restraint location in the tests of RUN No. 5507 (OH=400 mm) and RUN No. 5508 (OH=650 mm) in which the rupture disk did not open completely. In the test of RUN NO. 5604 (OH=650 mm) in which the rupture disk opened completely, the peak of the residual strain is observed at the distance of about 250 mm backward from the restraint location. This is due to the reason that the location on the test pipe constrained by the restraints became backward owing to the slide of the restraints along the axis of the test pipe and the bending of the restraints, as shown in Photo 4.2.

In the following is discussed the plastic collapse of the test pipe. Let M_y and M_u denote the moment required to yield plastic strain in the outer surface of the test pipe and the ultimate moment of the test pipe, respectively. M_y and M_u can be given as follows:

$$M_y = \sigma_y Z_e \quad , \quad M_u = \sigma_y Z_p + (\sigma_u - \sigma_y) Z_e \tag{2}$$

in which σ_y and σ_u denote the yield strength and the ultimate strength, respectively, and Z_e and Z_p are the elastic bending section modulus and the plastic bending section modulus, respectively. Z_e and Z_p can be reprensented using the inner and outer radii, r_i and r_o, as follows:

$$Z_e = \frac{\pi}{4 r_o} (r_o^4 - r_i^4) \quad , \quad Z_p = \frac{4}{3}(r_o^3 - r_i^3) \tag{3}$$

The strengths σ_y and σ_u were obtained from a tensile test at the temperature of 325°C as follows:

$$\sigma_y = 192 \text{ MPa} \ , \quad \sigma_u = 448 \text{ MPa}$$

The moments M_y and M_u are obtained as follows by substituting the above values of σ_y and σ_u, and the values of r_i and r_o corresponding to 4-inch & sch160 pipe into eqs.(2) and (3):

$$M_y = 1.859 \times 10^4 \text{ N·m}, \quad M_u = 4.454 \times 10^4 \text{ N·m}$$

Let F_y and F_u indicate the loads corresponding to M_y and M_u which act on the break location of the test pipe. Table 4.1 shows the comparison between the blowdown thrust force T obtatined from the test data and the calculated loads F_y and F_u. The average value of the blowdown thrust force from 0 sec to 0.2 sec was used as the value of T because the pipe movement settled down within above time. The value of T for

RUN No. 5604 is not given in the table since the accurate value could not be obtained in this case. In the test of RUN No.5506, T is nearly equal to F_y, which means that little plastic strain is caused in the outer surface of the test pipe near the restraint location. On the other hand, T is much larger than F_y and smaller than F_u in the tests of RUN No. 5507 and 5508, which indicates that relatively large plastic strain is caused in the outer surface of the test pipe near the restraint location. In the test of RUN No. 5604, T is assumed to be nearly equal to 70 KN, considering that the test conditions of RUN No. 5604 are the same as those of RUN No. 5506 and 5507. In this case, T is much larger than F_u, which means that platic collapse takes place in the test pipe. The abovementioned behaviors of the test pipe predicted by comparing T with F_y and F_u are coincident with those of the tests. It is also found that plastic collapse of the test pipe can be predicted by using the limit moment M_u.

4.3.2 Dynamic behaviors

The dynamic beahviors of the test pipe are discussed here based on the test data obtained from strain gages and accelerometers.

Figure 4.5 shows the comparison between the dynamic strains of the upper and lower surfaces of the test pipe. This figure suggests that the test pipe was subjected to bending becase of the symmetry of the strain distributions of both the surfaces.

Figure 4.6 shows the output of the strain gage mounted on the lower surface of the test pipe near the restraint location. The following are observed from the figure. ① Strain becomes larger in proportion to the overhang length. ② Strain varies stepwise. ③ Steady strain is larger than that caused at the first impact of the test pipe on the restraints and it is a maximum strain. The fact ① is due to the reason that the moment arm becomes large in proportion to the overhang length. The facts ② and ③ can be explained as follows. The strain-time curves have plateaux at the strains of 1500×10^{-6} for RUN No. 5506, 3000×10^{-6} for RUN No. 5507 and 5500×10^{-6} for RUN No. 5508. This is due to the reason that the movement of the test pipe caused just after pipe break was prevented by the restraints. However, a large blowdown thrust force continued to act on the test pipe even after the first impact of the test pipe on the restraints. Thus, the test pipe bend

at the restraint location and was deformed to a static equilibrium position. Therefore, the strain of the test pipe attained to a maximun at the steady state, when the movement of the test pipe settled down.

Figure 4.7 shows the outputs of the strain gages mounted on the surfaces of the test pipe near the restraint location and the mid location between the restraints and the pipe support. An oscillation with the frequency of about 160 Hz is observed in both XU112 and XU123 for RUN No. 5506 and XU123 for RUN No. 5507. This indicates that an oscillation of a beam type was induced in the test pipe when the overhang length was relatively short.

Figure 4.8 shows the accelerations of the test pipe. In the test of RUN No. 5506, the acceleration has an oscillation with the frequency of 160 Hz which is corresponding to that appearing in the strain gages mounted on the test pipe. In the test of RUN No. 5507, the great variation of the acceleration is observed at the time of 0.04 sec, when the strain of the test pipe near the restraint location also begins to increase as shown in Fig. 4.8. Generally speaking, the accerelations of the test pipe change greatly when a force acts on it. Therefore, the qualitative behavior of the test pipe can be deduced from the accerelations of the test pipe. It is inferred from Fig..4.8(d) that the following five events were caused in the test pipe in the test of RUN No. 5604.

① Event (0): A large blowdown force began to act on the test pipe by the break of a rupture disk. Afterwards the test pipe crashed into the restraints.

② Event (1): Recrash occurred between the test pipe and the R2 restraint which had been separate after the first crash. This can be confirmed by Fig. 4.11 which shows the decrease of the reaction force of the R1 restraint and the increase of that of the R2 restraint after the time of Event (1).

③ Event (2): The test pipe rotated on the plastic hinge and hit against the pipe itself. This can be confirmed by the time when the pressure transducer PU111 mounted near the collision point was damaged. The tear of the R1 restraint can be also inferred from Fig. 4.11 which shows the complete unloading of the reaction force of the R1 restraint at the time of Event (2).

④ Event (3): The tear of the R2 restraint can be inferred from Fig. 4.11 which shows the complete unloading of the reaction force of

the R2 restraint.

⑤ Event (4): The test pipe crashed into the test bed.

4.4 Deformation of Restraints

4.4.1 Residual deformations of restraints

Photograph 4.2 shows the deformations of restraints after tests. Little deformarion can be observed for RUN No. 5506, 5507 and 5508. On the other hand, both the restraints were torn just above the fixed bolts for RUN No. 5604. The tear of the restraints was initiated at the bottom of the screw of the restraints. Considering that the minimum diameter of the screw is 24 mm and that the tensile strength of the restraint material is 512 MPa, each bolt of the restraints can sustain a tensile load of about 230 KN. As shown in Fig. 4.11, the tensile load acting on each bolt of the restraints is at most 50 KN. Therefore, the restraint has a wide margin for tensile load. It is inferred from the aforementioned discussion that the tear of the restraints was initiated by the excessive tensile stress acting on the notch root of the screw of the bolt which was induced by a bending load. This can be confirmed by the views of the fixed volts shown in Photo. 4.2 (b) which indicates that large bending strain was caused near the tear location of the bolt.

The following are observed from Table 3.5 and Fig. 3.4 as regards the relation between the residual deformation of restraints and the overhang length. ① Residual deformation of the restraint is larger as the overhang length becomes shorter. ② The difference of the residual deformations of two restaints is small for the case of short overhang length such as RUN No. 5506, while the residual deformation of the R1 restraint is larger than that of the R2 restraint for the case of large overhang length such as RUN No. 5506 and 5507. The fact ① is due to the reason that the kinematic energy of the test pipe absobed by the restraints decreases with increase of the overhang length since the velocity of the test pipe at the impact of the test pipe on the restraints decreases with increase of the overhang length. On the other hand, the fact ② can be explained as follows. The R2 restraint does not work effectively in order to prevent the movement of the test pipe because the test pipe bent at the restraint location and is detached from the R2 restraint after the first impact of the test pipe on the restraints.

It can be seen from Fig. 3.4 that the residual strain in the straight section of the restraint is much smaller than that in the circular section. This indicates that the circular section is mainly deformed and the strain in the straight section is almost within the elastic range.

4.4.2 Dynamic behaviors

Figure 4.9 shows the typical outputs of the strain gages mounted on the restraints. A pair of strain gages such as XU135 and XU136 shown in the figure denotes the strain gages mounted on the outer and inner sides in the straight secion of the restraint, the locations of which are at the same height from the restraint support. On the other hand, the strain gages XU142 was mounted at the top of the R1 restraint. As shown in Fig. 4.9 (a), the vibrations with the frequencies of 300 Hz through 350 Hz are observed in the outputs of the strain gages mounted on the straight sections of the restraints. It is inferred that the vibrations were induced by the lateral movements of the restraints because there is a difference of 180 degrees in the phase of the vibration between the outputs of the pairs of strain gages mounted on the outer and inner sides of the restraints. The frequencies of the vibrations are approximately corresponding to that of the 2nd mode obtained by the ADINA code which is shown in Fig. 4.10. As shown in the figure, the 2nd mode vibration has the lowest frequency in the varations with the symmetrical mode shapes. It is concluded from the above discussion that the strain vibration observed in the straight section of the restraint is the lowest natural vibration of the symmetical mode induced by the first impact of the test pipe on the restraints.

As shown in Fig. 4.9 (a), the vibration with a frequency of 160 Hz is observed in the output of the strain gage XU142 mounted on the circular section of the R1 restraint for RUN No. 5506. This frequency is the same as that of the vibration of the test pipe appearing in the strain gages and accelerometer mounted on the test pipe. This means that the circular section of the restraint stuck to the test pipe and moved together with it.

It is found from Figs. 4.9 (a) and (b) that for RUN No. 5506 both the R1 and R2 restraints were subjected to a tensile strain in the

circular section because of the positive value of the average strain, whereas for other cases the R1 restraint was subjected to a tensile strain but the average strain of the R2 restraint was nearly equal to zero. This indicates that the R2 restraint does not work effectively to limit the pipe movement when the overhang length is large.

4.5 Reaction Forces of Restraints

The reaction forces of the restraints were measured using the load transducers WU131 to WU134 for the R1 restraint and WU141 to WU144 for the R2 restraint, respectively. The total reaction forces F_{R1} and F_{R2} of the R1 and R2 restraints can be calculated as follows:

$$F_{R1} = (WU131 + WU132 + WU133 + WU134)/2$$

$$F_{R2} = (WU141 + WU142 + WU143 + WU144)/2$$

Figure 4.11 shows the results of WU131 and WU141. In the first place, we will discuss the results of RUN No. 5506, 5507 and 5508. For RUN No. 5506, whose overhang length is the shortest, the values of WU131 and WU141 are alwavs positive. On the other hand, for RUN No. 5507 and 5508, the value of WU131 is always positive but that of WU141 becomes equal to zero at the times of 0.1 sec for RUN No. 5507 and 0.02 sec for RUN No. 5508, respectively. Especially, the value of WU141 for RUN No. 5508 has only the first peak. It is concluded from the above discussion that both of the two restraints was effective to limit the pipe movement for the case of relatively short overhang length such as RUN No. 5506, whereas for the cases of relatively long overhang length such as RUN No. 5507 and 5508, only the R1 restraint is effetive to limit the pipe movement after an early stage in the impact of the test pipe on the restraints. Although the maximum reaction forces of the R1 and R2 restraints are observed at the first peak for RUN No. 5506, the maximum reaction forces of the R1 restraint are observed after the first peak for RUN No. 5507 and 5508. This is due to the reason that for these cases the reaction force of the R1 restraint increased according as that of the R2 restraint decreased.

Next, we will discuss the results of RUN No. 5604 in which the overhang length was 650 mm and the rupture disk opened completely. The reaction forces of the restraints for RUN No. 5604 have the same tendency as those for RUN No. 5507 and 5508 in a short time range.

As for a long time range, the reaction force of the R1 restraint WU131 starts to increase and that of R2 restraint WU141 begins to decrease after the time of 0.1 sec. This means that the test pipe collided again with the R2 restraint, which kept apart from the test pipe after the first impact of the test pipe on the restraints. Then WU131 and WU141 have constant values after the times of 0.22 sec and 0.25 sec, respectivley, which are corresponding to the times when the tear of the restraints occurred. The reaction forces of the restraints do not return to zero after the tear of restraints, since large residual strain owing to the bend of the restraints along the pipe axis was caused at the locations of the restraint where the strain gages were mounted to measure the reaction forces of the restraint. The conversion from the strain to the load for WU131, WU141 and so on is based on the assumption that the strains of the strain gages used in the load transducers are within the elastic range. Therefore, the reaction forces of the restraint may be inaccurate, when the restraints slided along the pipe axis and they were subjected not only to a tensile force but also to a bending moment.

Figures 4.12 (a) and (b) show the relation between the reaction forces of the restraints and the overhang length. The results of RUN No. 5604 are not depicted in the figures because of the reason mentioned in the preceding paragraph. Figure 4.12 (a) indicates that the reaction forces of the restraints at the first impact decrease with increase of the overhang length. It is also observed from Figs. 4.12 (a) and (b) that, even in the case of relatively large overhang length such as RUN No. 5507 and 5508, the R2 restraint sustained fairly large reaction force regarding the first impact, although it sustained no force at the steady state.

Figure 4.13 shows the time history of the blowdown thrust force obtained from the tatal reaction force of the restraints as follows:

$$T = F_R \frac{L - OH}{L}$$

in which

T = Blowdown thrust force

F_R = Total reaction force of restraints

L = Length of test pipe

OH = Overhang length

In the figure, the result is also depicted for RUN No. 5509 which was performed to obtain the blowdown thrust force by the load transducer

attached at the elbow adjacent to the break location. The restuls of RUN No. 5506 and 5507 are in comparatively good agreement with that of RUN No. 5509. On the other hand, a large blowdown thrust force is obtained for RUN No. 5508, although the rupture disk did not open completely. Table 4.2 shows the thrust coefficients defined as follows:

$$\eta_{max} = \frac{T_{max}}{P_{max}A} \quad , \qquad \eta_{ss} = \frac{T_{ss}}{P_{ss}A}$$

in which

T_{max} = Maximum blowdown thrust force
T_{ss} = Steady state blowdown thrust force
P_{max} = Pressure in the pressure vessel at the time when the blowdown thrust force reaches maximum
P_{ss} = Pressure in the pressure vessel at the steady state
A = Break area of the test pipe

The value of $f_D L/D$, in which f_D, L and D denote Darcy's friction coefficient, length of the piping and pipe diameter respectively, is equal to about 1.1 for the present system. Thus, according to the chart obtained by Moody[3] the discharge coefficient is equal to about 1.0 at the steady state. Compared with the Moody's result, RUN No. 5506 and 5507 give reasonable discharge coefficient, whereas RUN No. 5508 gives much larger value than the Moody's one owing to the oriffice effect of the remainder of the rupture disk.

Table 4.3 shows the dynamic load factor DLF defined as follows:

$$DLF = \frac{F_{R,max}}{T_{ss}}$$

in which

$F_{R,max}$ = Total reaction force of restraints at the first impact
T_{ss} = Steady state blowdown thrust force

It is observed from the table that the dynamic load factor decreases with increase of the overhang length.

Table 4.1 Comparison between Blowdown Thrust Force and Calculated Loads F_y and F_u

RUN No.	OH (mm)	F_y (kN)	F_u (kN)	T (kN)
5506	250	74.36	178.2	77.7
5507	400	46.48	111.4	68.4
5508	650	28.60	68.52	58.6
5604	650→900	20.66	49.49	—

Table 4.2 Thrust Coefficient Obtained from Experimental Data

RUN No.	A (cm^2)	T_{max} (N)	T_{ss} (N)	P_{max} (MPa)	P_{ss} (MPa)	η_{max}	η_{ss}
5506	47.52	8.16×10^4	6.14×10^4	13.20	11.12	1.31	1.17
5507	46.75	7.84×10^4	6.54×10^4	13.36	10.92	1.27	1.29
5508	23.28	7.17×10^4	5.28×10^4	13.56	10.76	2.27	2.13

The valves of T_{max} and P_{max} correspond to those at the time of 0.1sec.
The valves of T_{ss} and P_{ss} correspond to those at the time of 1.0sec.

Table 4.3 Dynamic Load Factor Obtained from Experimental Data

RUN No.	OH (mm)	$F_{R,max}$ (N)	T_{ss} (N)	DLF
5506	250	1.89×10^5	6.14×10^4	3.08
5507	400	1.10×10^5	6.54×10^4	1.68
5508	650	8.55×10^4	5.28×10^4	1.62

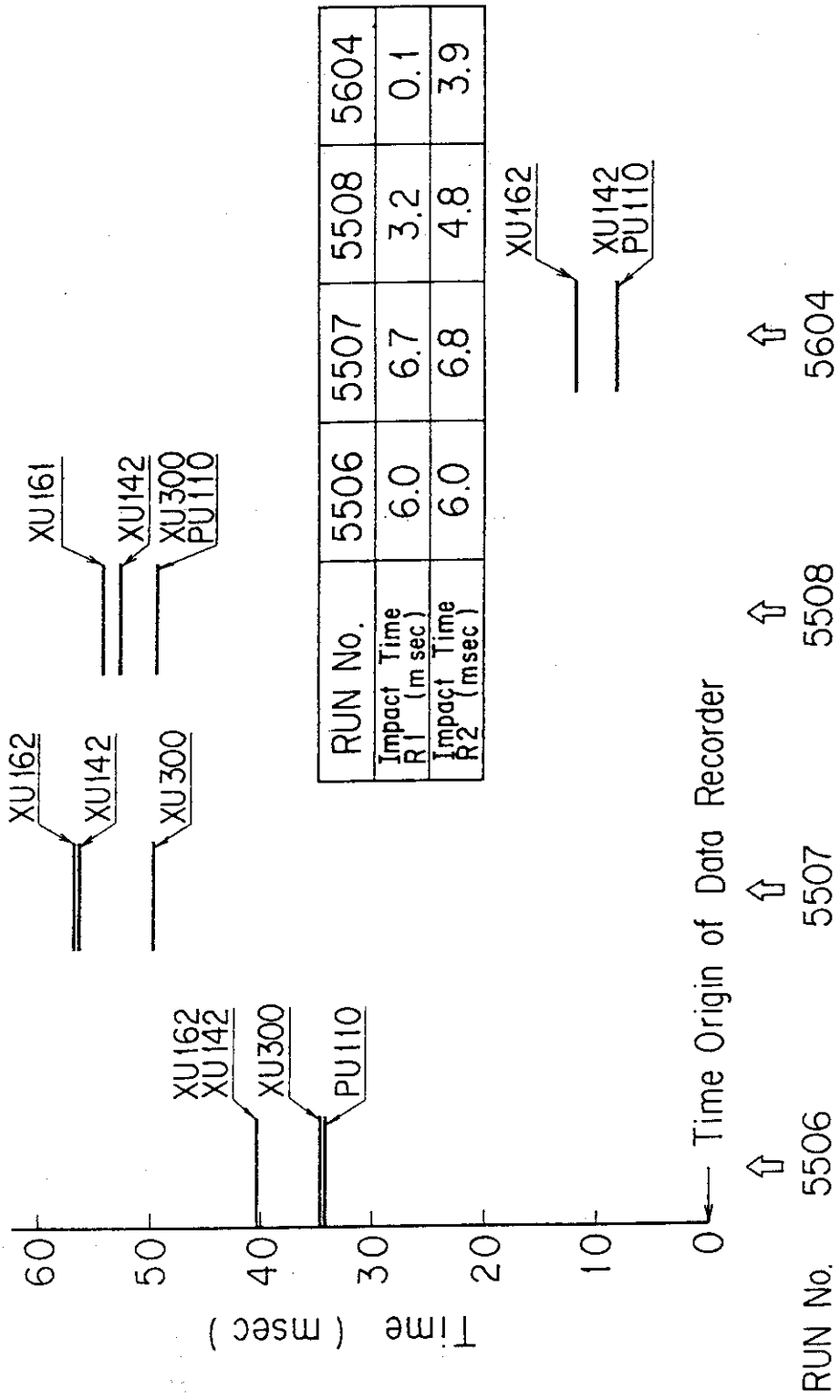

Fig. 4.1 Time Sequence of Major Events

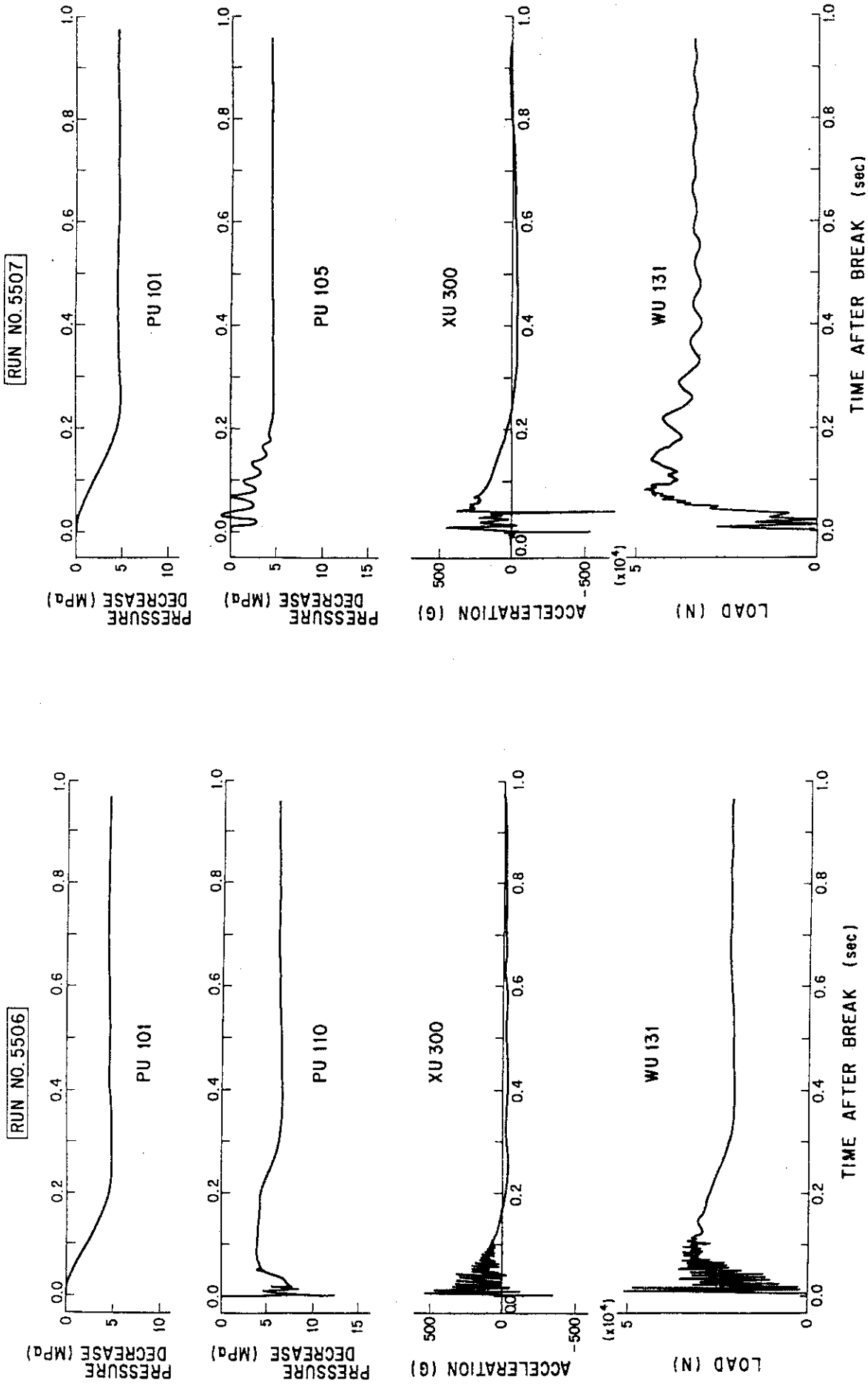

Fig. 4.2 Selected Data for Each Test

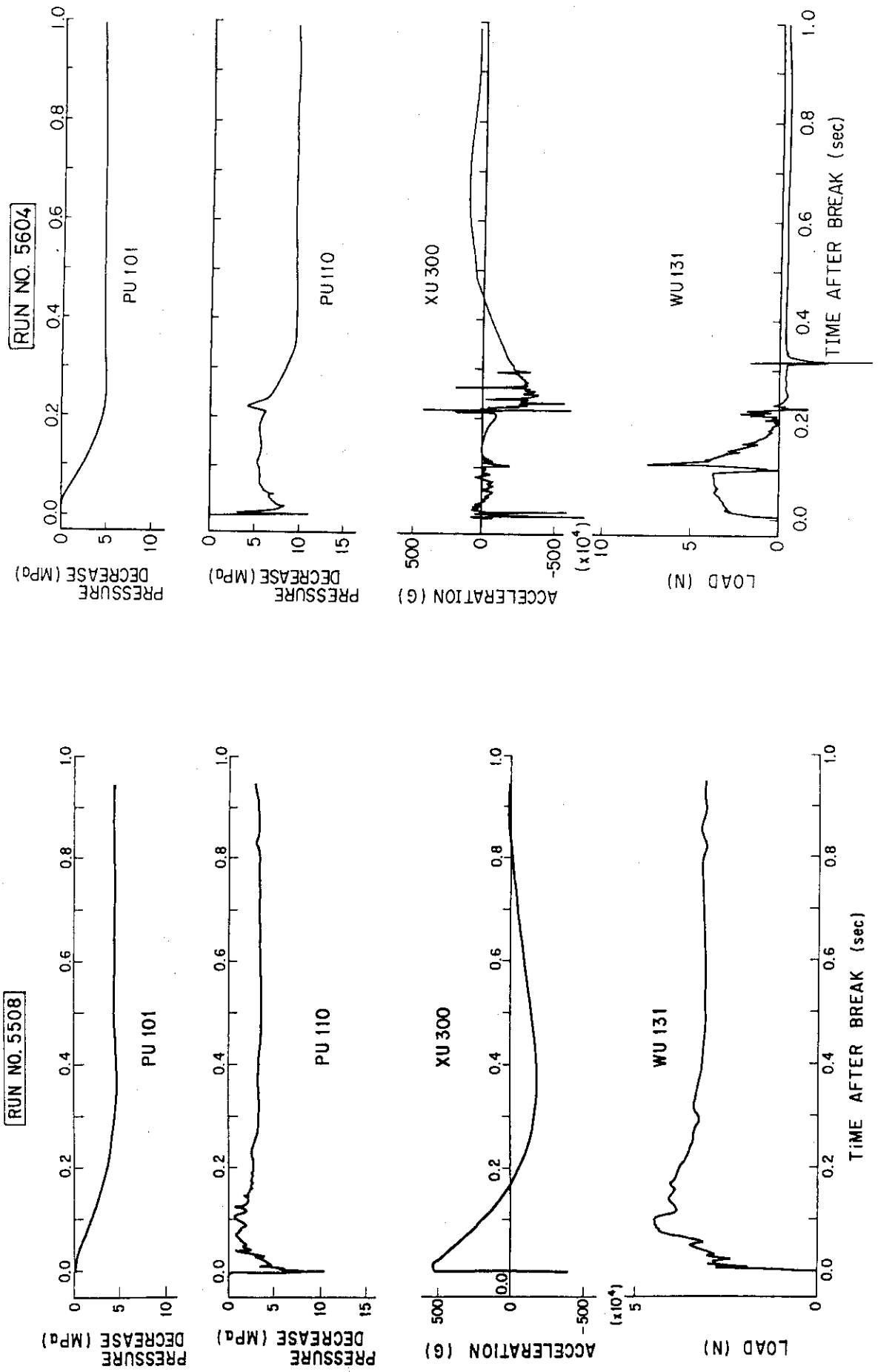

Fig. 4.2 (Continued)

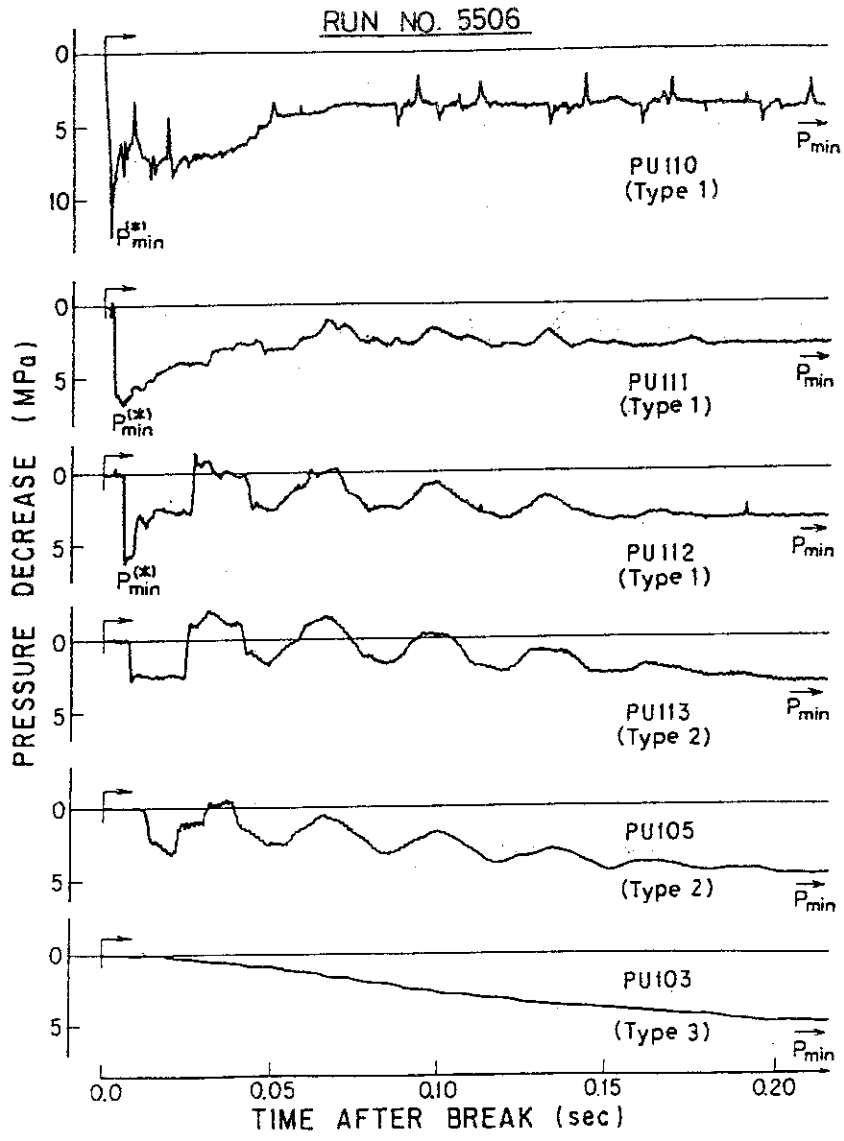

Fig. 4.3 Pressure vs. Time Curves in Subcooled Decompression Process

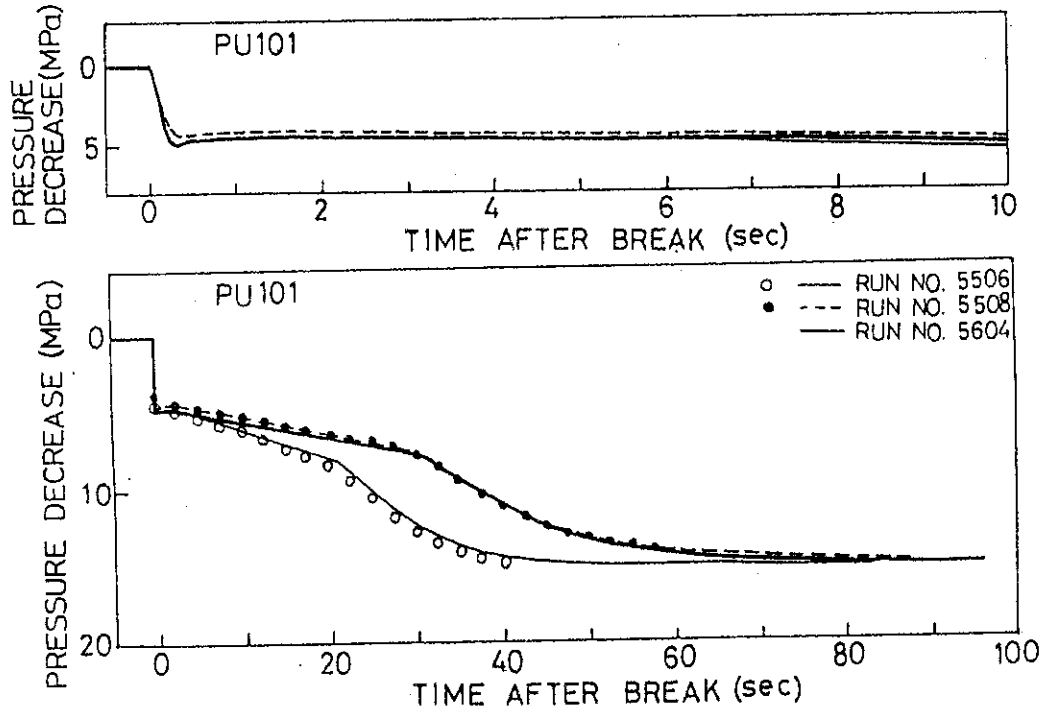

Fig. 4.4 Pressure Variation in Pressure Vessel

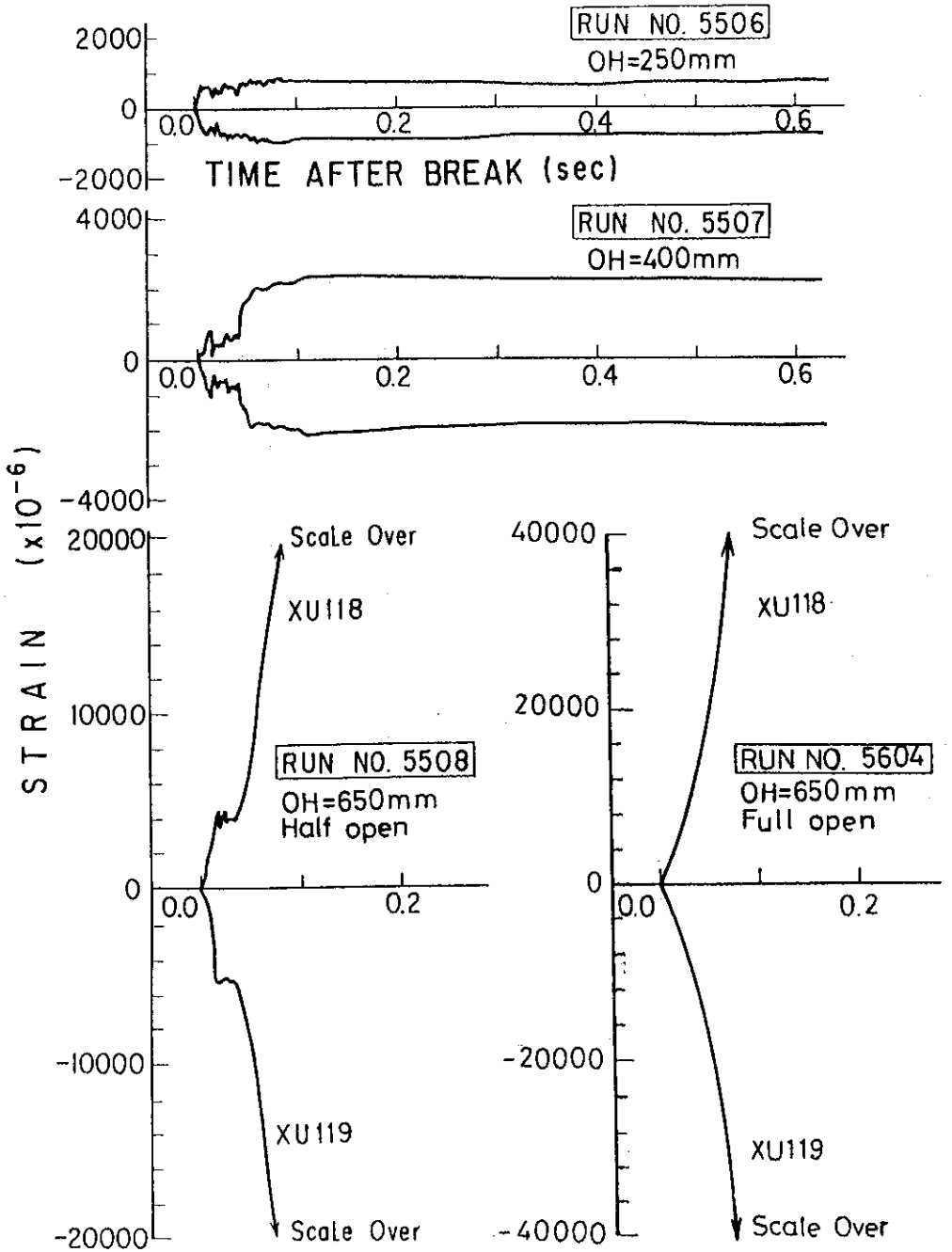

Fig. 4.5 Comparison between Dynamic Strains of Upper and Lower Surfaces of Test Pipe

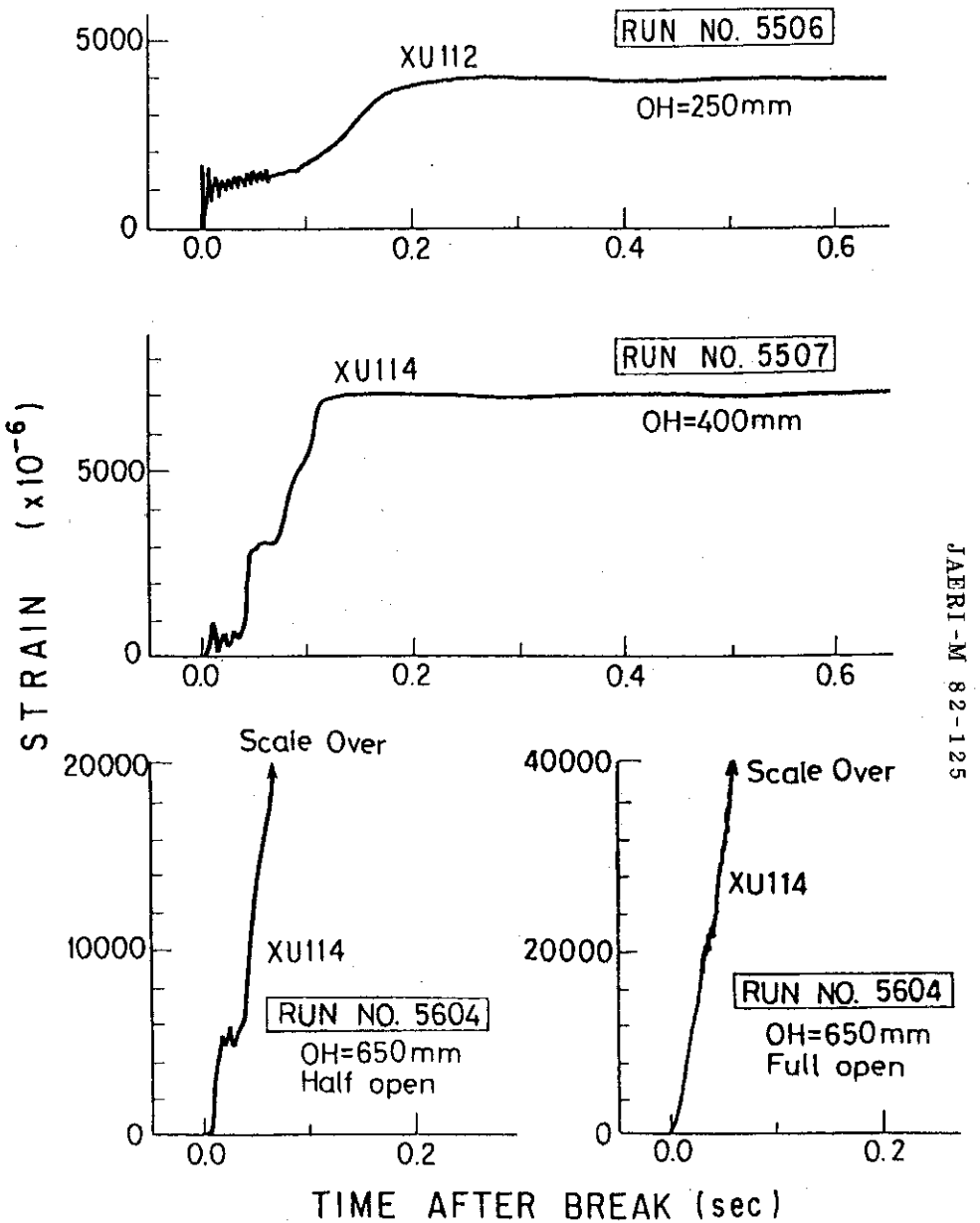

Fig. 4.6 Selected Dynamic Strains of Test Pipe at the neighborhood of Restraints

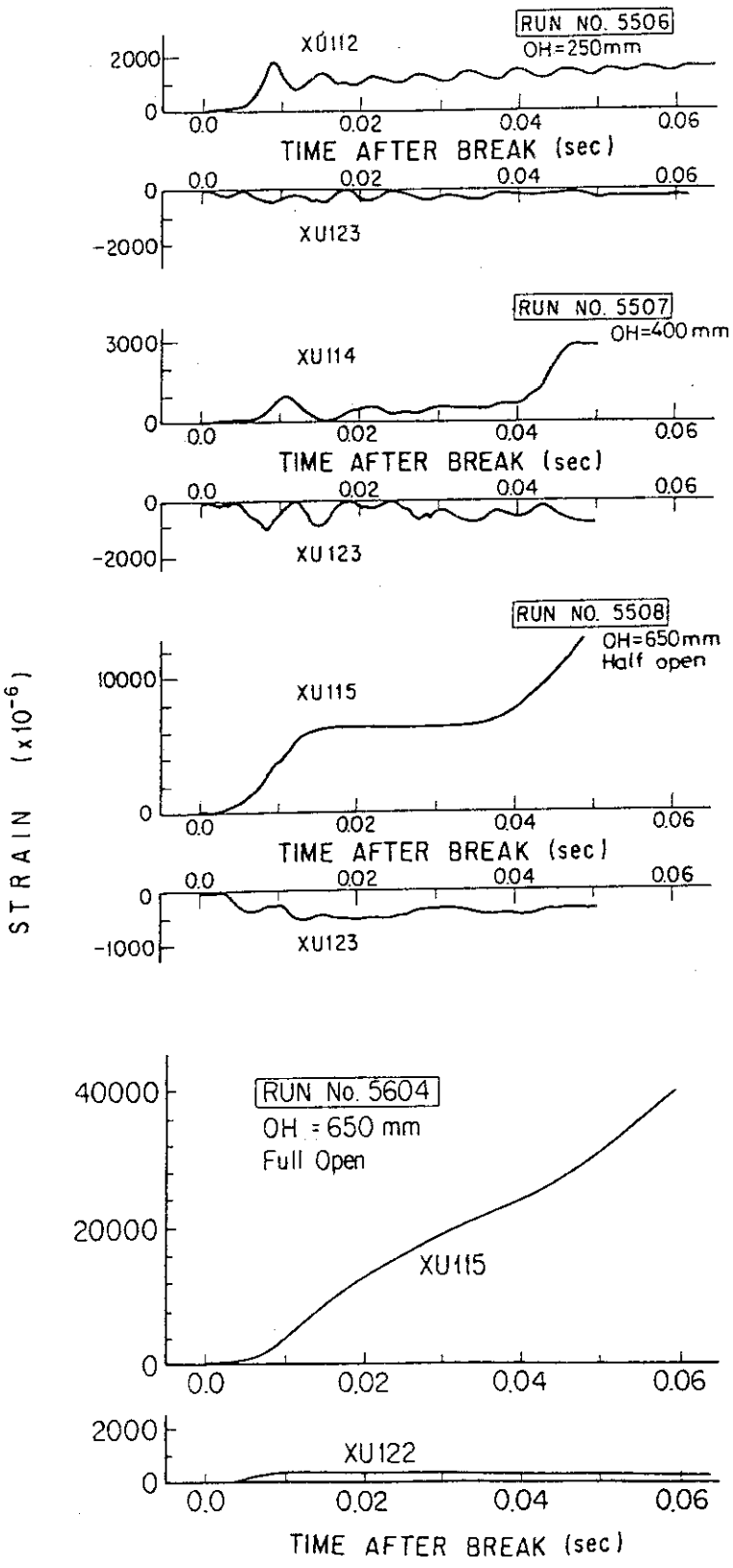

Fig. 4.7 Selected Dynamic Strains of Test Pipe

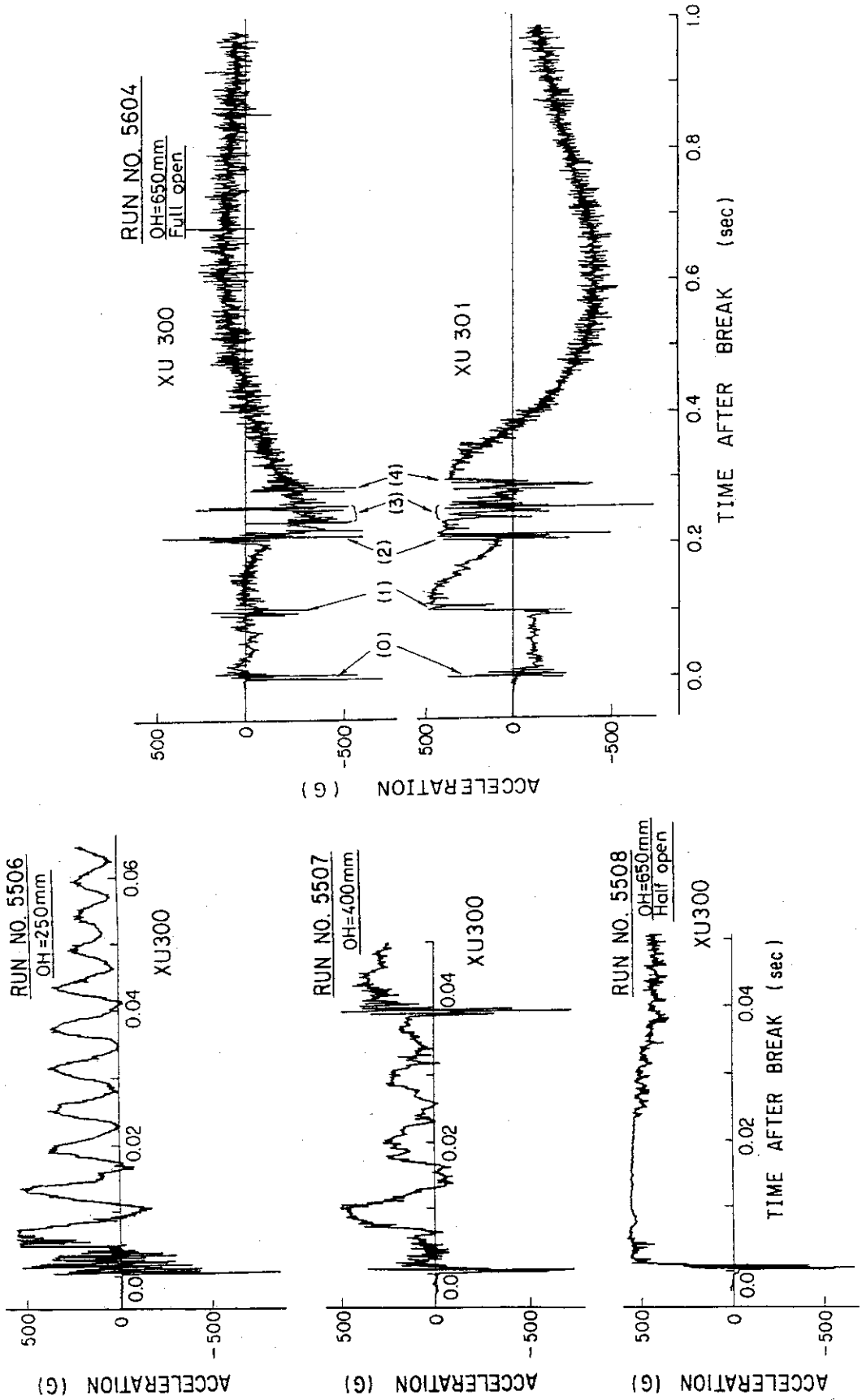

Fig. 4.8 Acceleration of Test Pipe

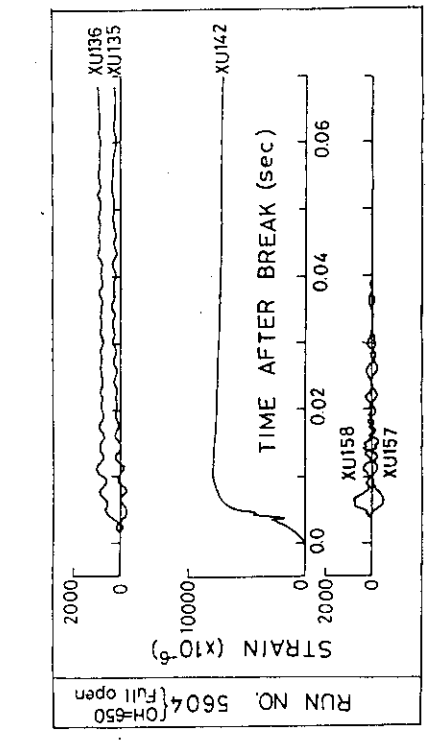

(a) 0 ~ 0.06 sec

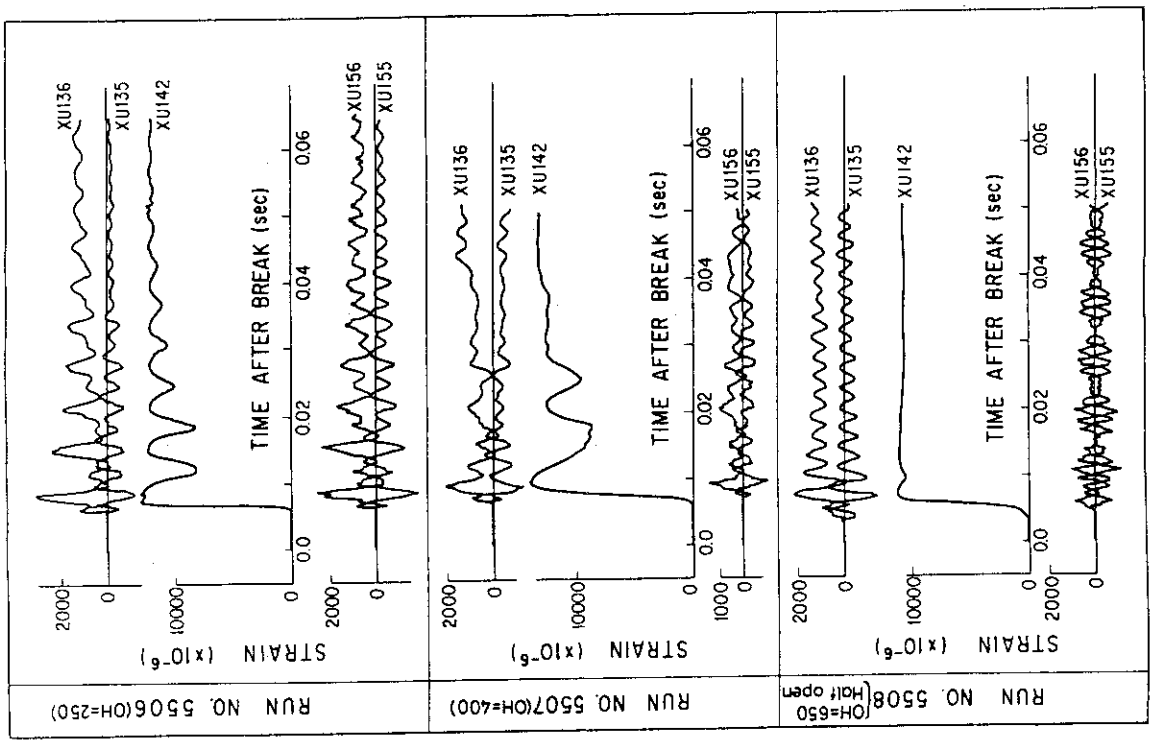

Fig. 4.9 Selected Dynamic Strains of Restraints

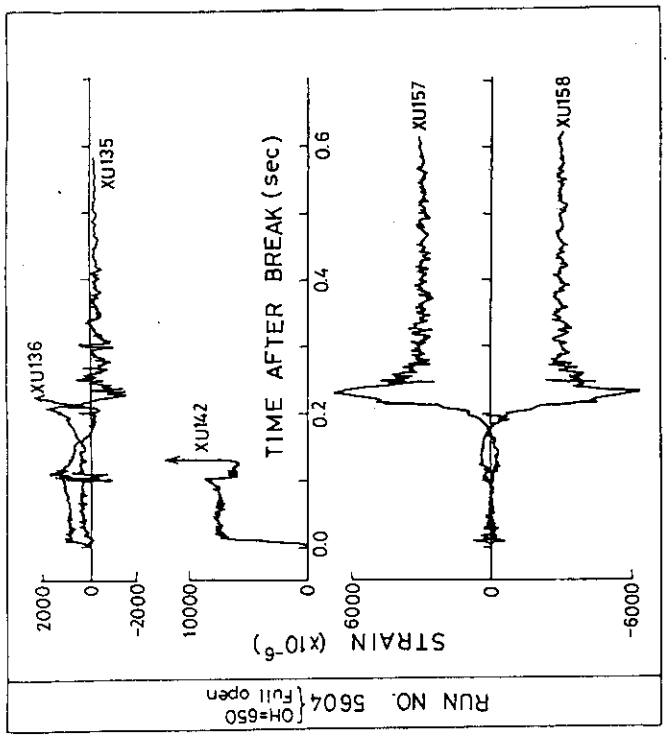

Fig.4.9 (Continued)

(b) 0 ∿ 0.6 sec

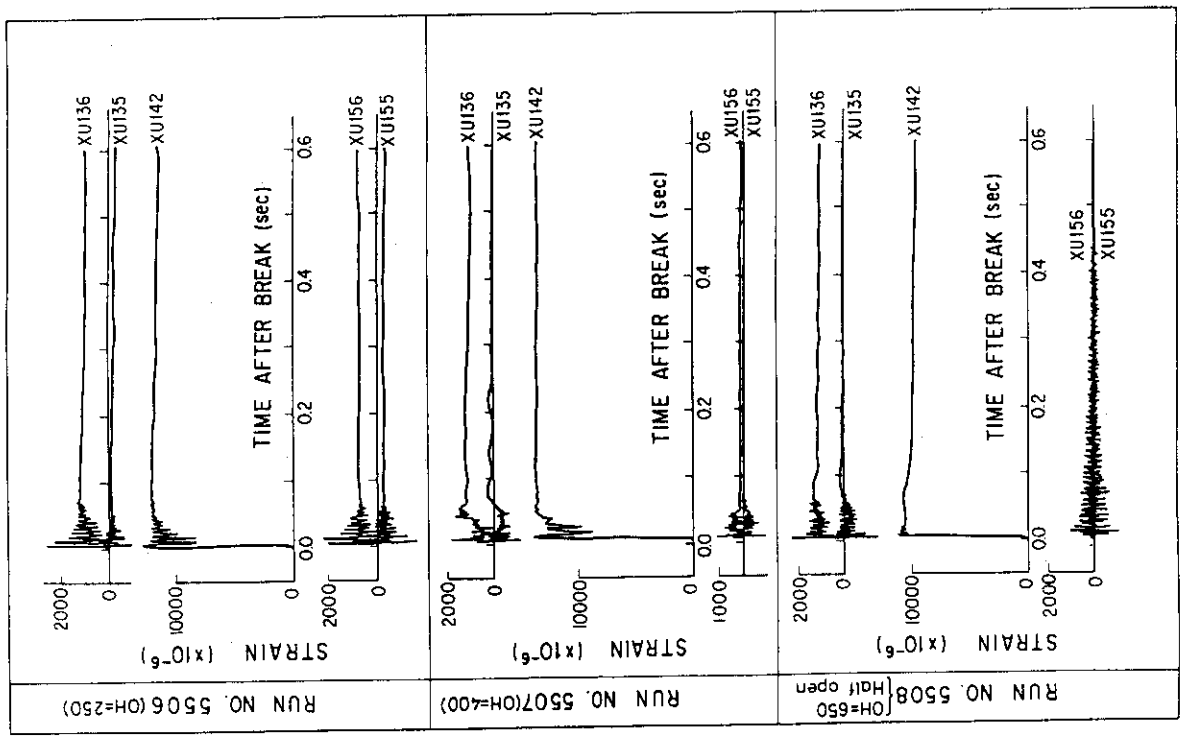

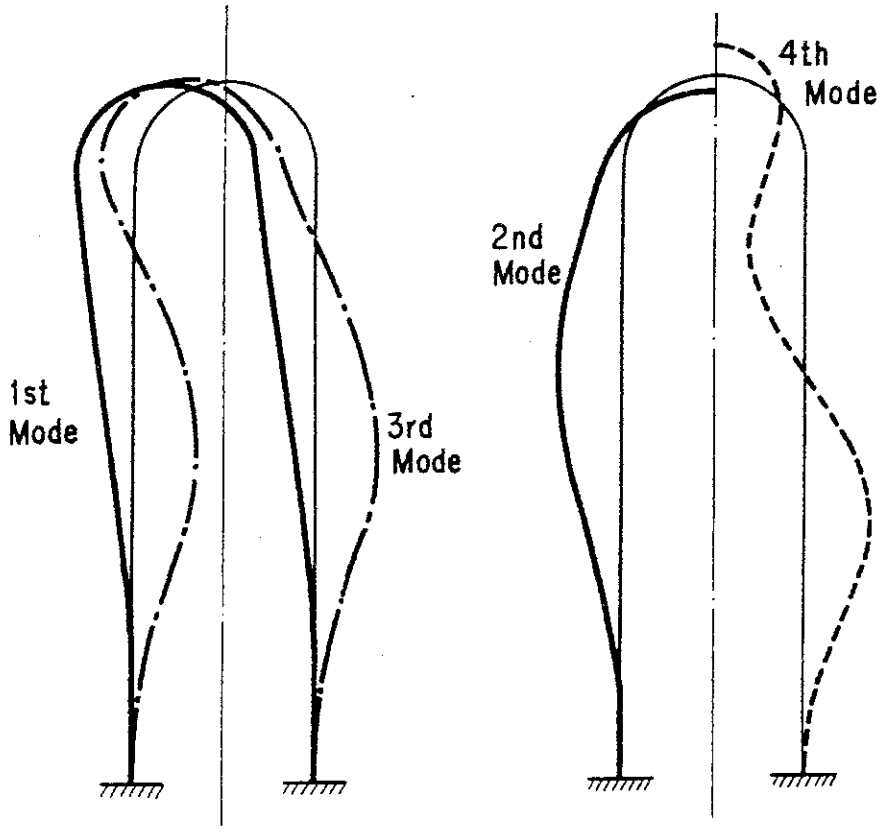

Frequency (Hz)			
1st Mode	2nd Mode	3rd Mode	4th Mode
78	289	415	750

Fig. 4.10 Natural Frequencies and Mode Shapes of Restraint Obtained by ADINA Code

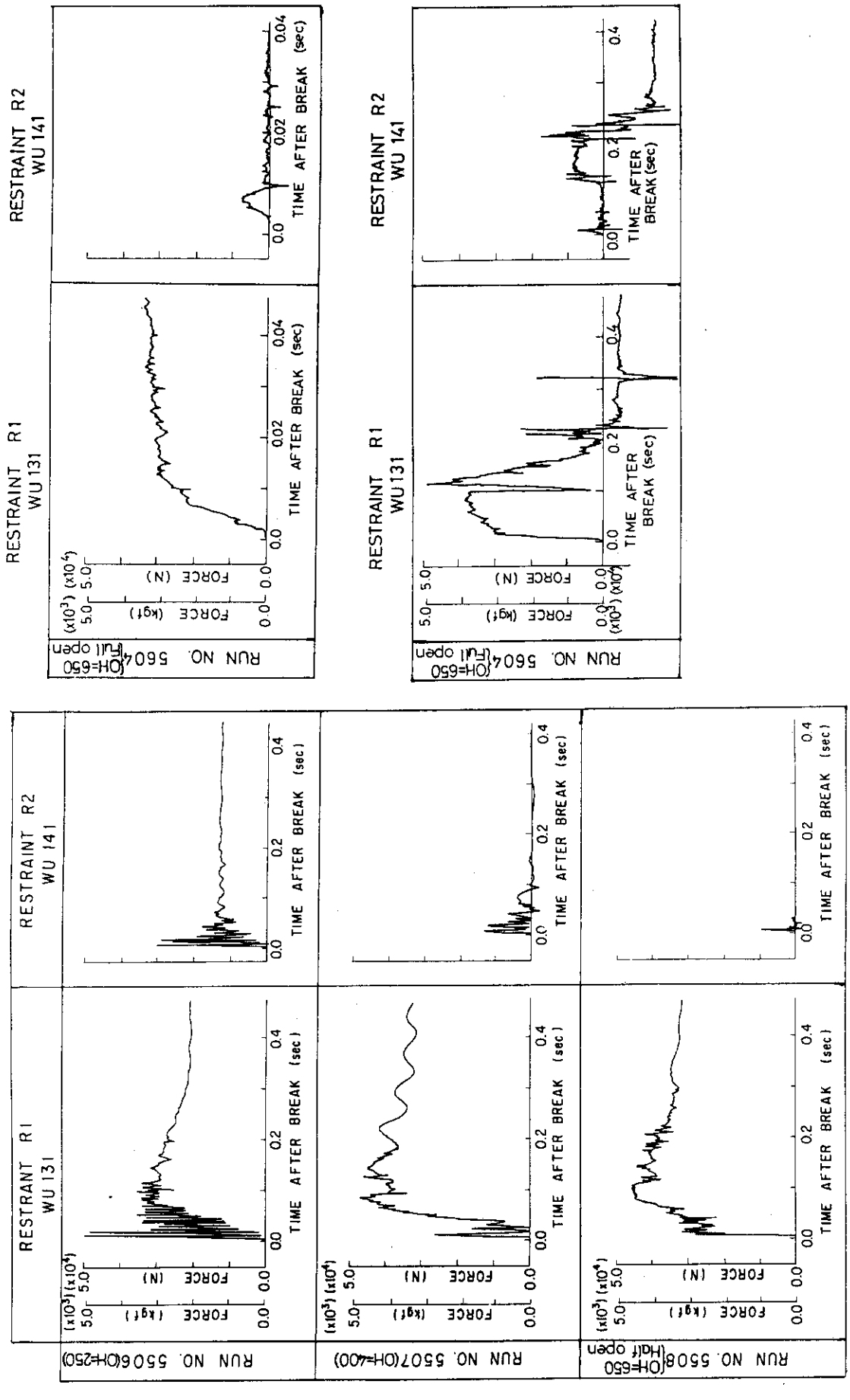

Fig. 4.11 Selected Restraint Reaction Forces

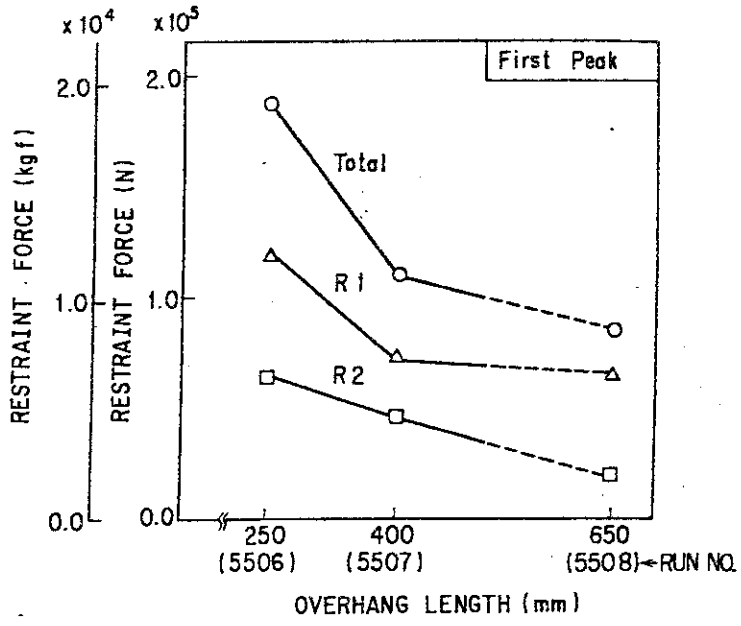

(a) First Peak

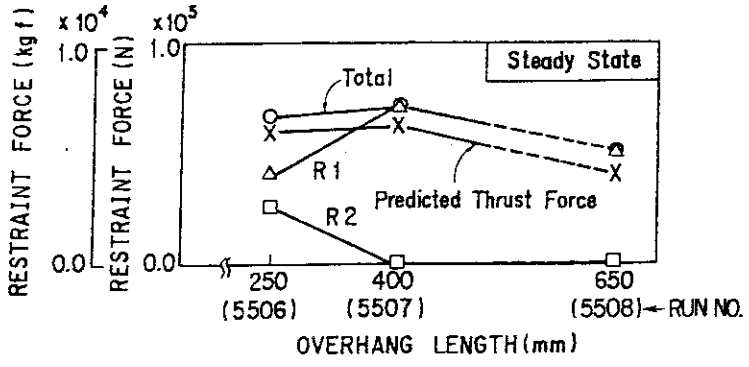

(b) Steady State

Fig. 4.12 Restraint Reaction Forces vs. Overhang Length

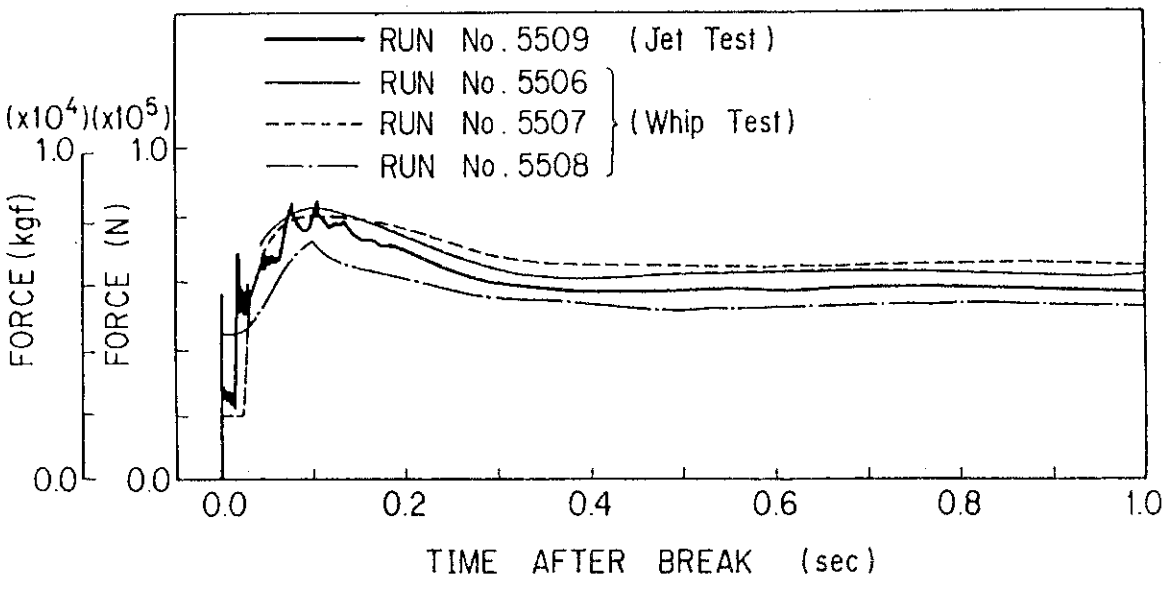

Fig. 4.13 Blowdown Thrust Force Obtained from Restraint Reaction Forces

(a) RUN No. 5506 (OH=250mm)

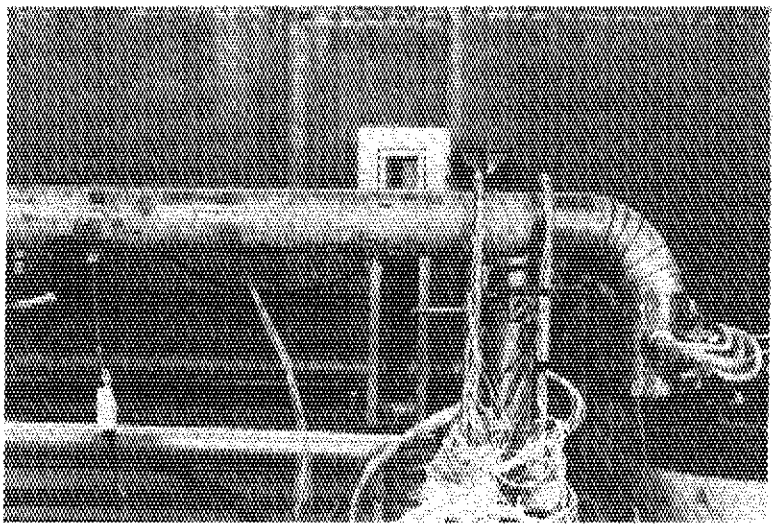

(b) RUN No. 5507 (OH=400mm)

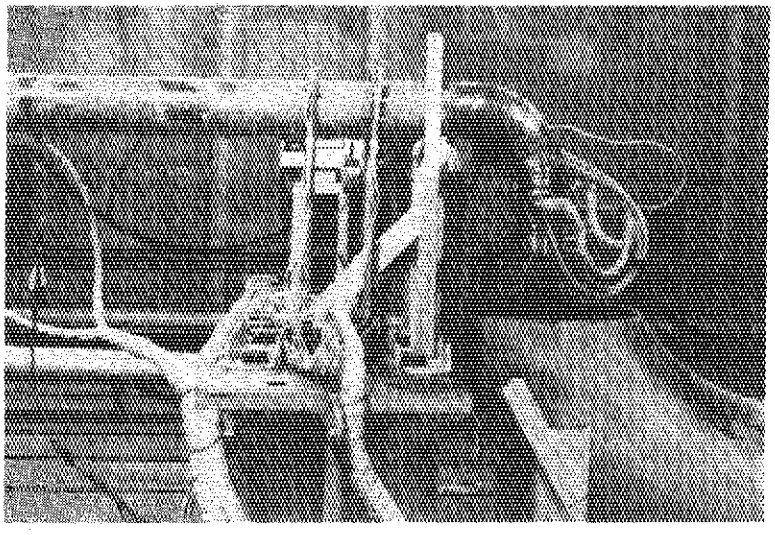

(c) RUN No. 5508 (OH=650mm, Half open)

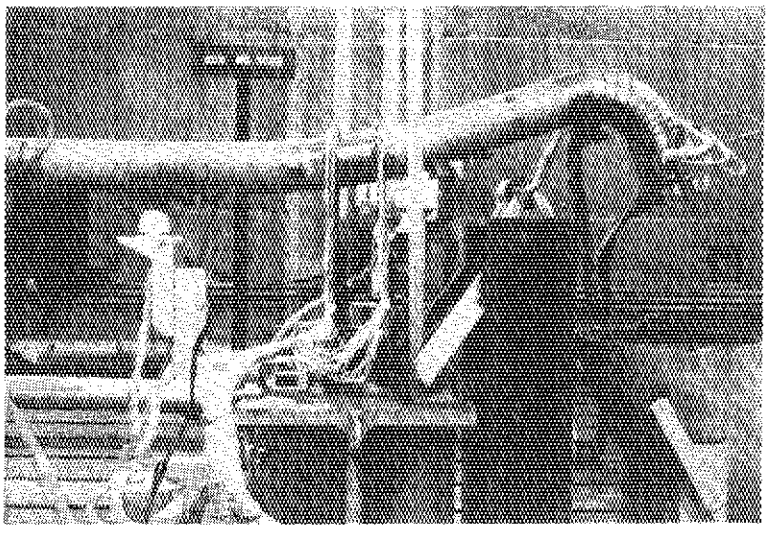

Photo. 4.1 View of Pipe Deformation after Test

(d) RUN No. 5604 (OH=650mm, Full open)

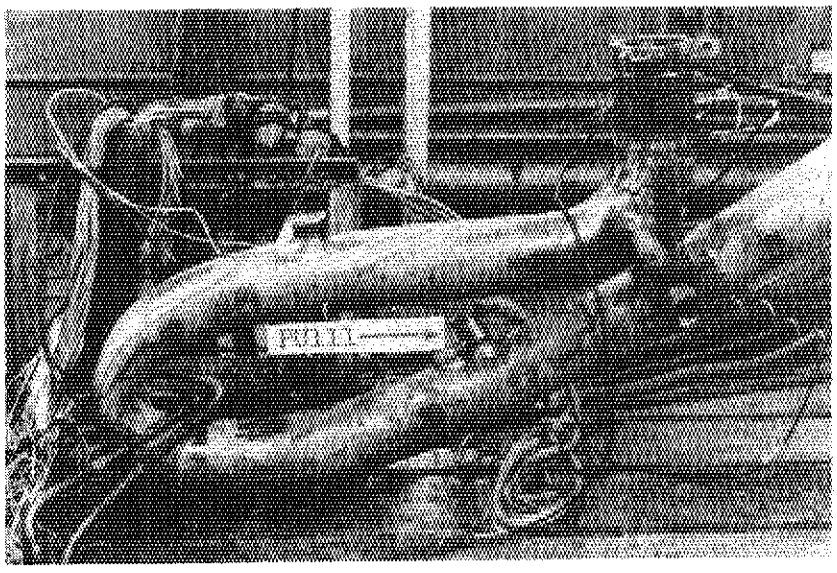

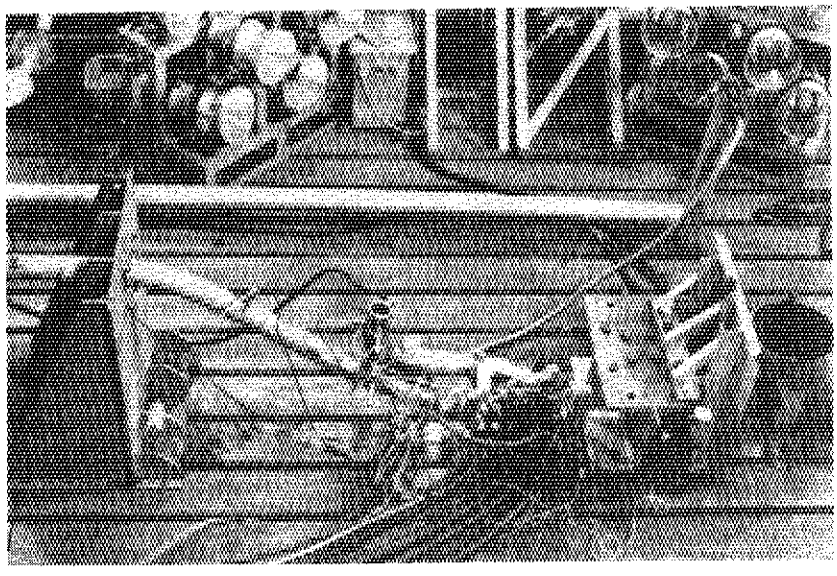

Photo. 4.1 (Continued)

(a) RUN No.5506, 5507 and 5508

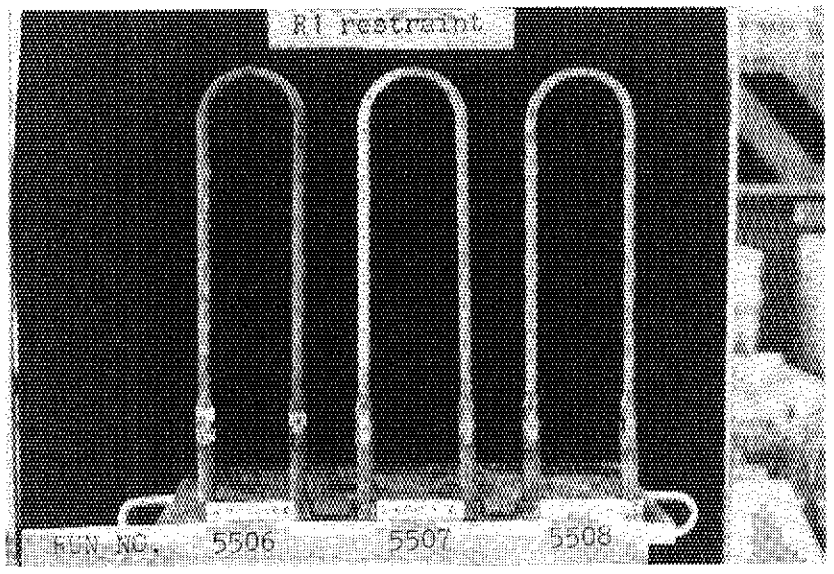

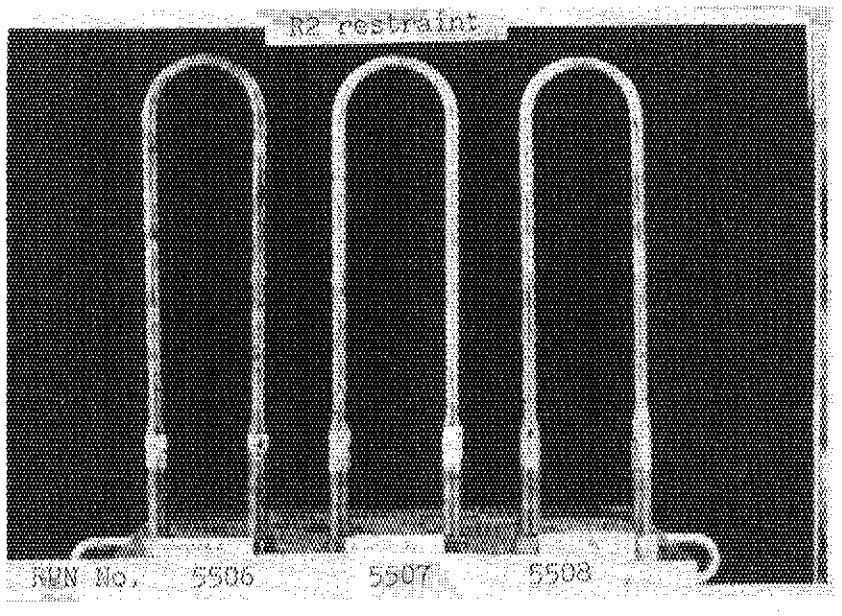

Photo. 4.2 View of Restraint Deformation after Test

(b) RUN No. 5604

R1 restraint

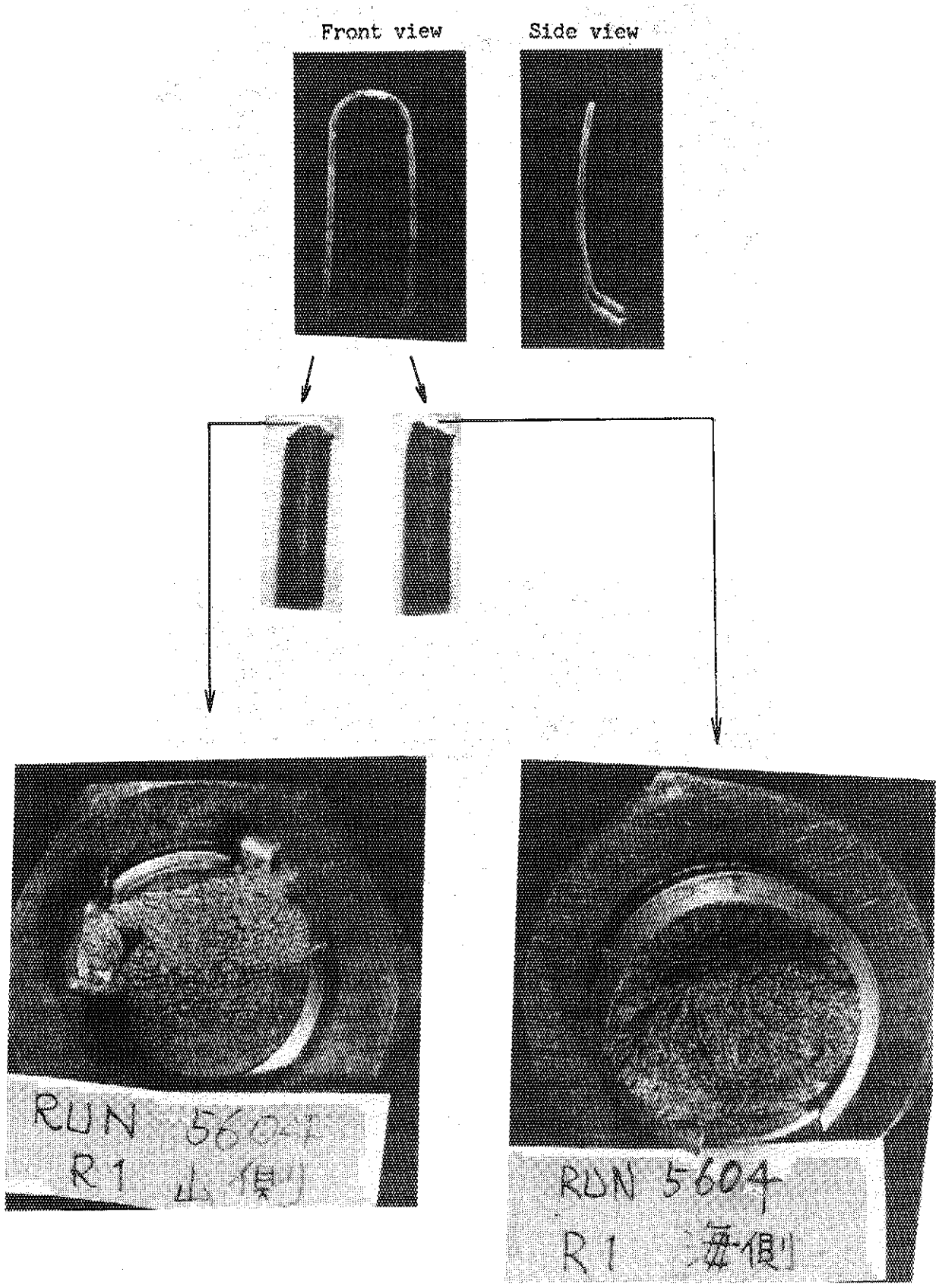

Photo. 4.2 (Continued)

(b) RUN No. 5604

R2 restraint

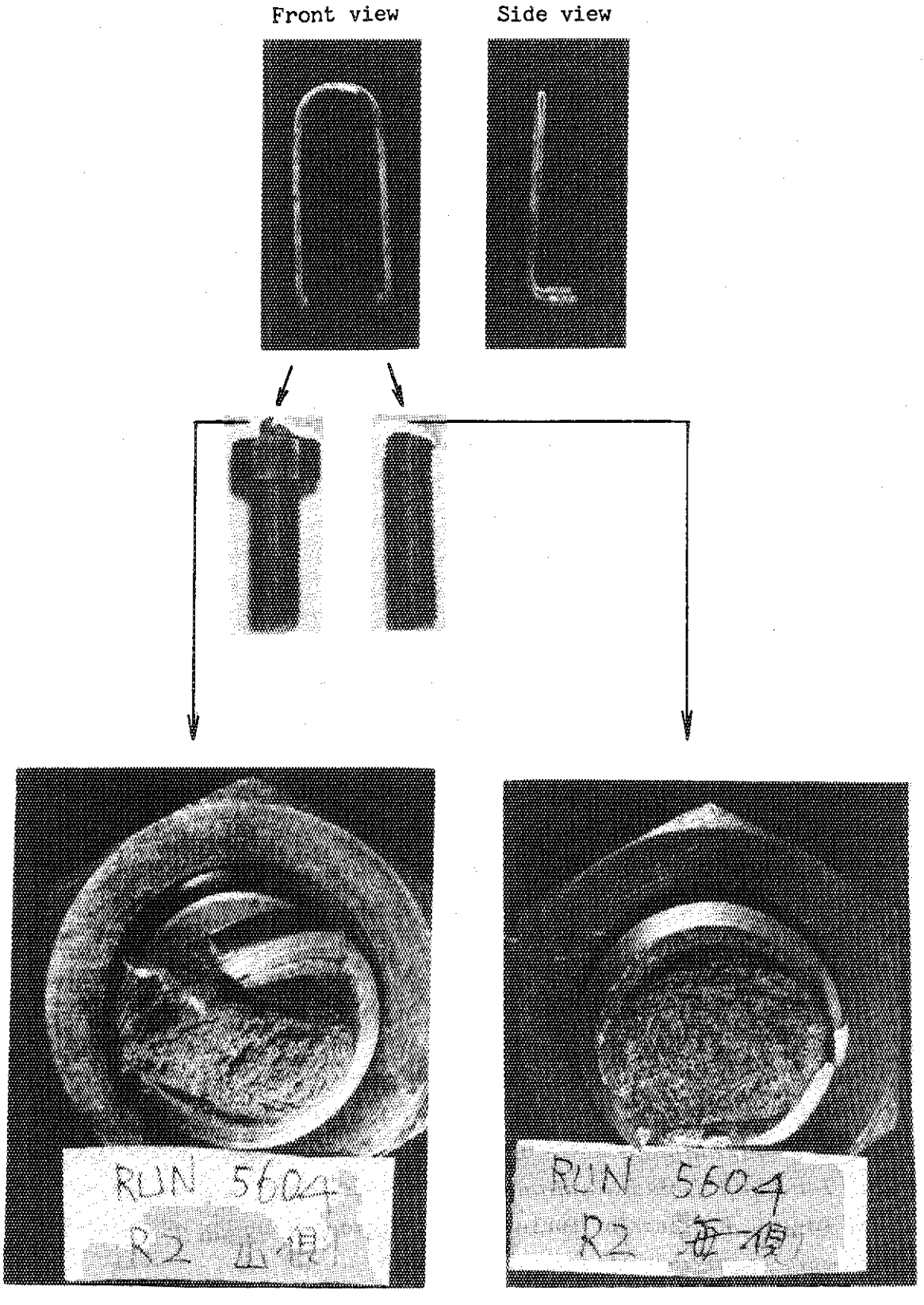

Photo. 4.2 (Continued)

5. CONCLUDING REMARKS

Four pipe whip tests were performed under the PWR LOCA conditions by varying the overhang length. The following conclusions are obtained from the tests.

(1) The whipping of the pipe can be prevented more effectively by the restraints as the overhang length becomes shorter.

(2) The load acting on the restraint support structure becomes larger as the overhang length becomes shorter.

(3) The restraint farther from the break location does not limit the pipe movement except for the first impact when the overhang length is larger. Thus, two restraints should be installed close to each other

(4) The ultimate moment M_u of the pipe at the restraint location can be used to predict the plastic collapse of the whipping pipe.

(5) The restraints slide along the pipe axis and are subjected to a bending moment, when the overhang length is larger. In this case, the restraints may be torn at the fixed bolt, because excessively high stress is caused at the bottom of the screw in the fixed bolt owing to a bending moment.

Based on the above conclusions, let us consider the practical case. In nuclear power plants, restraints are installed as close to the hypothetical break location, mamely, weld line, of the elbow as possible. Thus, the test of RUN No. 5506, in which the overhang length was 250 mm is closest to the practical case among the present pipe whip tests. In this case, both the restraints worked effectively to limit the pipe movement and little deformation could be found in the pipe.

ACKNOWLEDGEMENTS

The authors wish to make their acknowledgement to the members of the Committee on the Assessment of Safety Research for Nuclear Reactor Structural Components at JAERI (Chairman: Prof. Y. Ando, University of Tokyo) for their fruitful comments. Acknowledgement is also due to Dr. M. Nozawa, director of Nuclear Safety Research Center at JAERI for his support throughout this work.

5. CONCLUDING REMARKS

Four pipe whip tests were performed under the PWR LOCA conditions by varying the overhang length. The following conclusions are obtained from the tests.

(1) The whipping of the pipe can be prevented more effectively by the restraints as the overhang length becomes shorter.

(2) The load acting on the restraint support structure becomes larger as the overhang length becomes shorter.

(3) The restraint farther from the break location does not limit the pipe movement except for the first impact when the overhang length is larger. Thus, two restraints should be installed close to each other

(4) The ultimate moment M_u of the pipe at the restraint location can be used to predict the plastic collapse of the whipping pipe.

(5) The restraints slide along the pipe axis and are subjected to a bending moment, when the overhang length is larger. In this case, the restraints may be torn at the fixed bolt, because excessively high stress is caused at the bottom of the screw in the fixed bolt owing to a bending moment.

Based on the above conclusions, let us consider the practical case. In nuclear power plants, restraints are installed as close to the hypothetical break location, mamely, weld line, of the elbow as possible. Thus, the test of RUN No. 5506, in which the overhang length was 250 mm is closest to the practical case among the present pipe whip tests. In this case, both the restraints worked effectively to limit the pipe movement and little deformation could be found in the pipe.

ACKNOWLEDGEMENTS

The authors wish to make their acknowledgement to the members of the Committee on the Assessment of Safety Research for Nuclear Reactor Structural Components at JAERI (Chairman: Prof. Y. Ando, University of Tokyo) for their fruitful comments. Acknowledgement is also due to Dr. M. Nozawa, director of Nuclear Safety Research Center at JAERI for his support throughout this work.

REFERENCES

(1) Ueda, S., Isozaki, I., Miyazaki, N., Kurikara, R., Kato, R., Saito, K. and Miyazono, S., Pipe Rupture Test Results; 4 Inch Pipe Whip Tests under BWR Operational Condition ---- Clearance Parameter Experiments (RUN 5405, 5406, 5407), JAERI-M 9496 (1980)

(2) Kurihara, N., Ueda, S., Isozaki, T., Miyazaki, N., Kato, R., Saito, K. and Miyazono, S., Pipe Rupture Test Results; 4 Inch Pipe Whip Test under BWR LOCA Conditions --- Overhang length Parameter Tests (RUN 5407, 5501, 5504, 5503), JAERI-M 82-022 (1982)

(3) Moody, F.J., "Fluid Reaction and Impingement Loads", Nuclear Power Plants, (1973), pp.219-216.

APPENDIX A ELECTRICAL MEASUREMENTS

(a) Pressures in the pressure vessel (A.1-A.16)

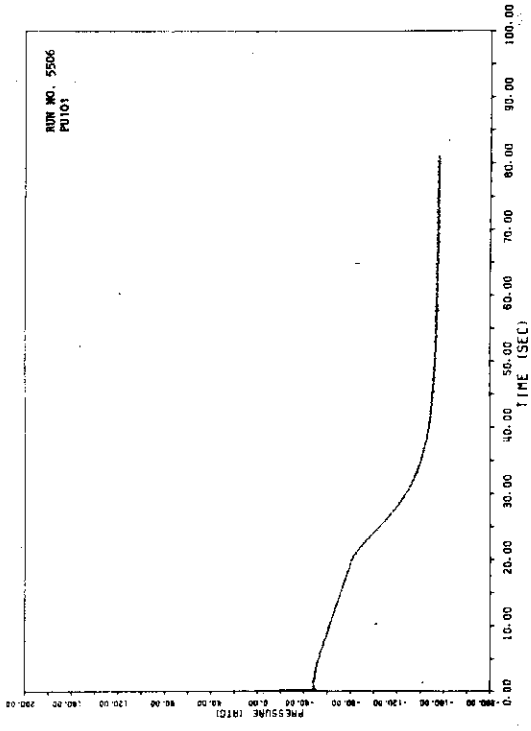

A.2

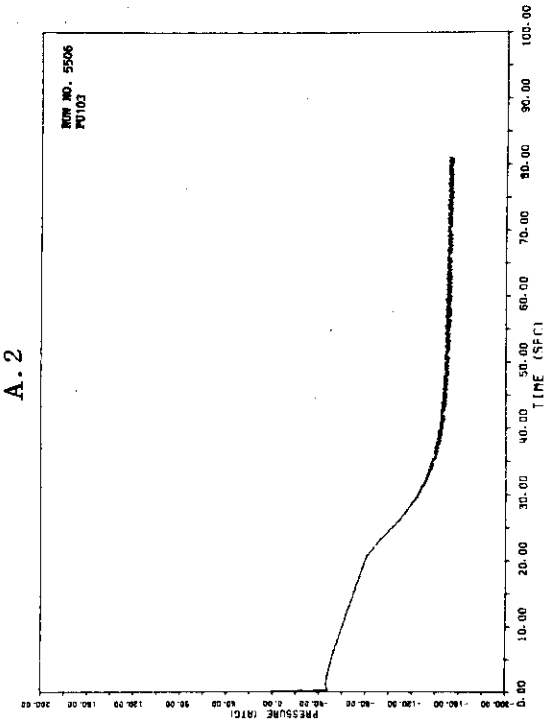

A.4

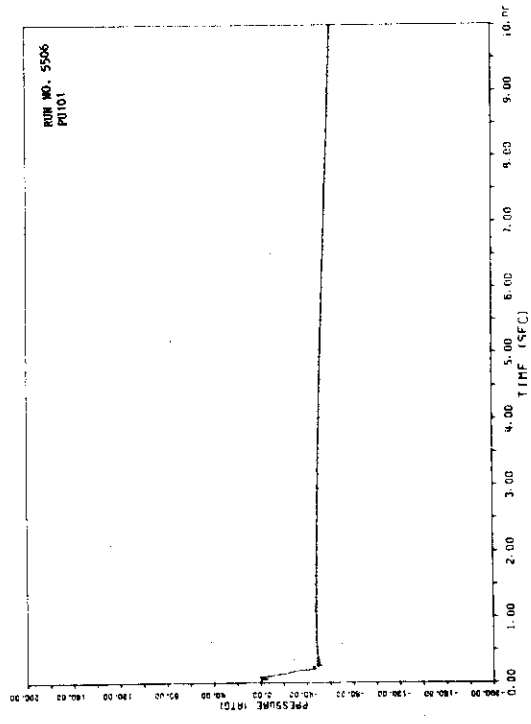

A.1

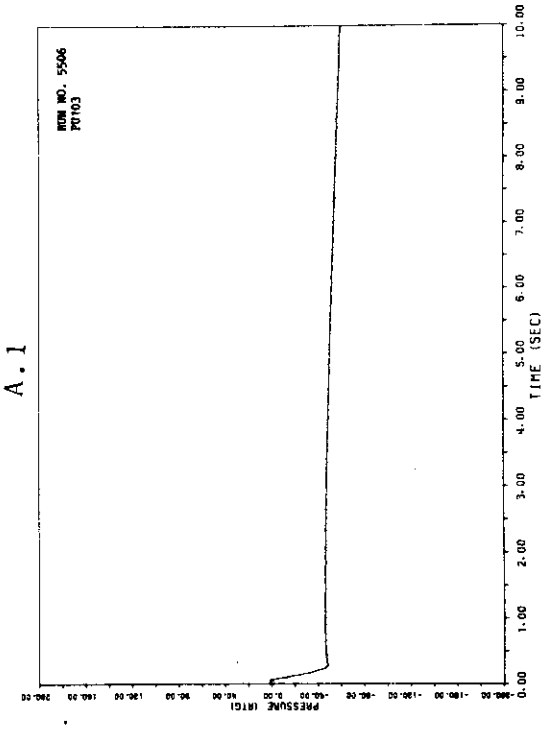

A.3

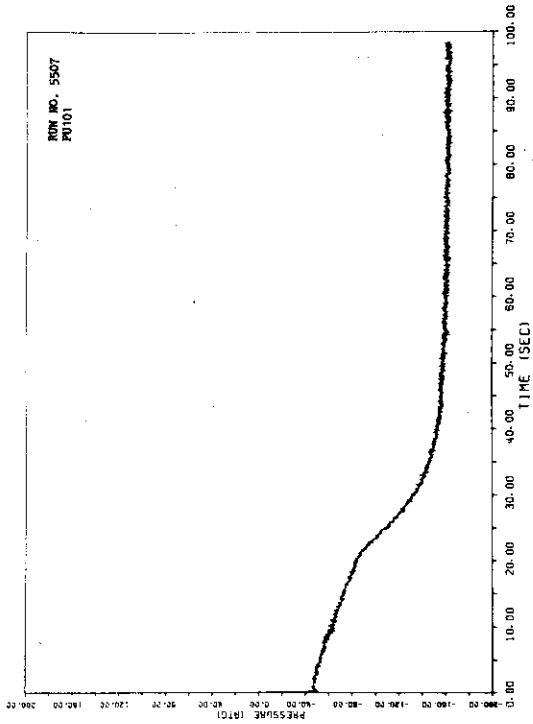
RUN NO. 5507
PU101
PRESSURE (ATG)
TIME (SEC)

A.6

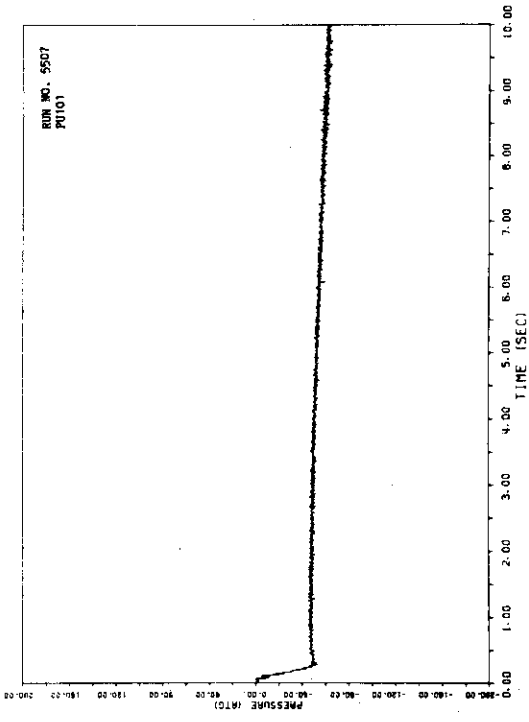
RUN NO. 5507
PU101
PRESSURE (ATG)
TIME (SEC)

A.5

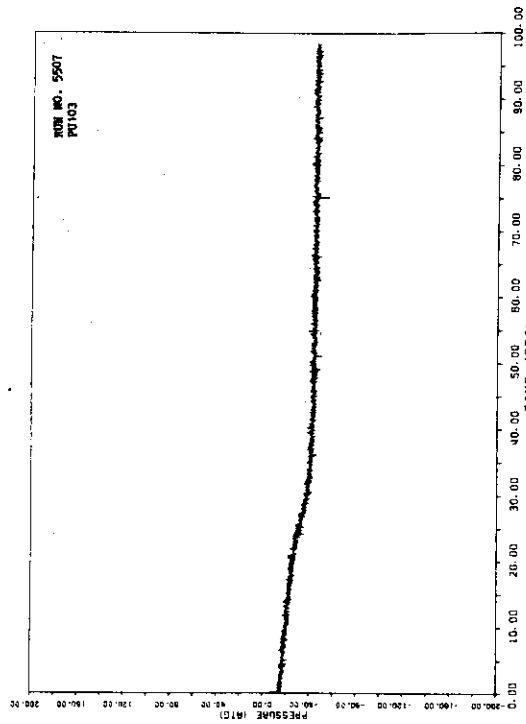
RUN NO. 5507
PU103
PRESSURE (ATG)
TIME (SEC)

A.8

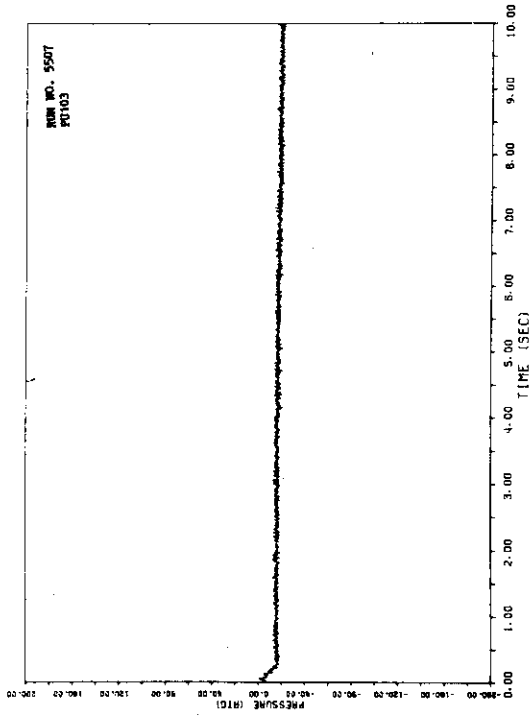
RUN NO. 5507
PU103
PRESSURE (ATG)
TIME (SEC)

A.7

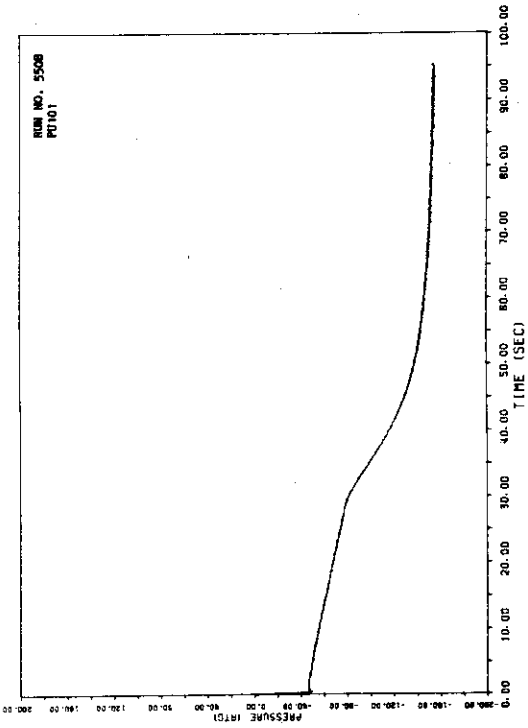

A.10

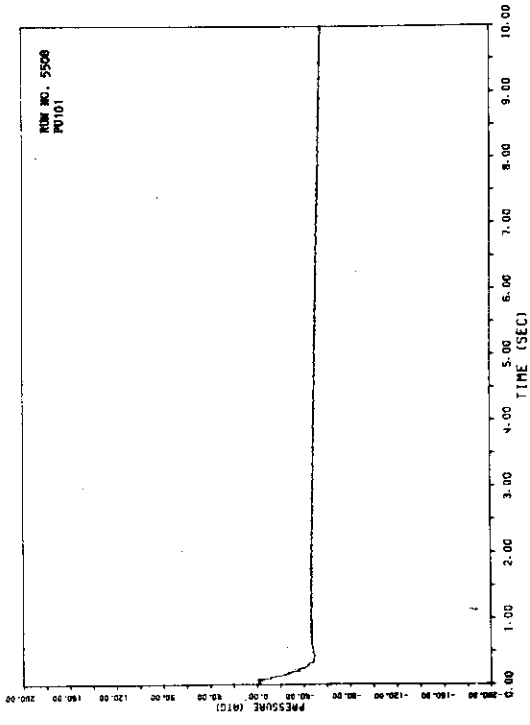

A.9

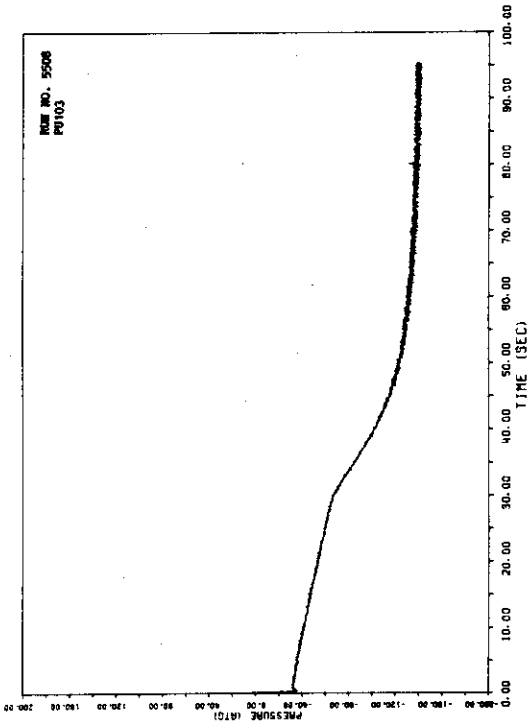

A.12

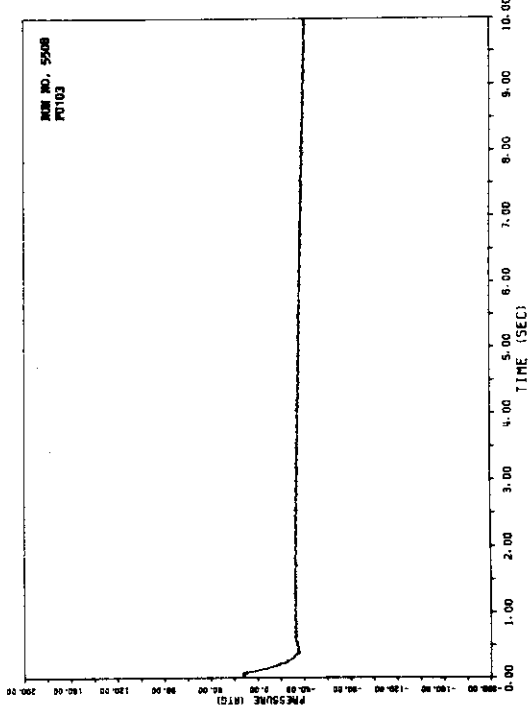

A.11

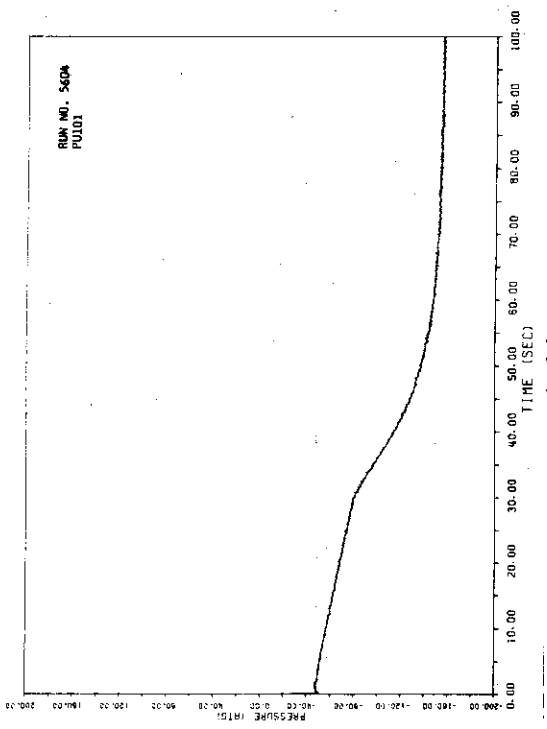

A.14

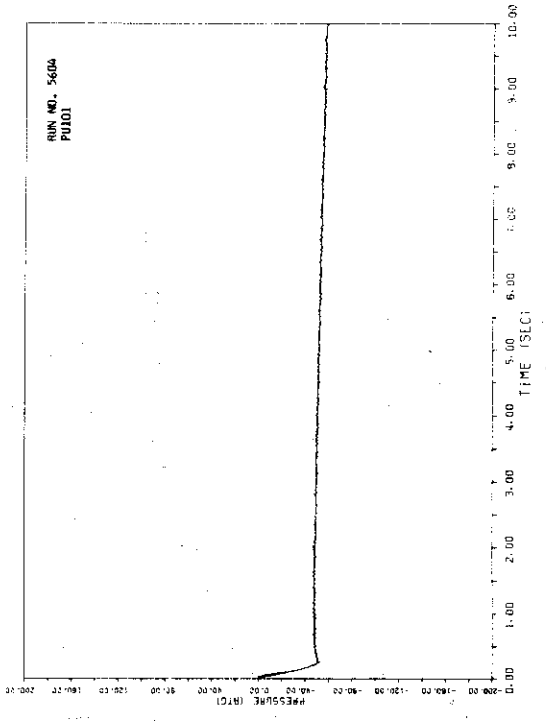

A.13

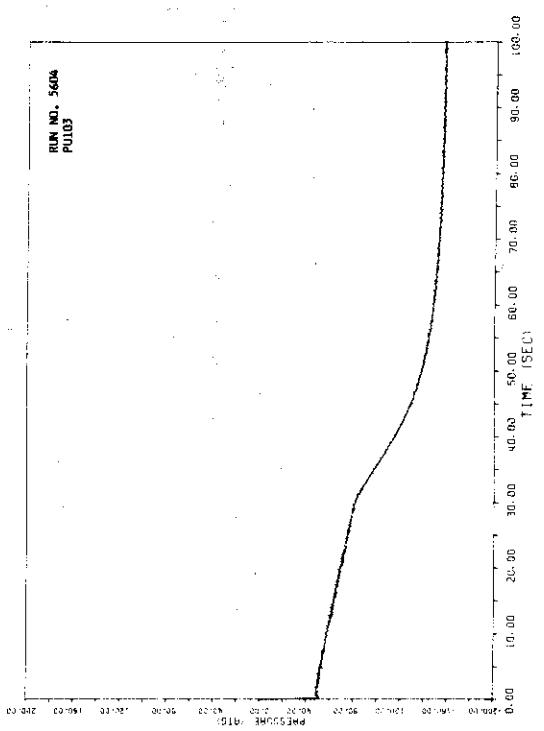

A.16

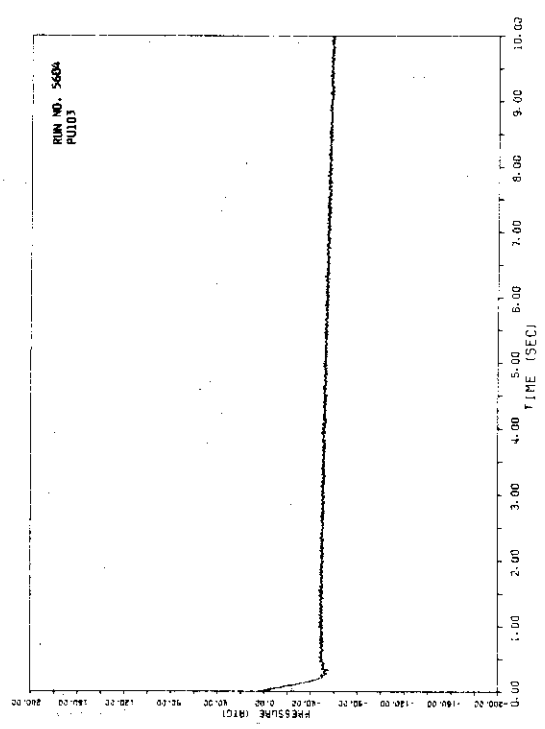

A.15

(b) Pressures in the piping (A.17-A.87)

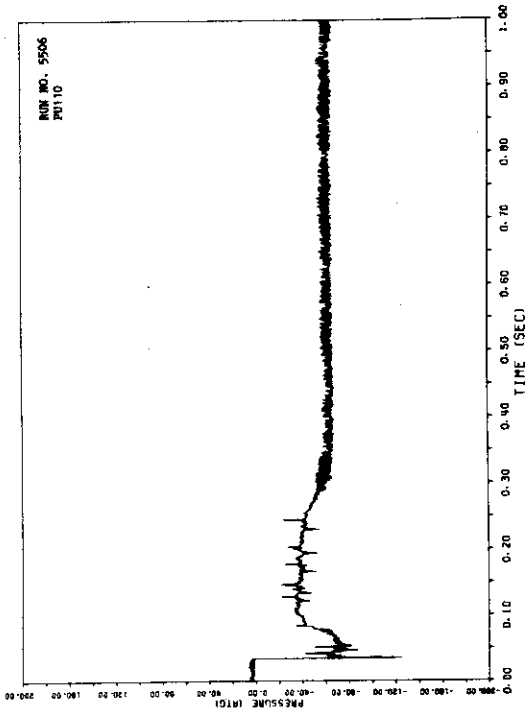

A.18

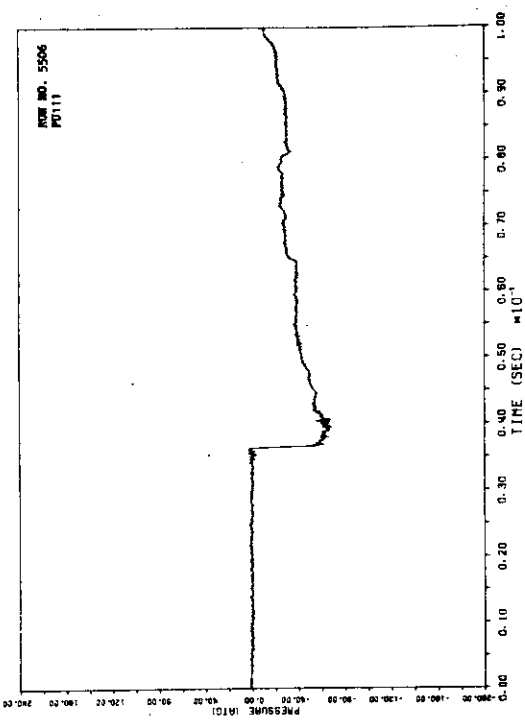

A.20

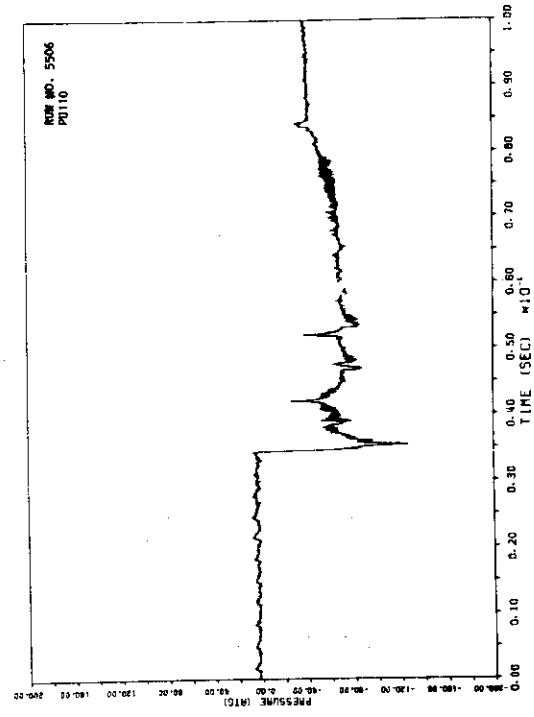

A.17

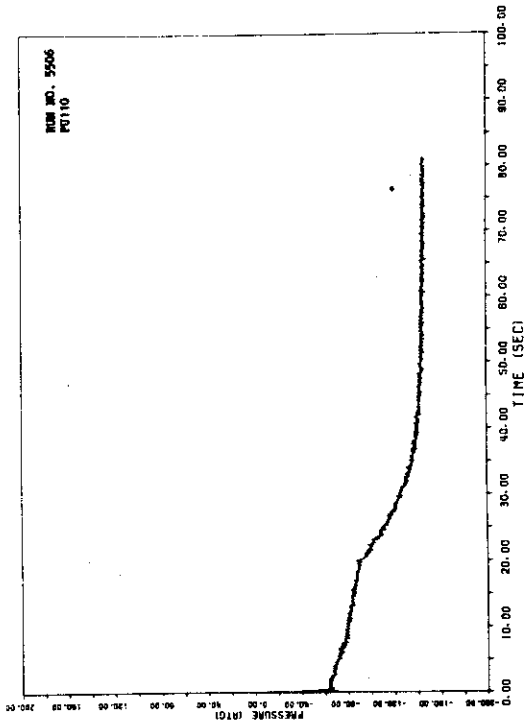

A.19

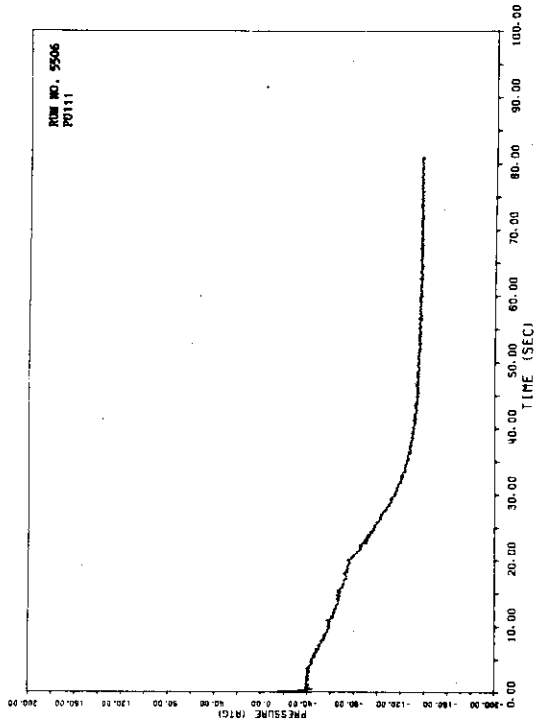

A.22

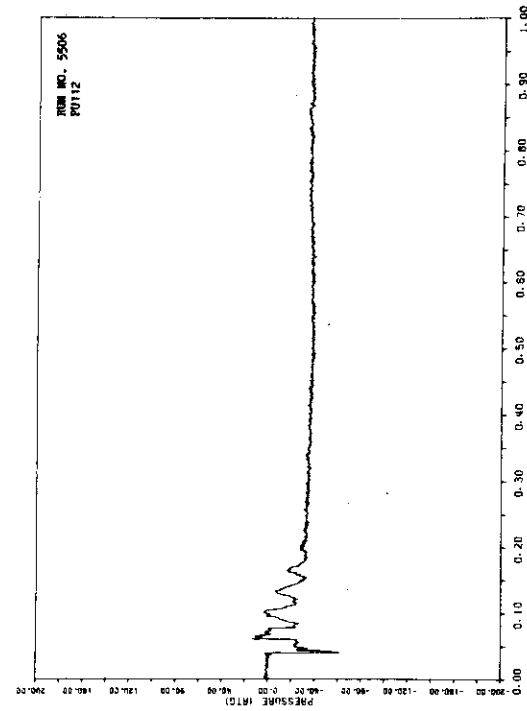

A.24

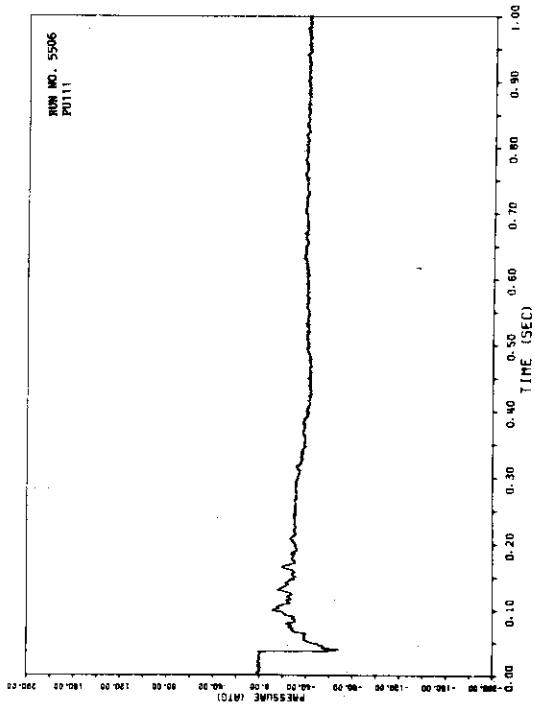

A.21

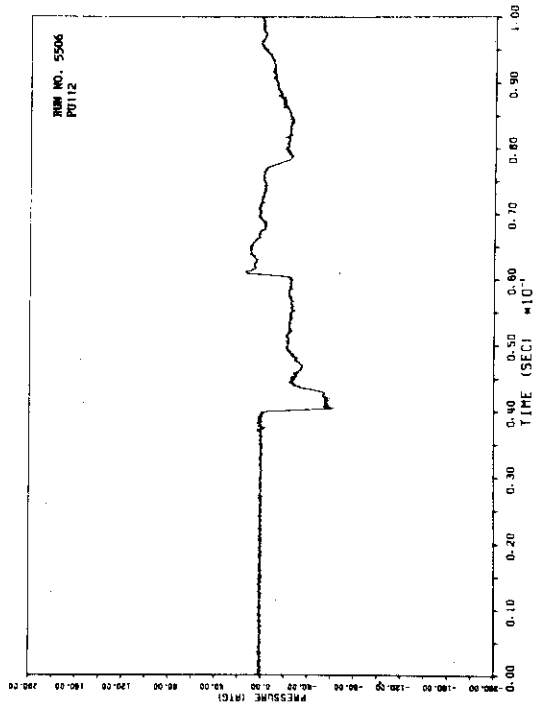

A.23

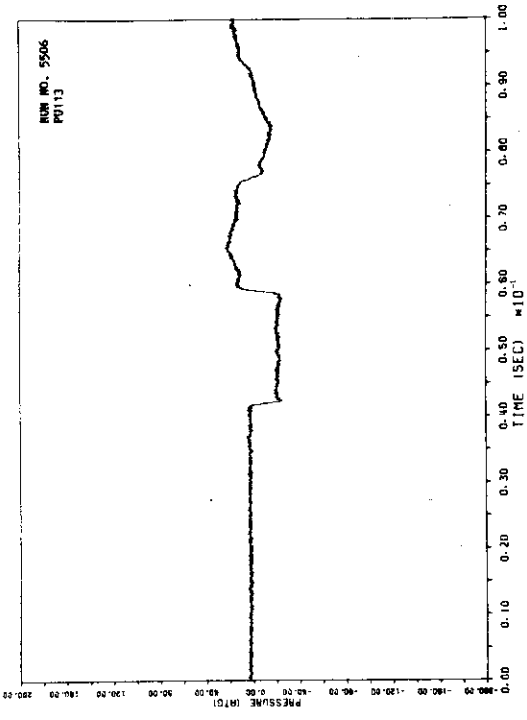

A.26

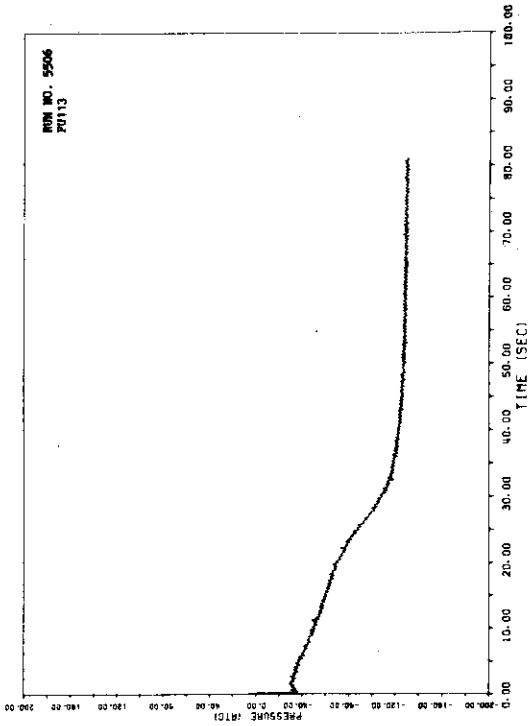

A.28

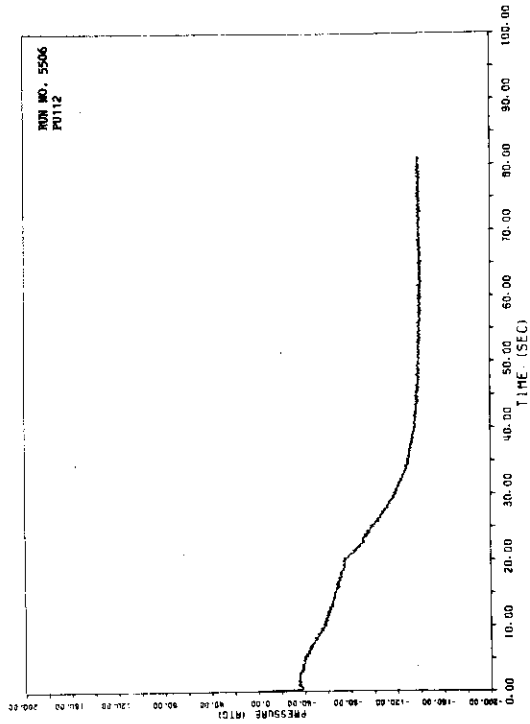

A.25

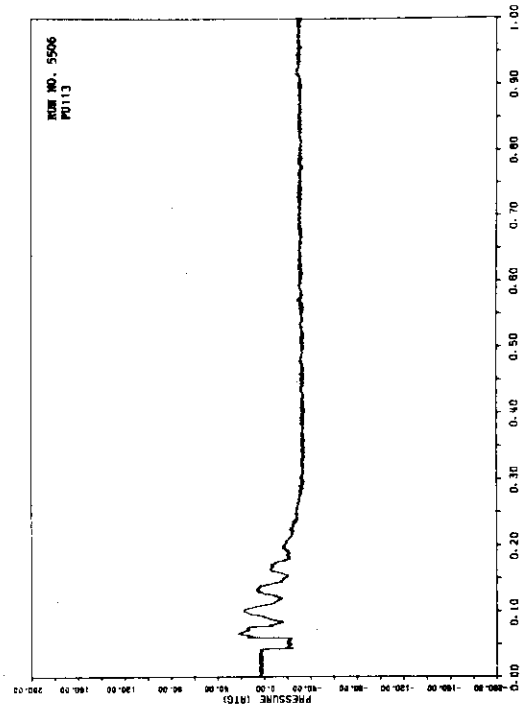

A.27

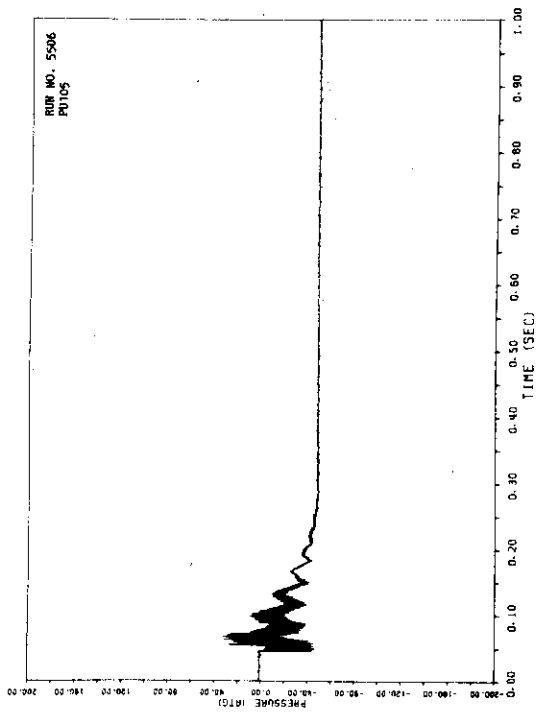

A.30

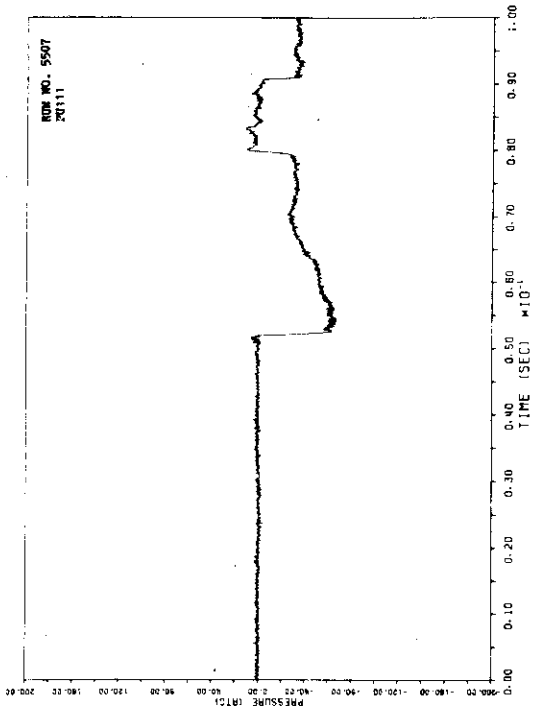

A.32

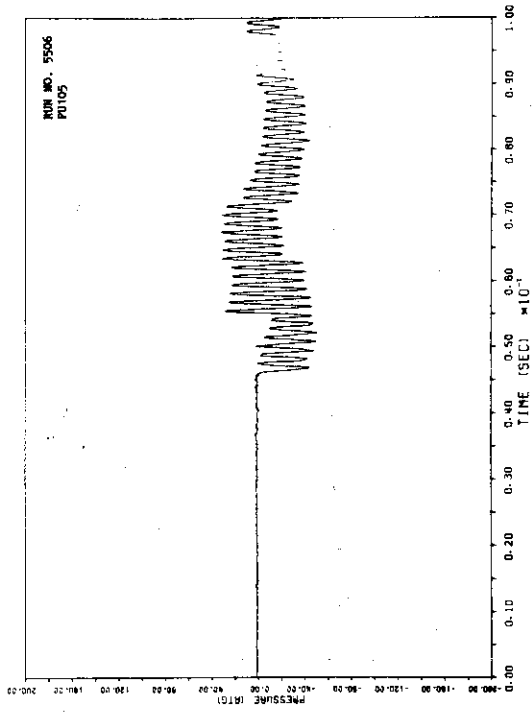

A.29

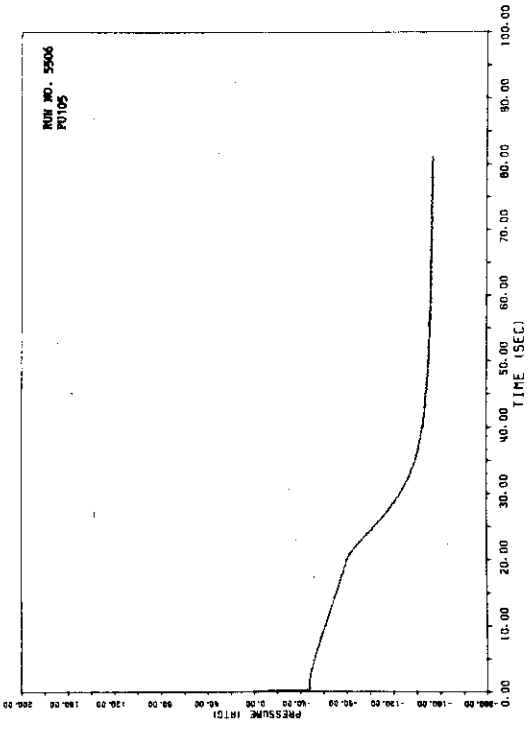

A.31

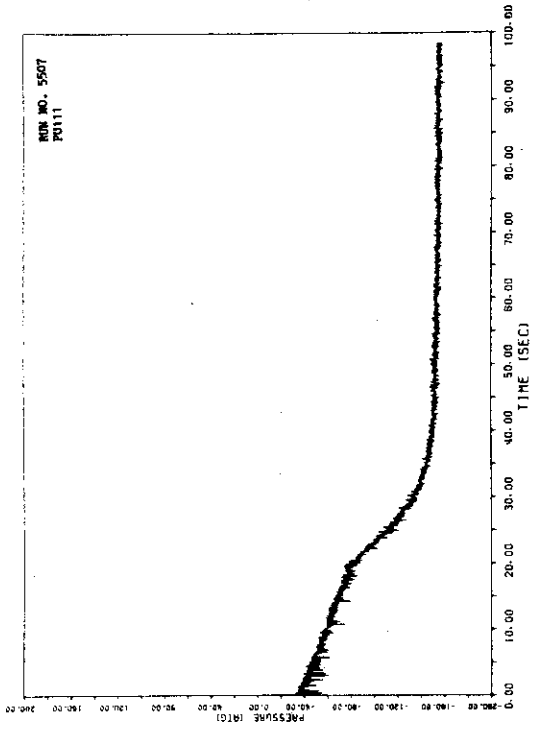

A.34

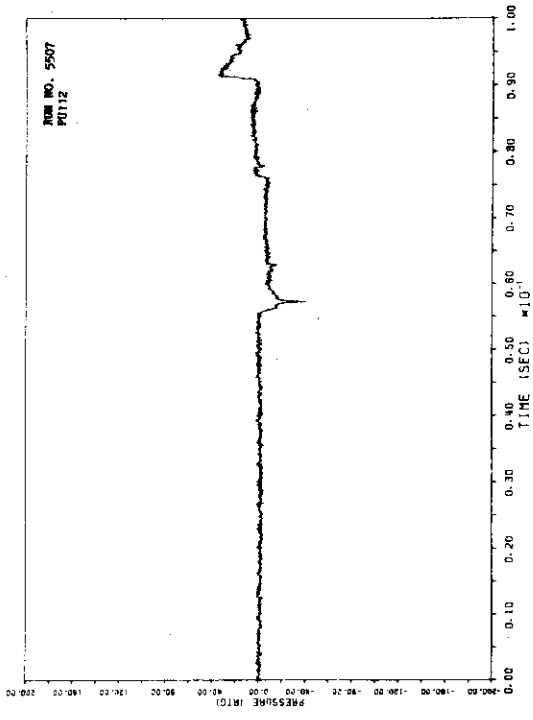

A.36

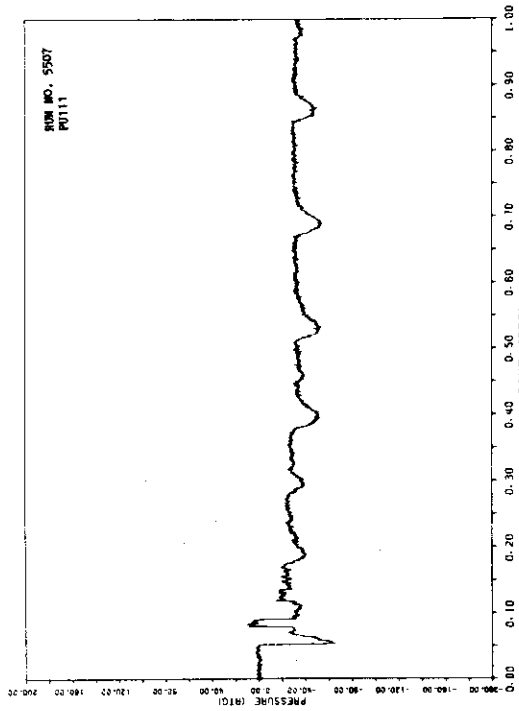

A.33

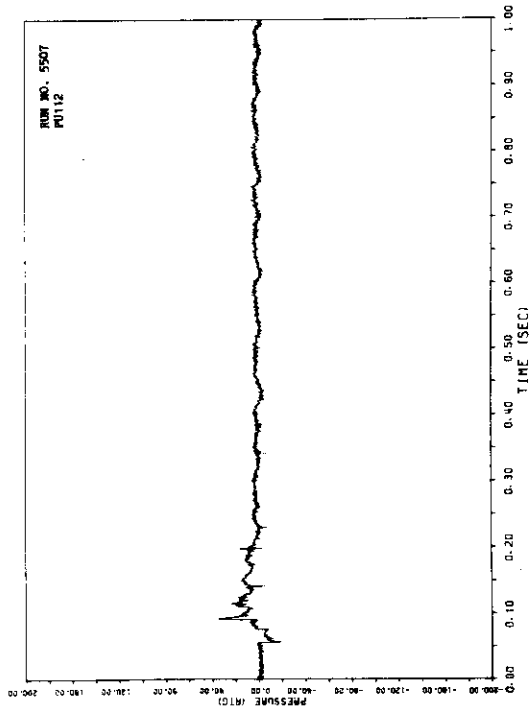

A.35

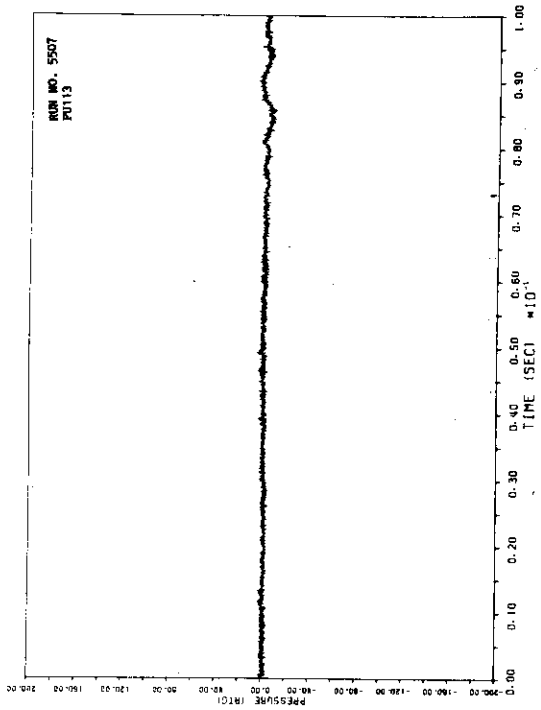

A.38

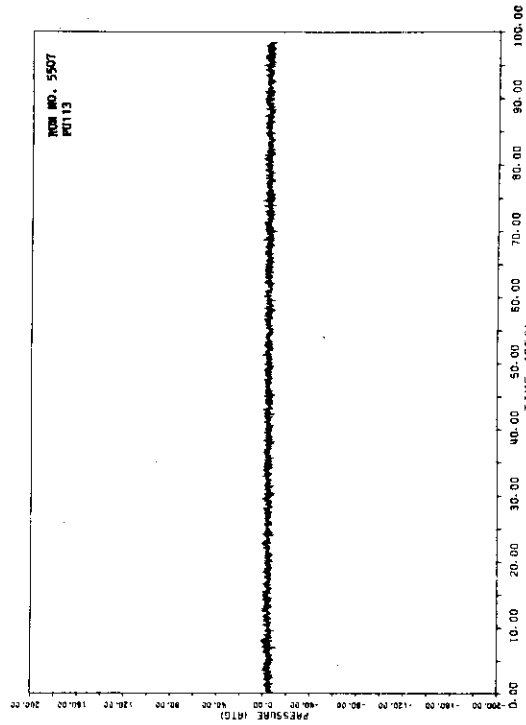

A.40

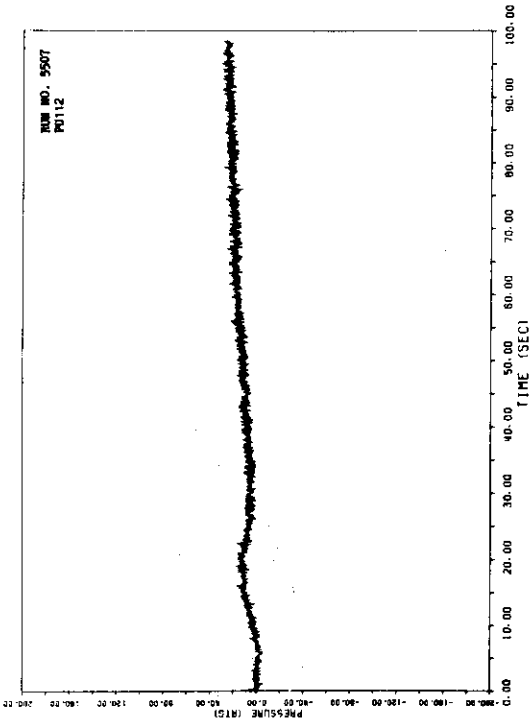

A.37

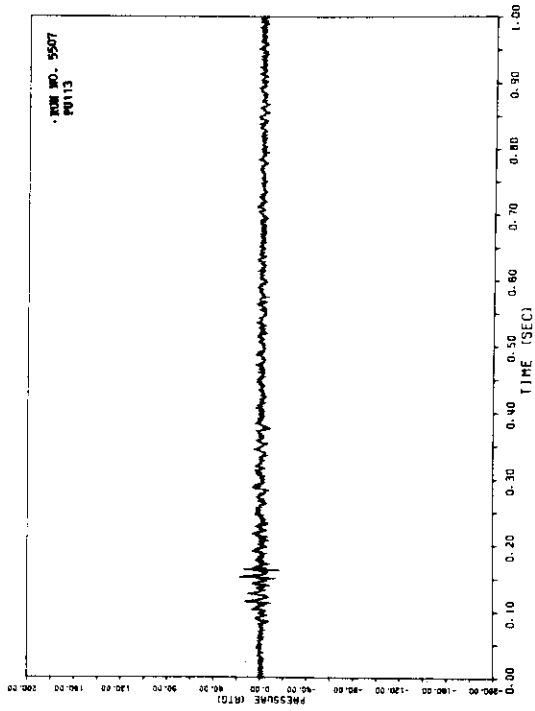

A.39

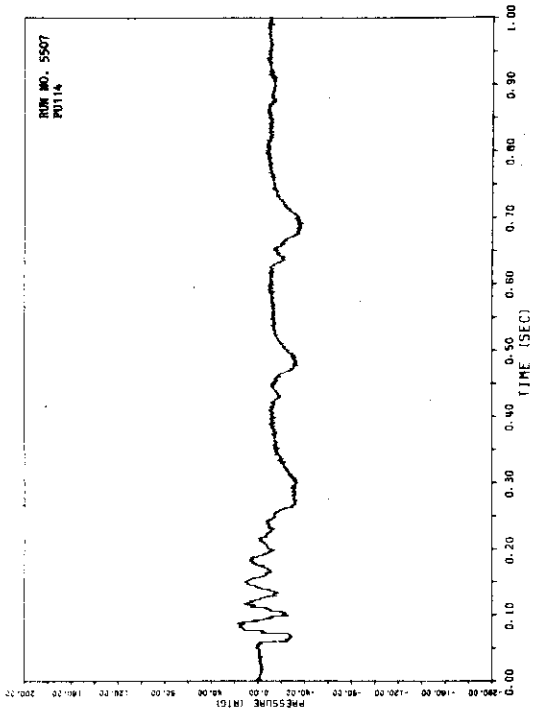

A.42

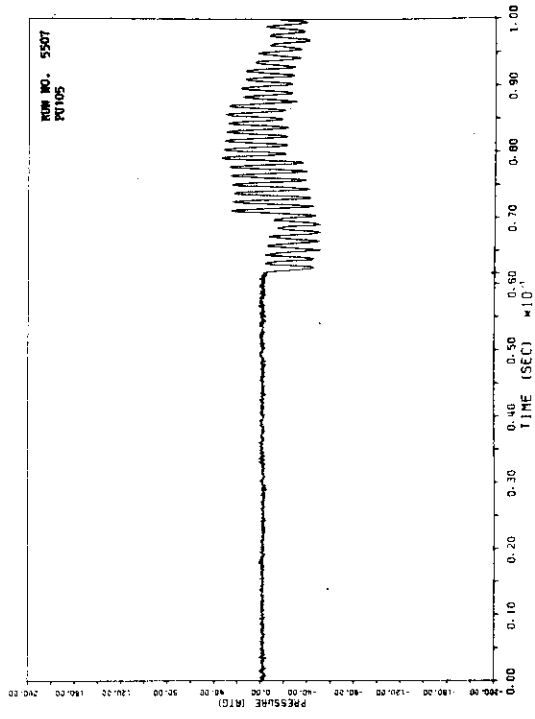

A.44

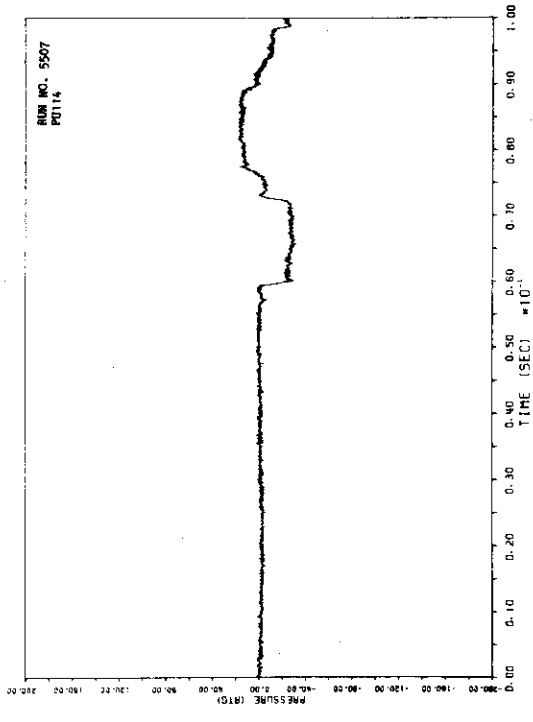

A.41

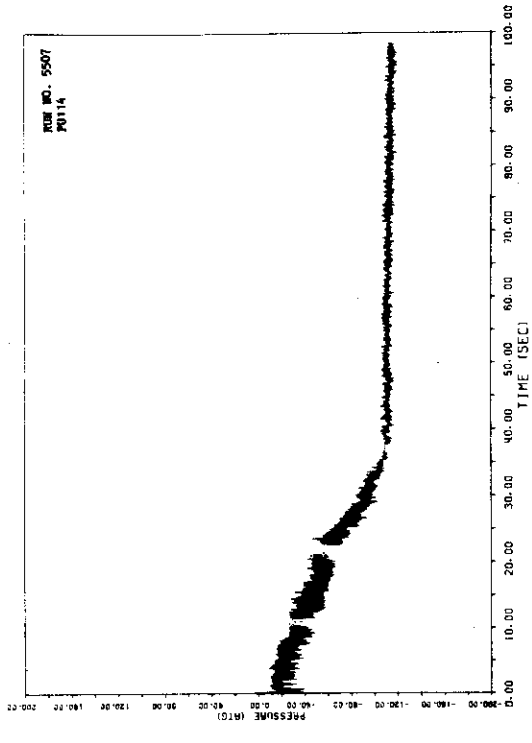

A.43

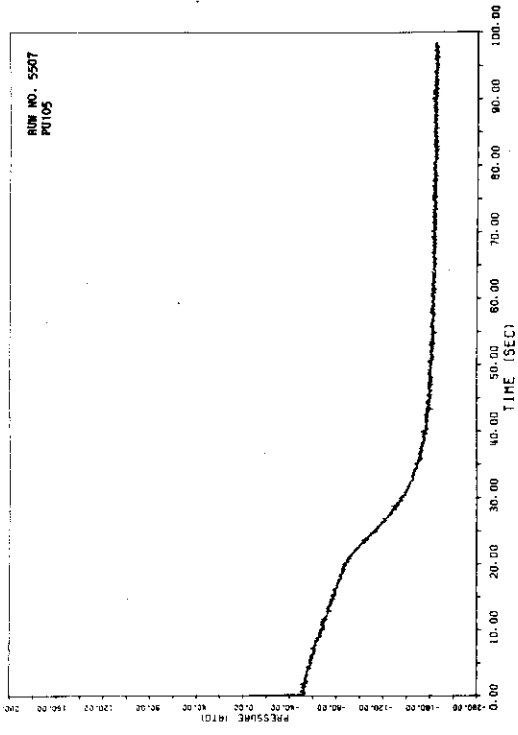

A.46

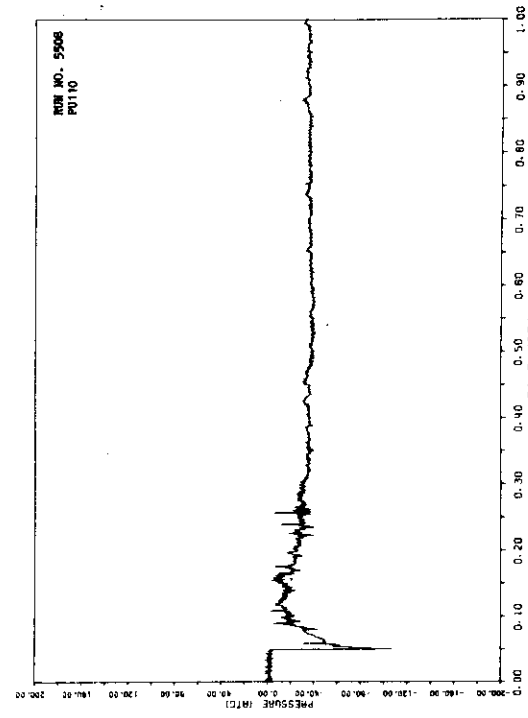

A.48

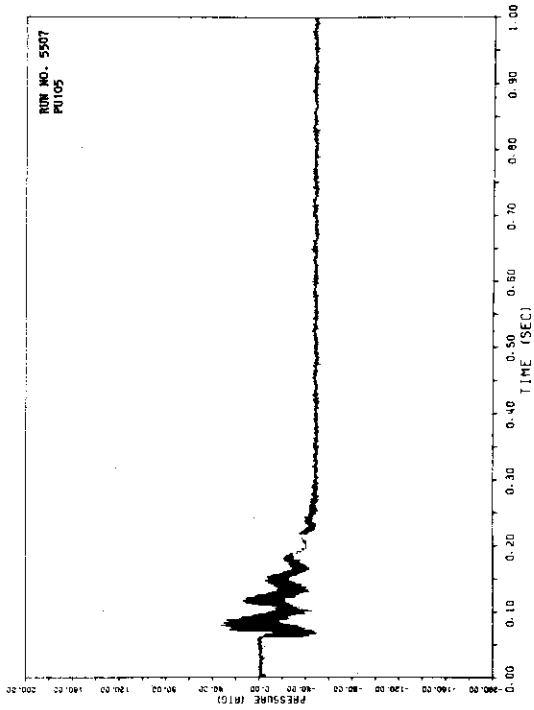

A.45

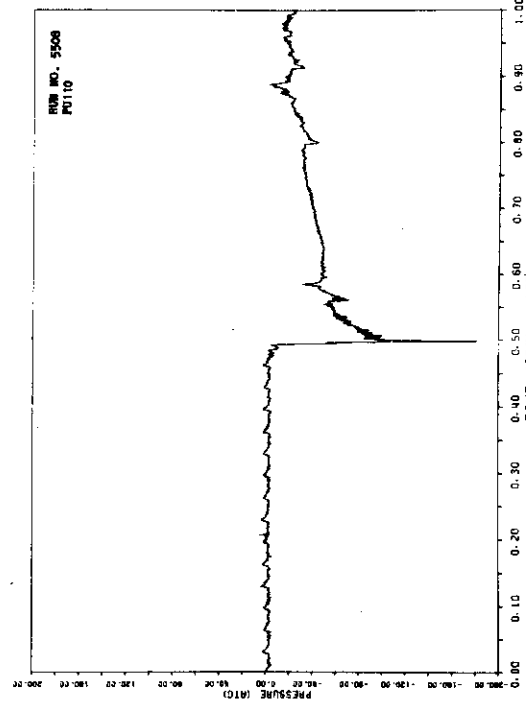

A.47

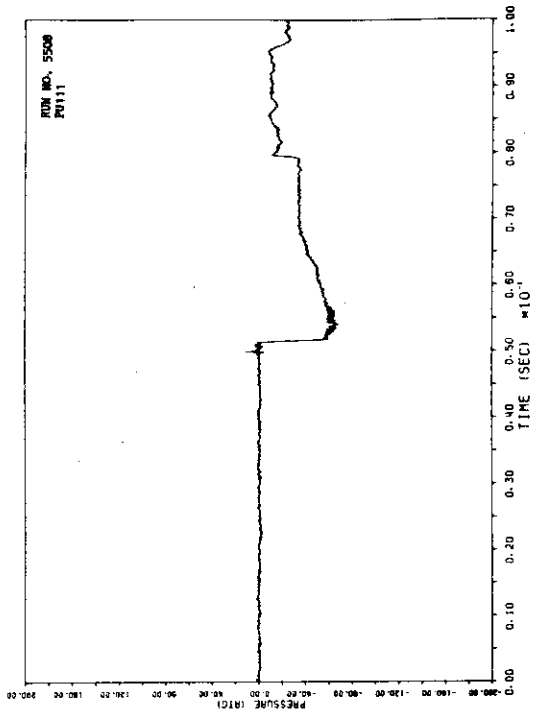

A.50

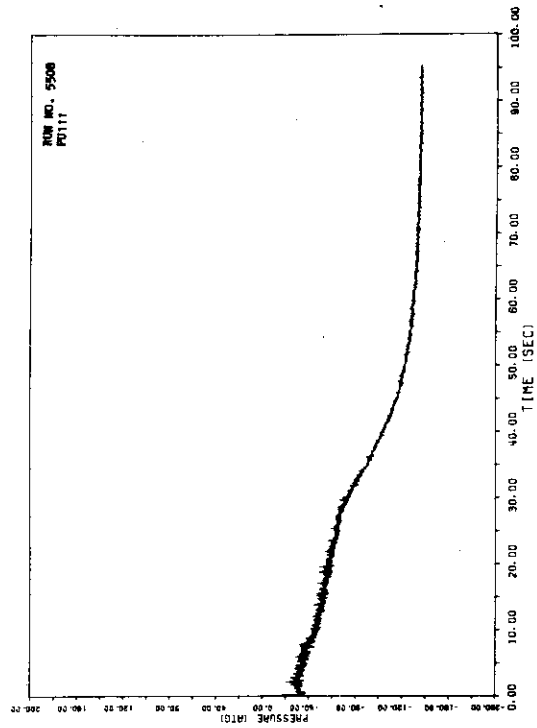

A.52

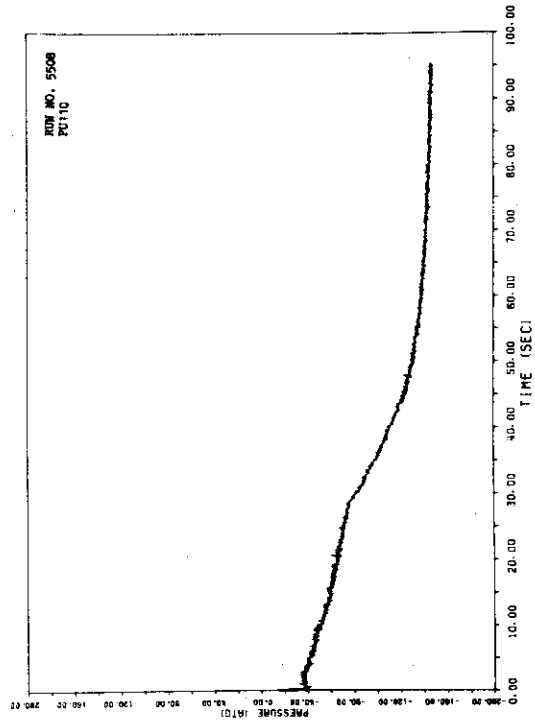

A.49

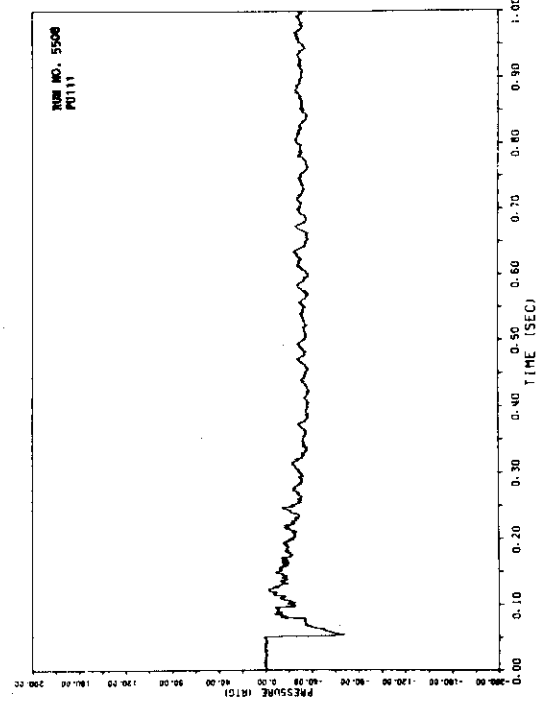

A.51

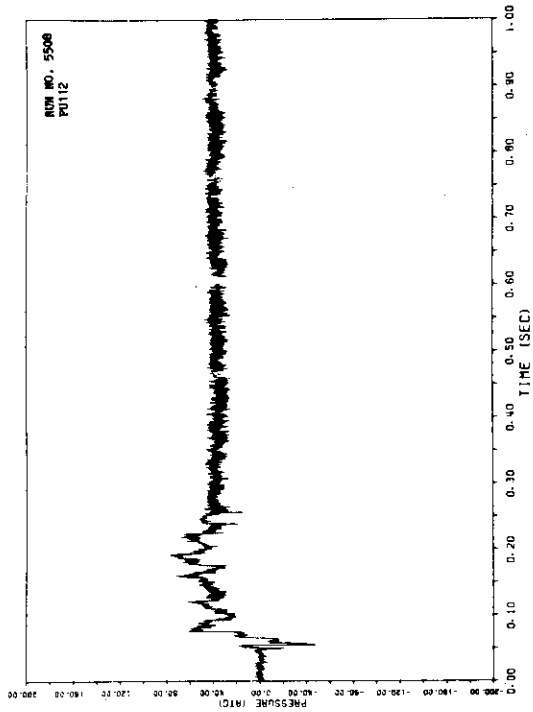

A.54

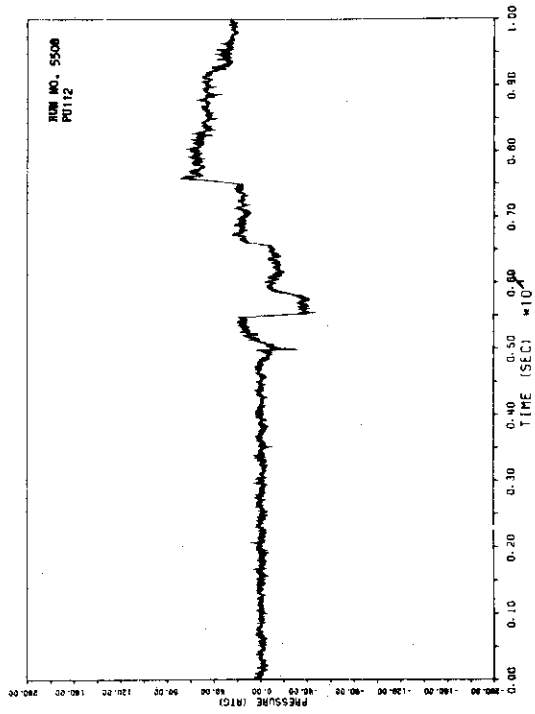

A.53

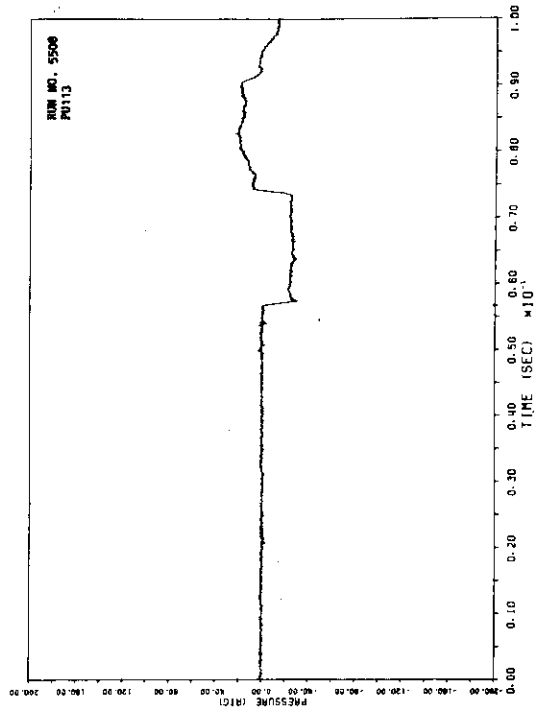

A.56

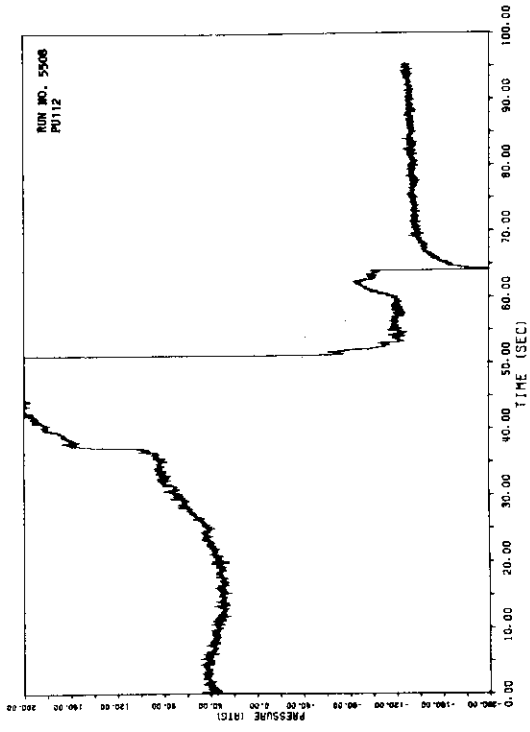

A.55

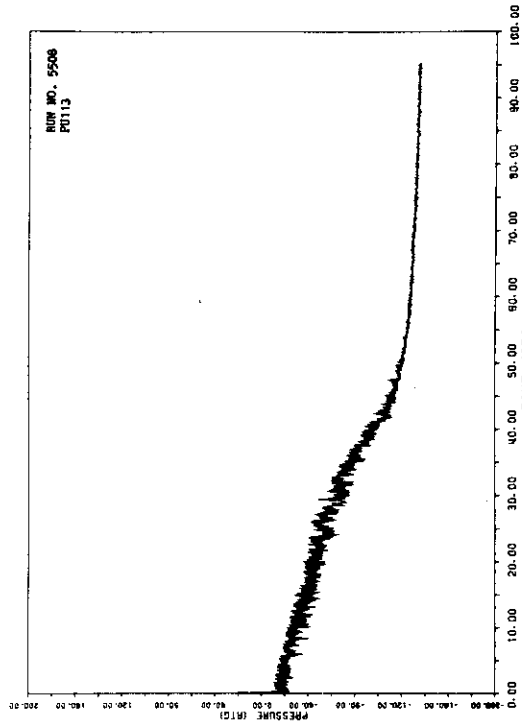

A.58

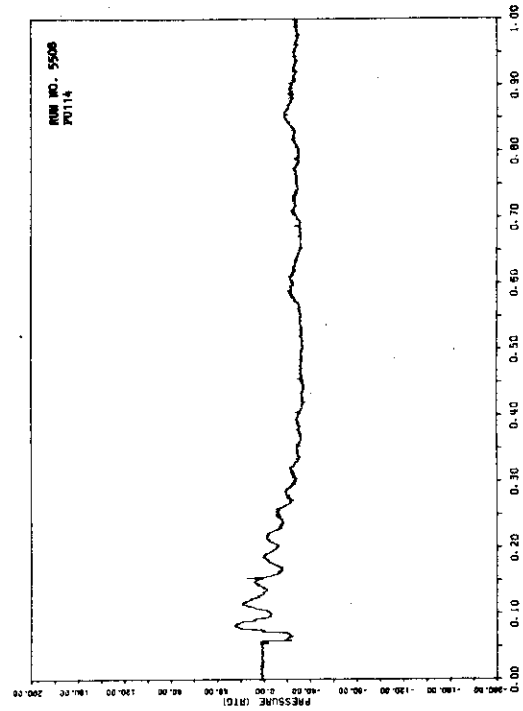

A.60

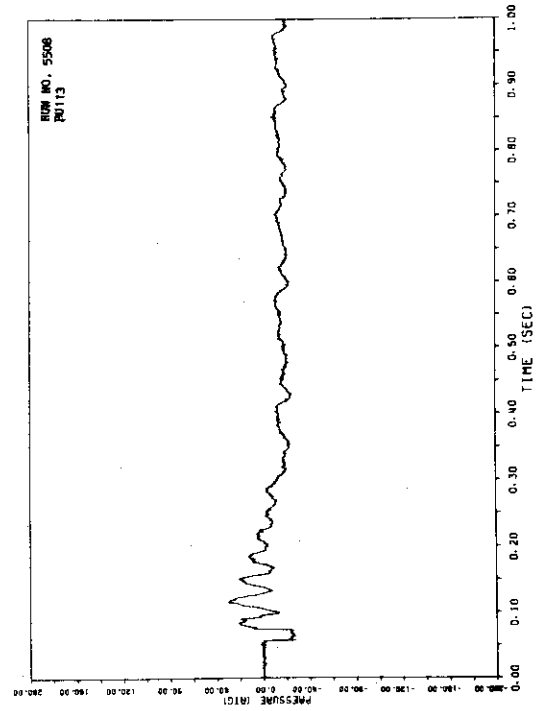

A.57

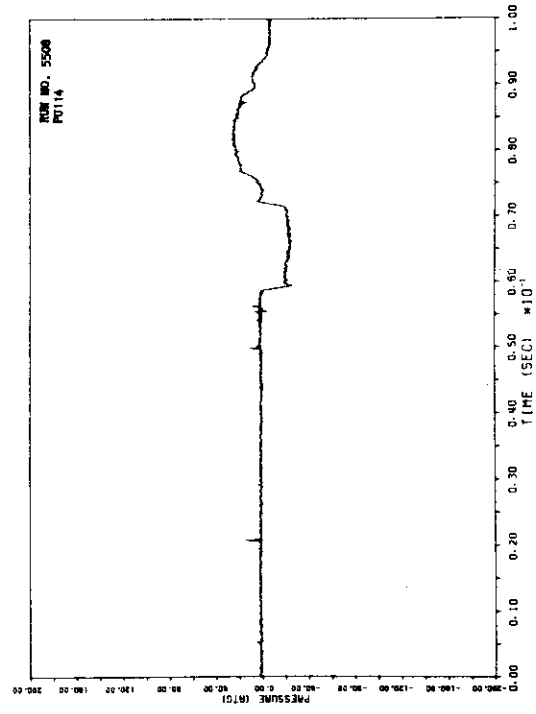

A.59

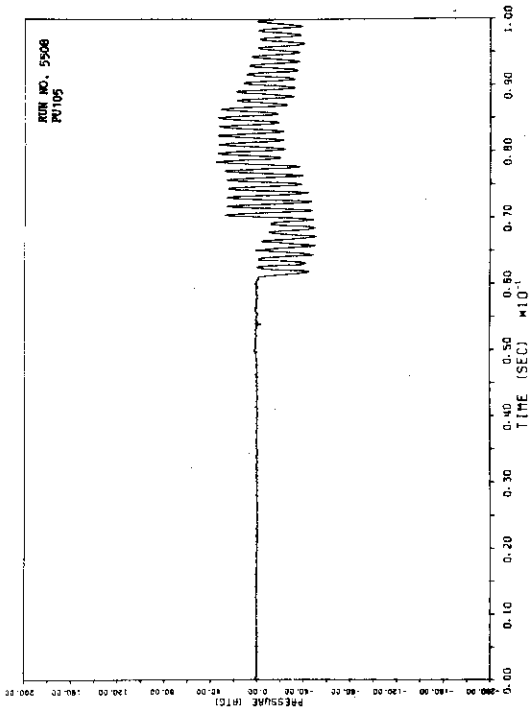

A.62

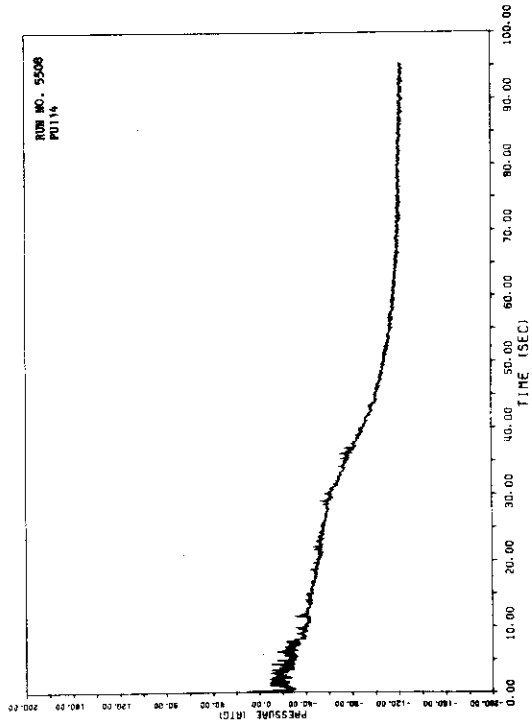

A.61

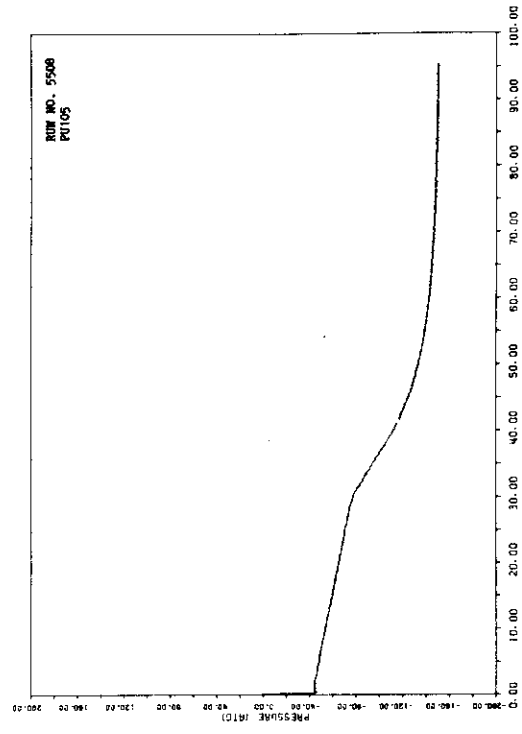

A.64

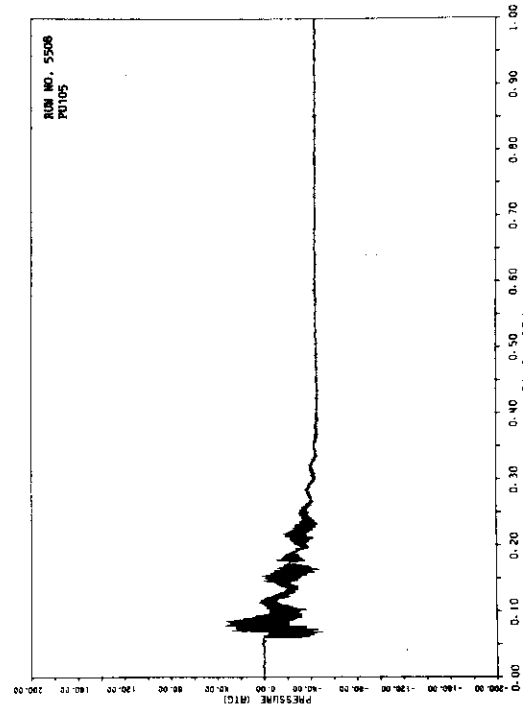

A.63

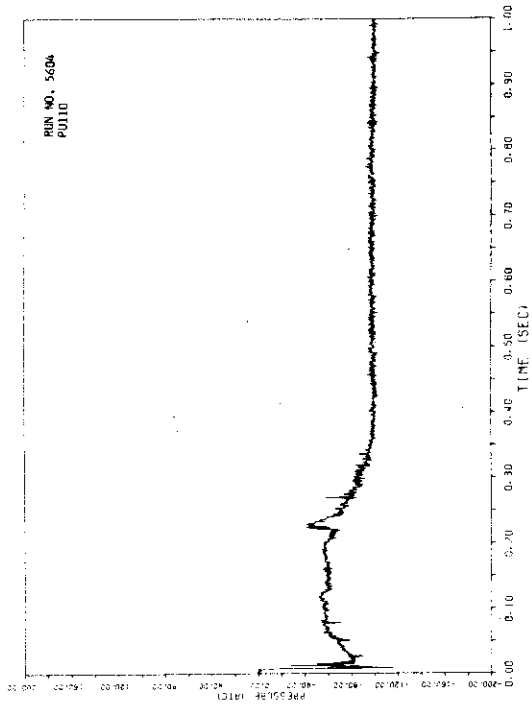

A.66

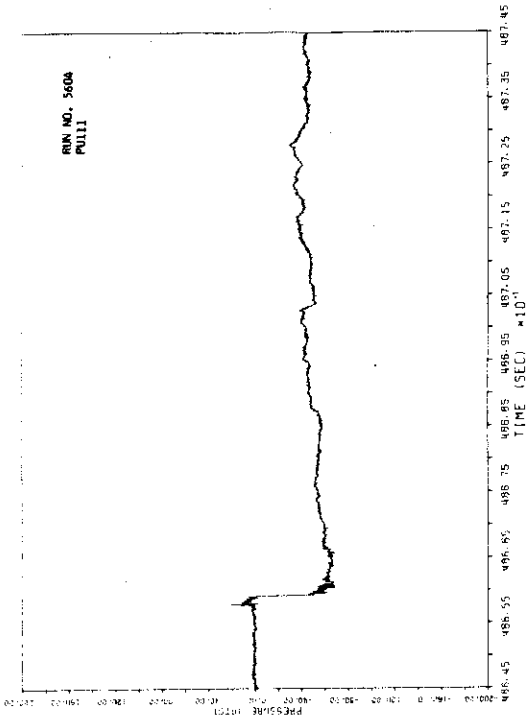

A.68

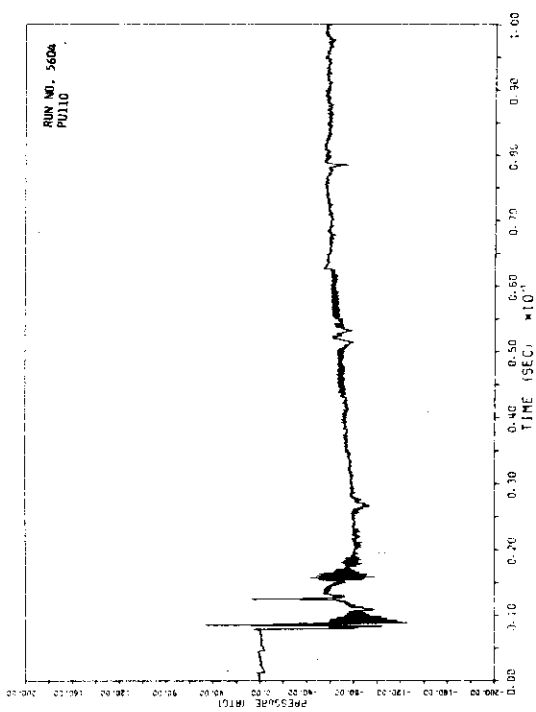

A.65

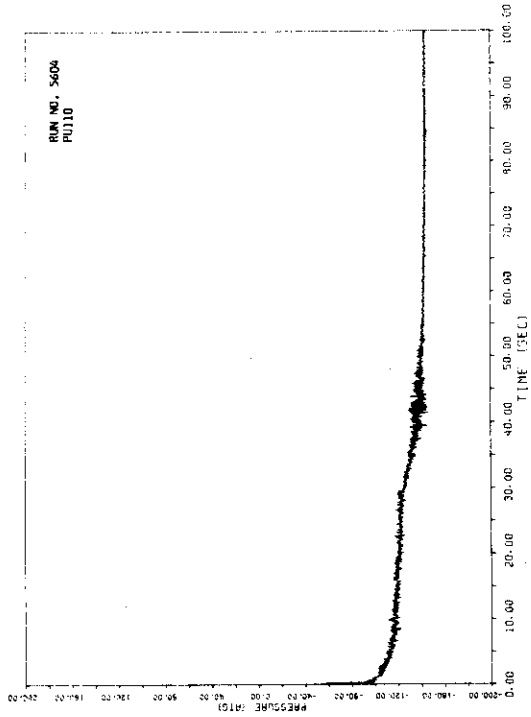

A.67

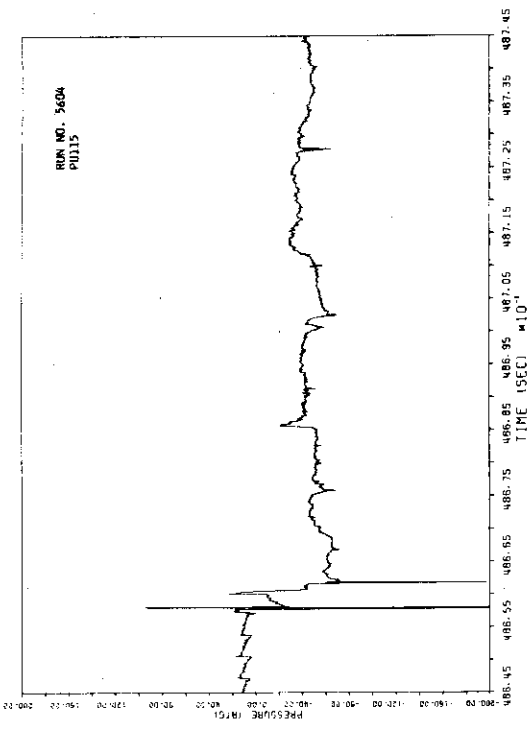

A.70

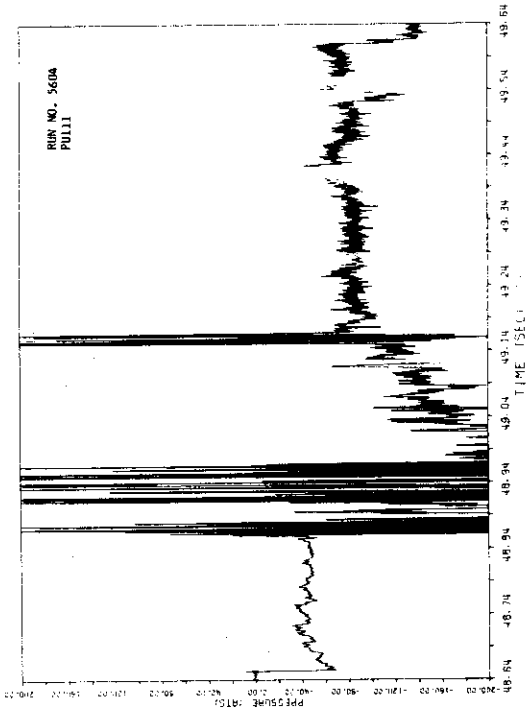

A.69

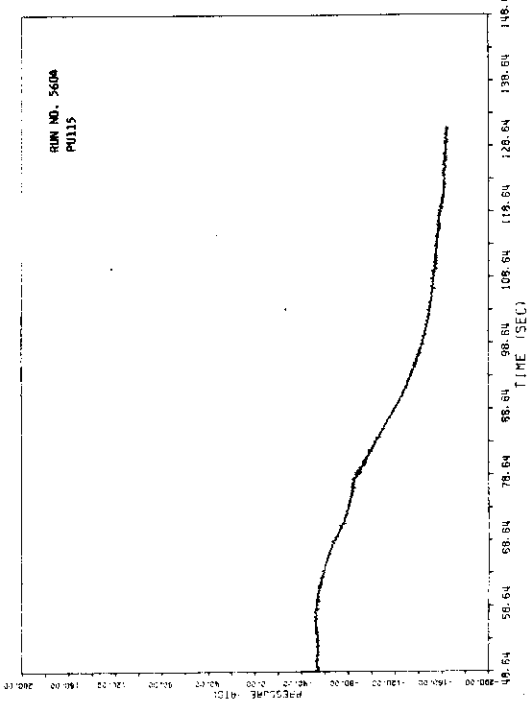

A.72

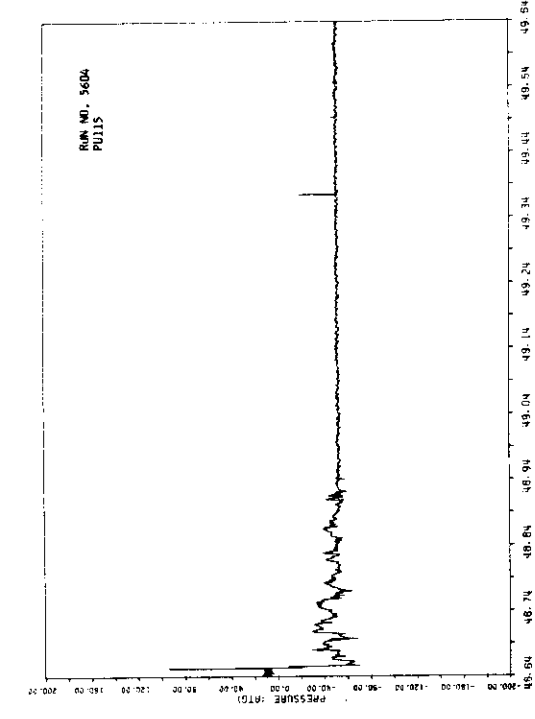

A.71

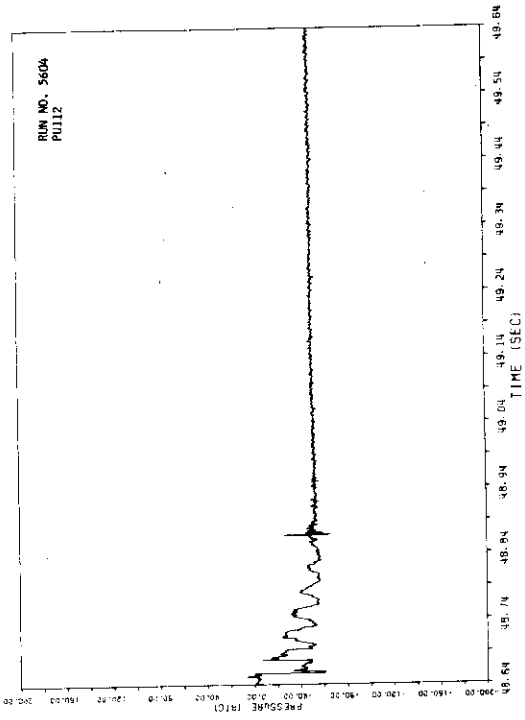

A.74

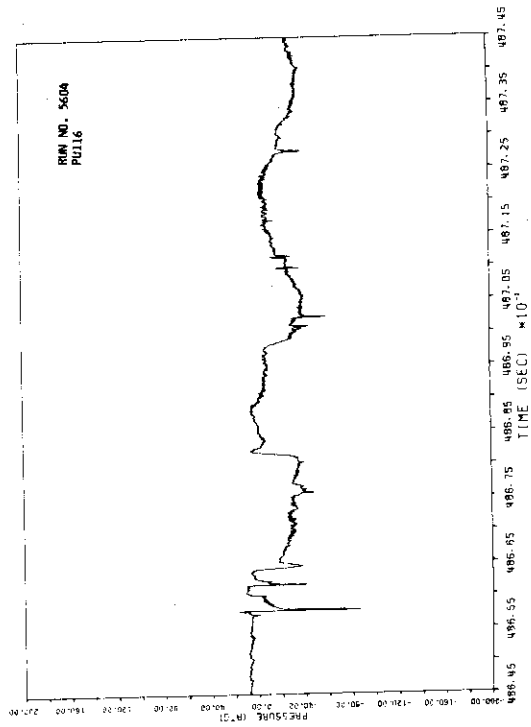

A.76

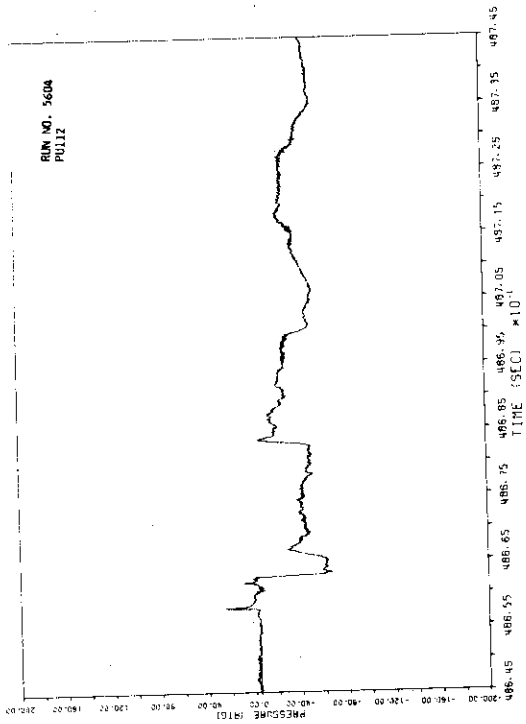

A.73

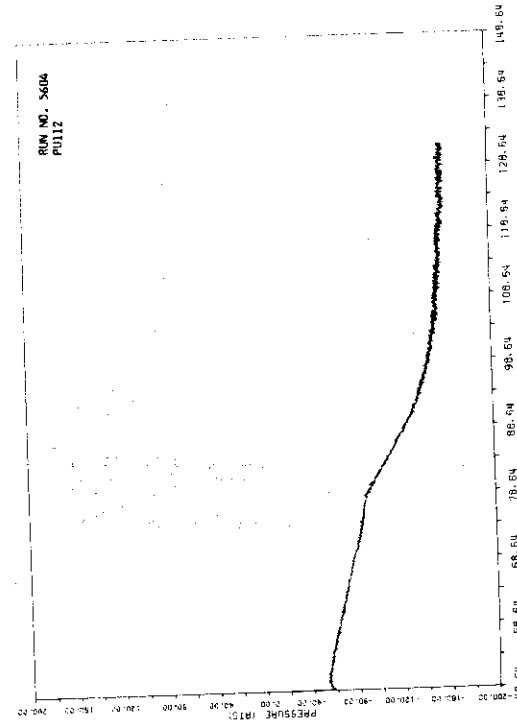

A.75

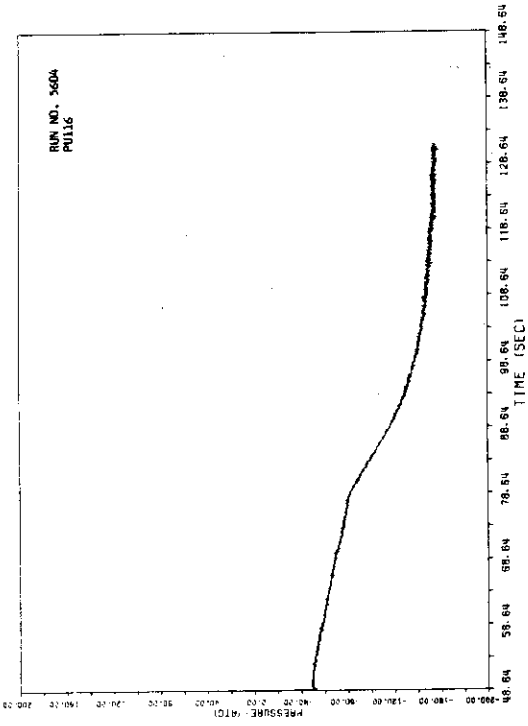

A.78

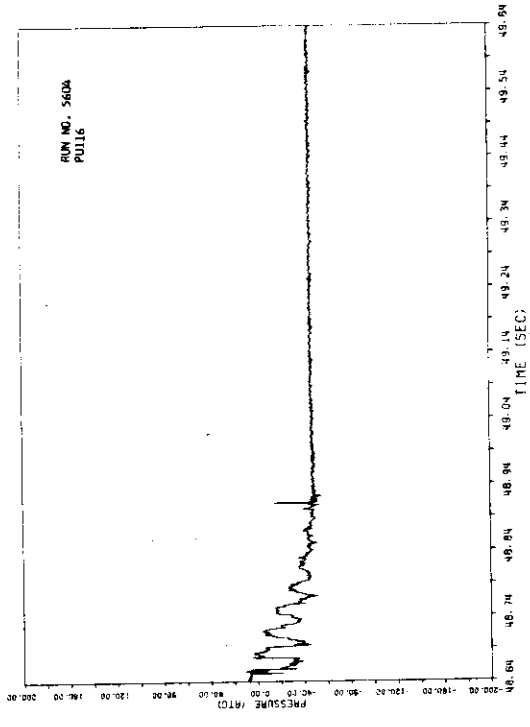

A.77

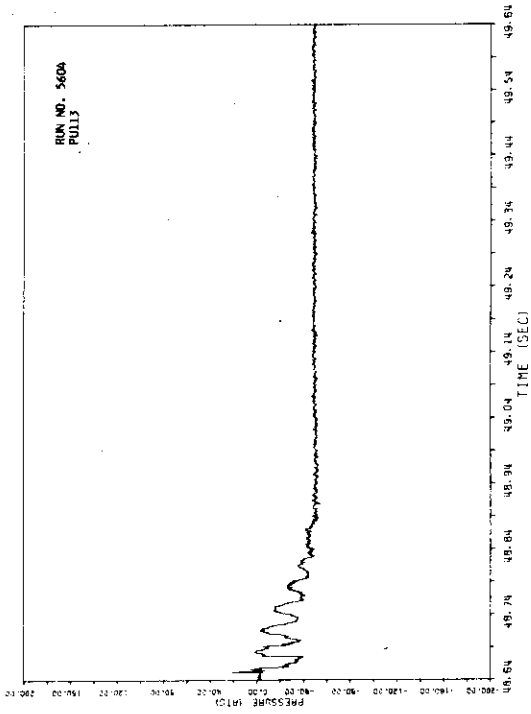

A.80

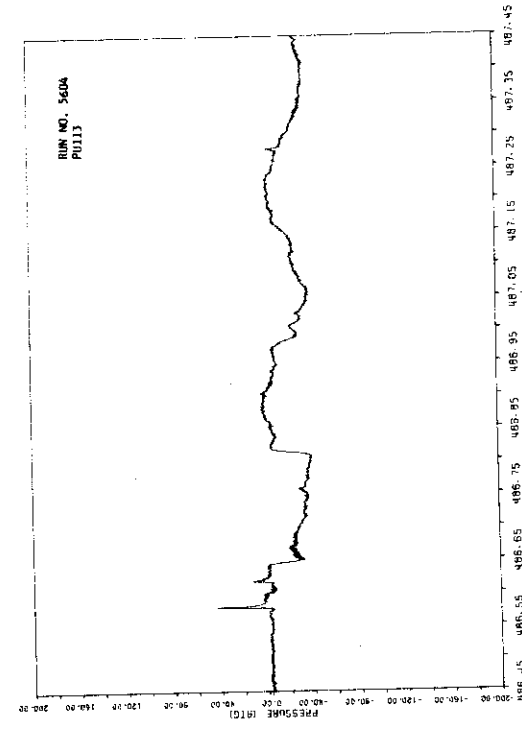

A.79

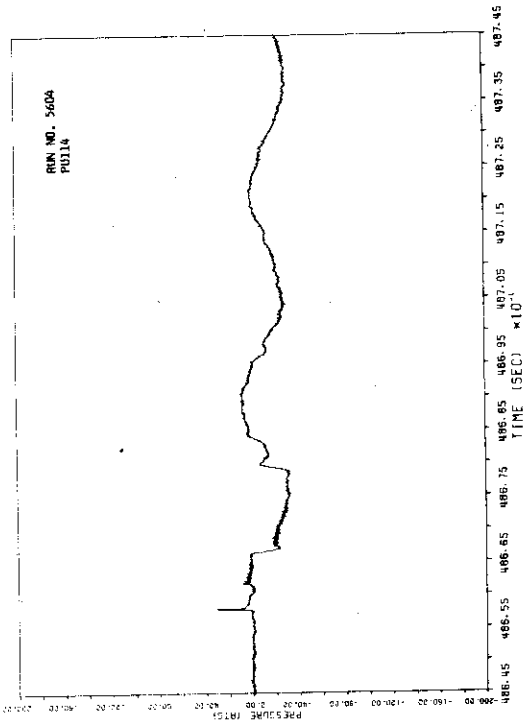

A.82

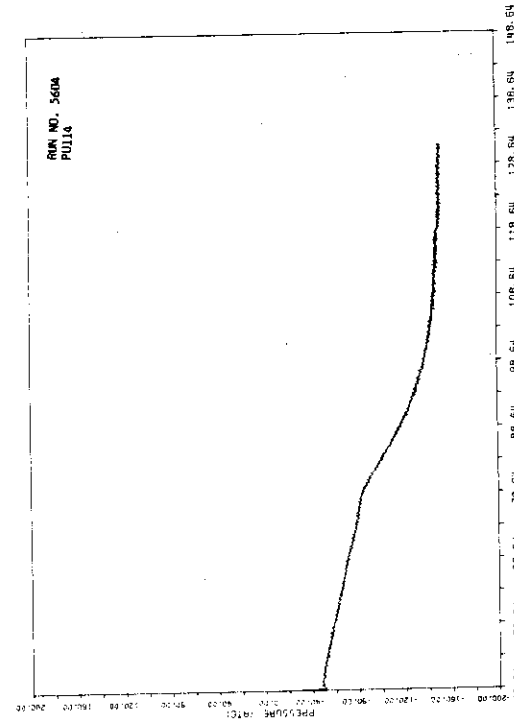

A.84

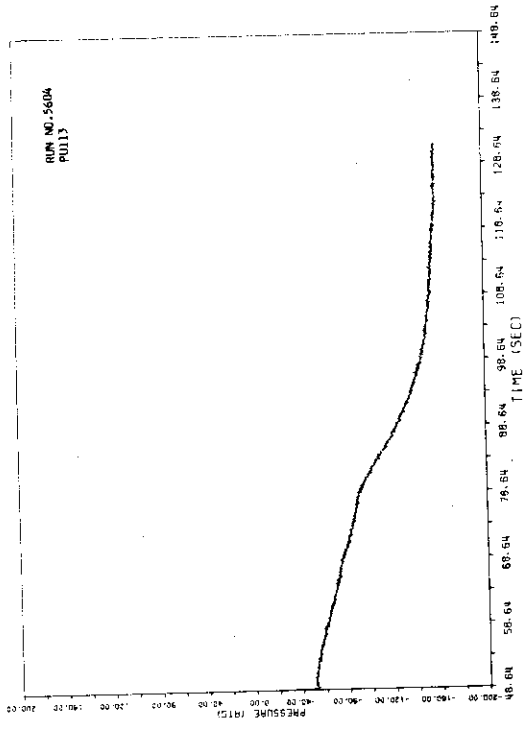

A.81

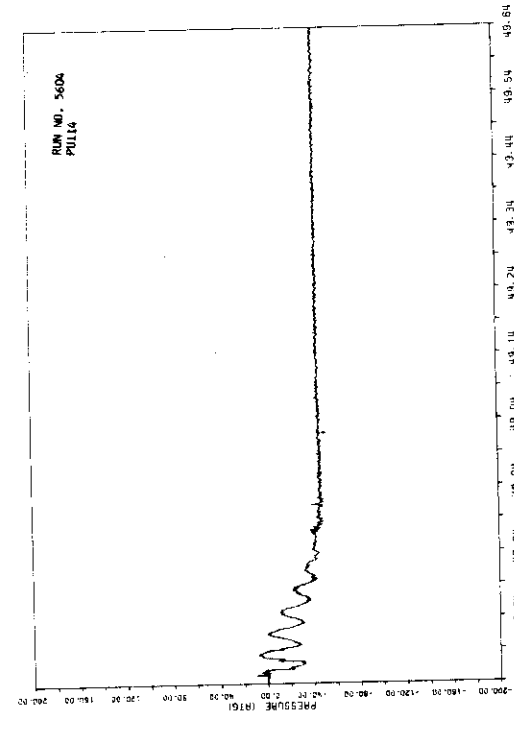

A.83

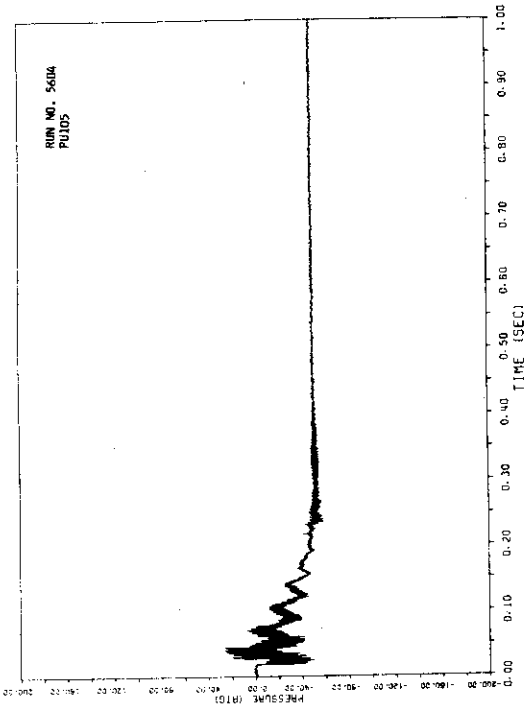
RUN NO. 5604
PU105
TIME (SEC)

A.86

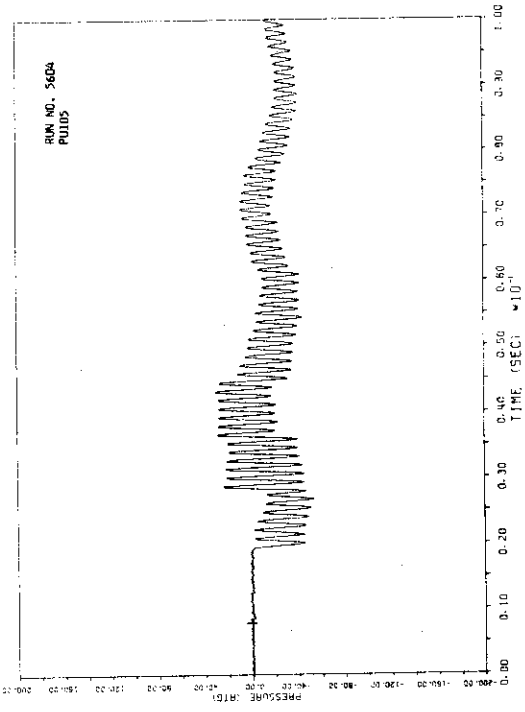
RUN NO. 5604
PU105
TIME (SEC)

A.85

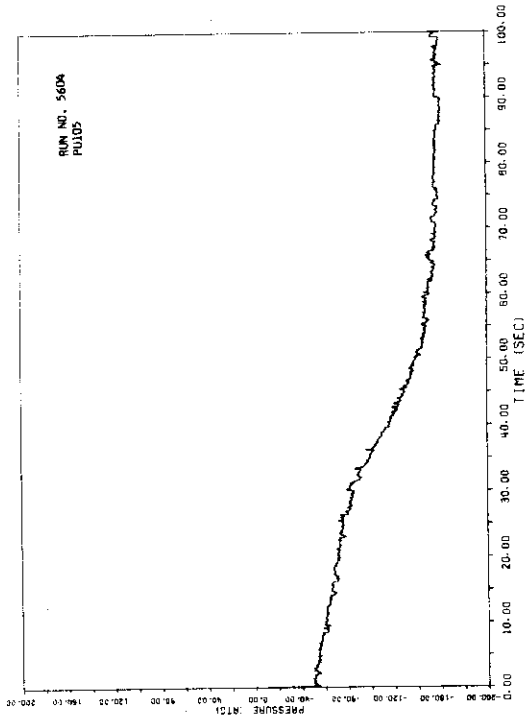
RUN NO. 5604
PU105
TIME (SEC)

A.87

(c) Fluid temperatures in the pressure vessel and piping (A.88-A.106)

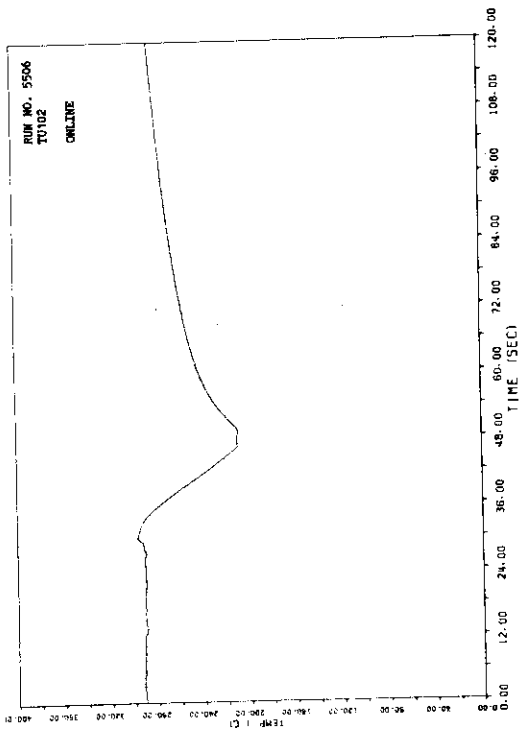

A.89

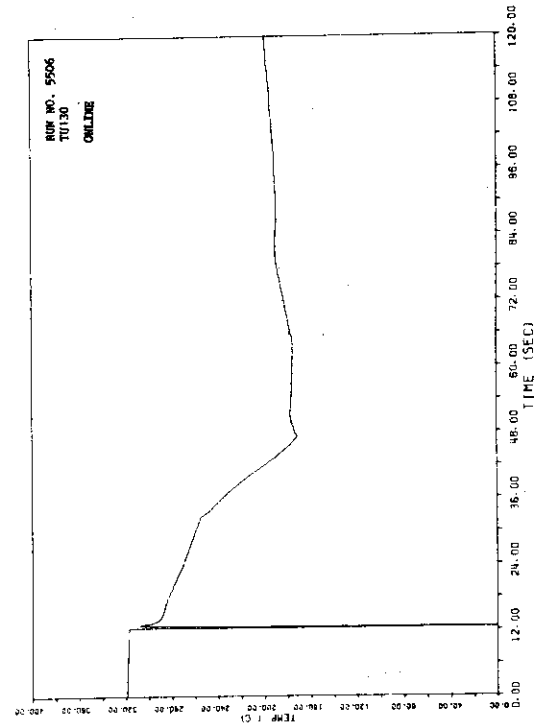

A.91

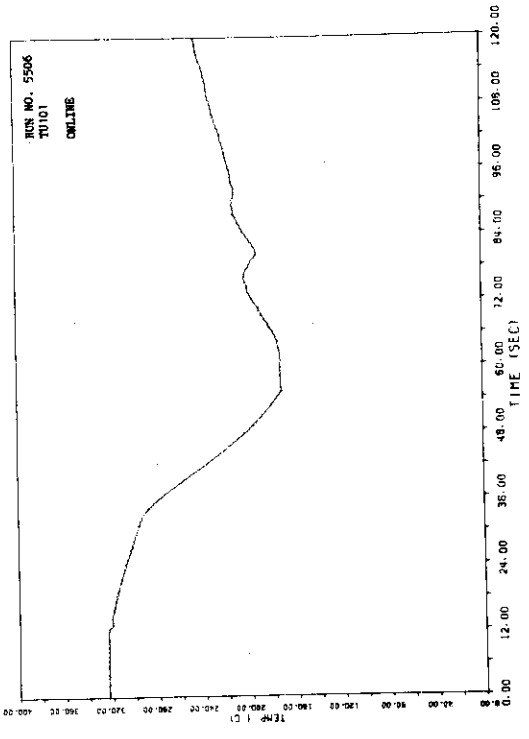

A.88

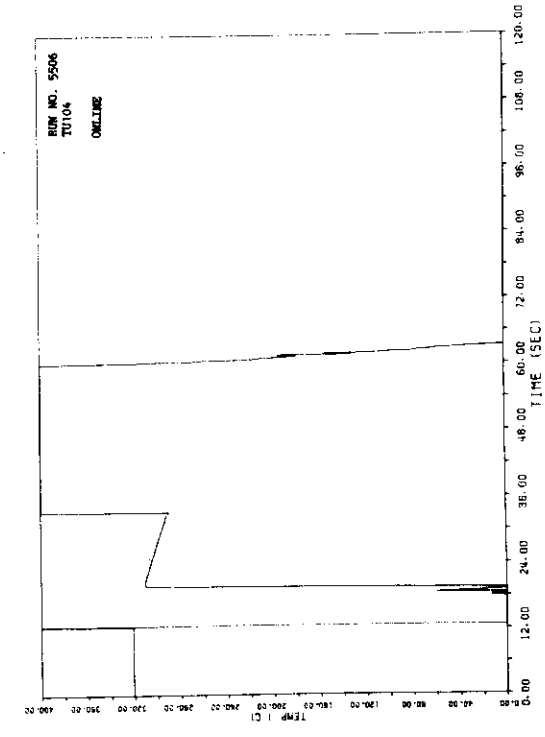

A.90

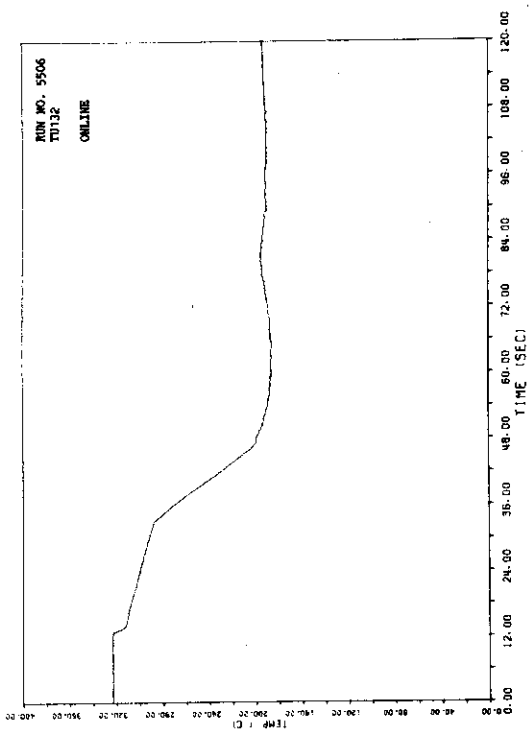

A.93

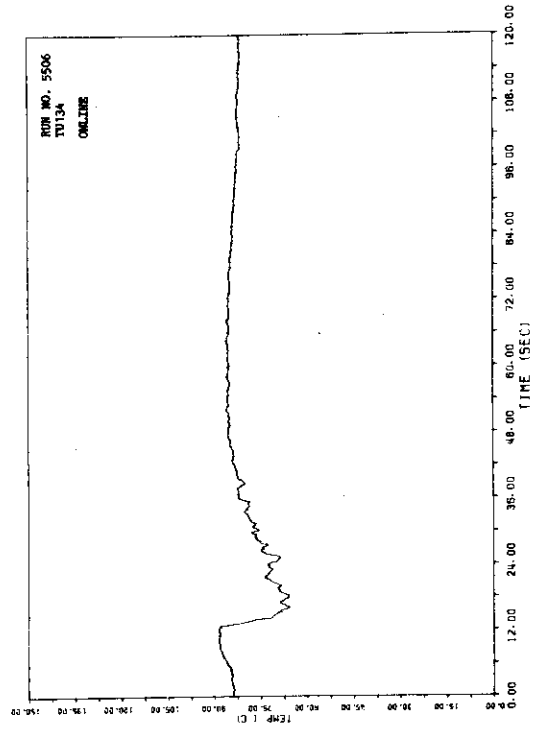

A.95

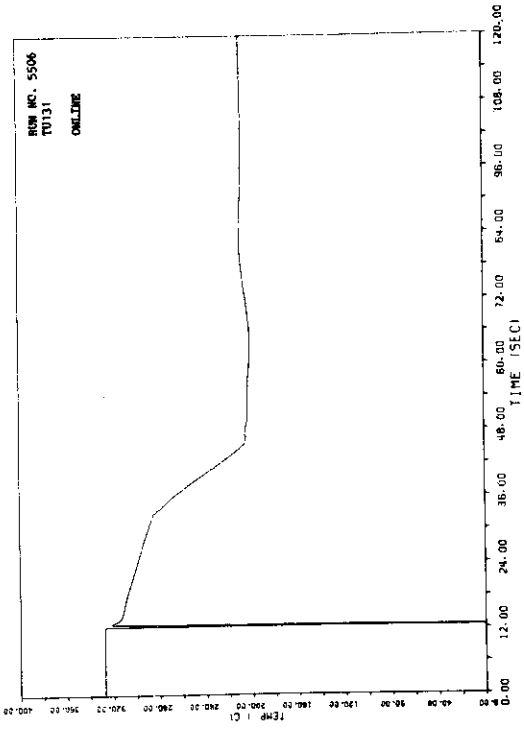

A.92

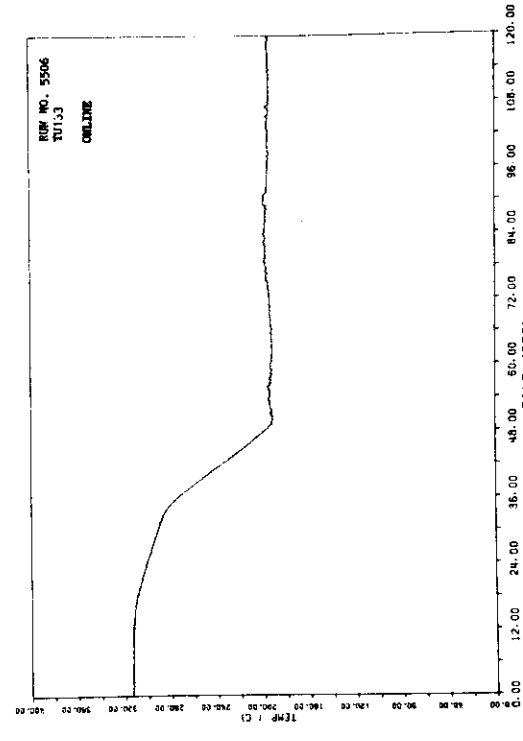

A.94

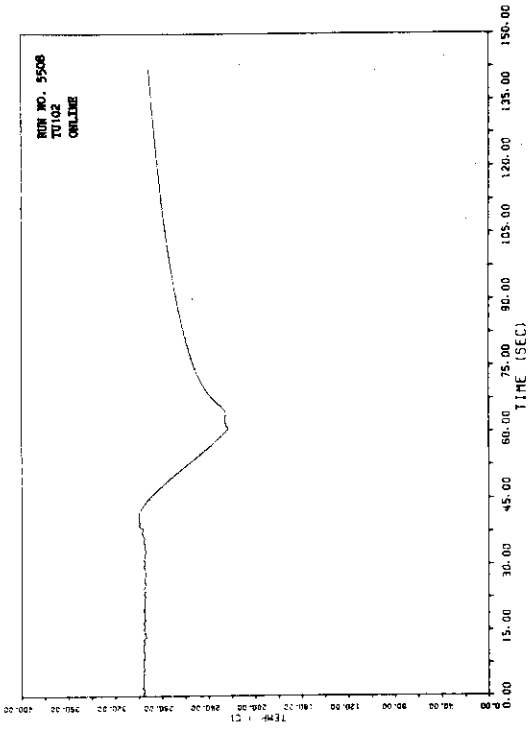

A.97

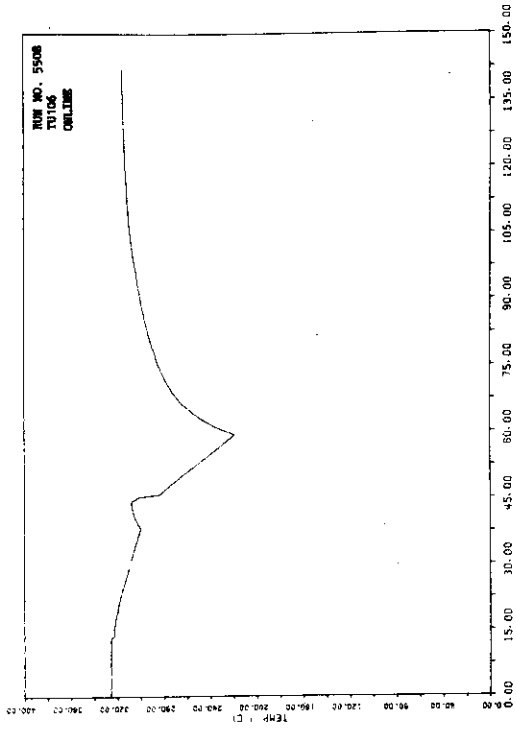

A.99

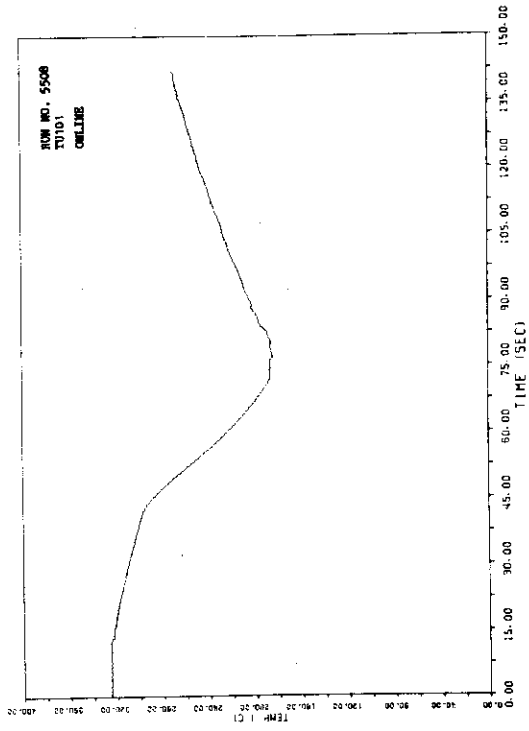

A.96

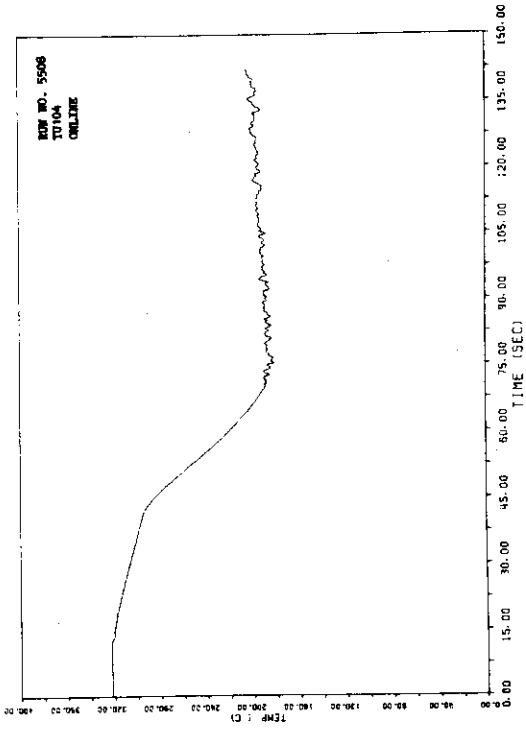

A.98

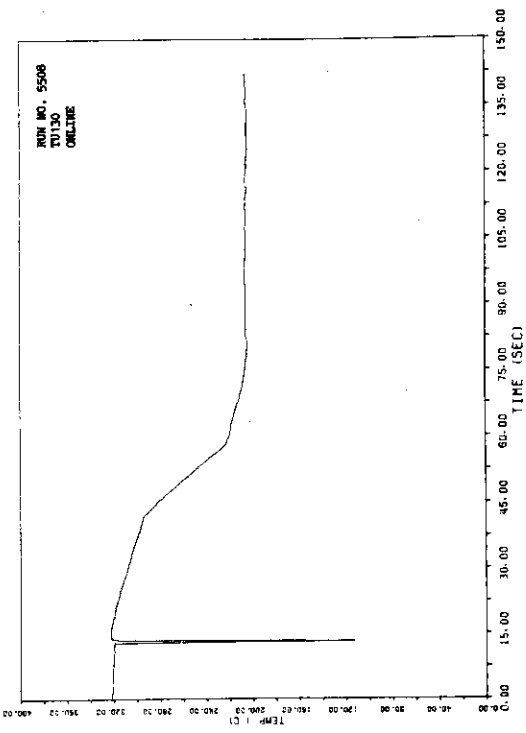

A.101

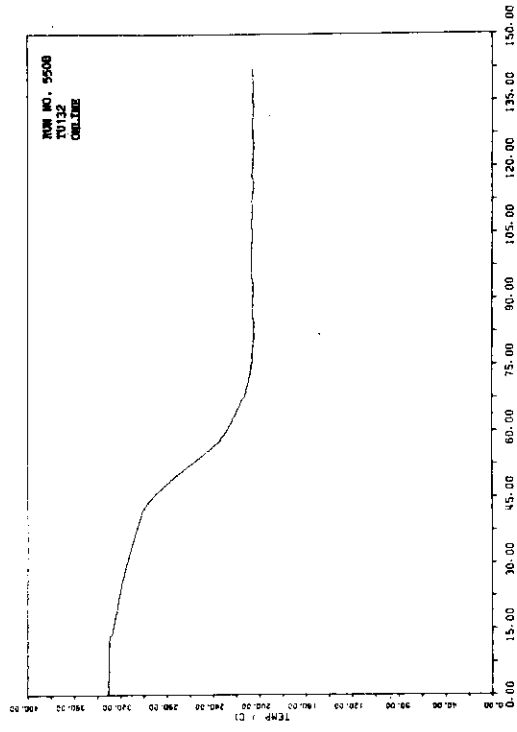

A.103

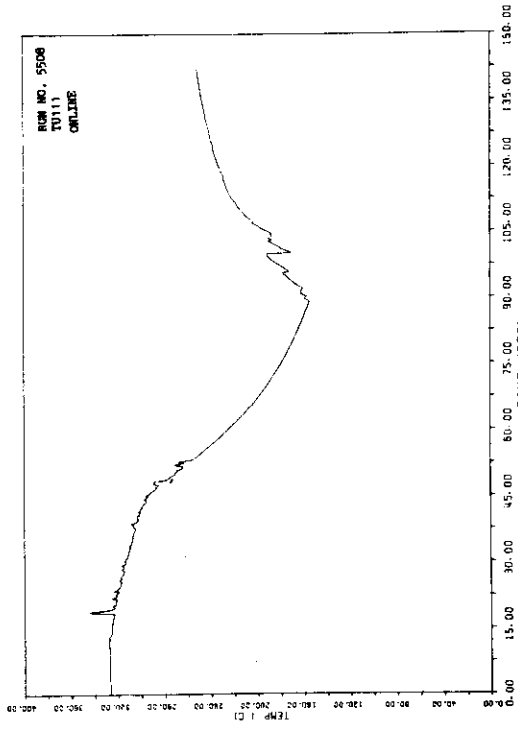

A.100

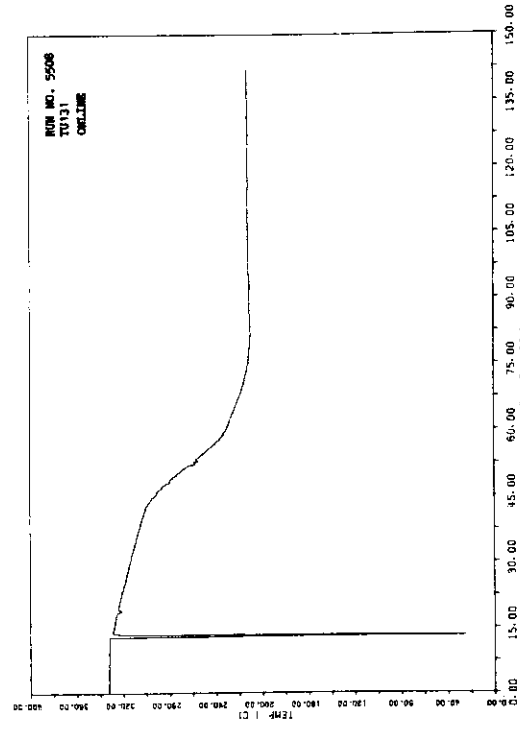

A.102

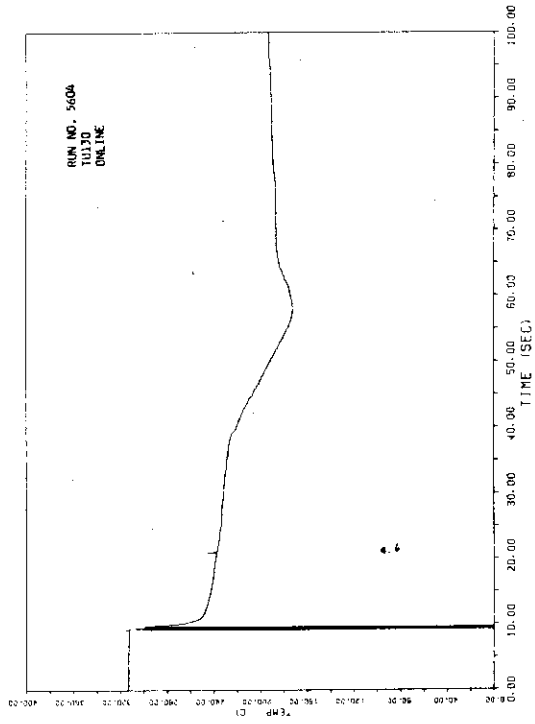

A.105

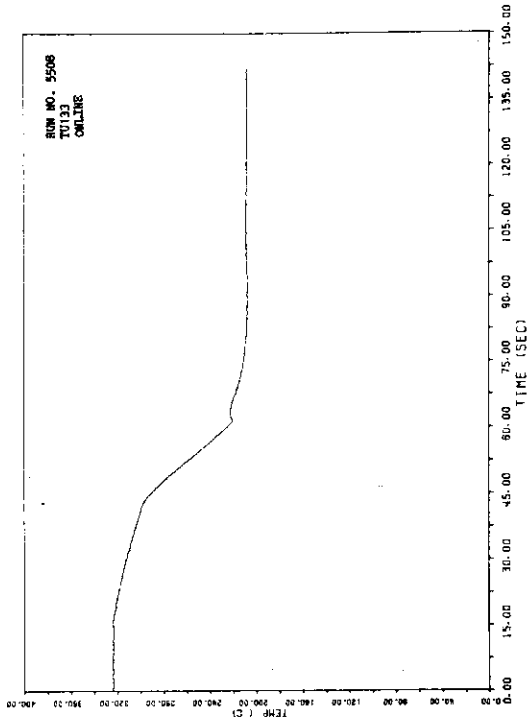

A.104

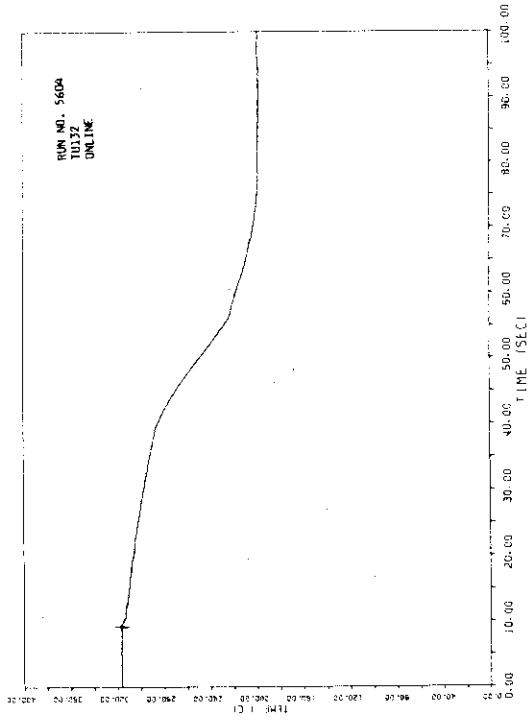

A.106

(d) Strains of the test pipe (A.107-A.218)

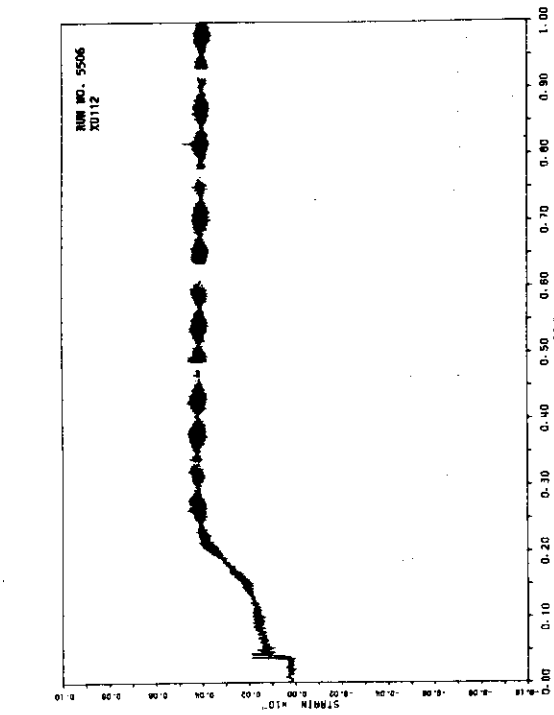

A.108

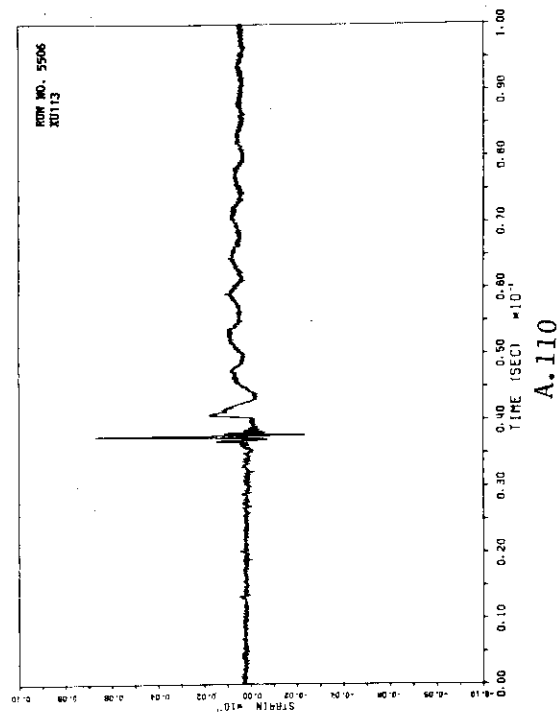

A.110

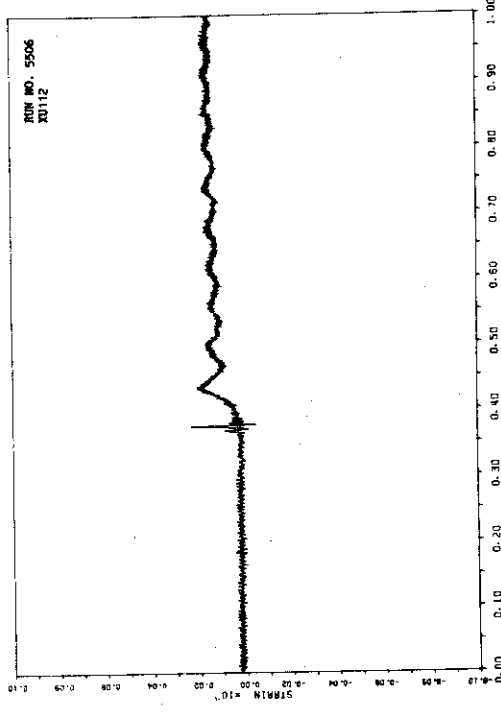

A.107

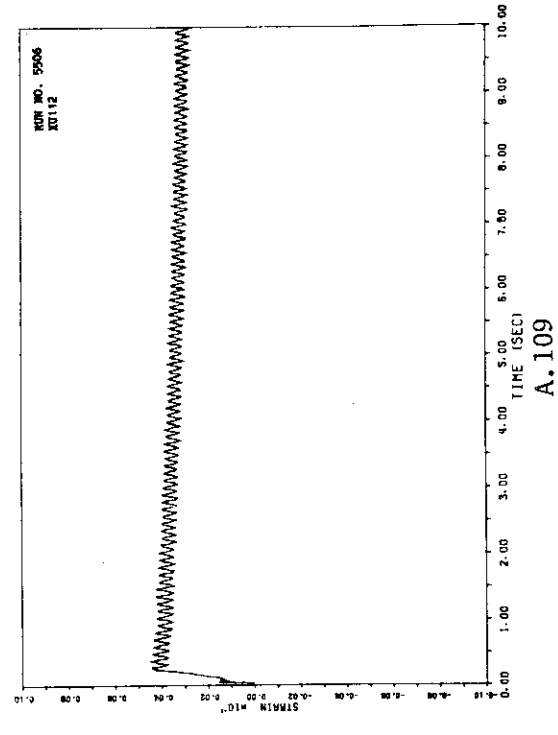

A.109

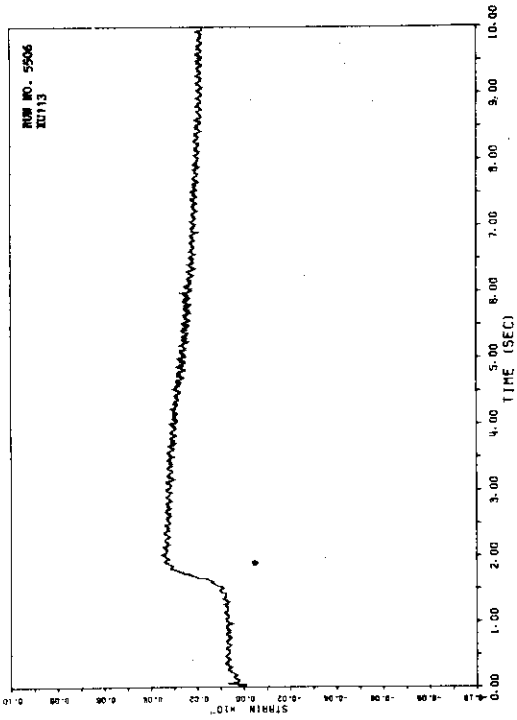

A.112

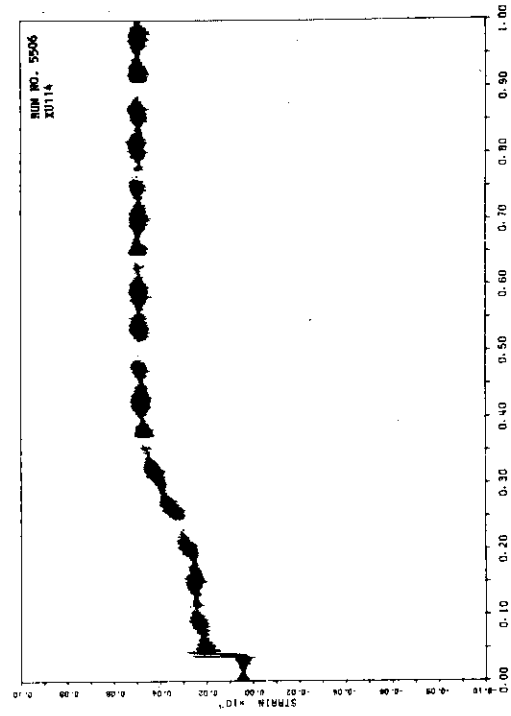

A.114

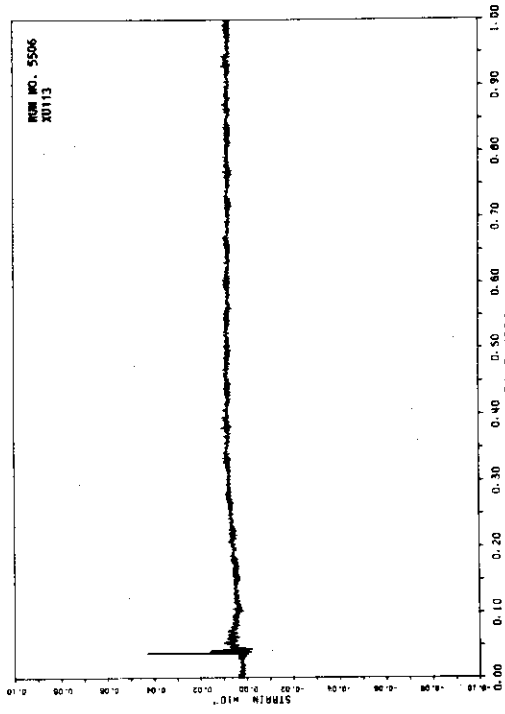

A.111

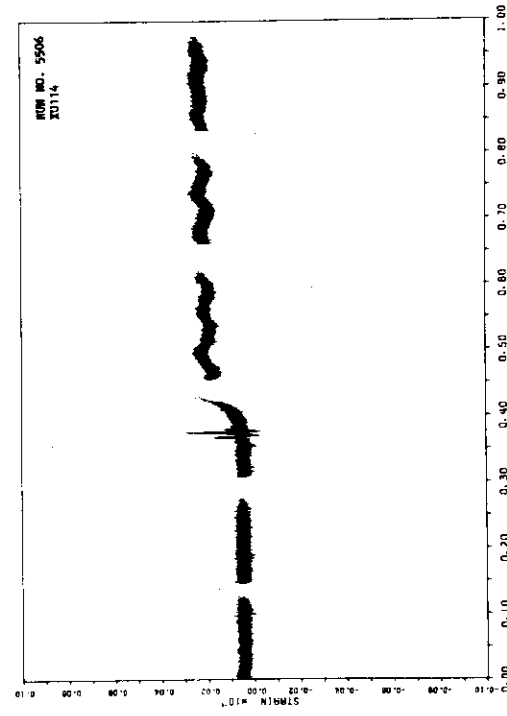

A.113

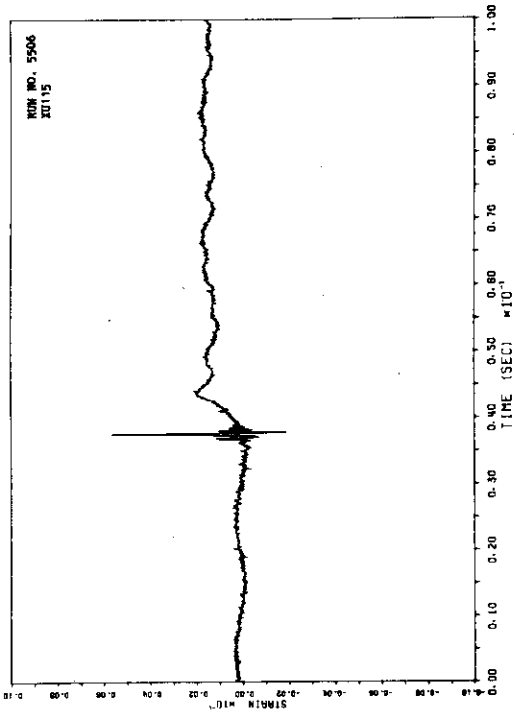

A.116

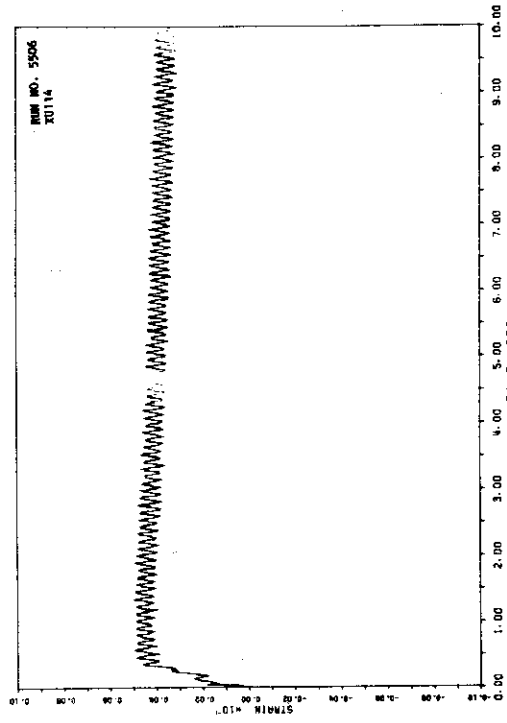

A.115

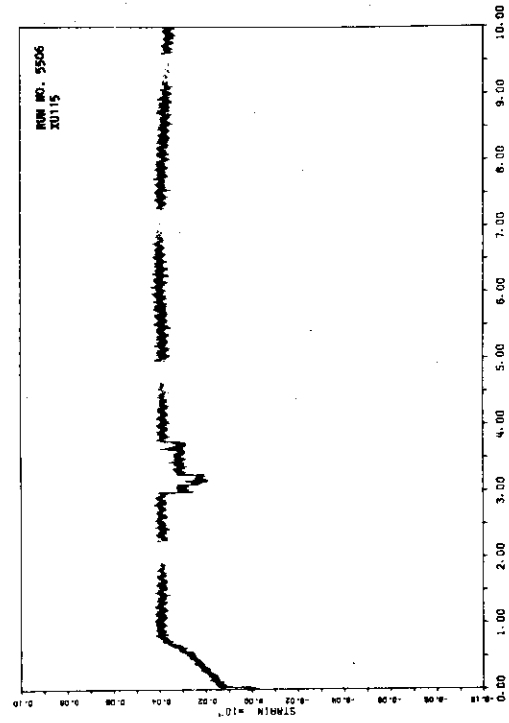

A.118

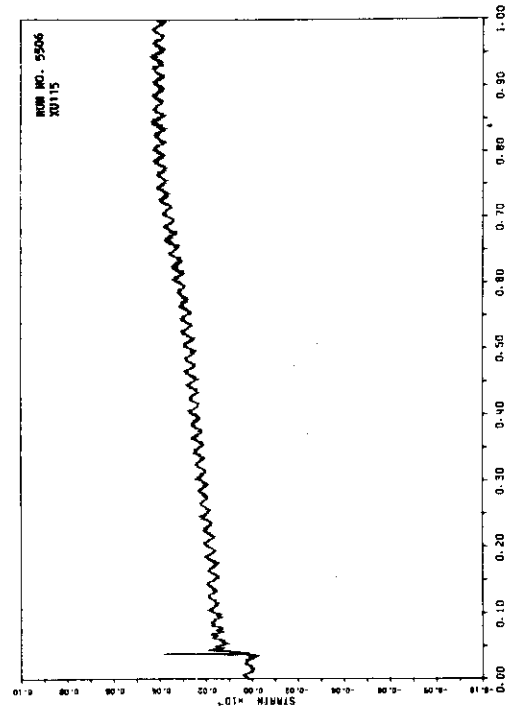

A.117

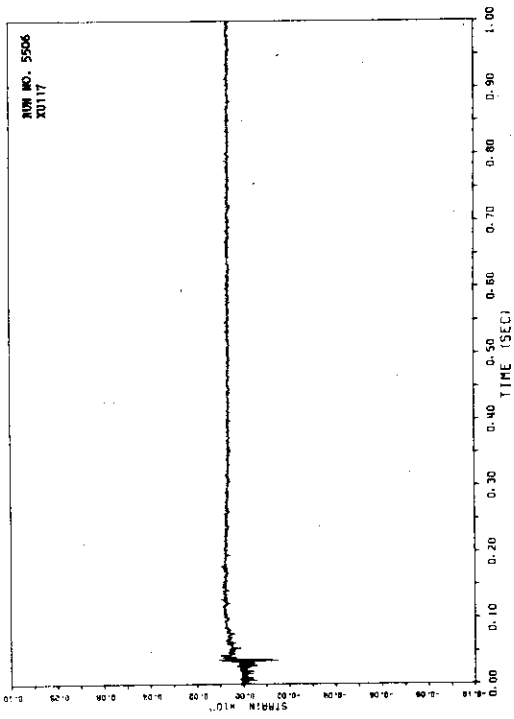

A.120

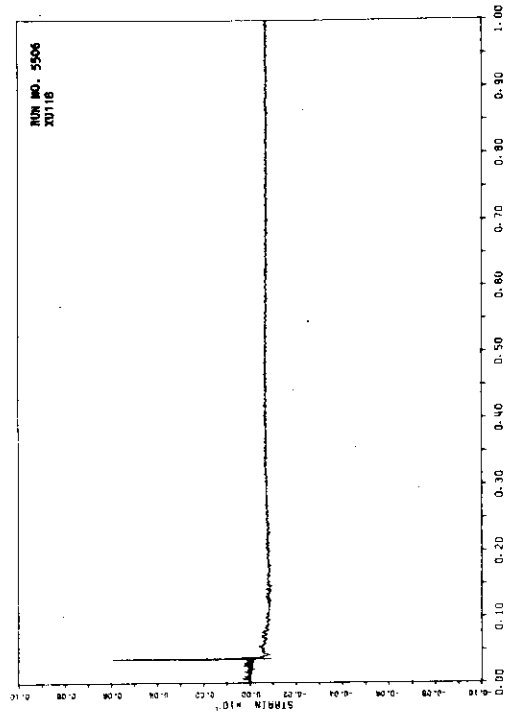

A.122

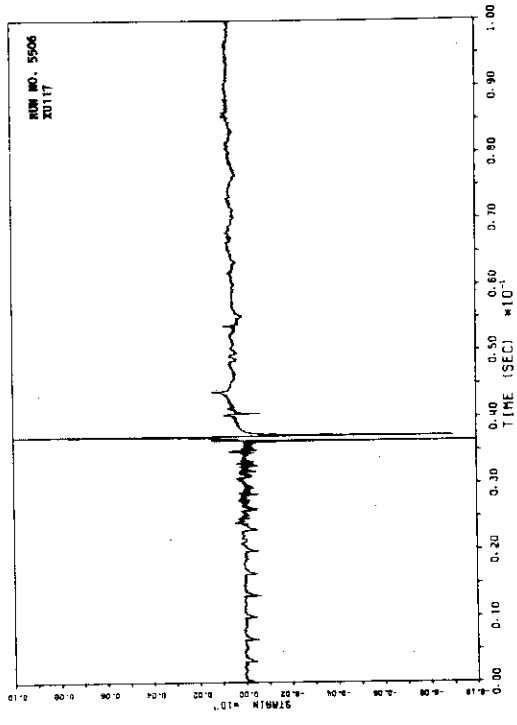

A.119

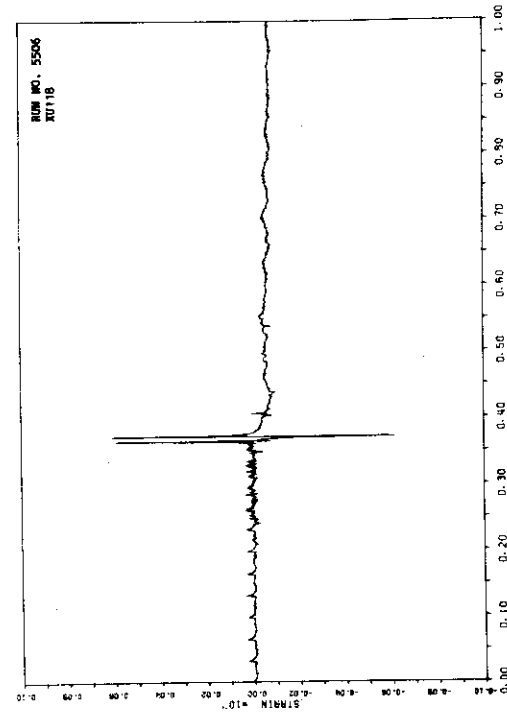

A.121

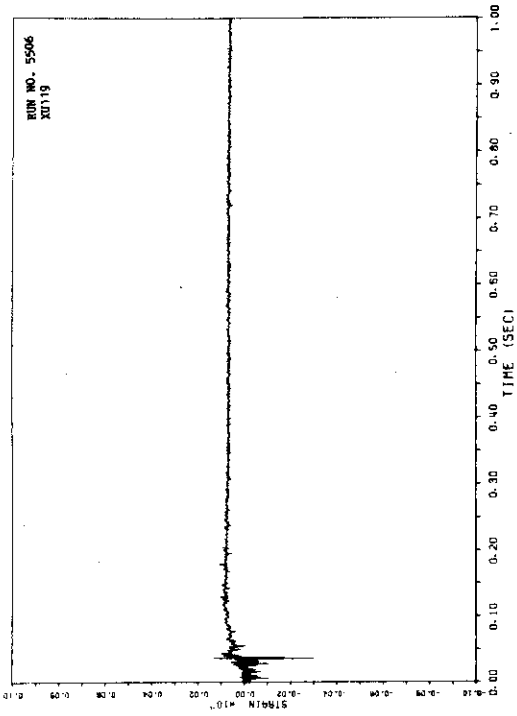

A.124

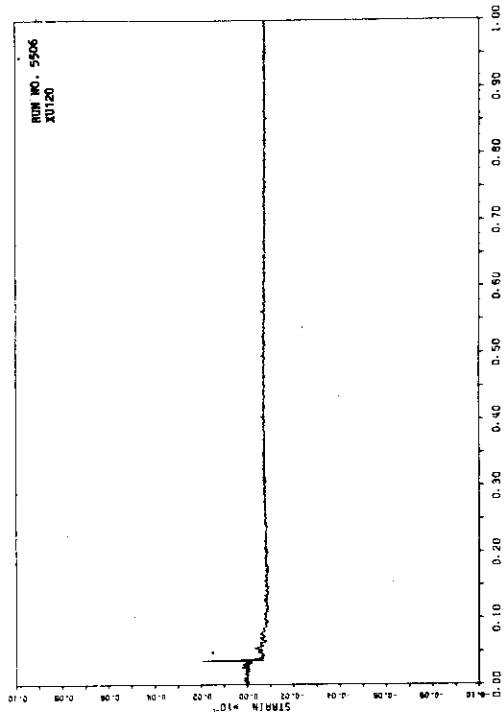

A.126

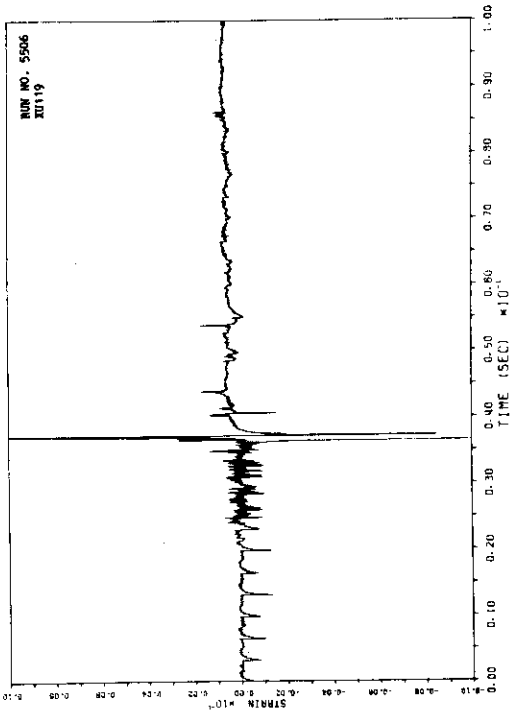

A.123

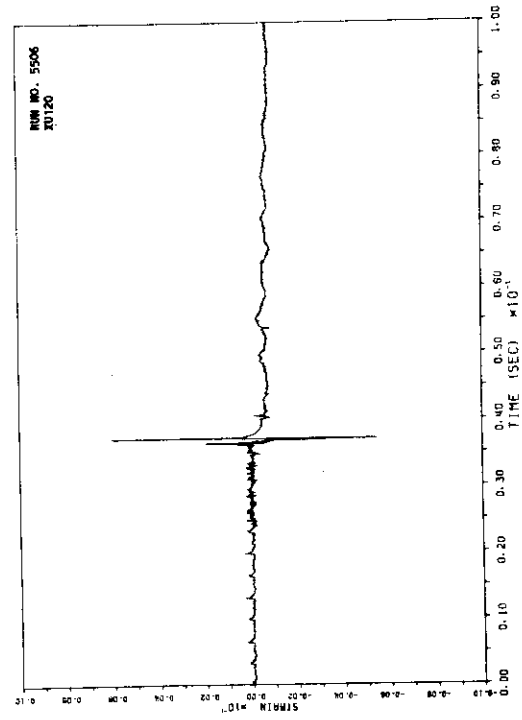

A.125

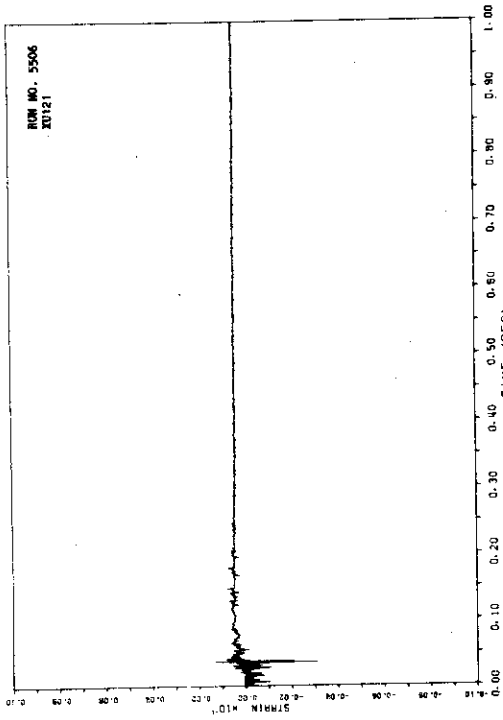

A.128

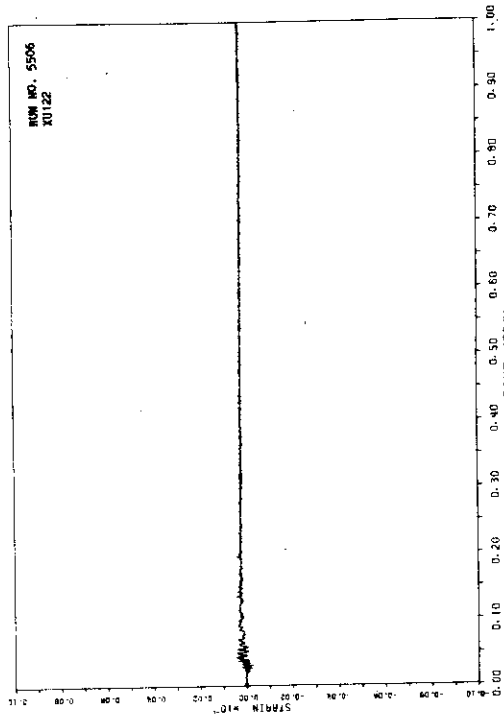

A.130

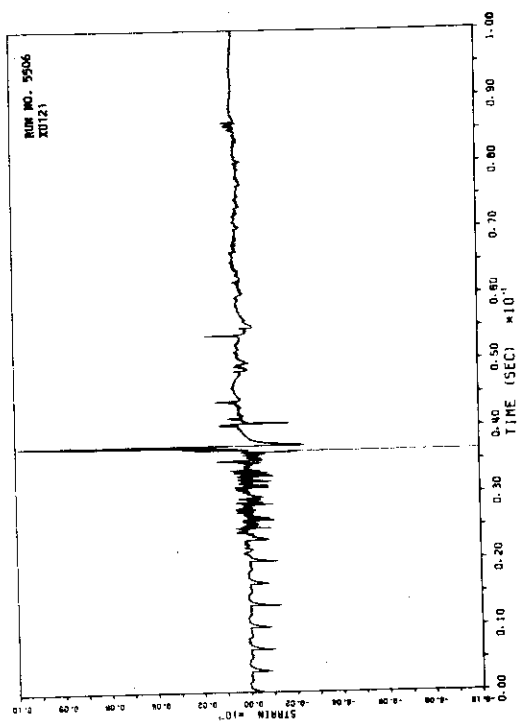

A.127

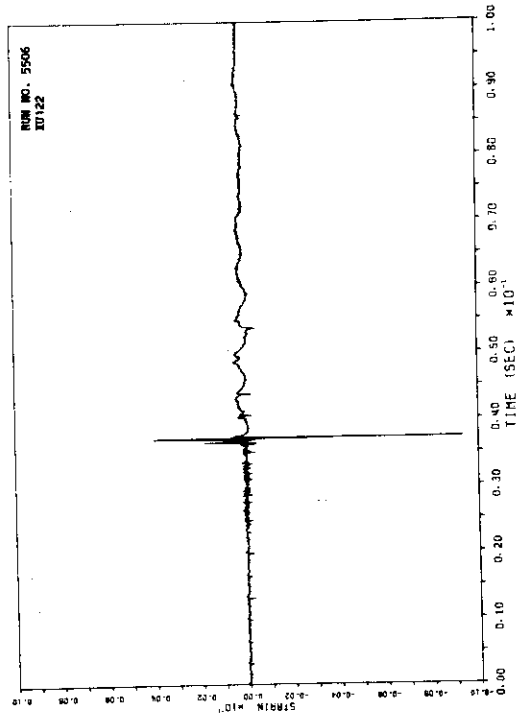

A.129

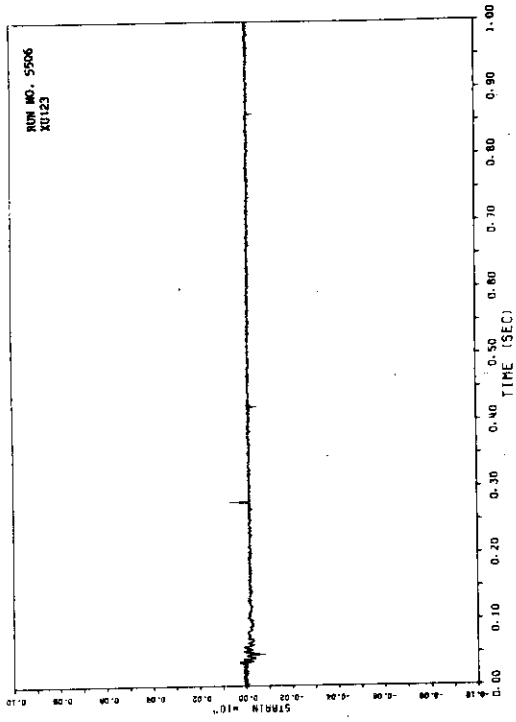

A.132

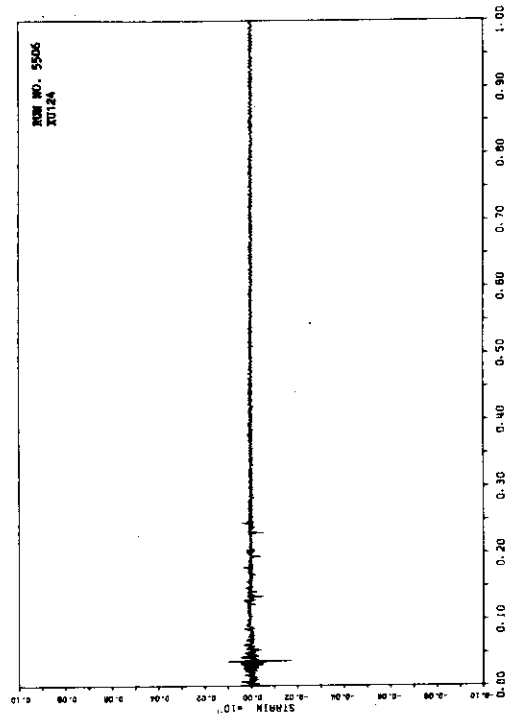

A.134

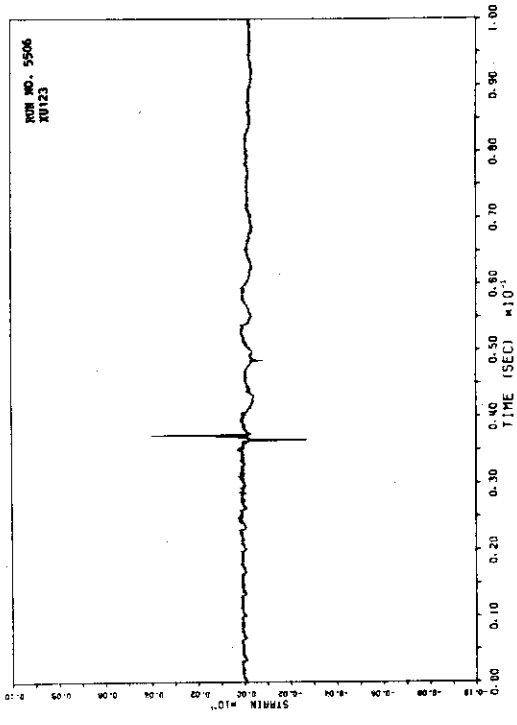

A.131

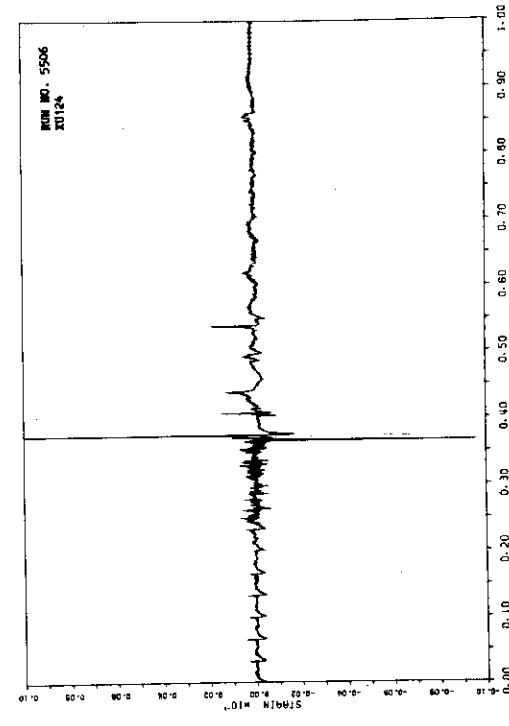

A.133

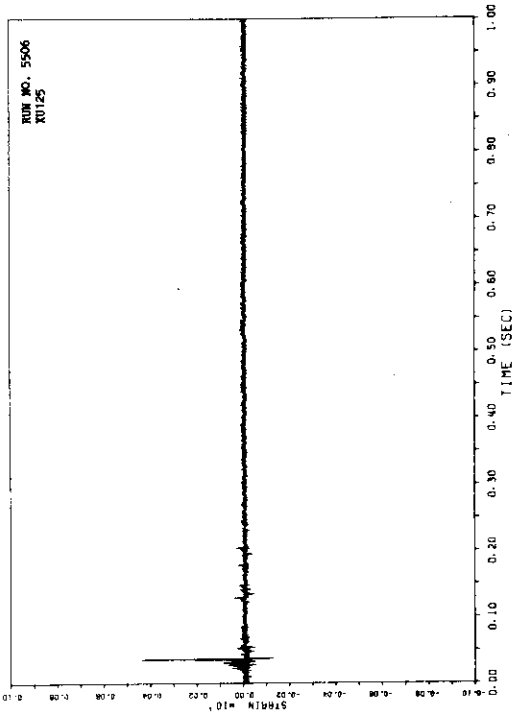

A.136

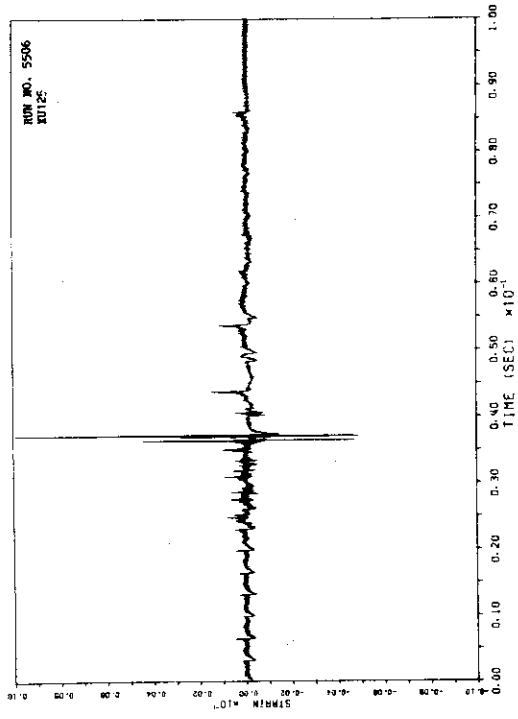

A.135

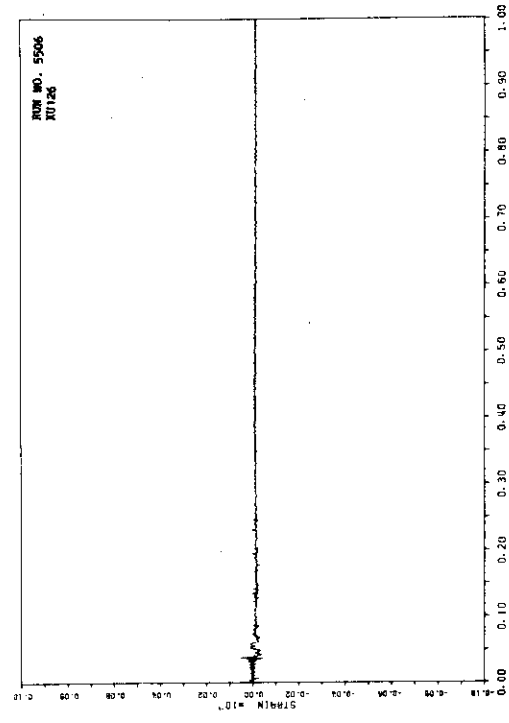

A.138

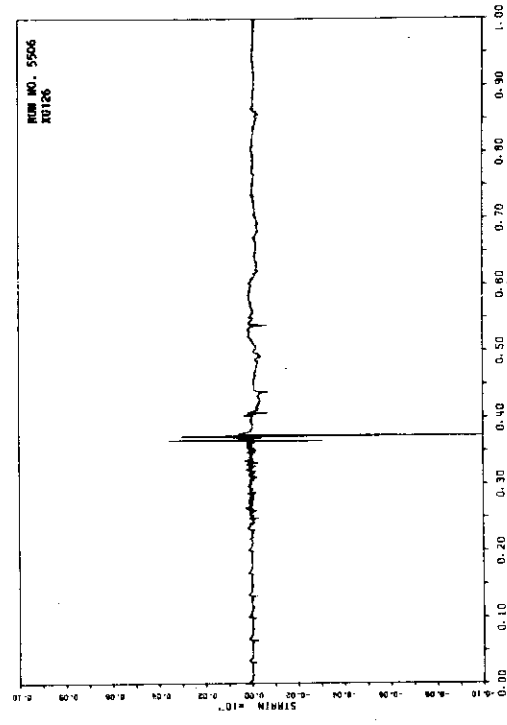

A.137

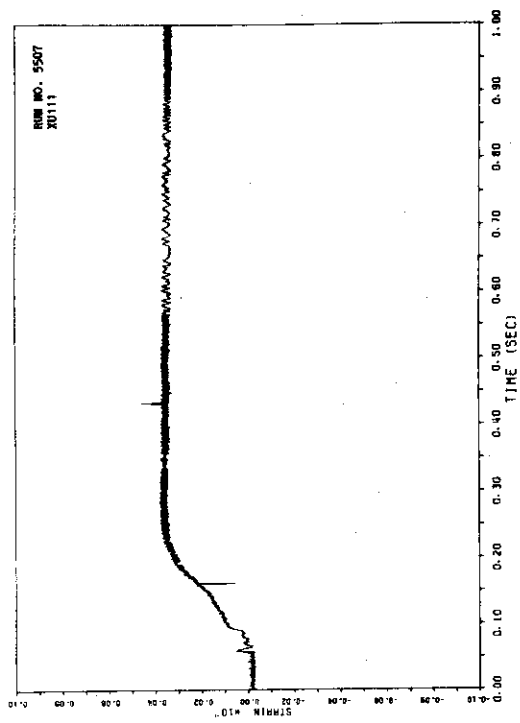

A.140

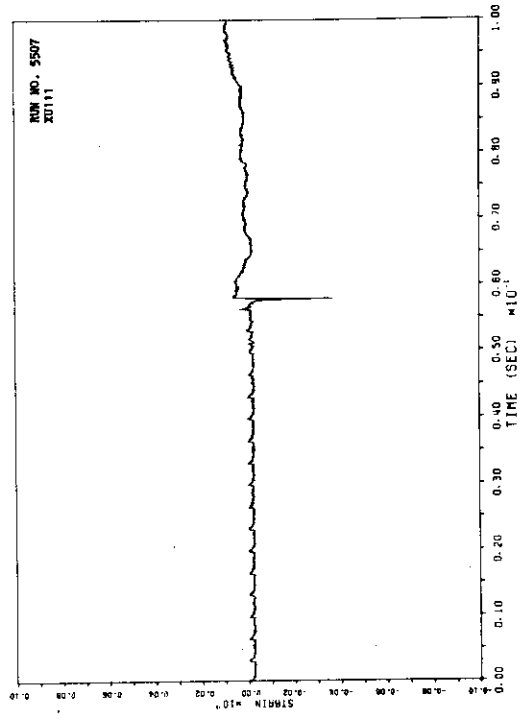

A.139

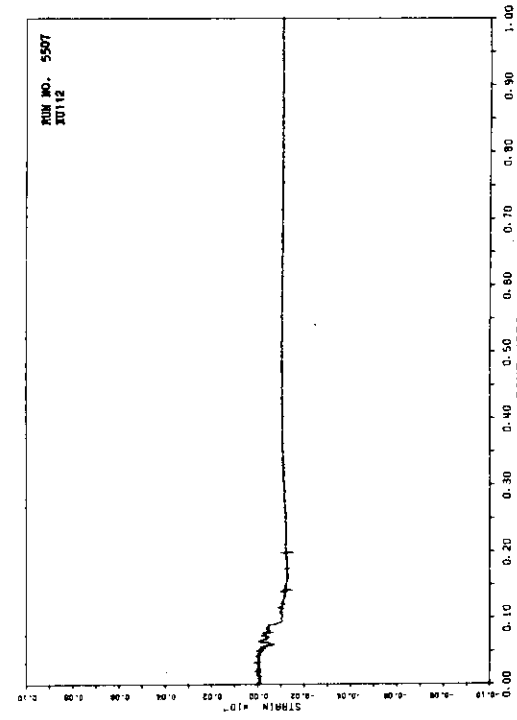

A.142

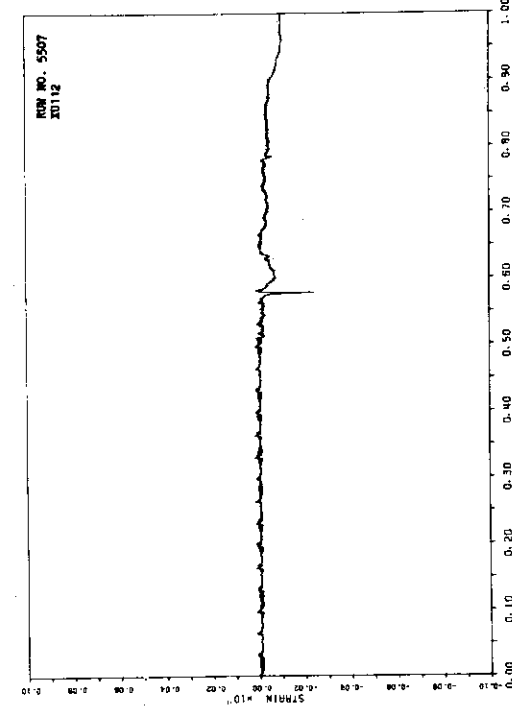

A.141

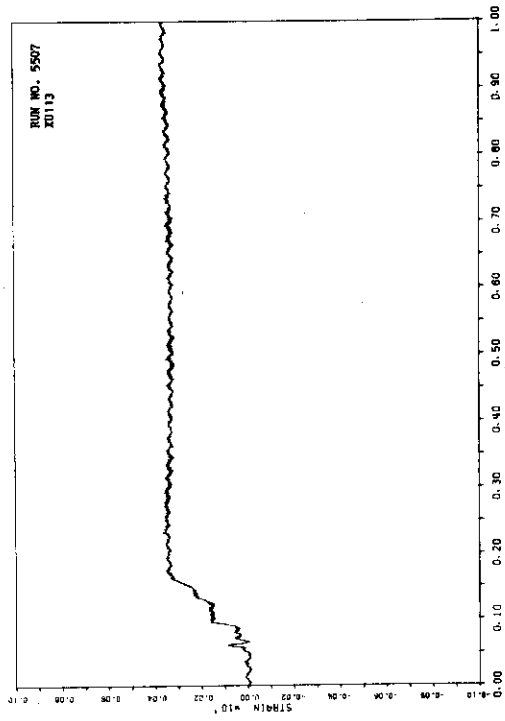

A.144

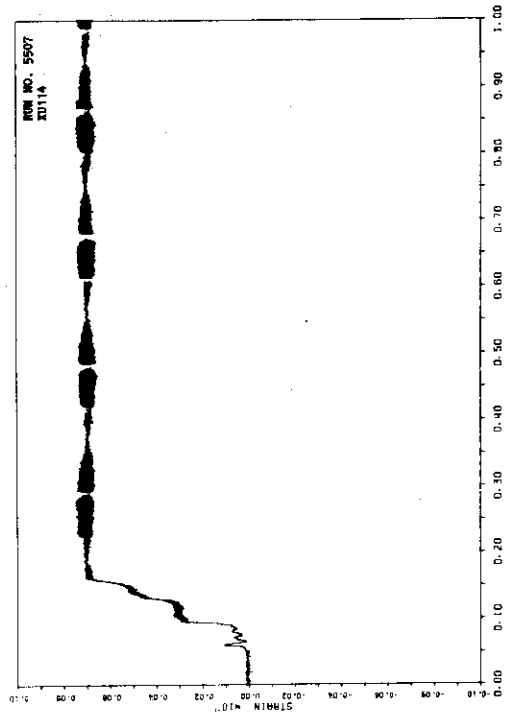

A.146

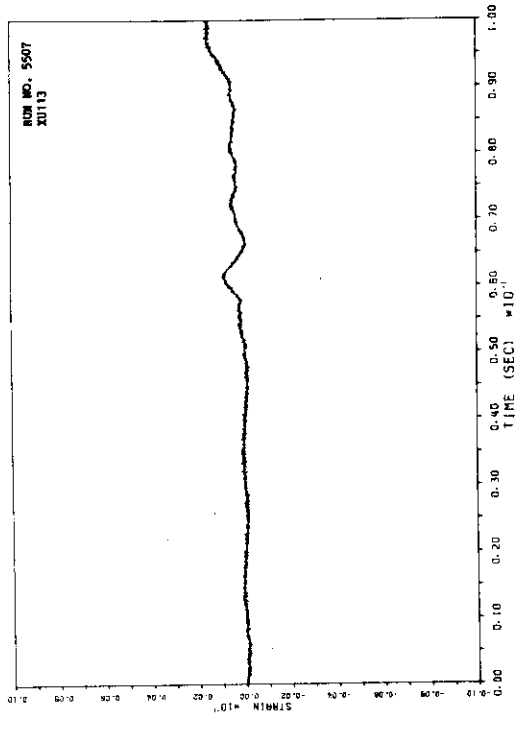

A.143

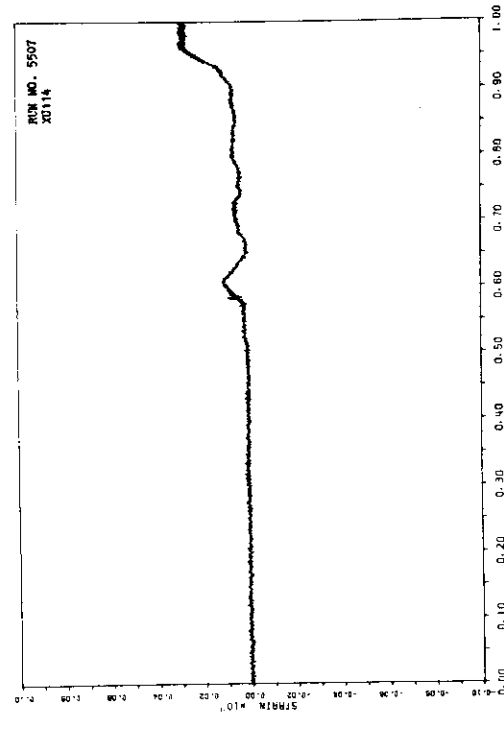

A.145

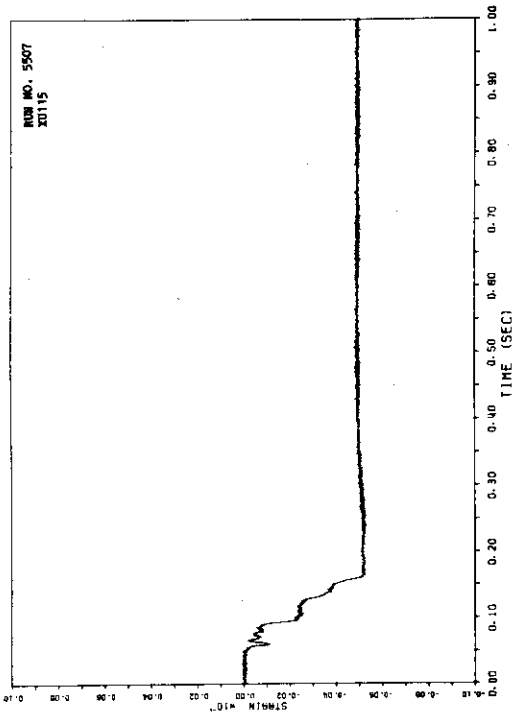

A.148

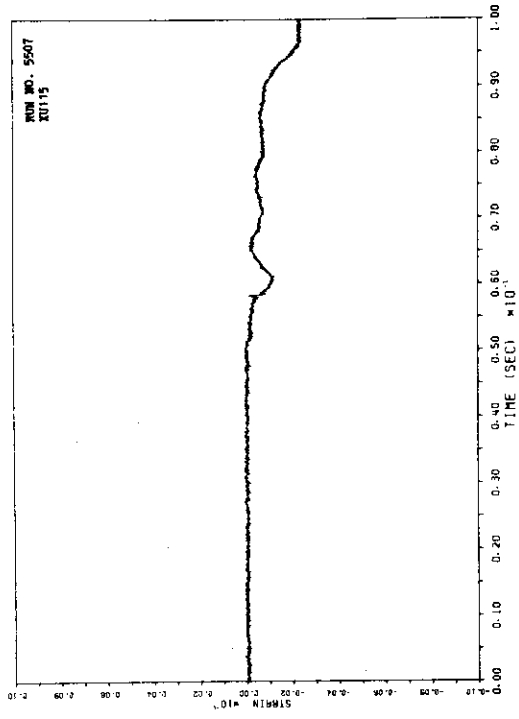

A.147

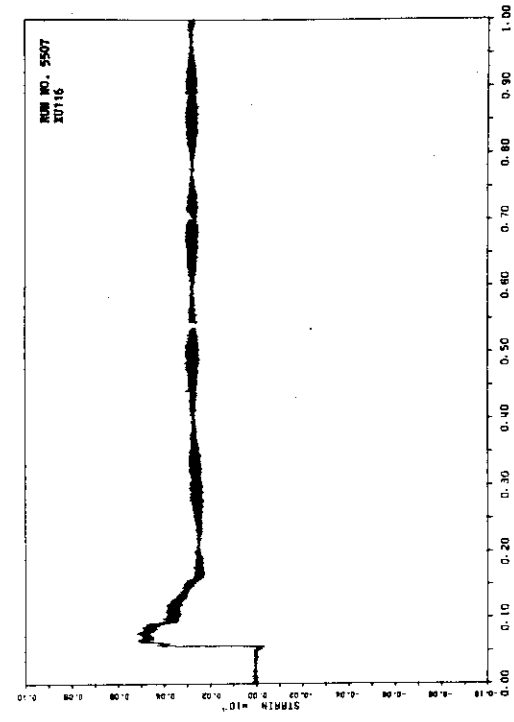

A.150

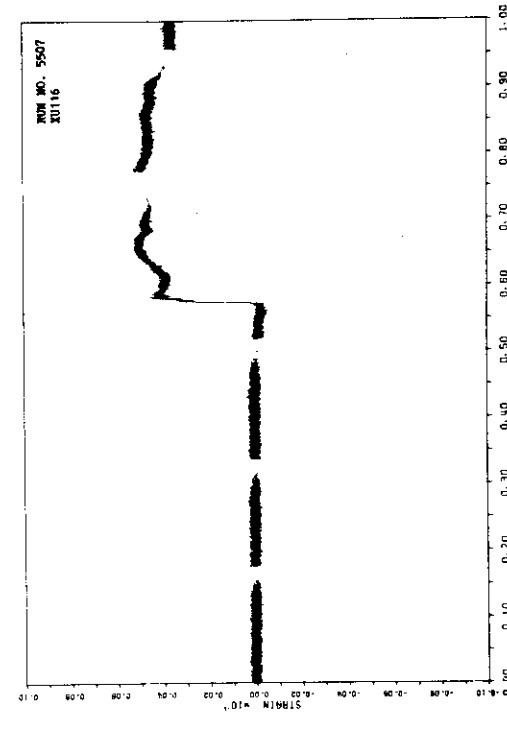

A.149

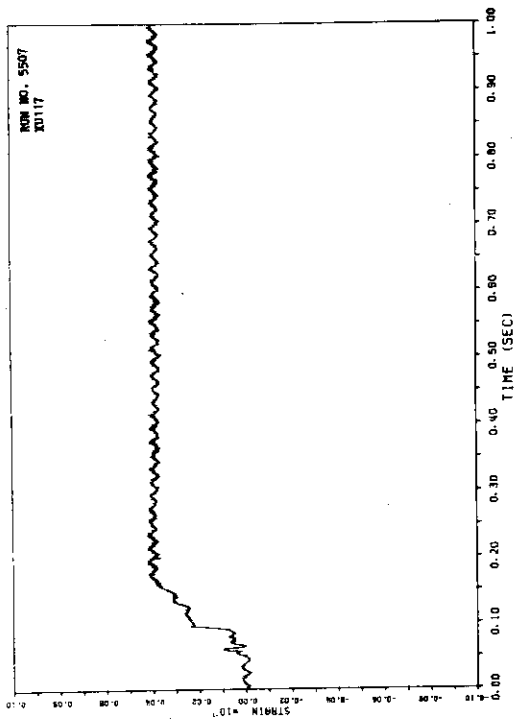

A.152

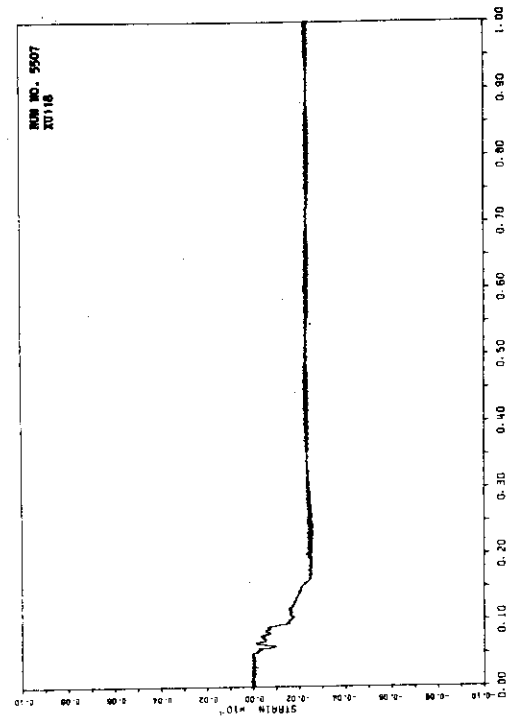

A.154

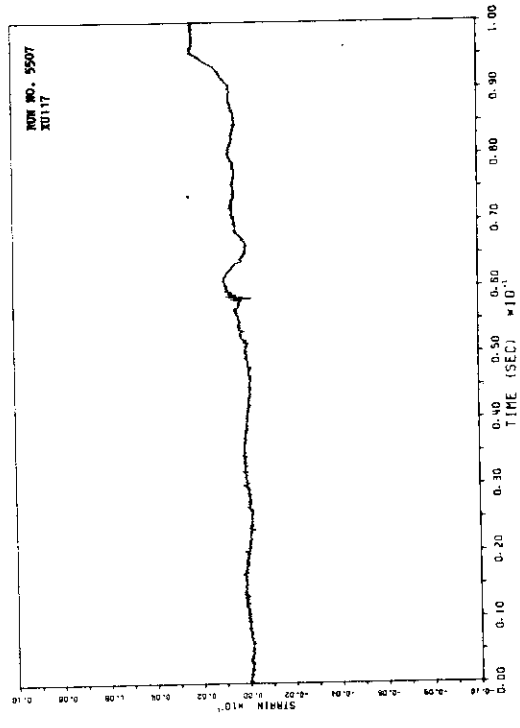

A.151

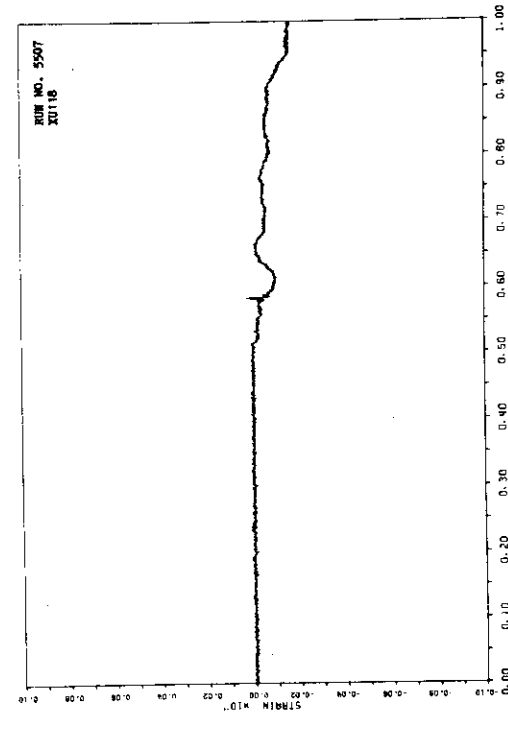

A.153

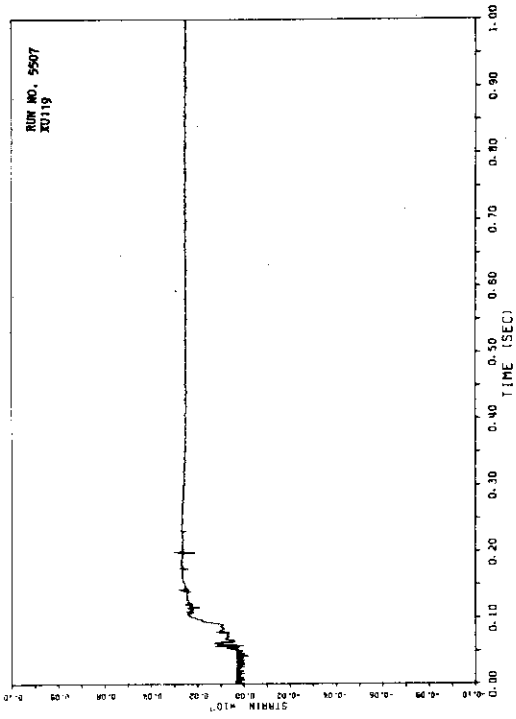

A.156

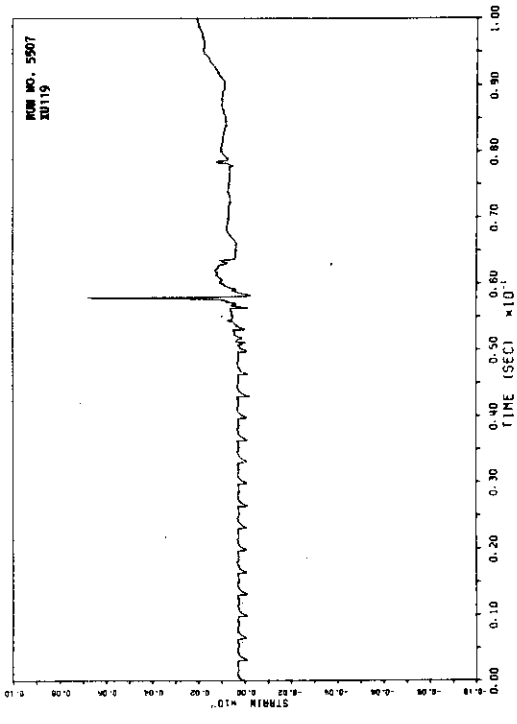

A.155

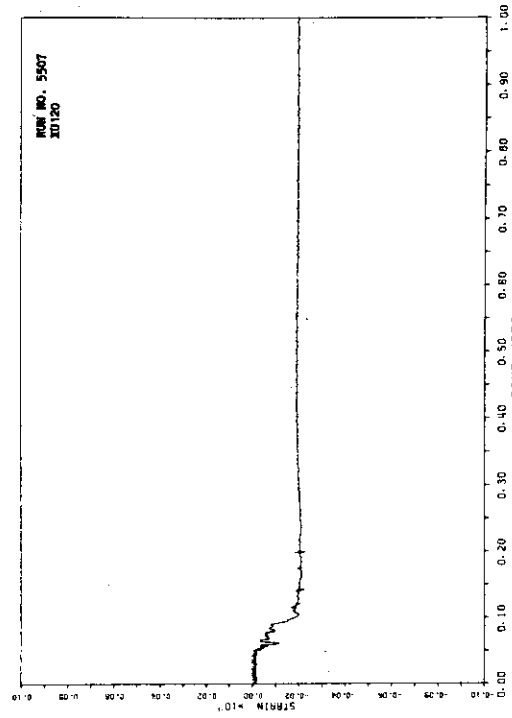

A.158

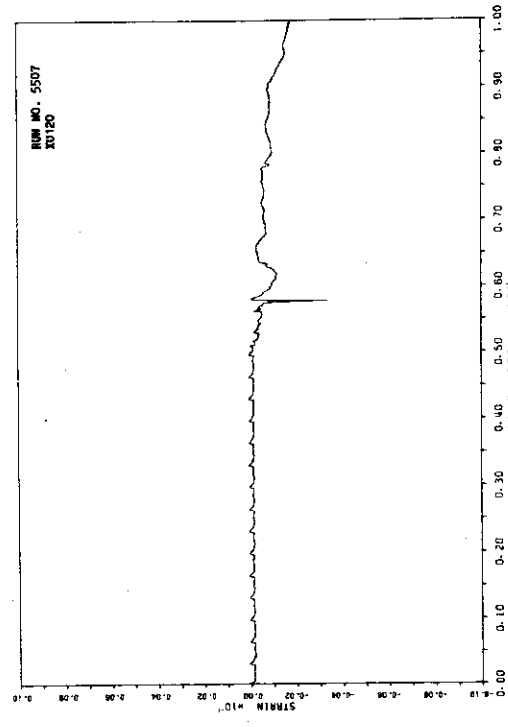

A.157

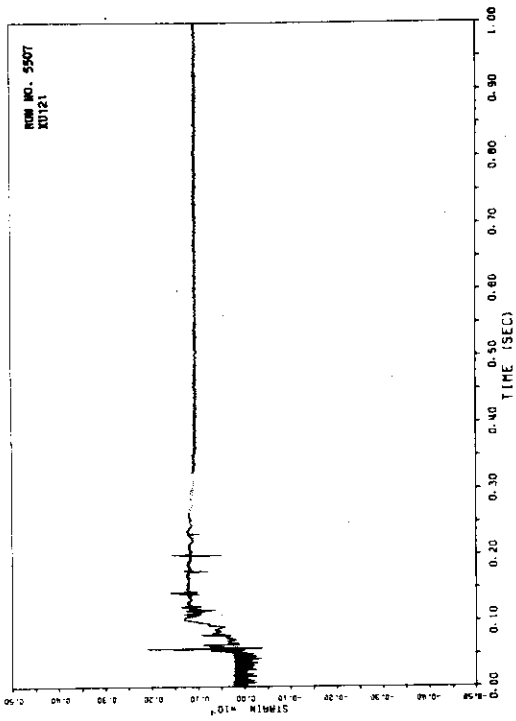

A.160

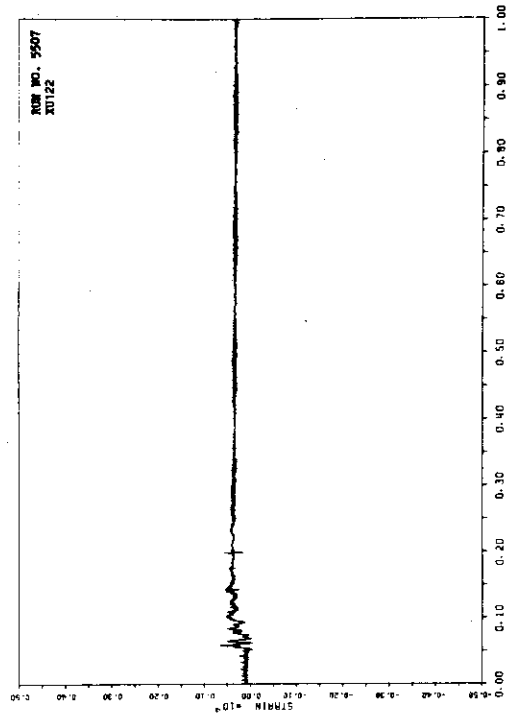

A.162

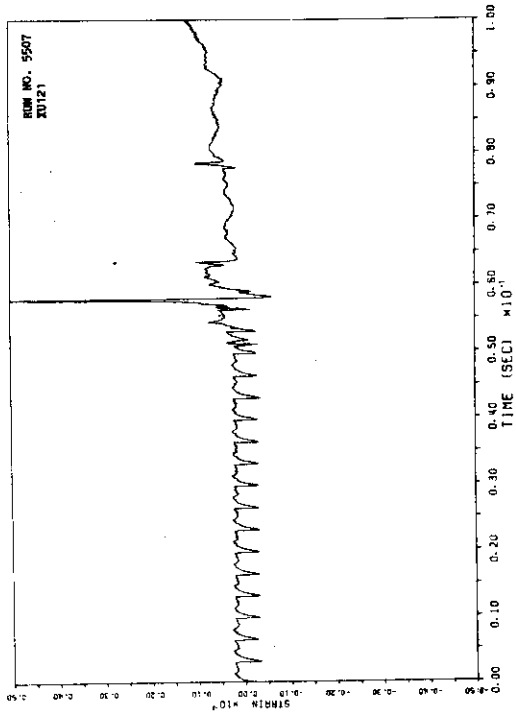

A.159

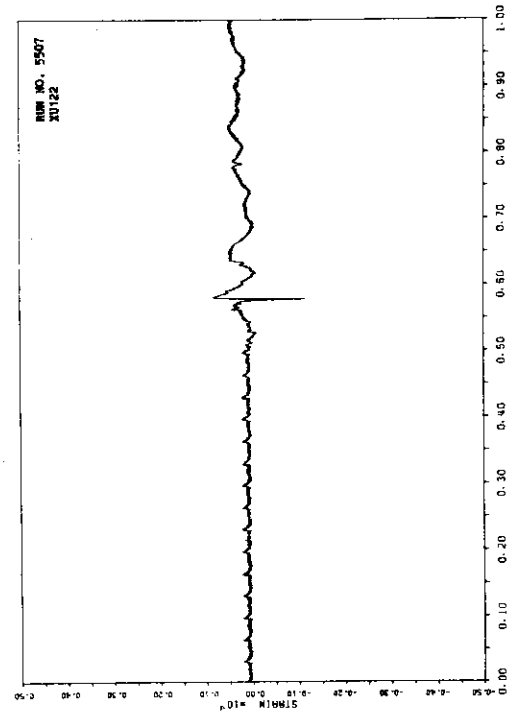

A.161

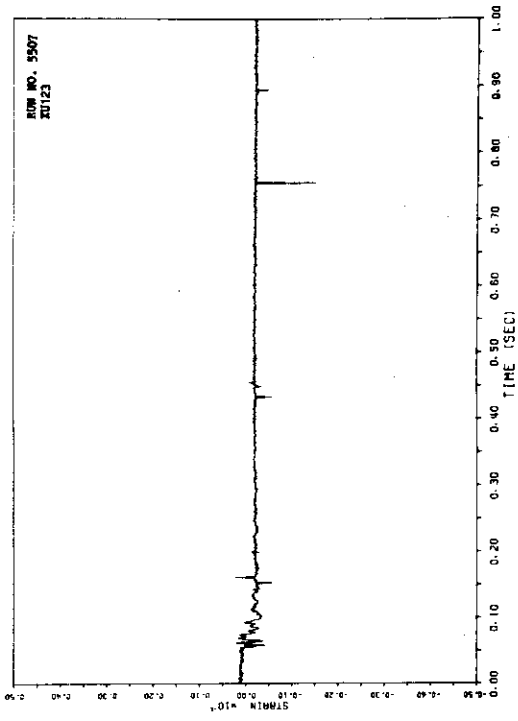

A.164

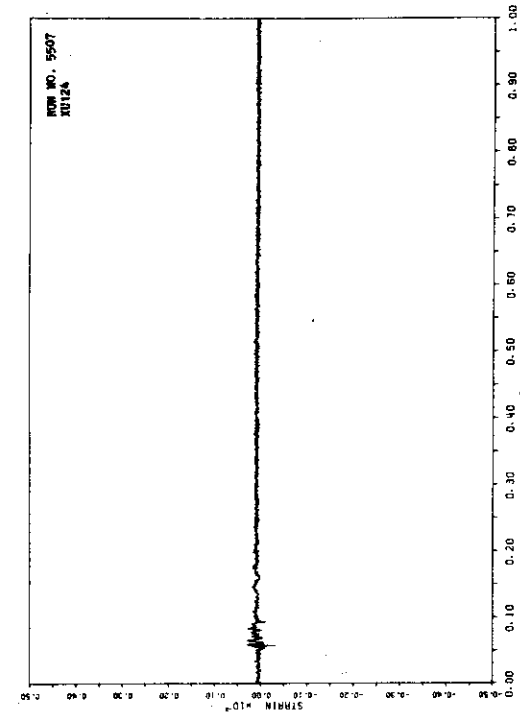

A.166

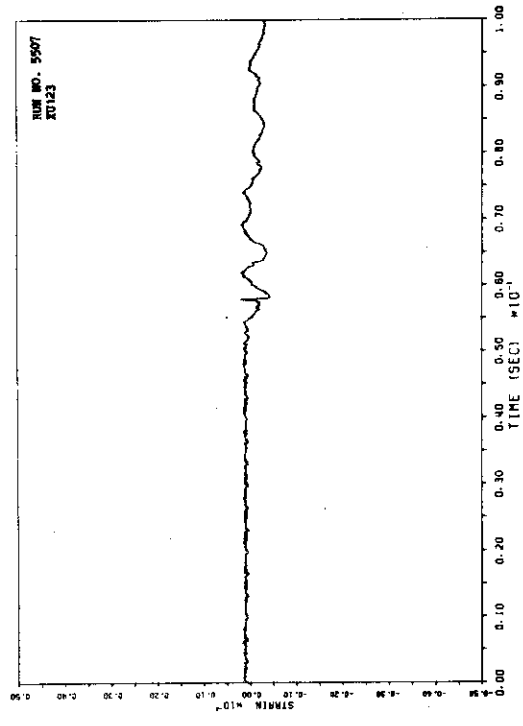

A.163

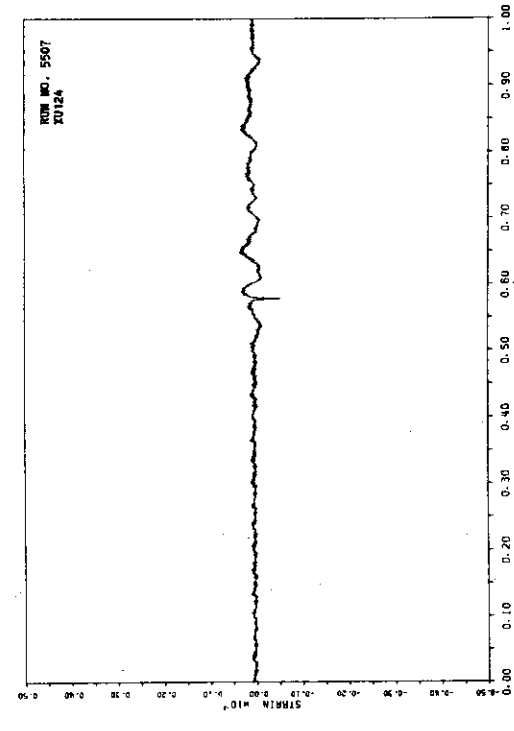

A.165

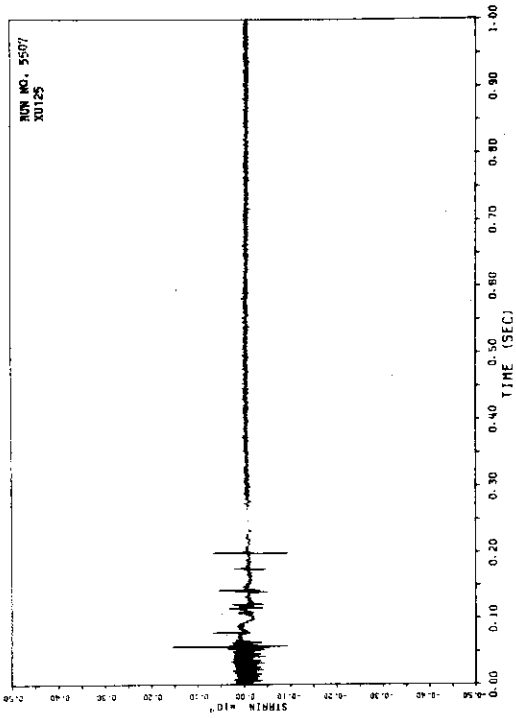

A.168

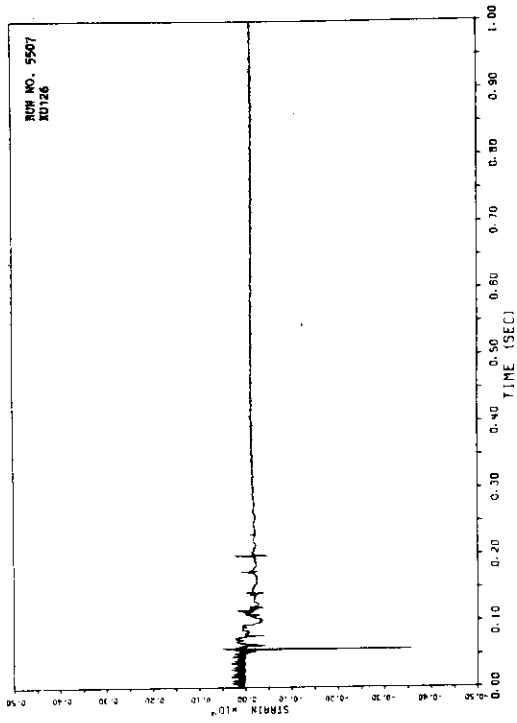

A.170

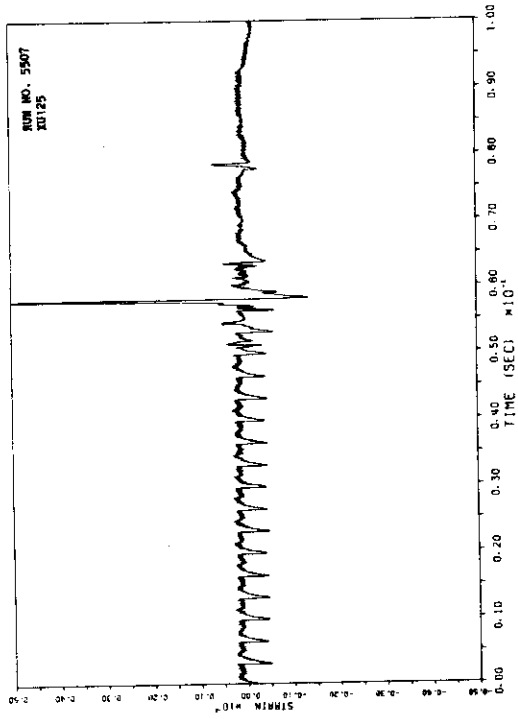

A.167

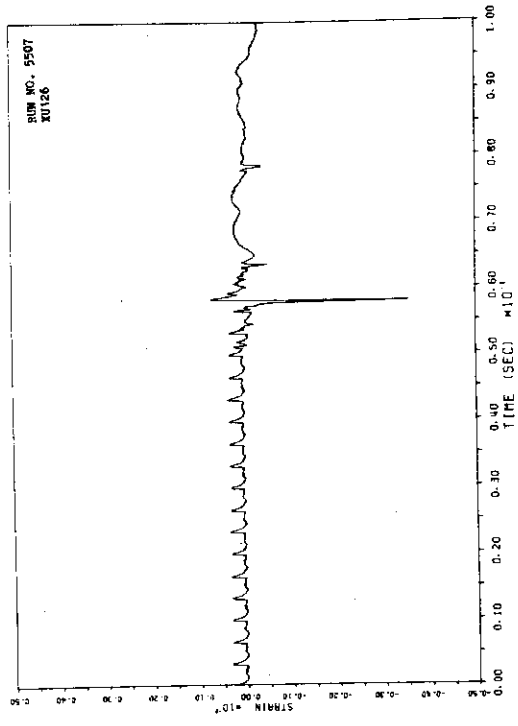

A.169

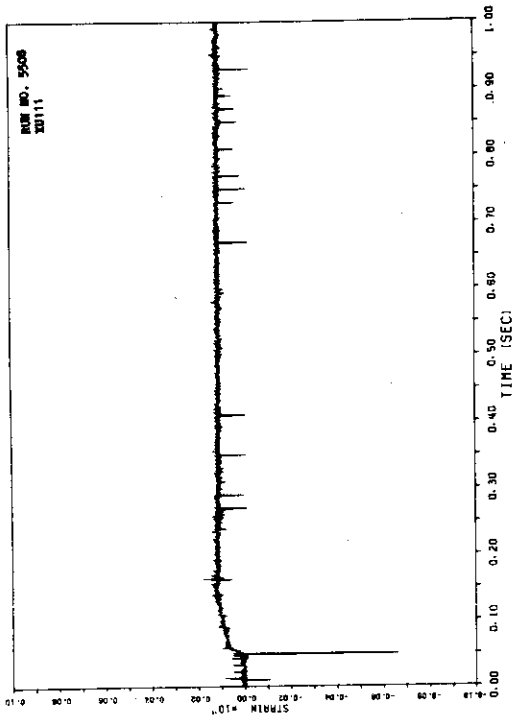

A.172

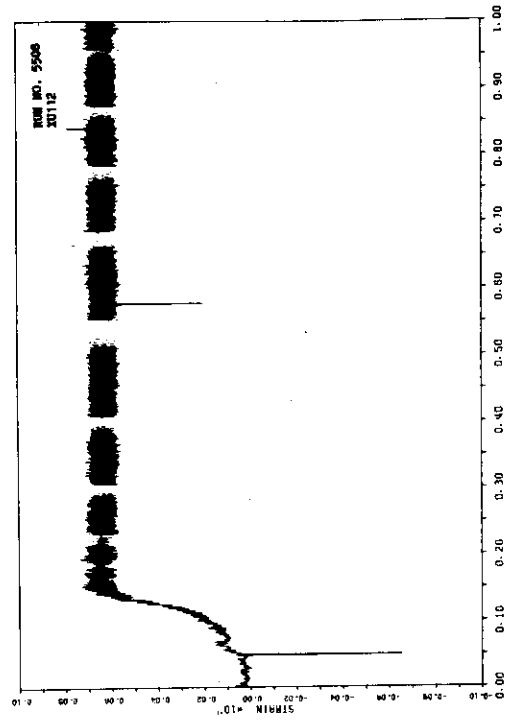

A.174

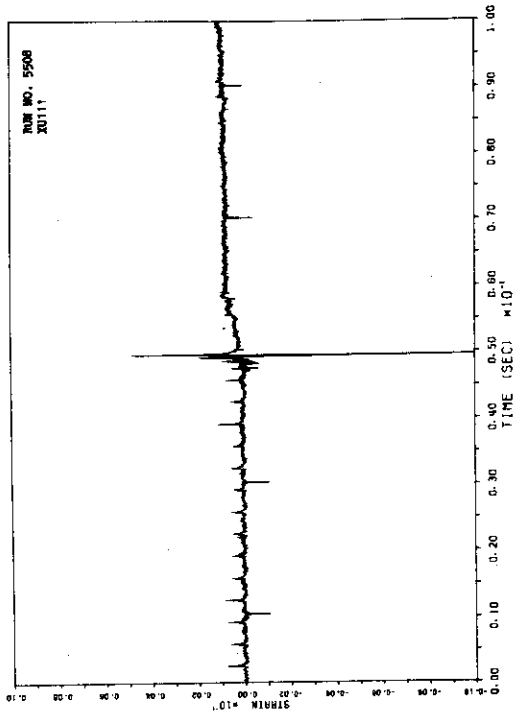

A.171

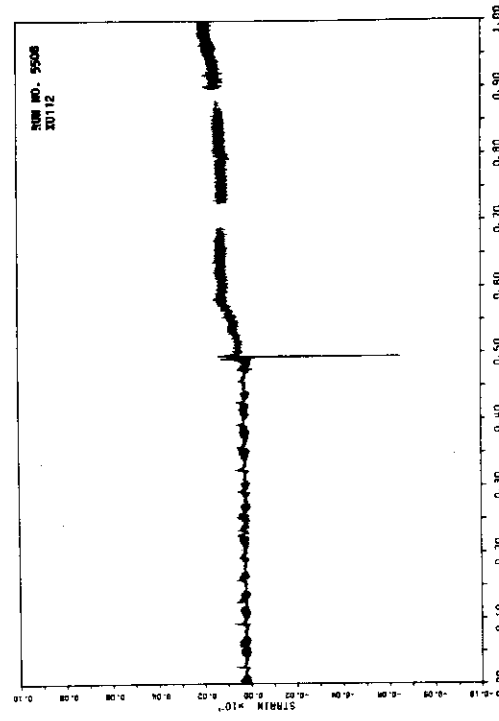

A.173

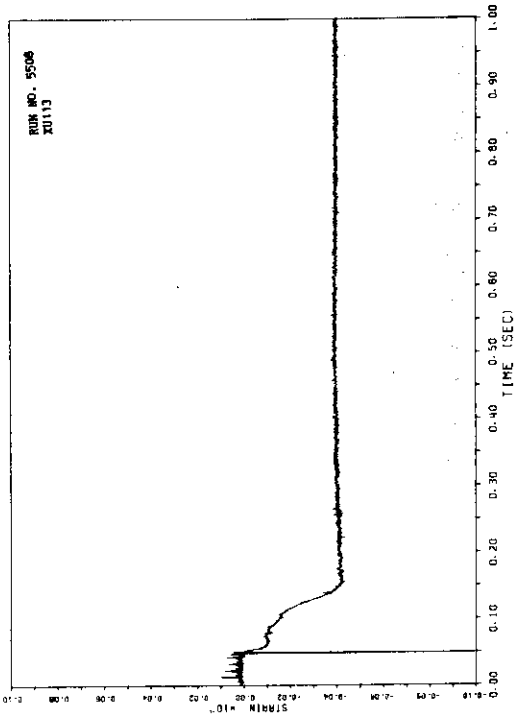

A.176

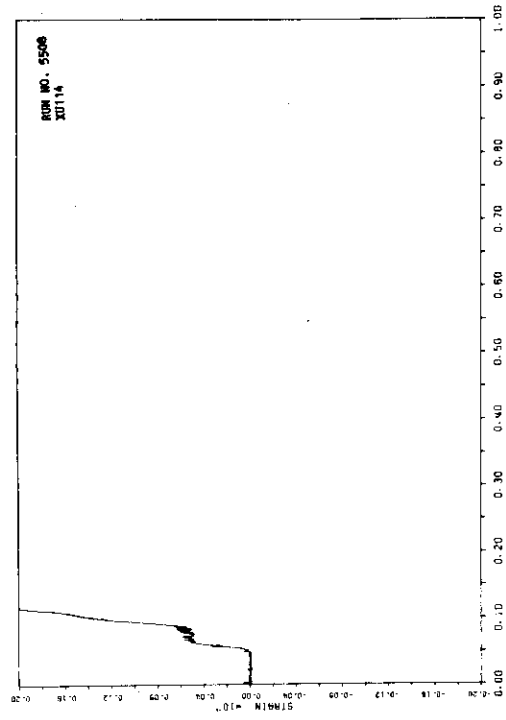

A.178

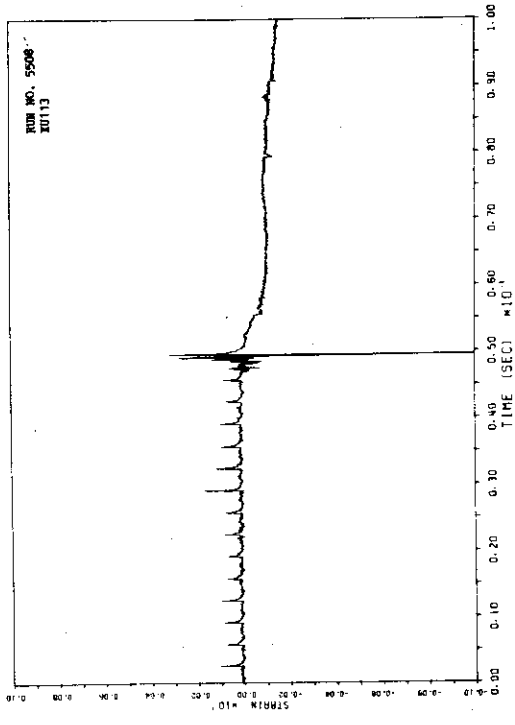

A.175

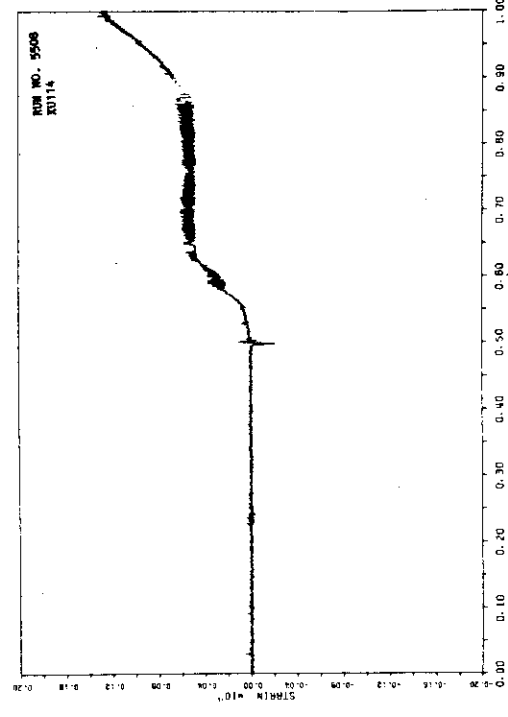

A.177

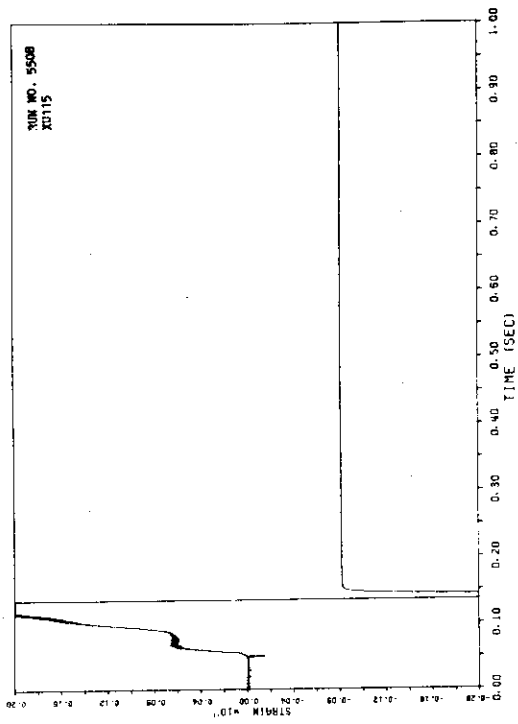

A.180

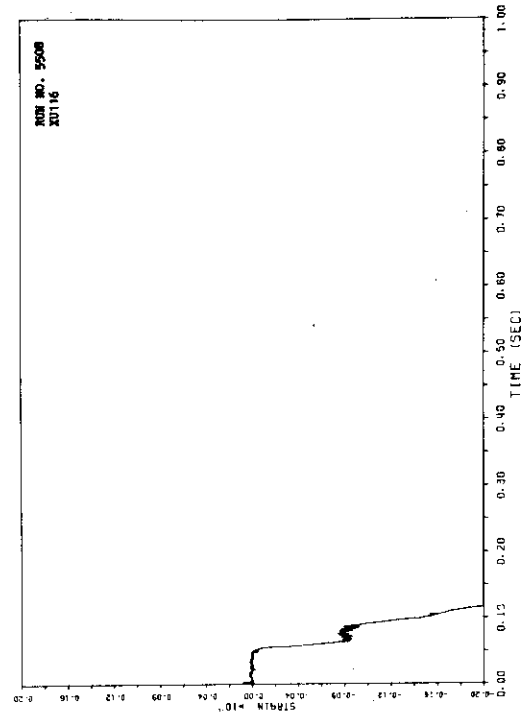

A.182

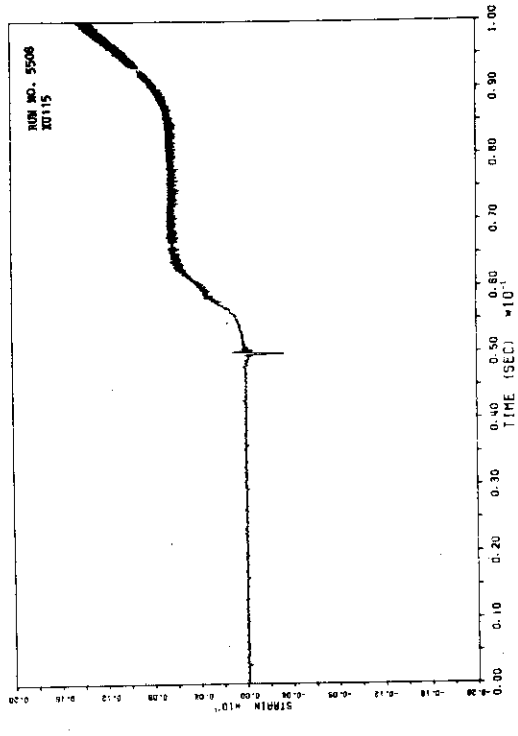

A.179

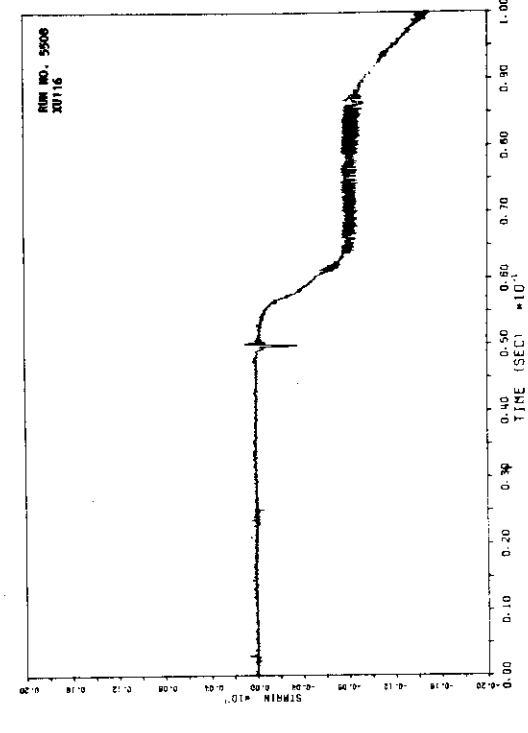

A.181

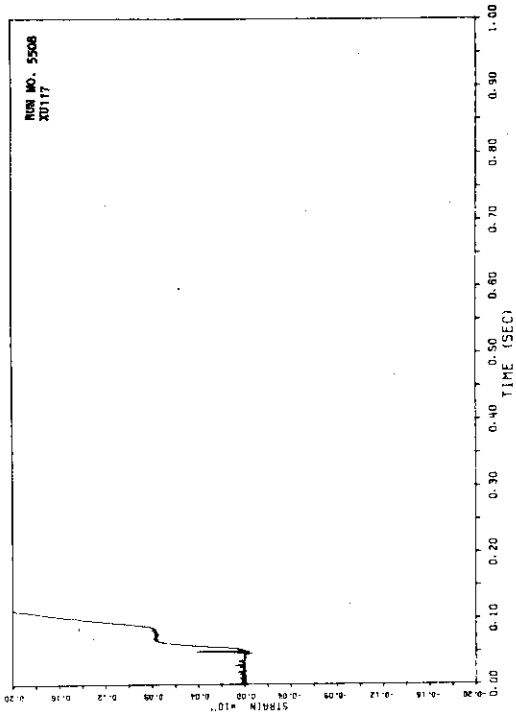

A.184

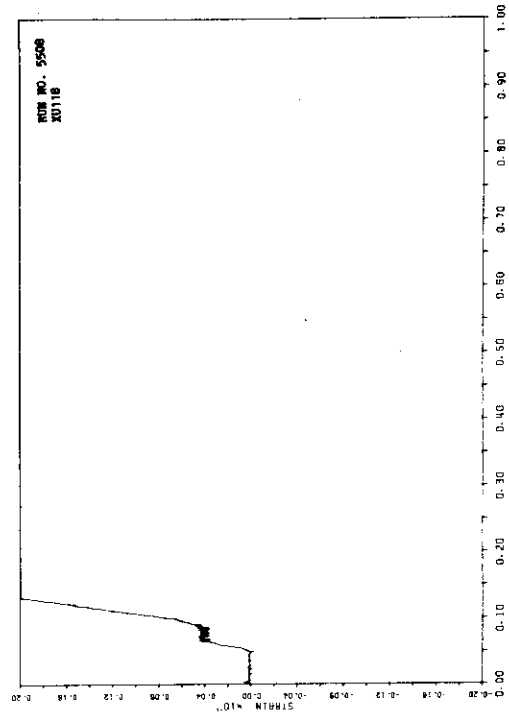

A.186

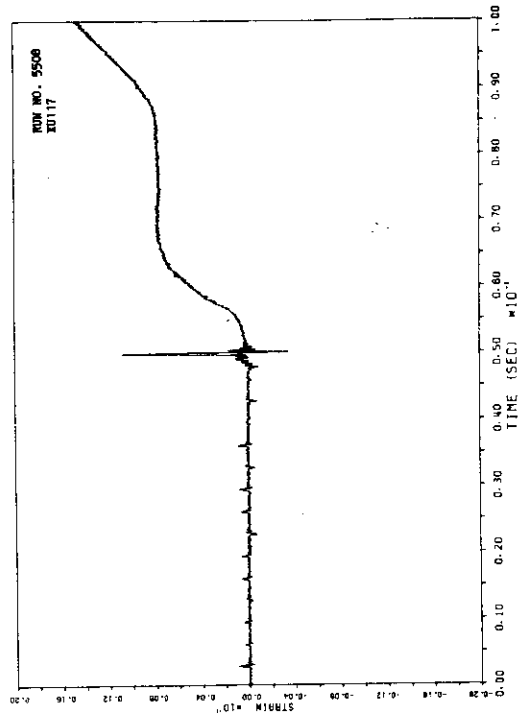

A.183

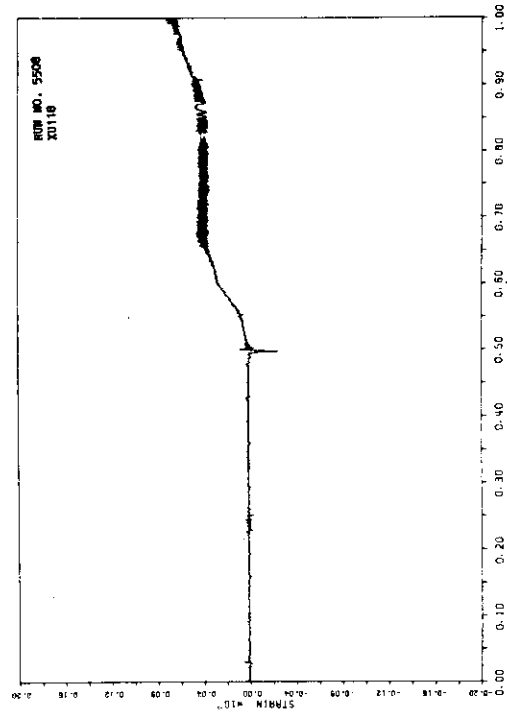

A.185

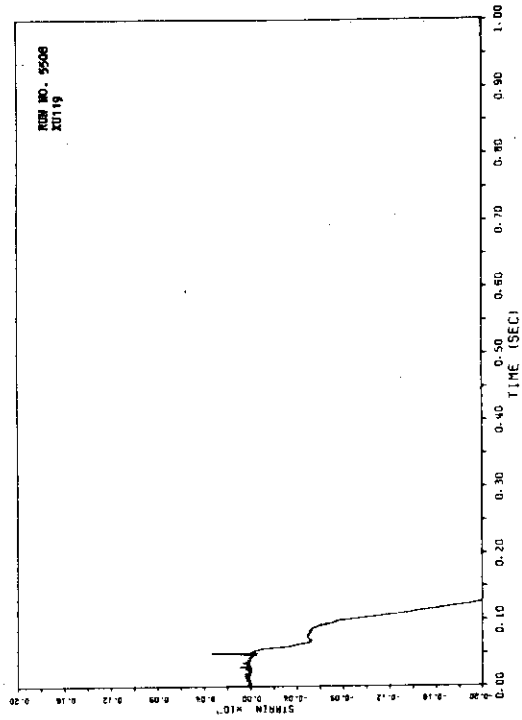

A.188

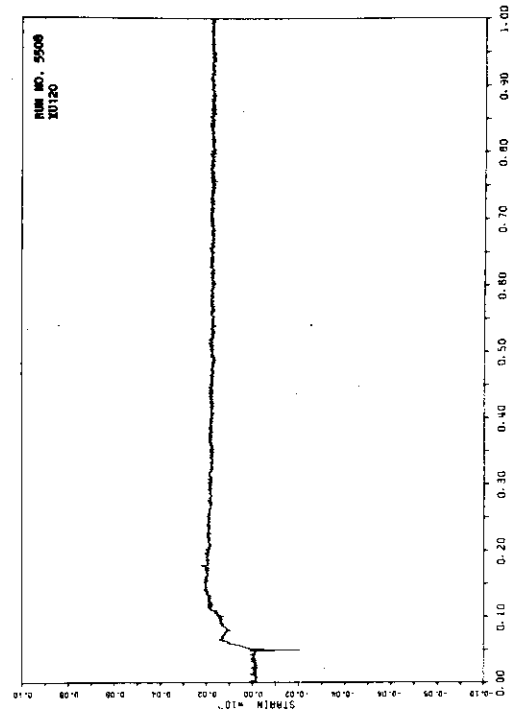

A.190

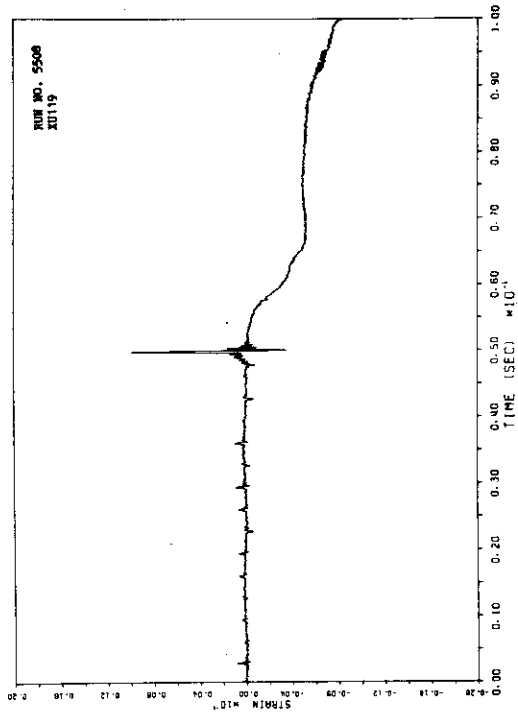

A.187

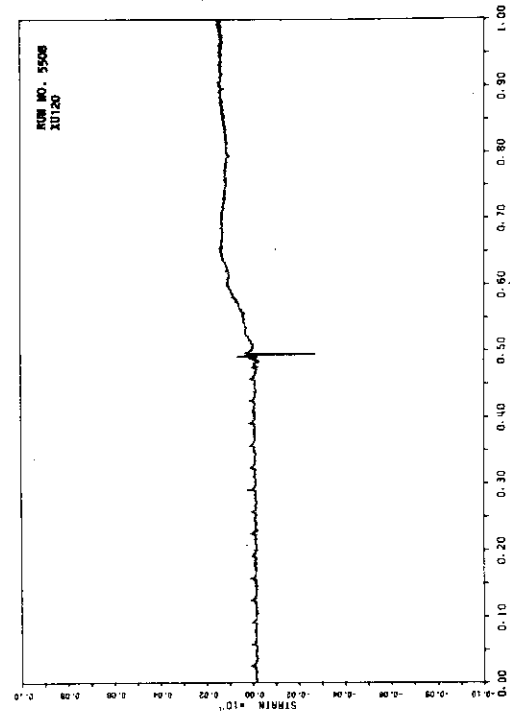

A.189

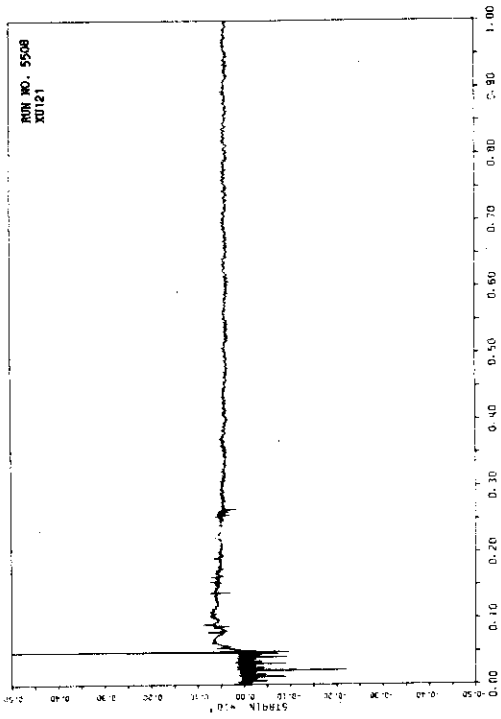

A.192

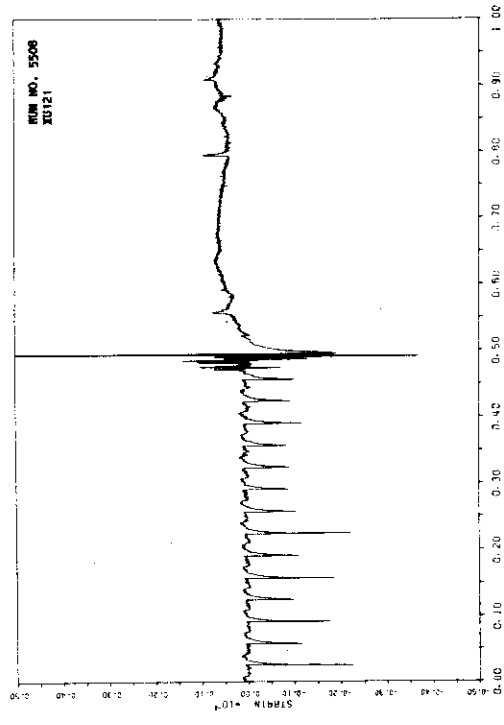

A.191

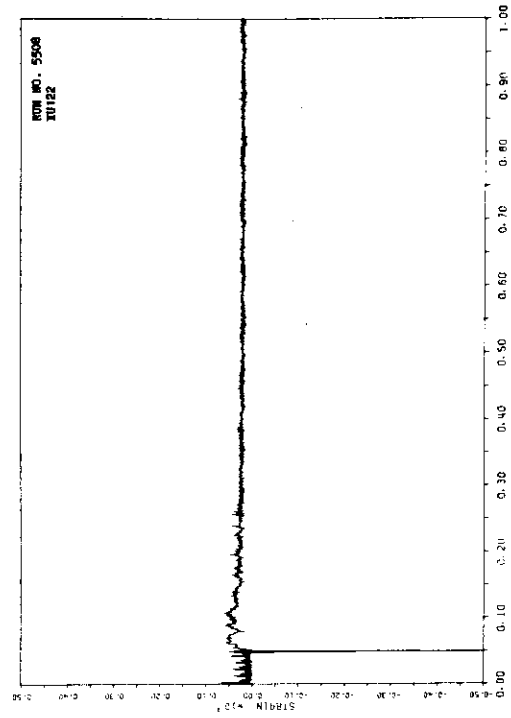

A.194

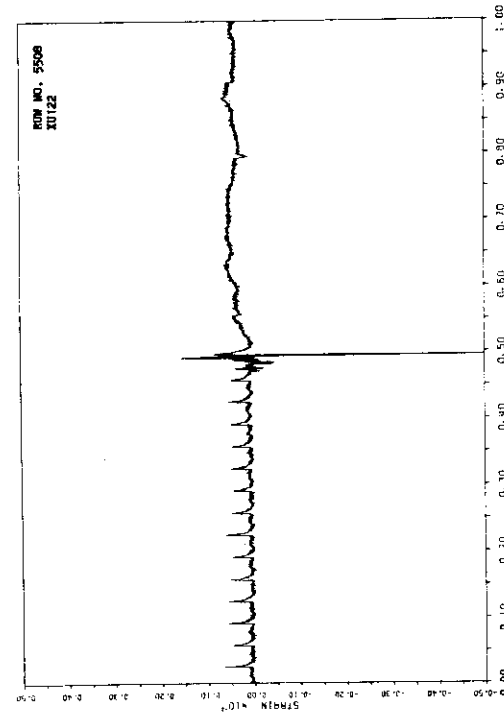

A.193

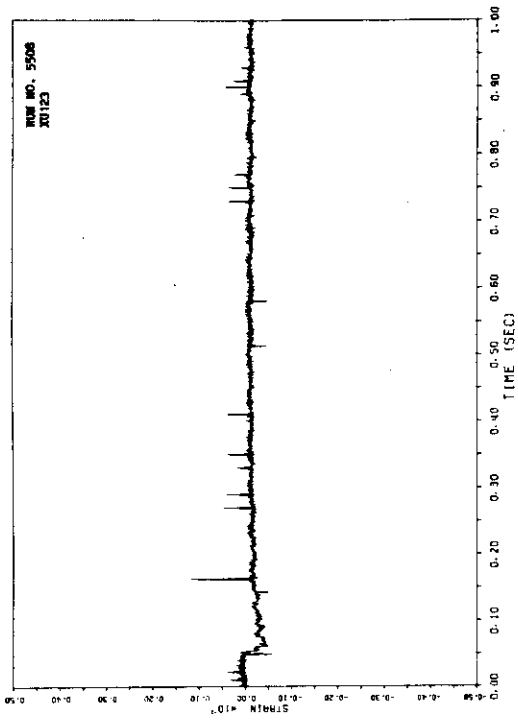

A.196

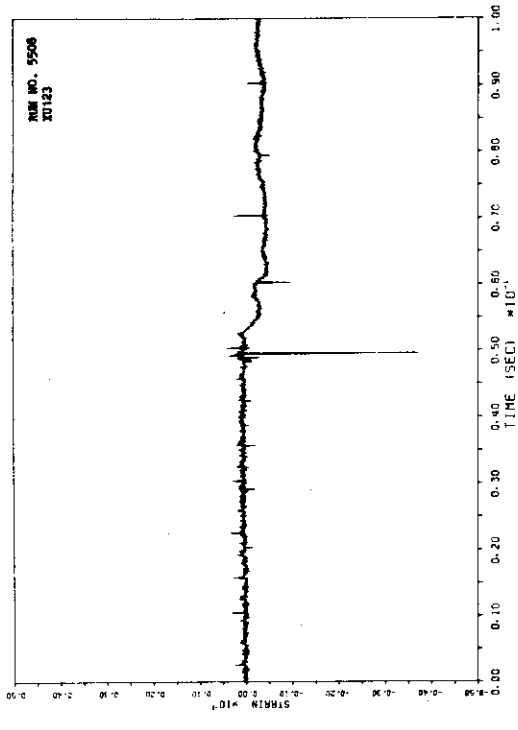

A.195

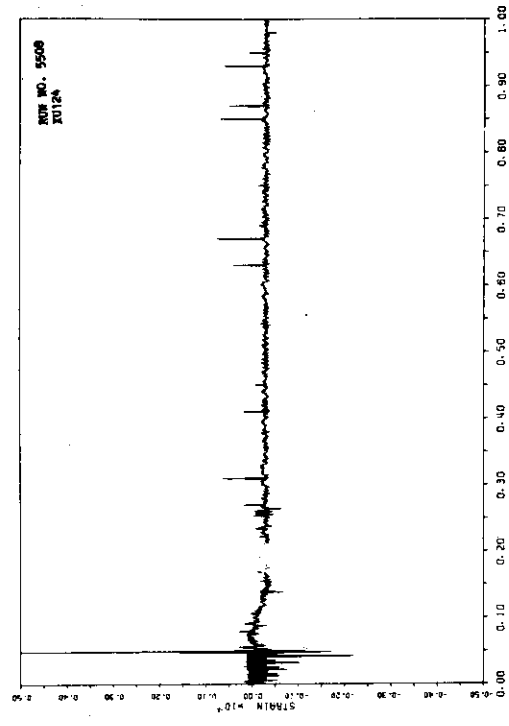

A.198

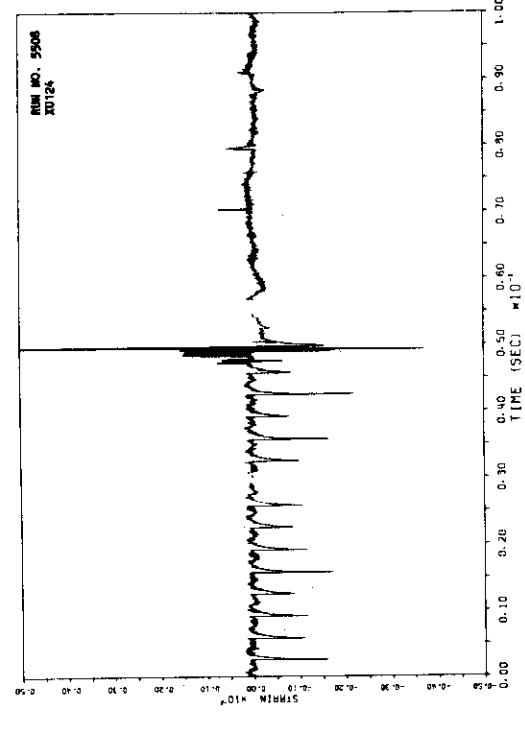

A.197

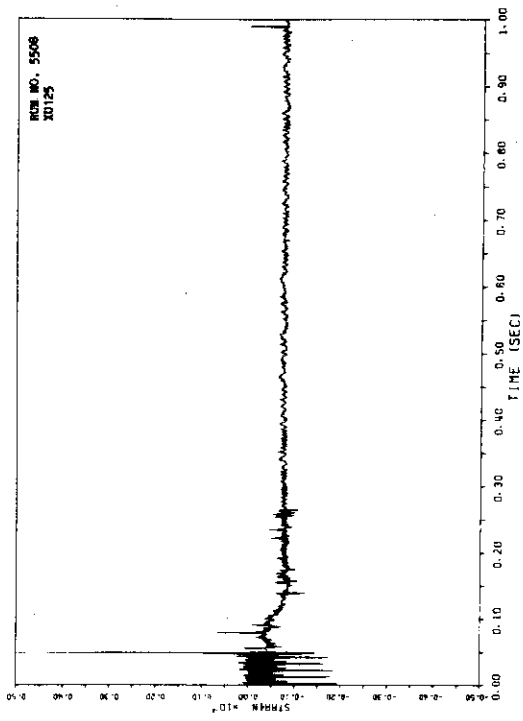

A.200

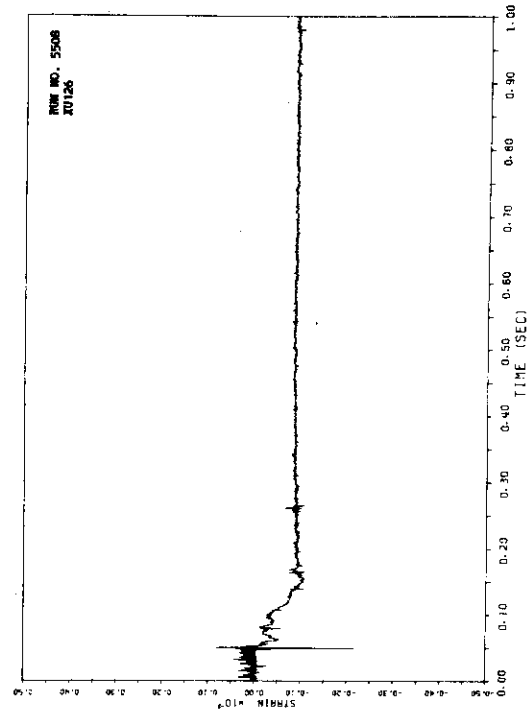

A.202

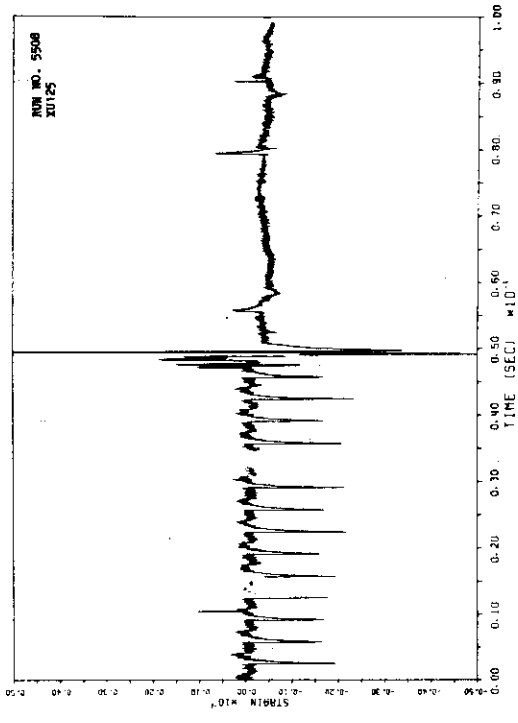

A.199

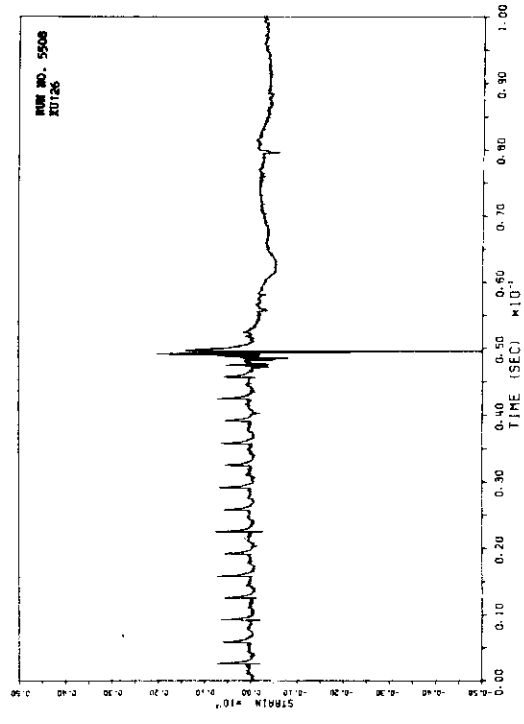

A.201

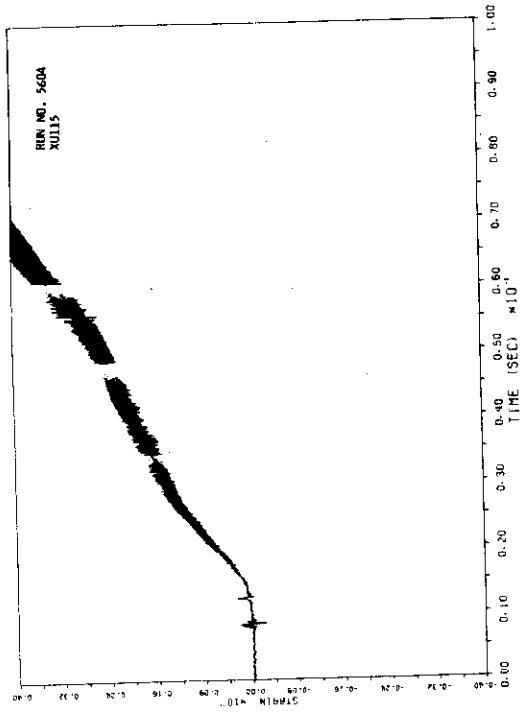

A.204

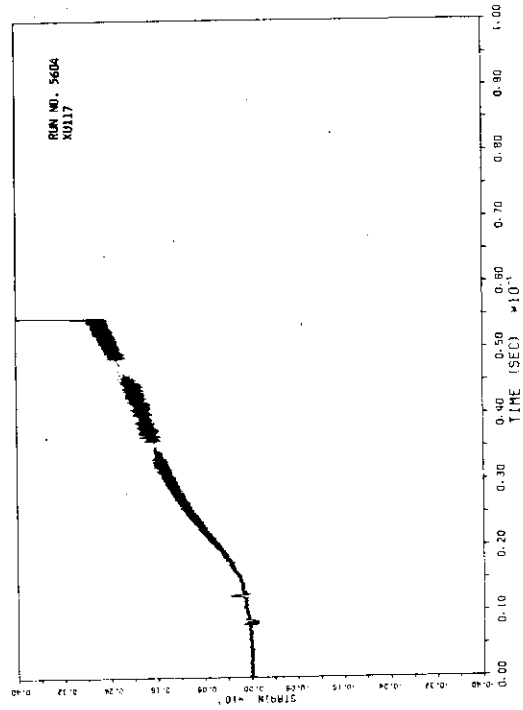

A.206

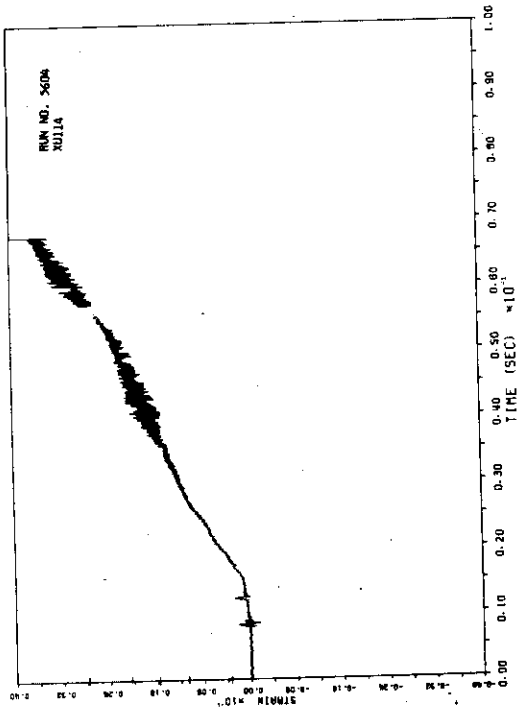

A.203

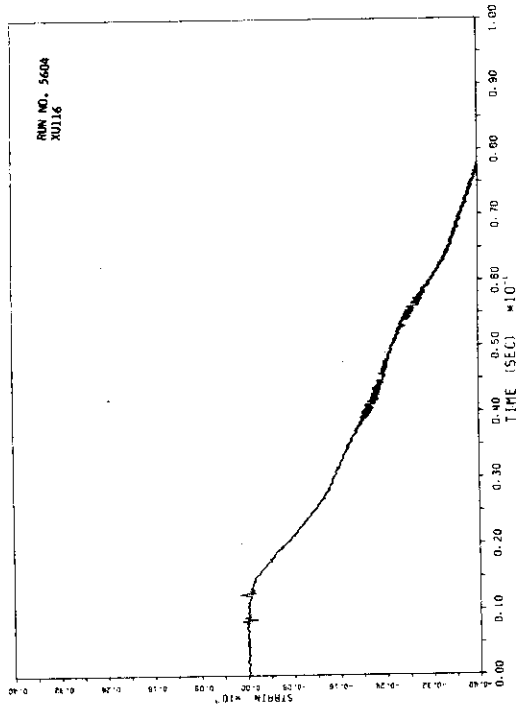

A.205

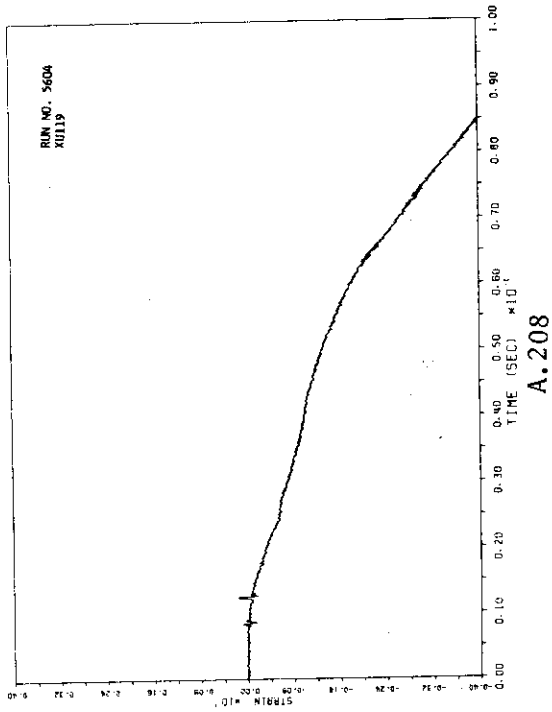

A.208

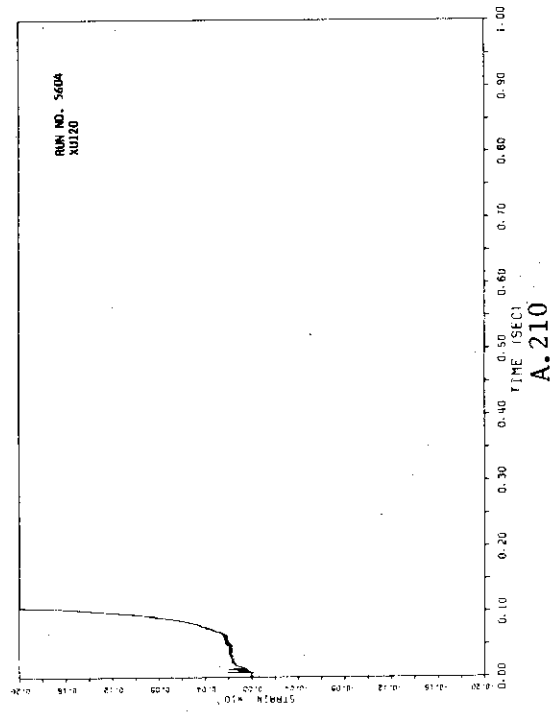

A.210

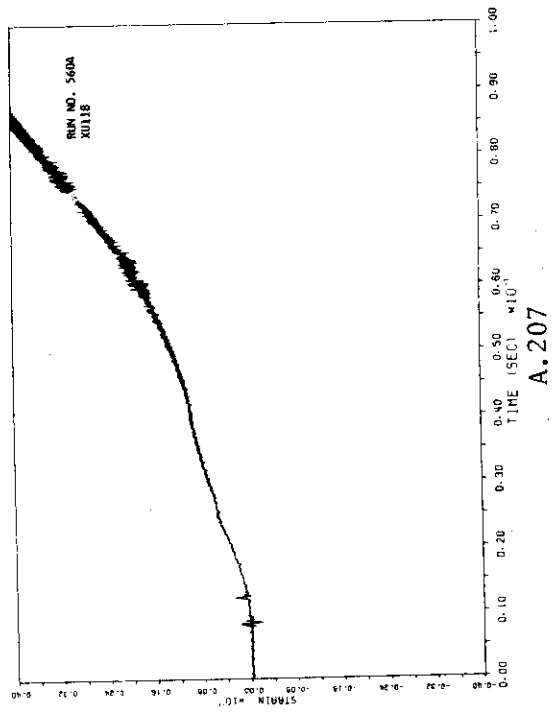

A.207

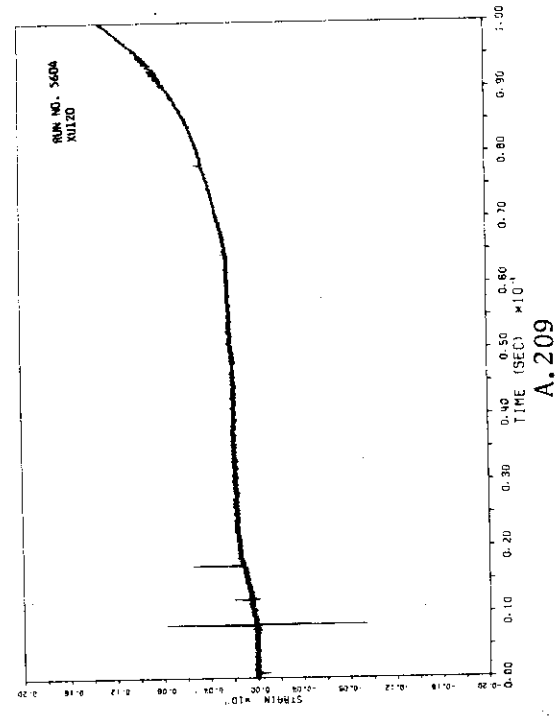

A.209

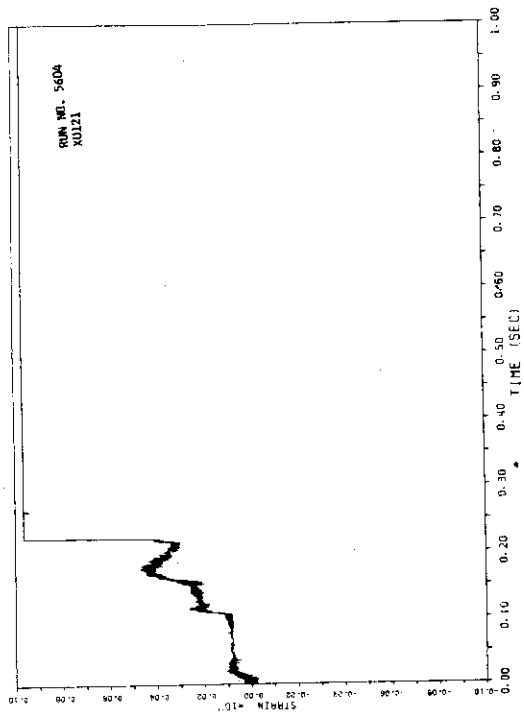

A.212

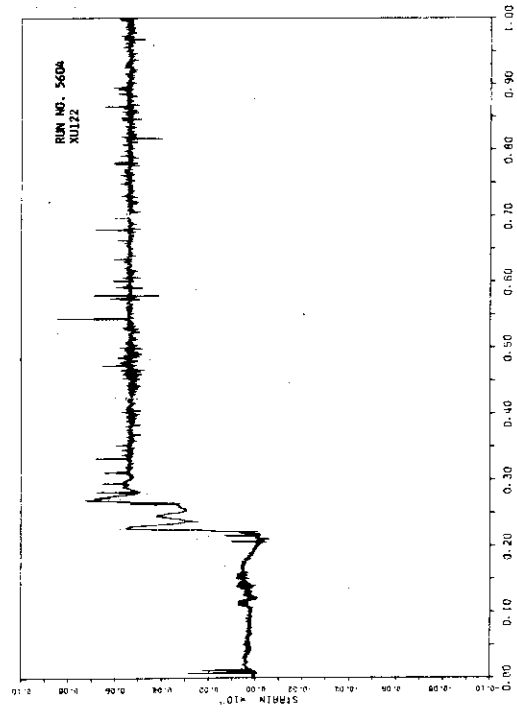

A.214

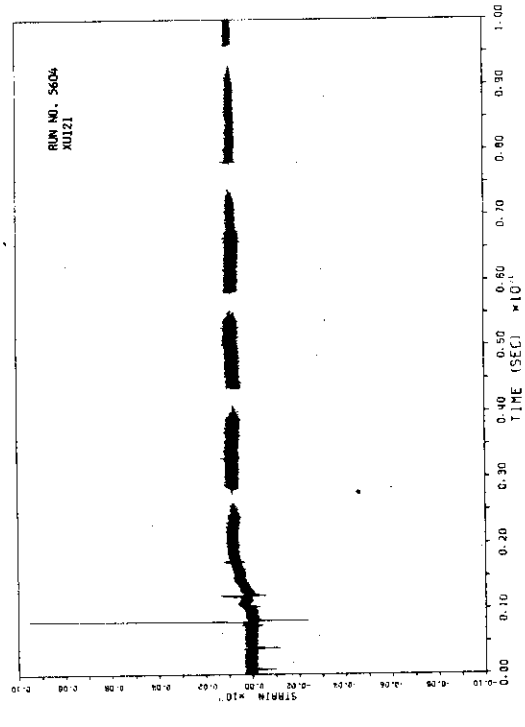

A.211

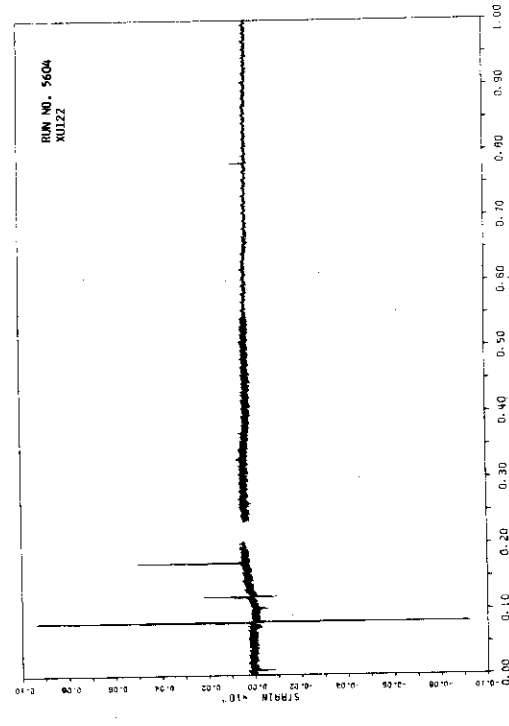

A.213

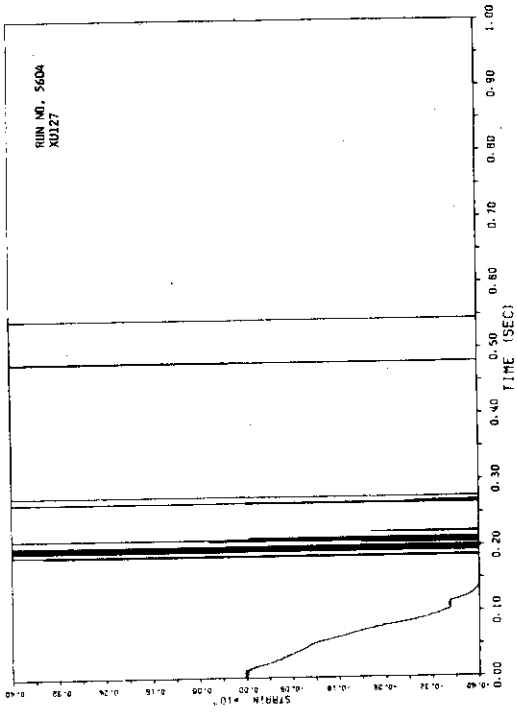

A.216

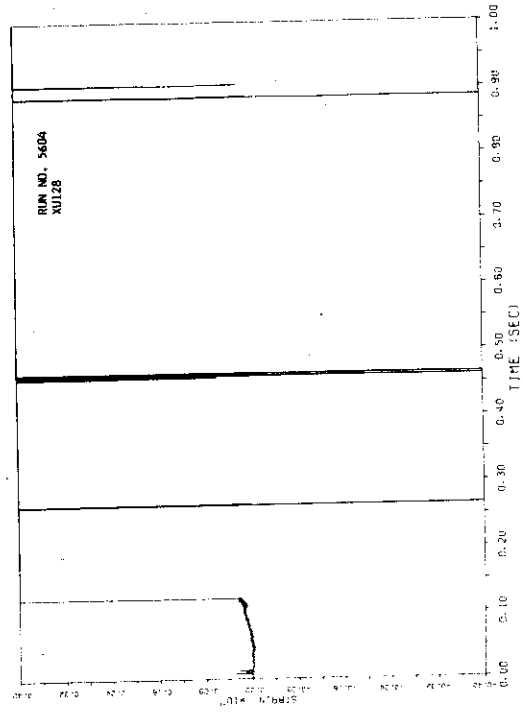

A.218

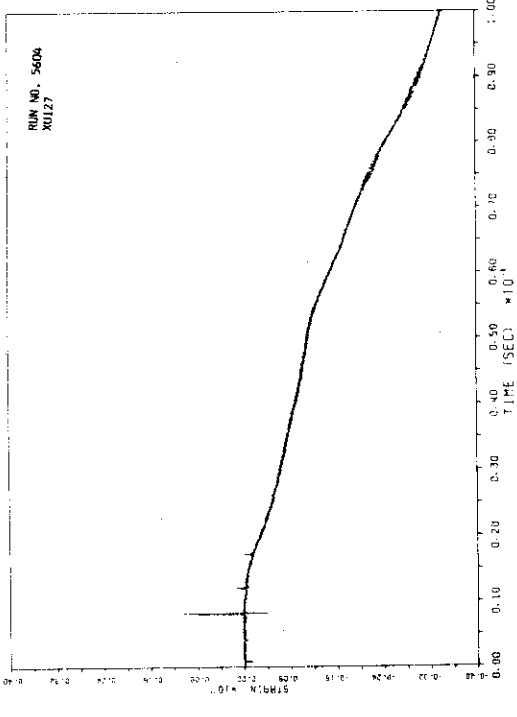

A.215

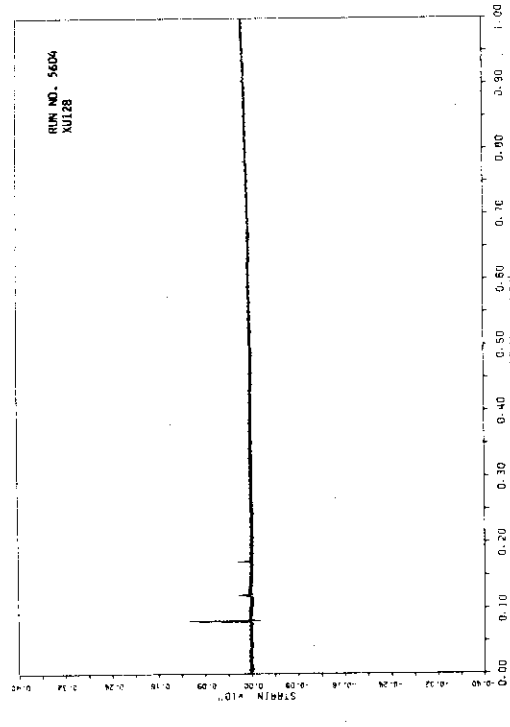

A.217

(e) Strains of the restraints (A.219-A.436)

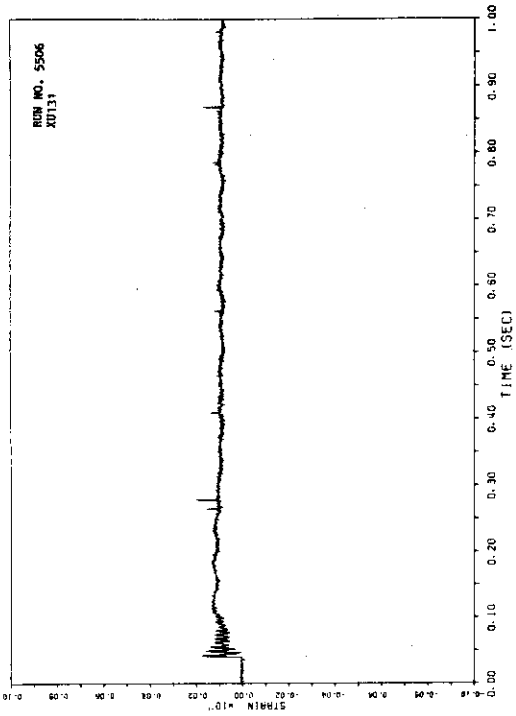

A.220

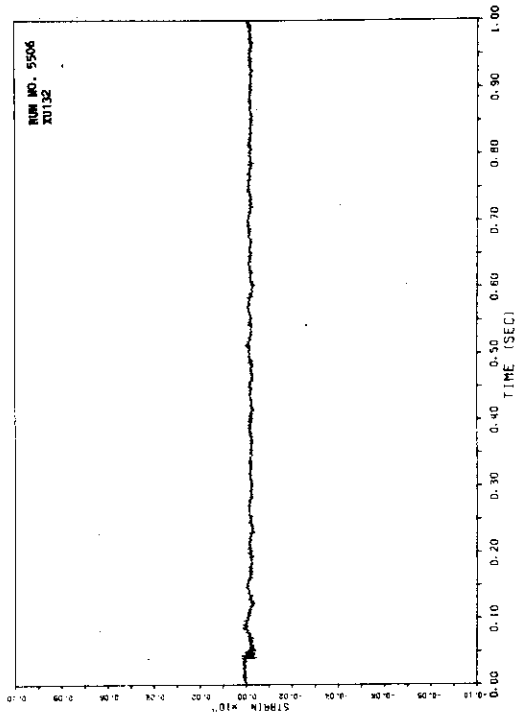

A.222

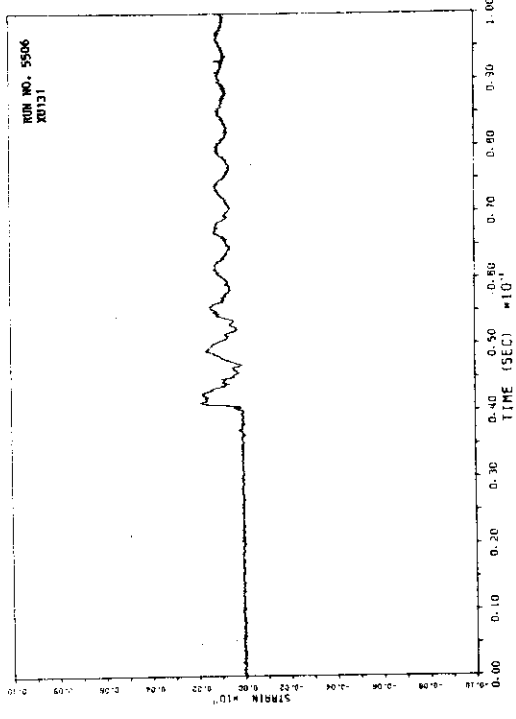

A.219

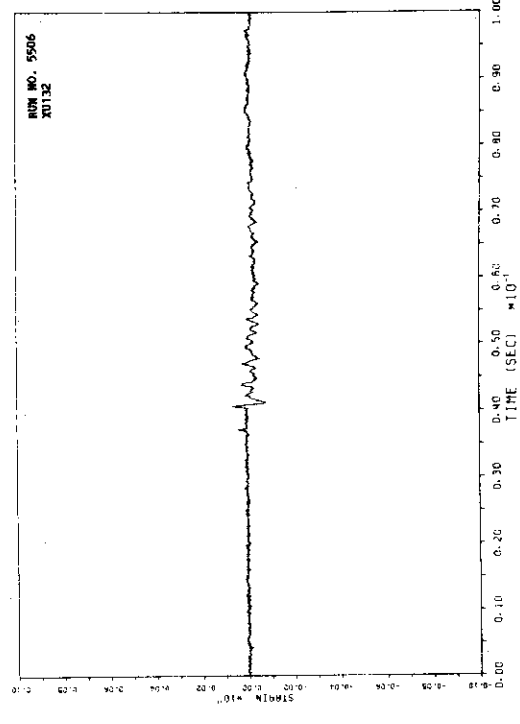

A.221

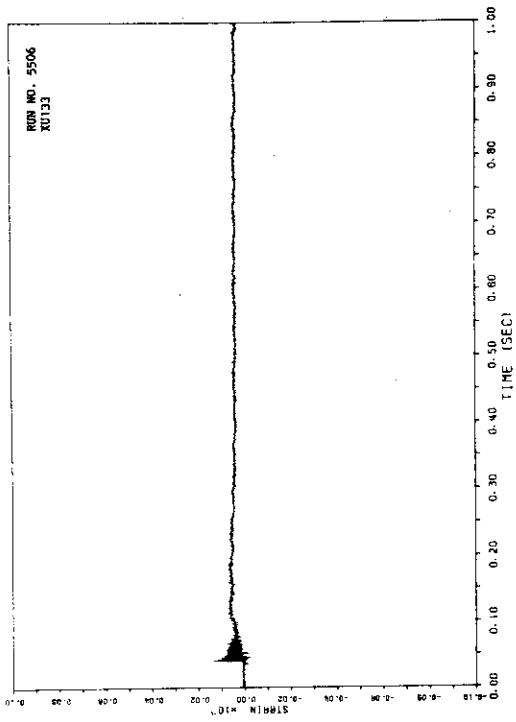

A.224

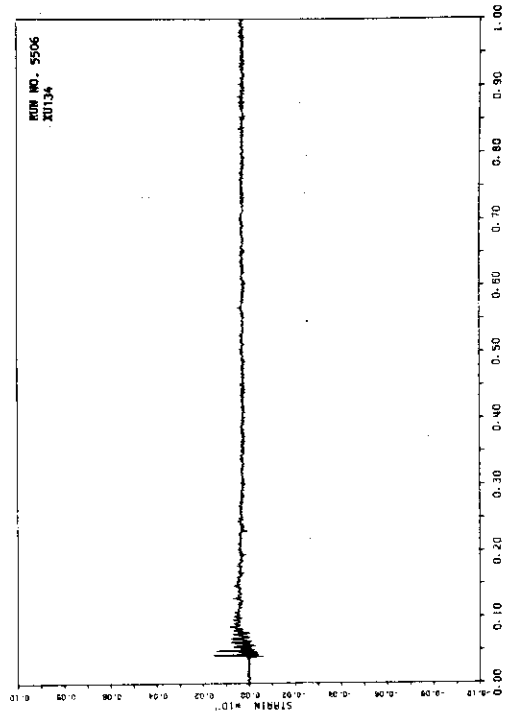

A.226

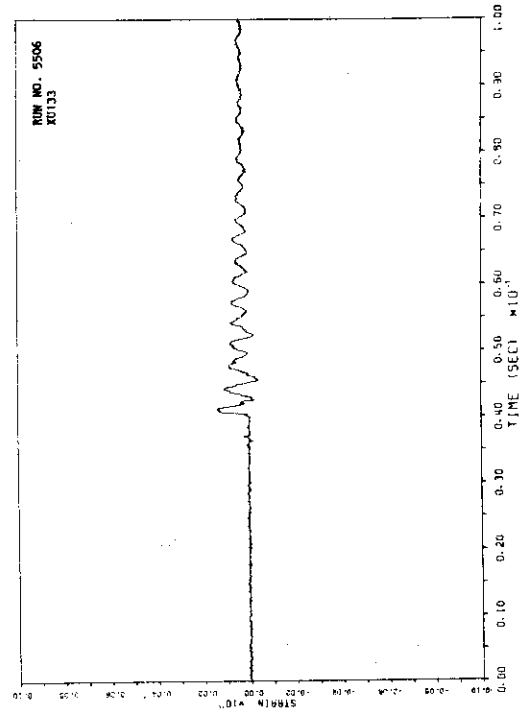

A.223

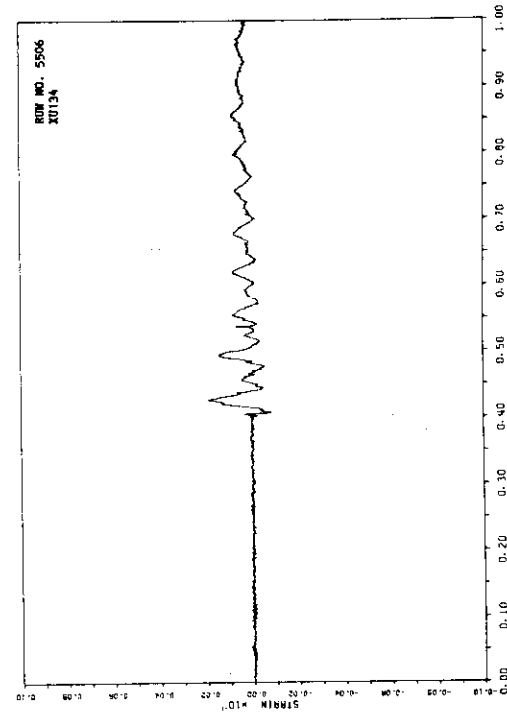

A.225

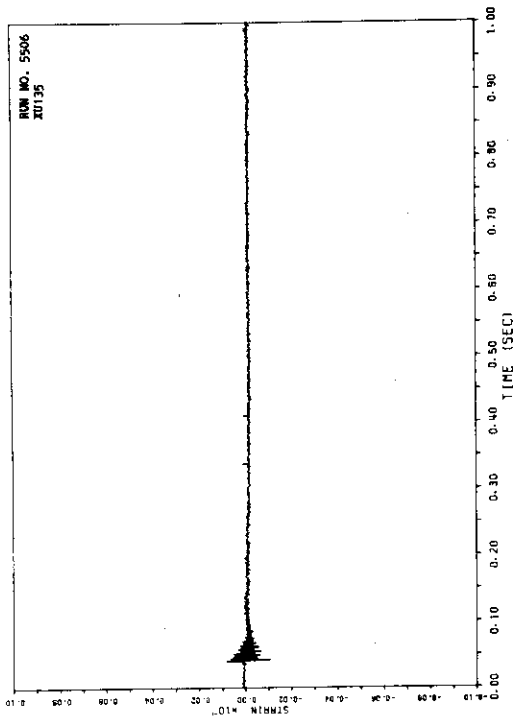

A.228

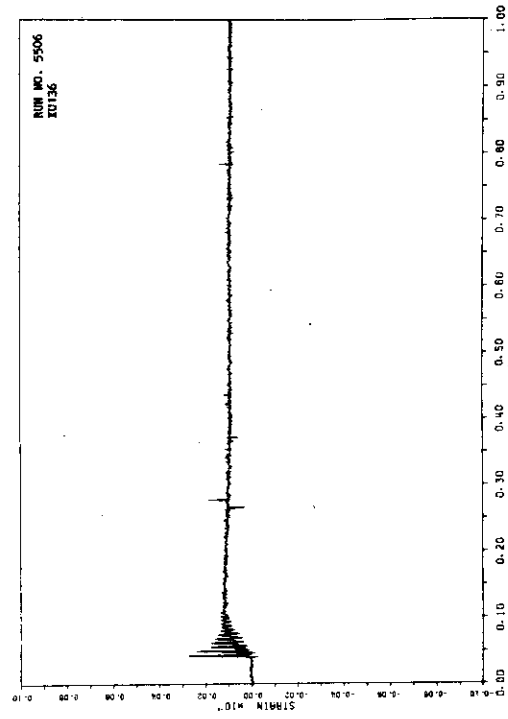

A.230

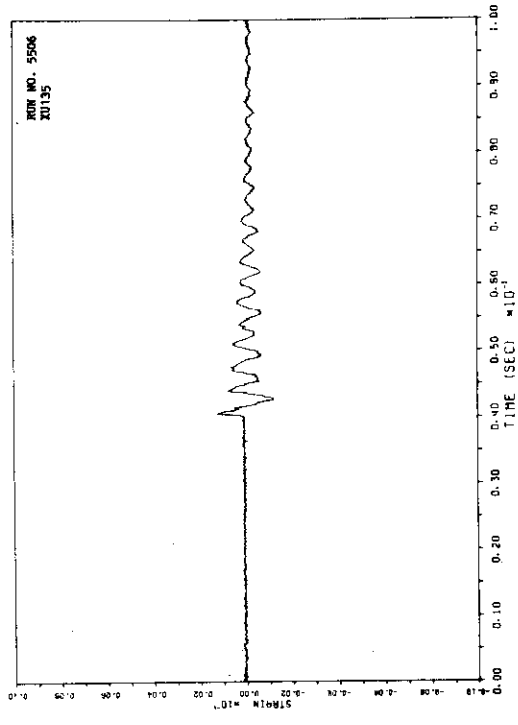

A.227

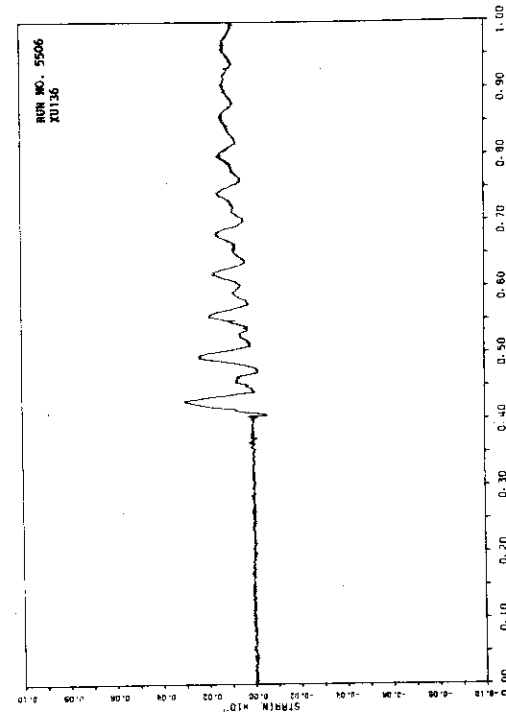

A.229

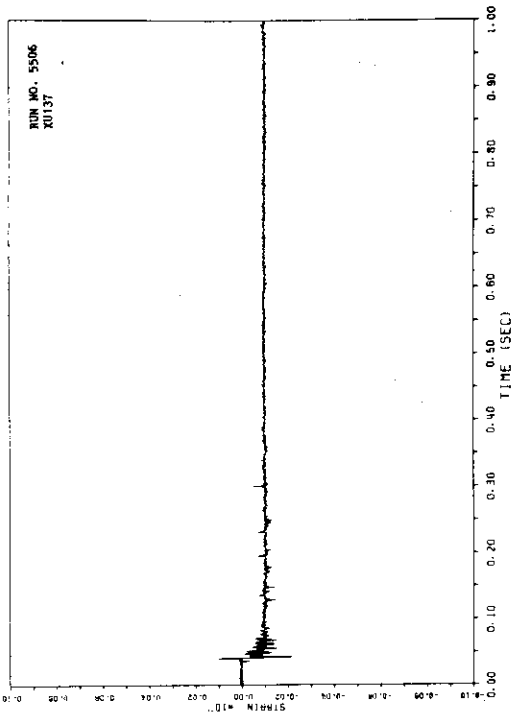

A.232

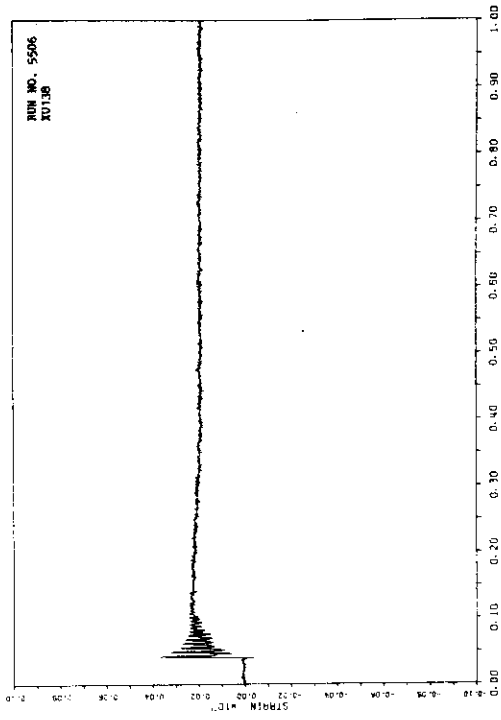

A.234

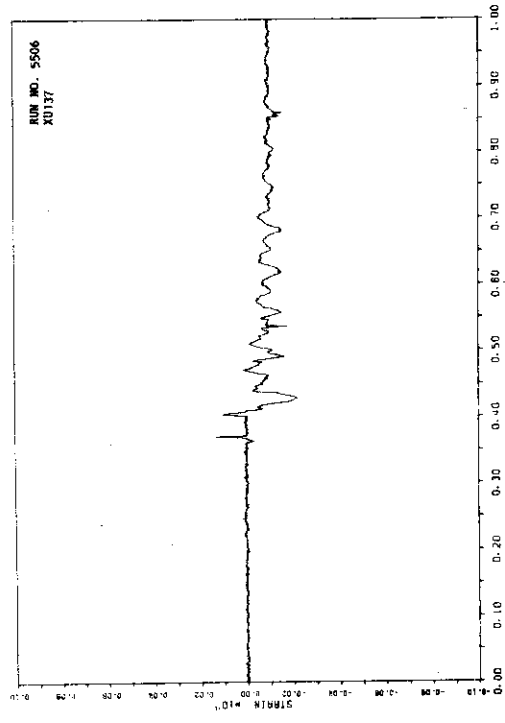

A.231

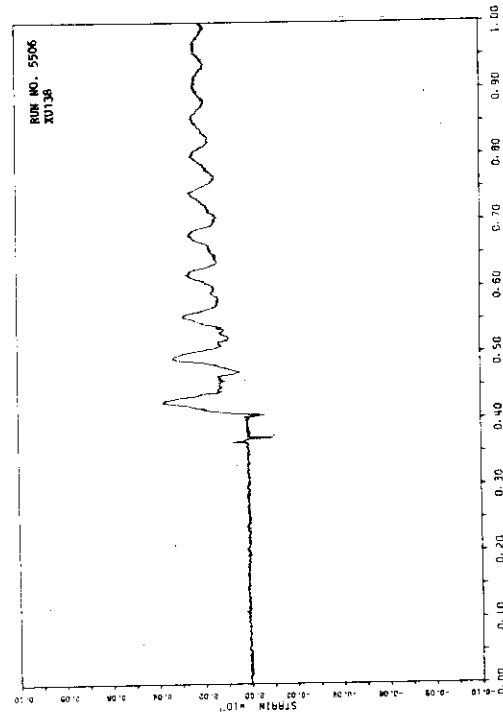

A.233

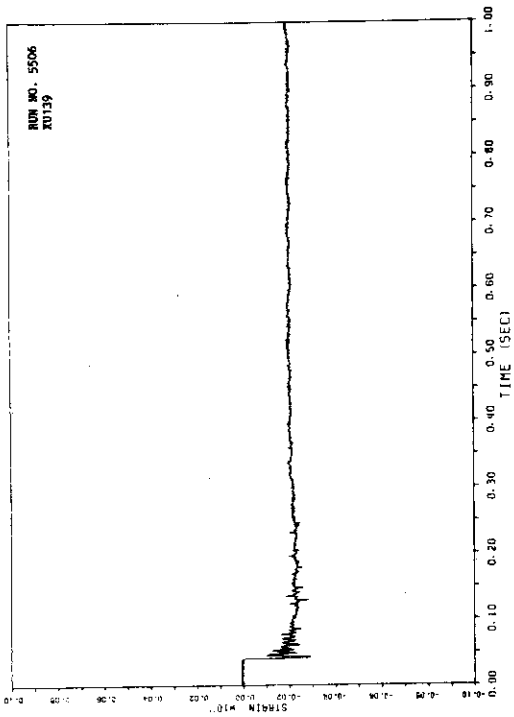

A.236

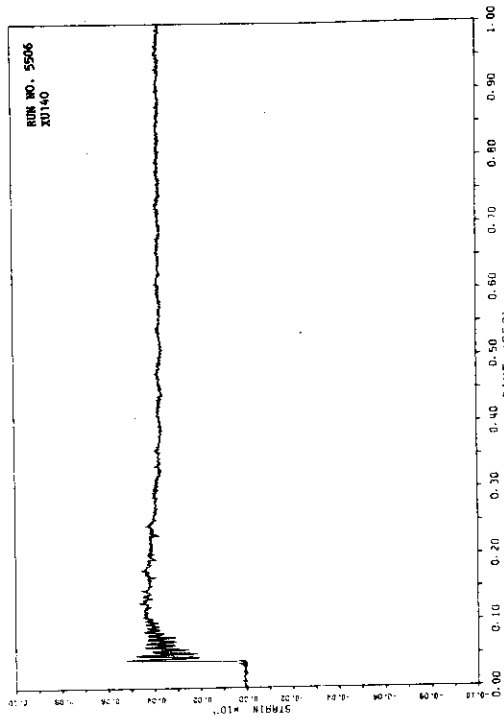

A.238

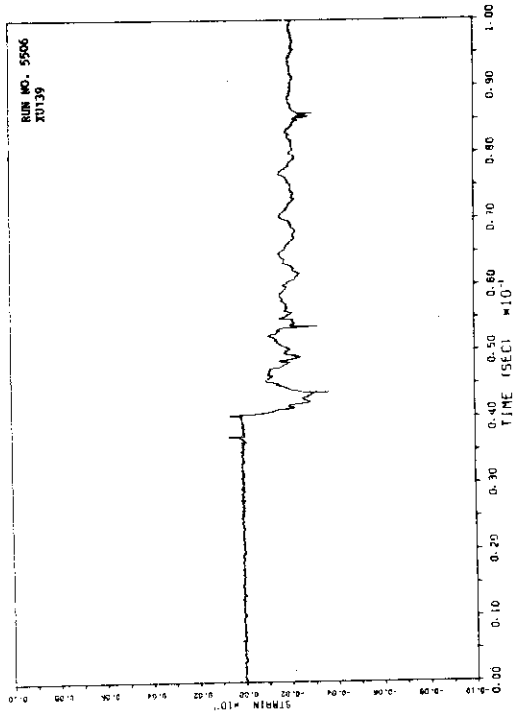

A.235

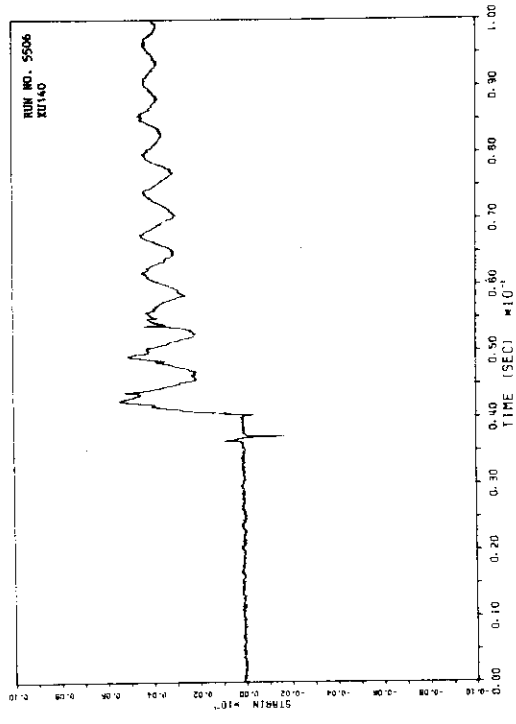

A.237

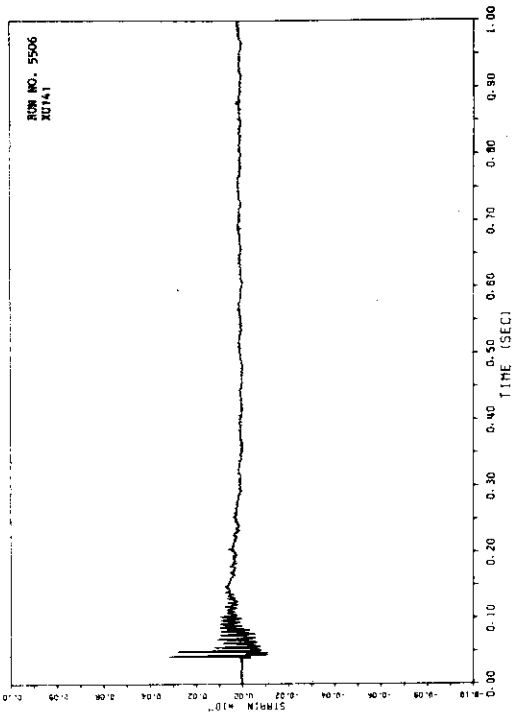

A.240

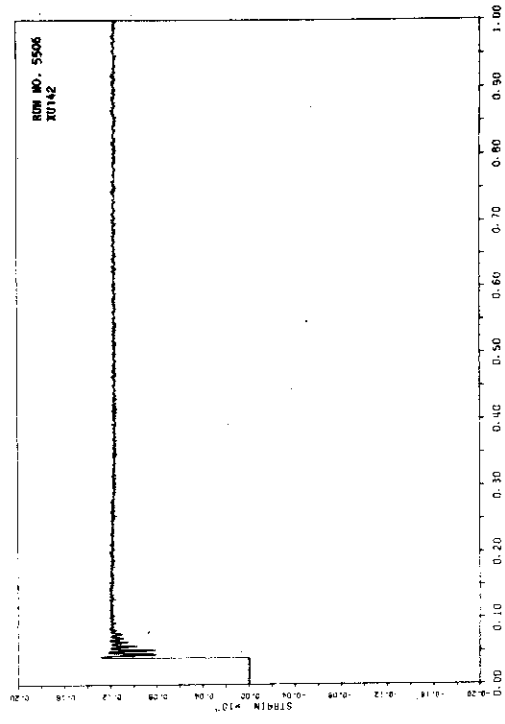

A.242

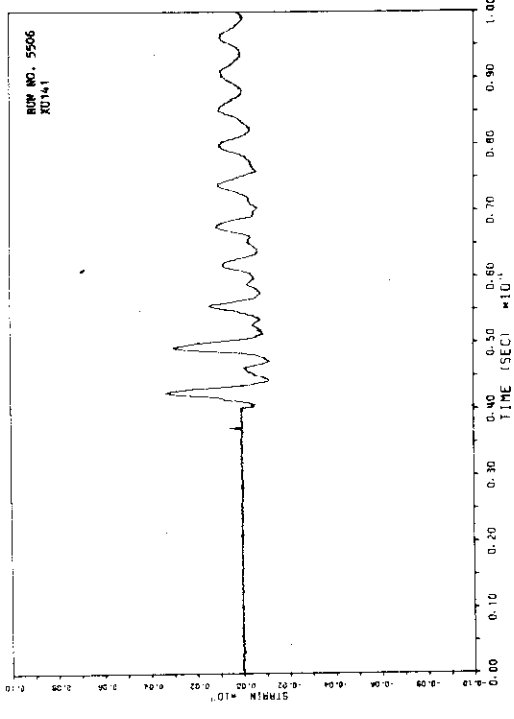

A.239

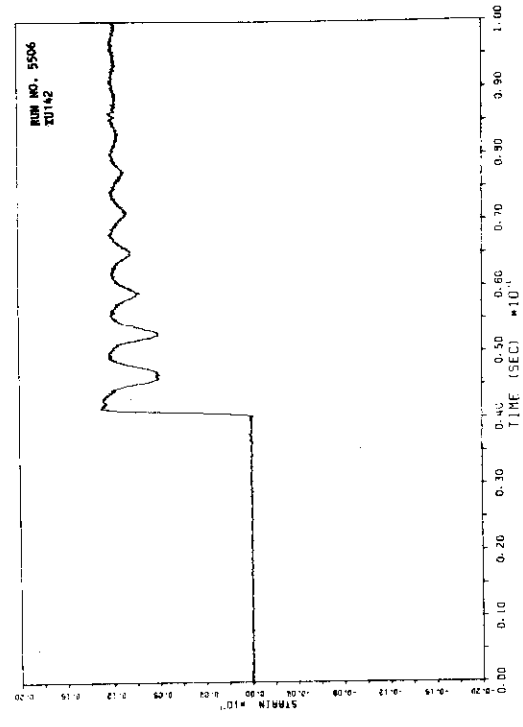

A.241

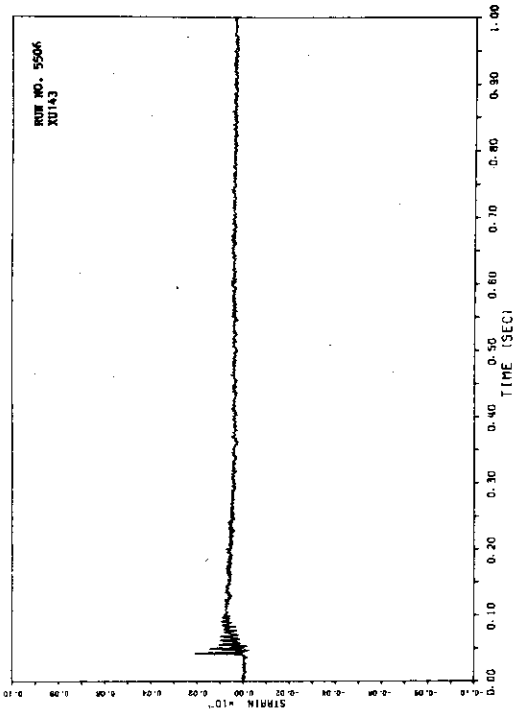

A.244

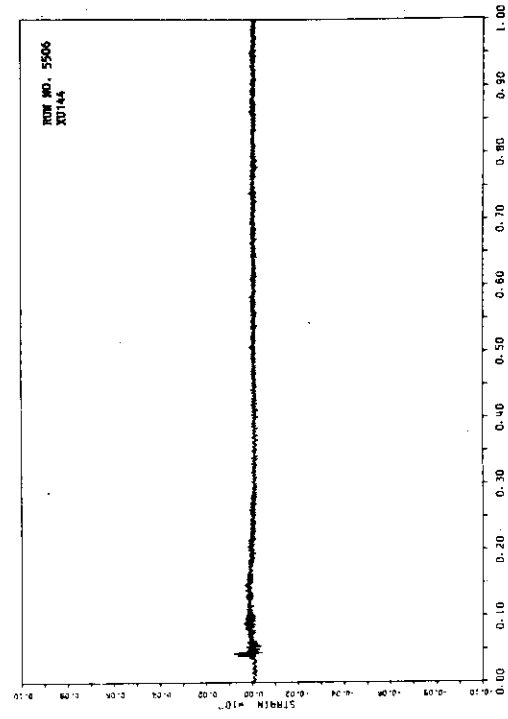

A.246

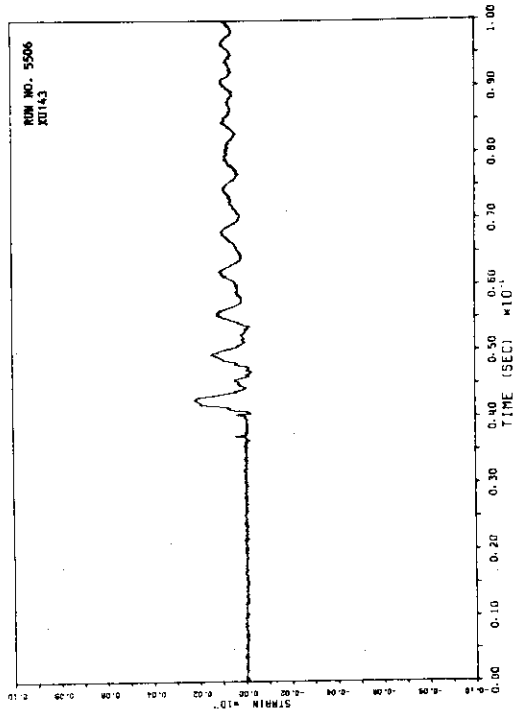

A.243

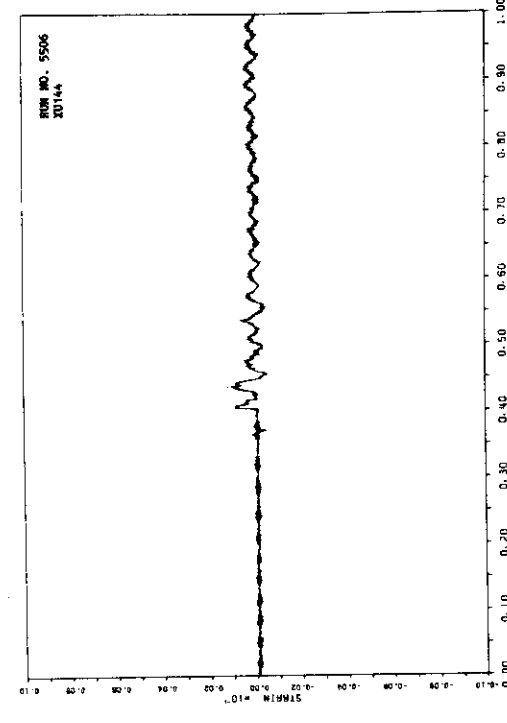

A.245

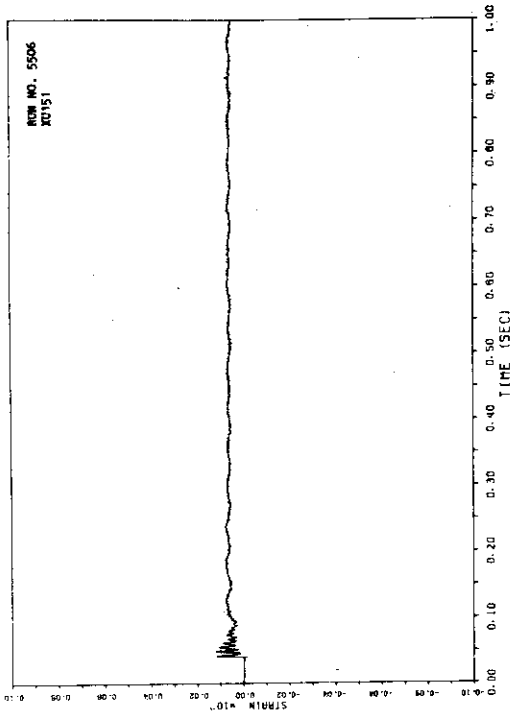

A.248

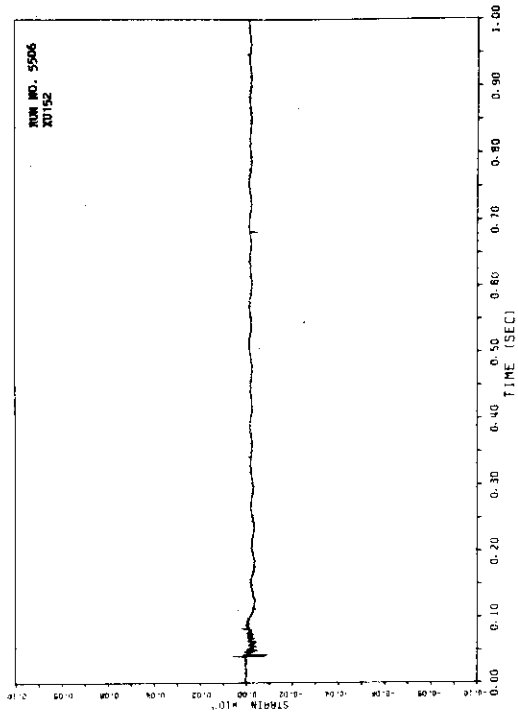

A.250

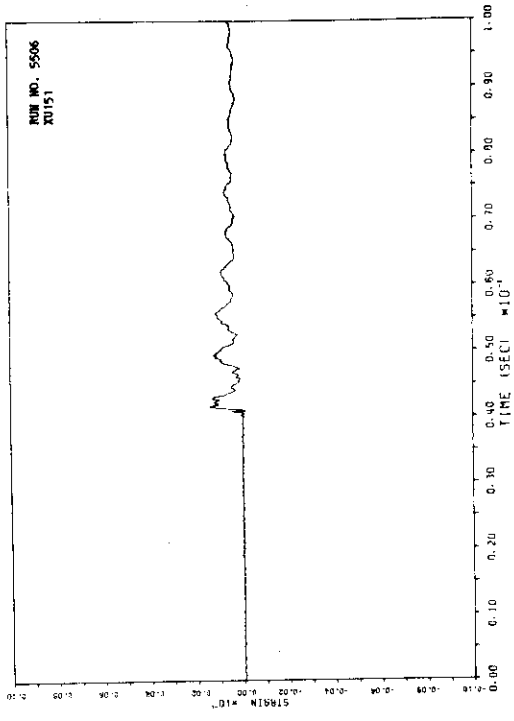

A.247

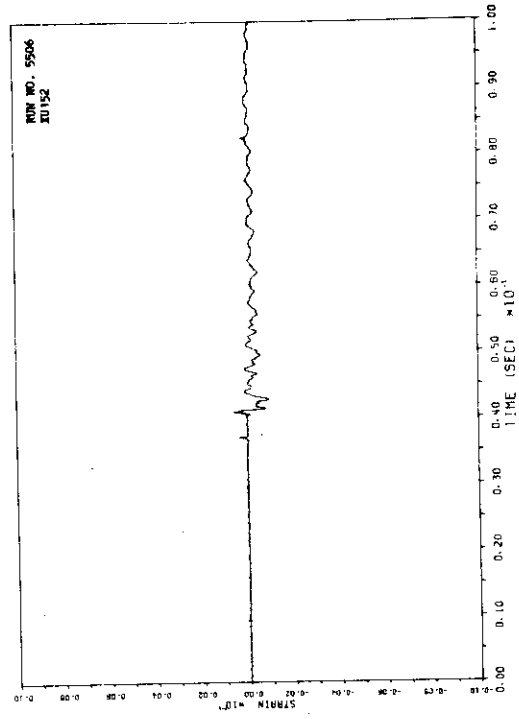

A.249

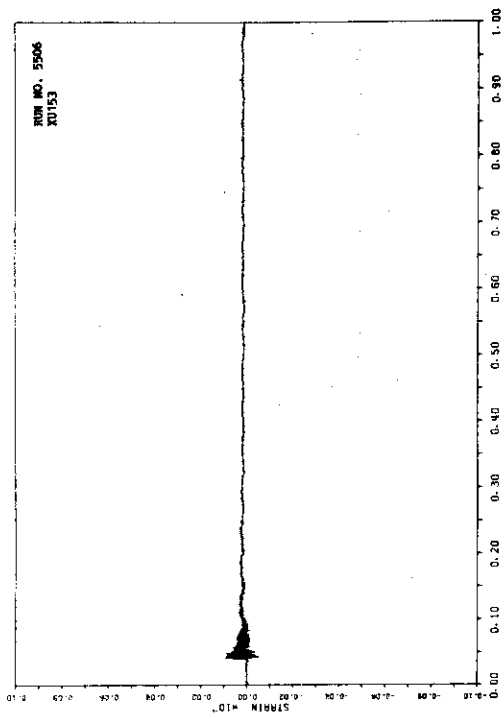

A.252

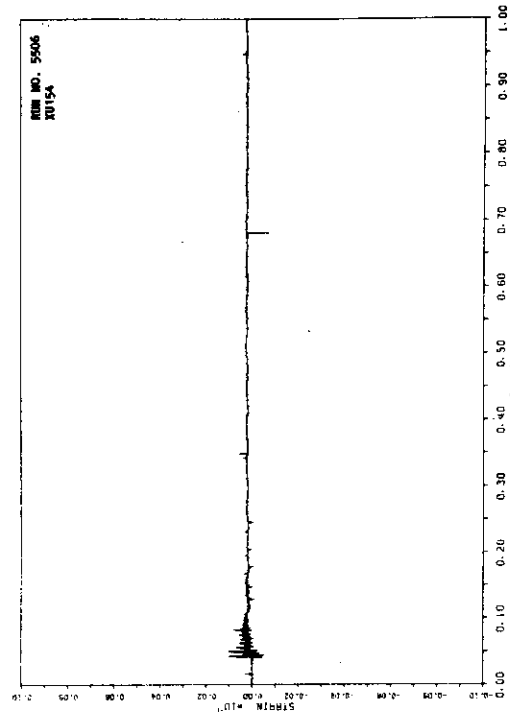

A.254

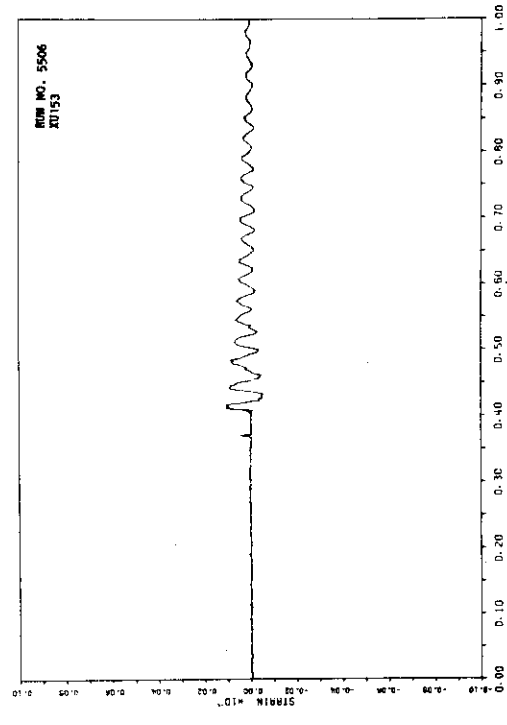

A.251

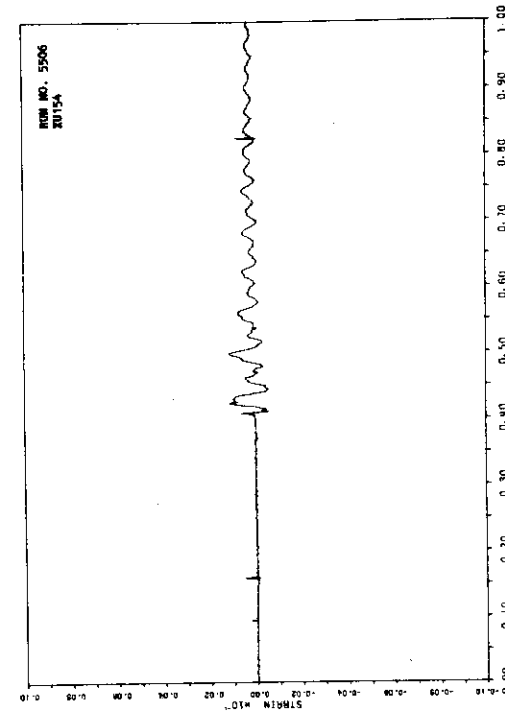

A.253

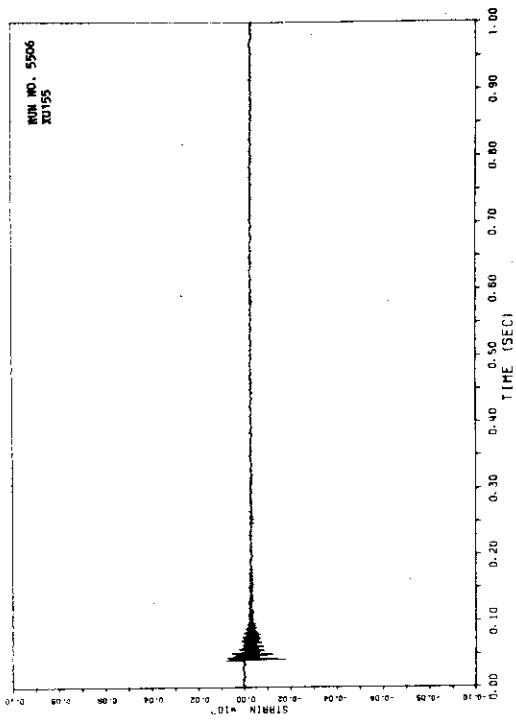

A.256

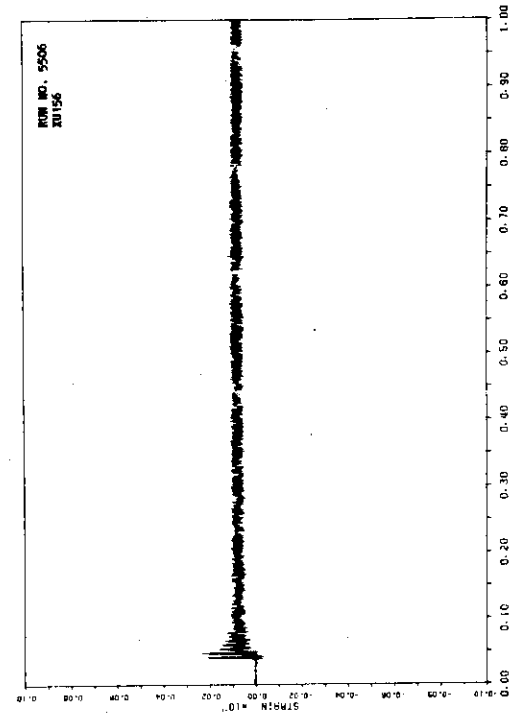

A.258

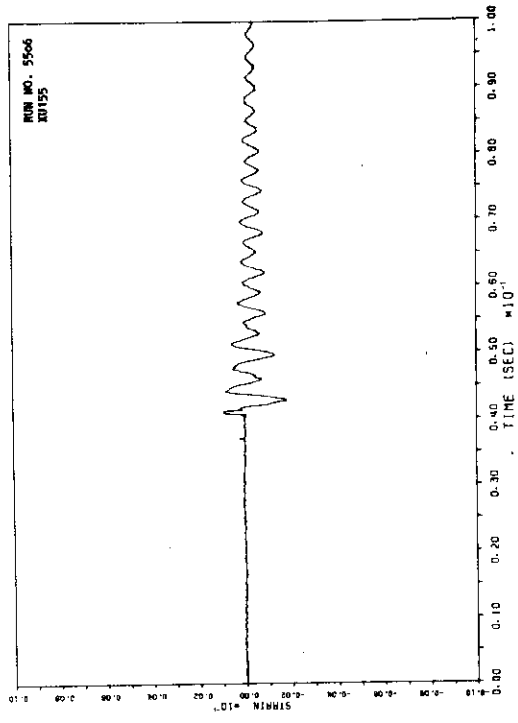

A.255

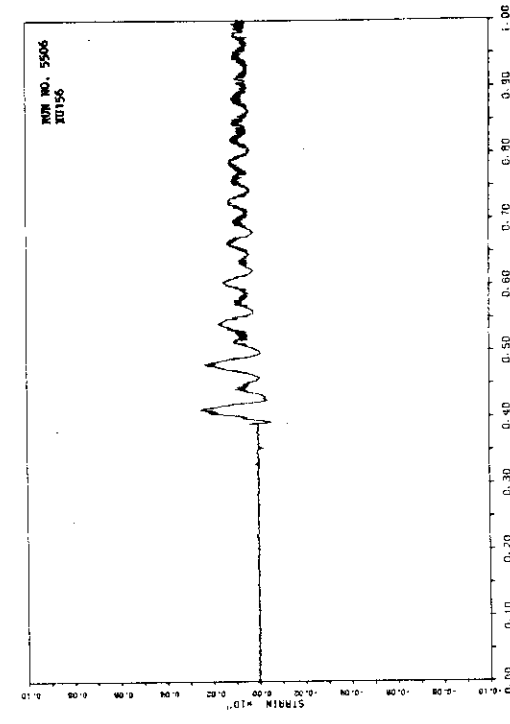

A.257

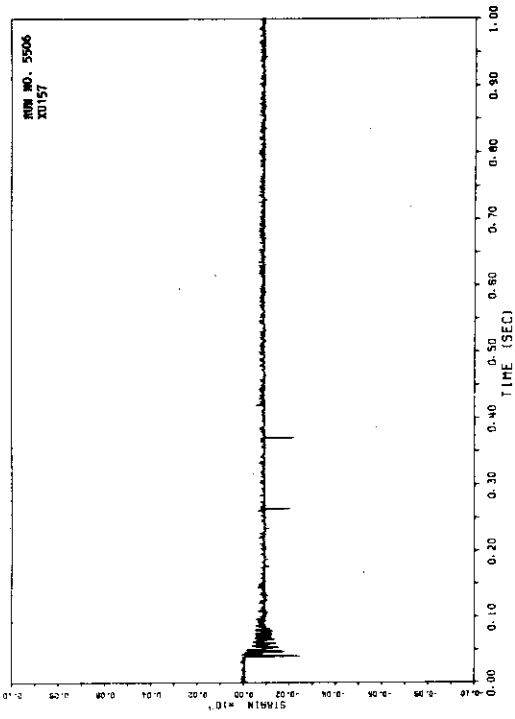

A.260

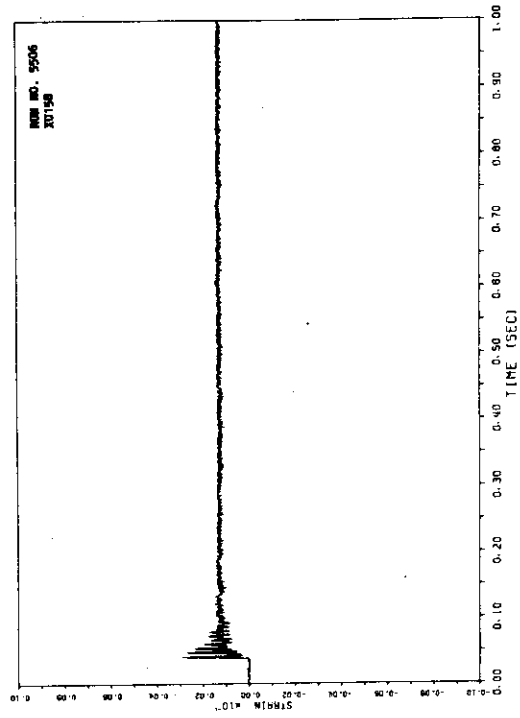

A.262

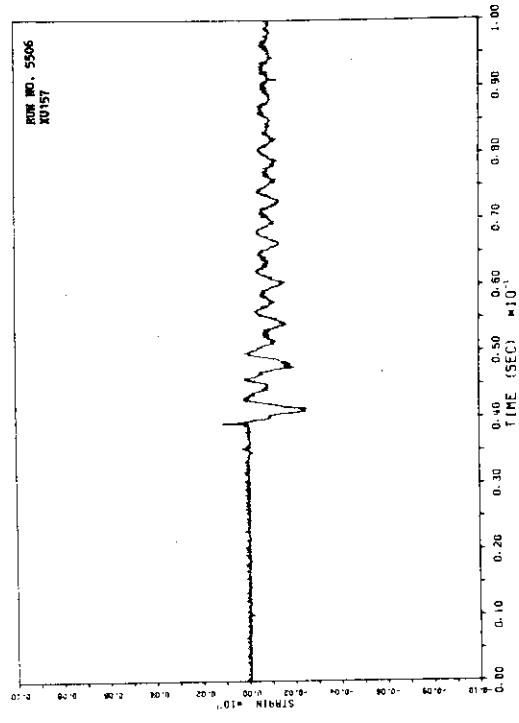

A.259

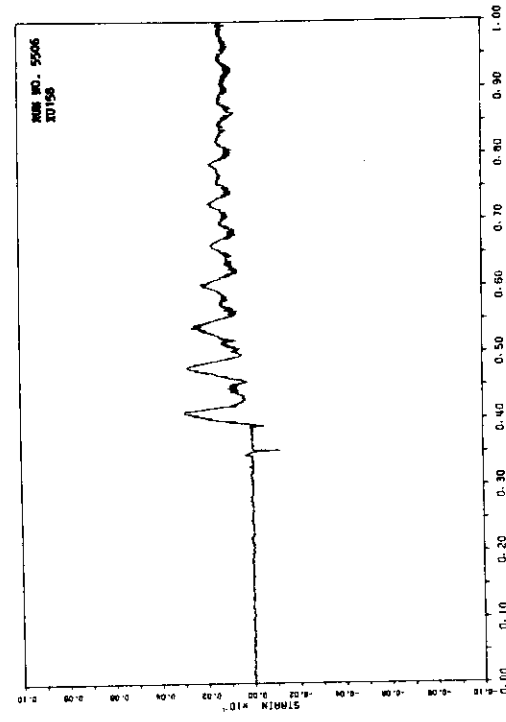

A.261

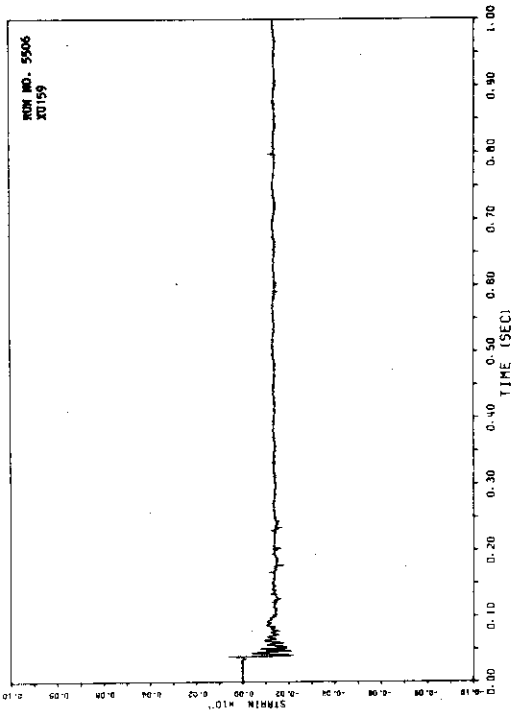

A.264

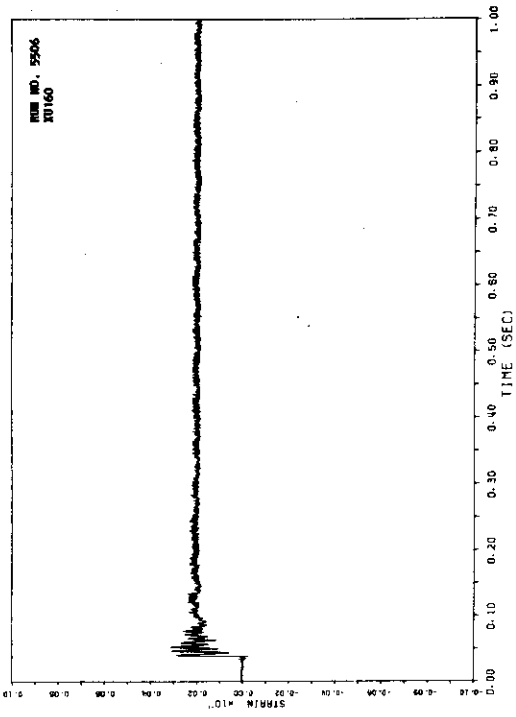

A.266

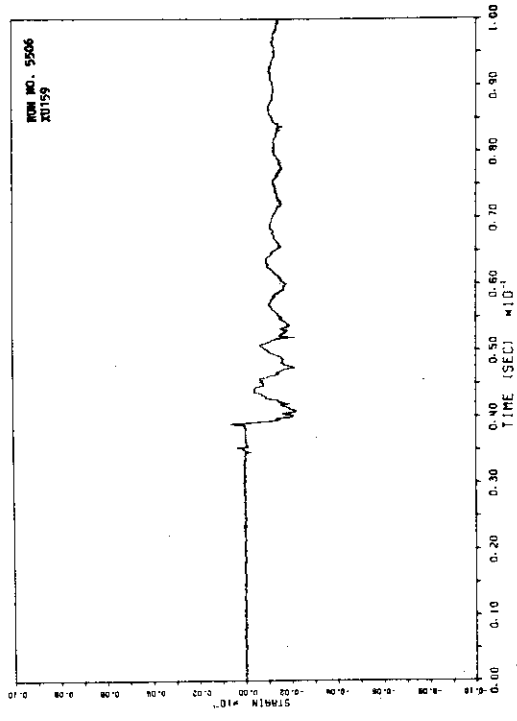

A.263

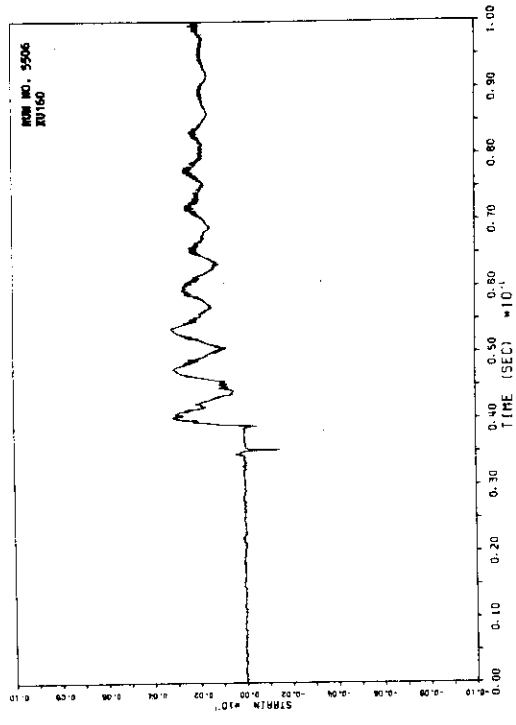

A.265

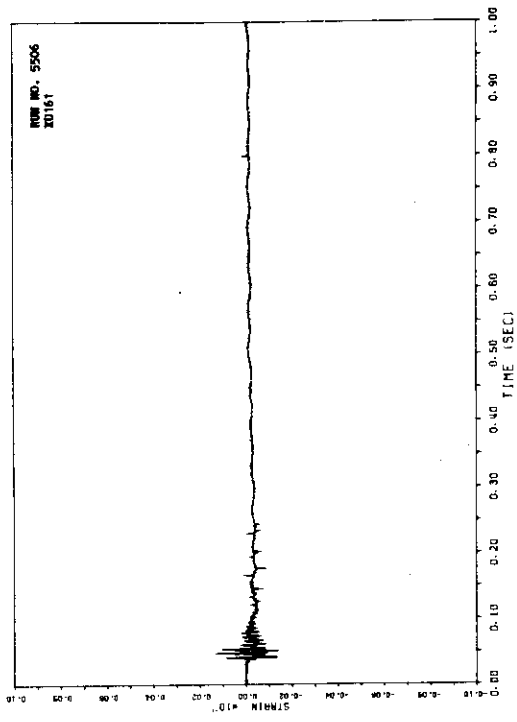

A.268

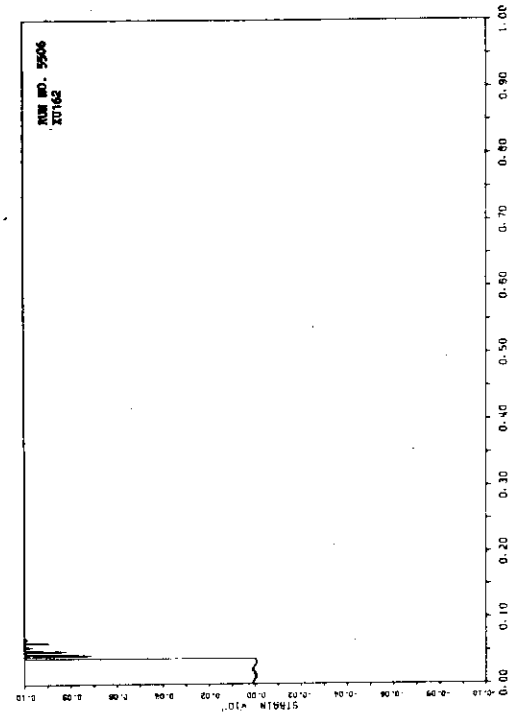

A.270

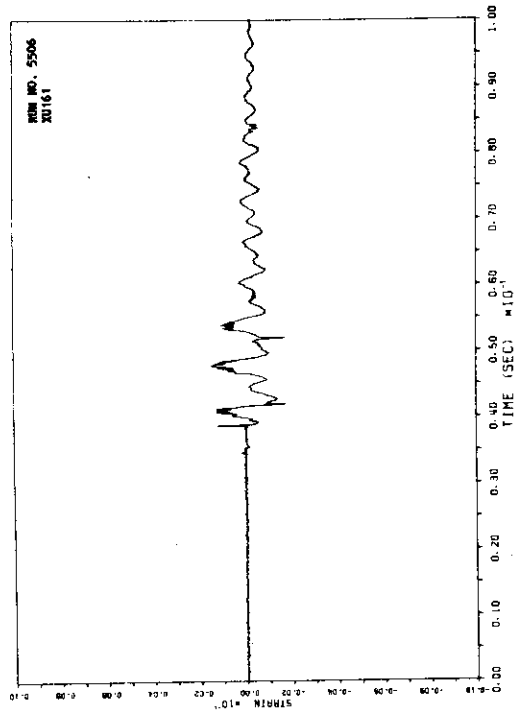

A.267

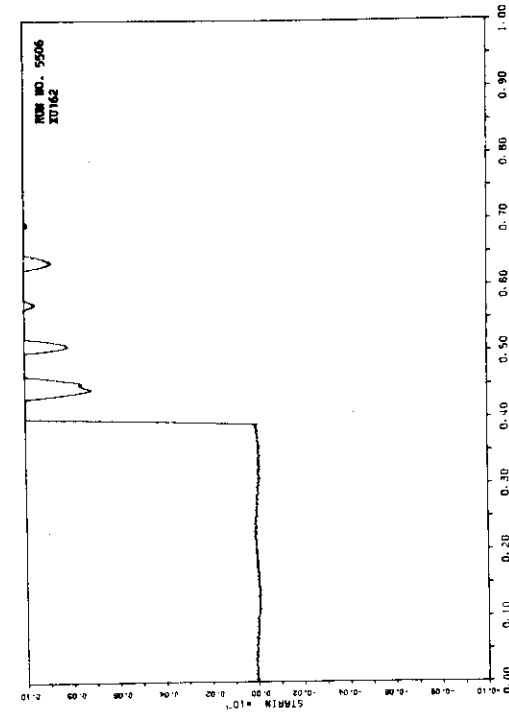

A.269

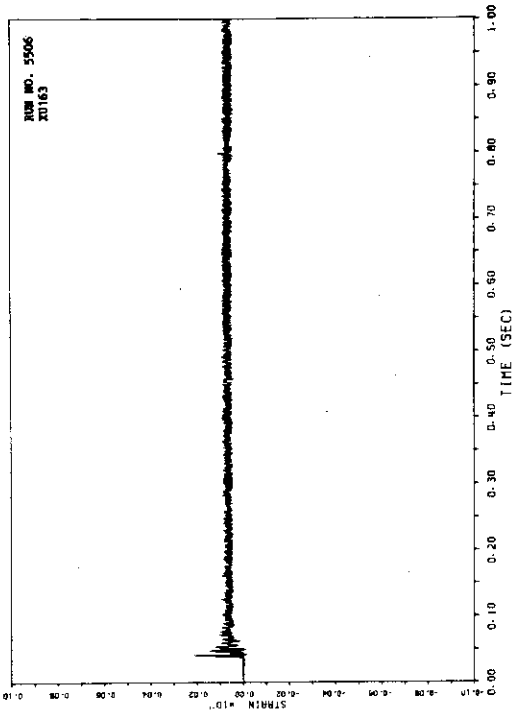

A.272

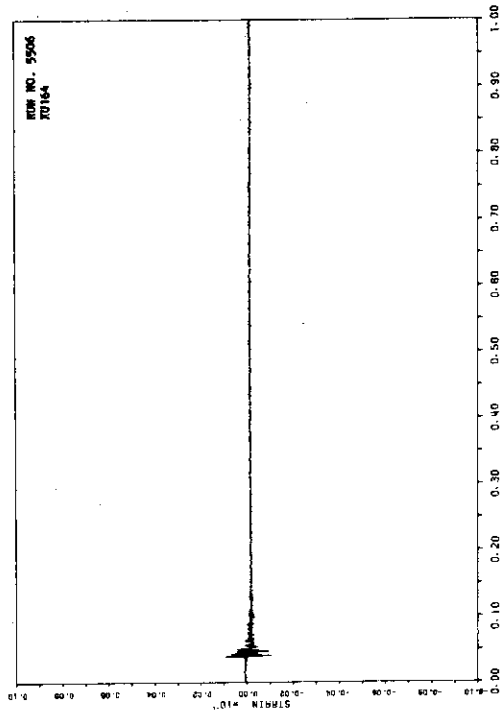

A.274

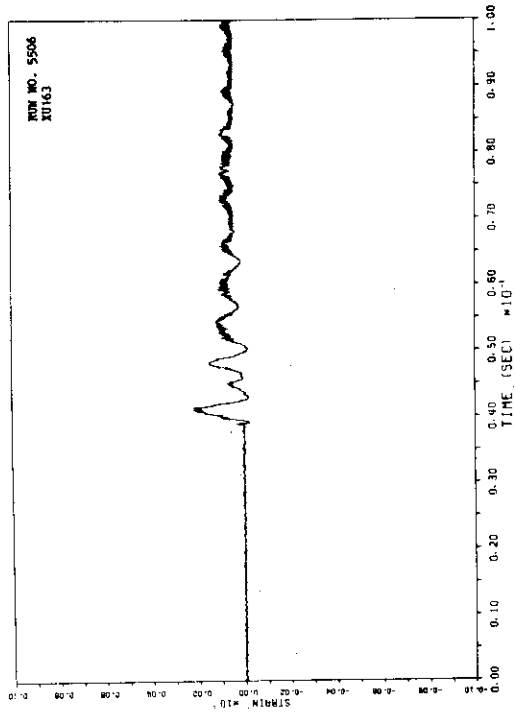

A.271

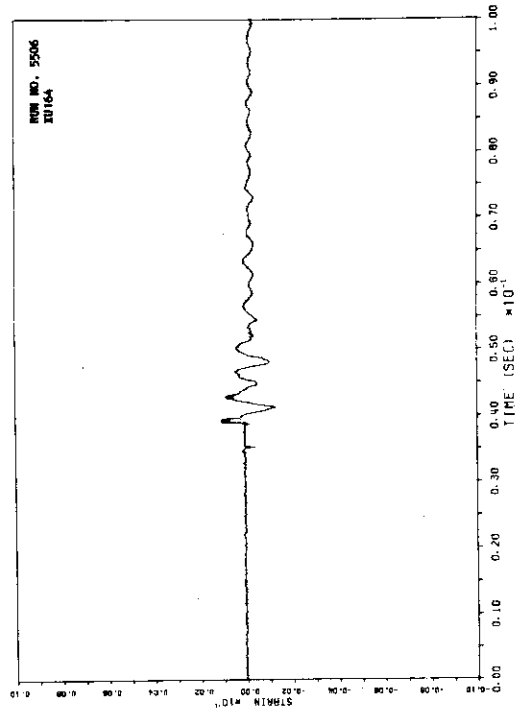

A.273

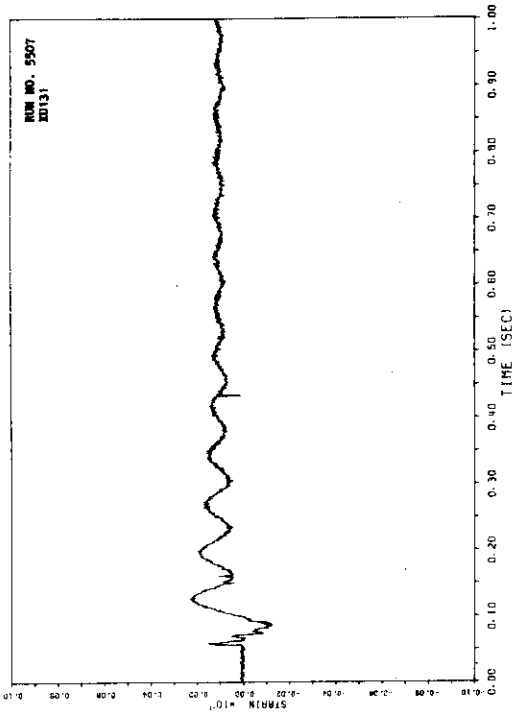

A.276

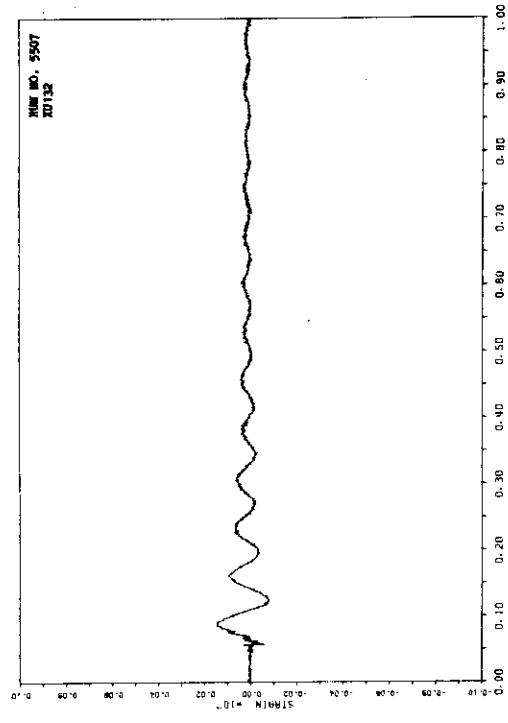

A.278

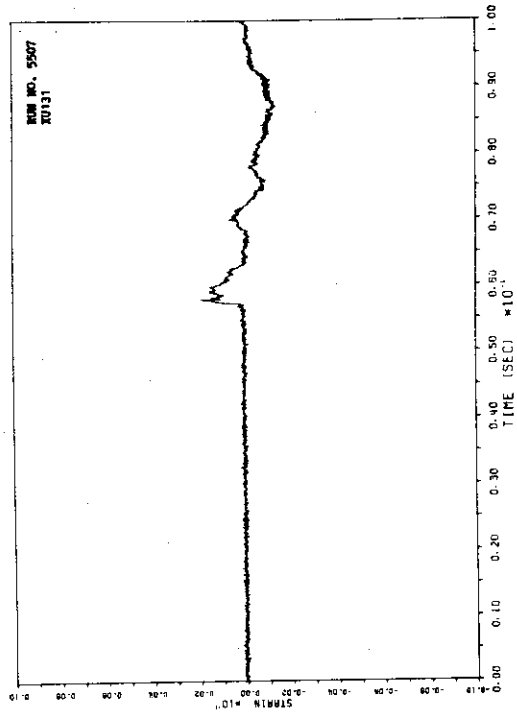

A.275

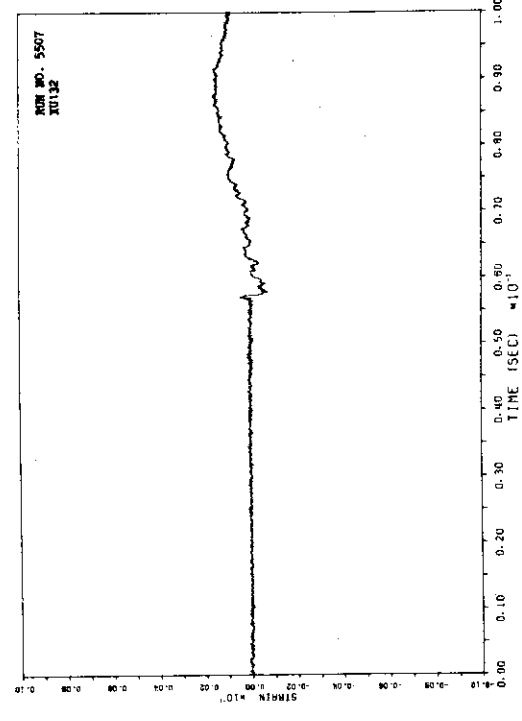

A.277

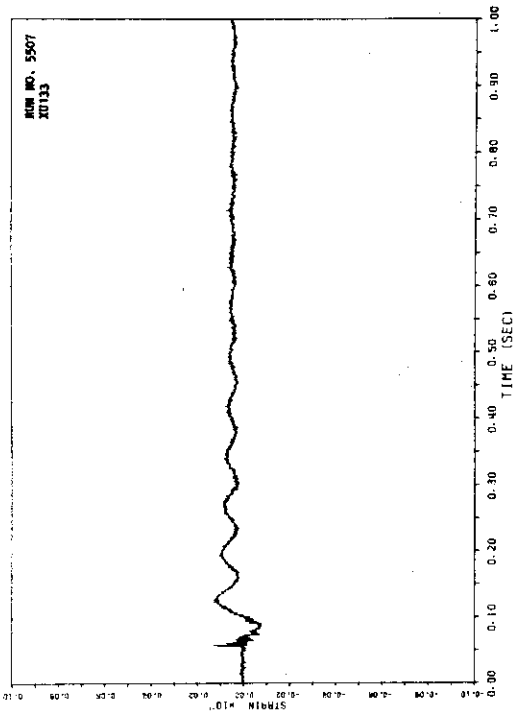

A.280

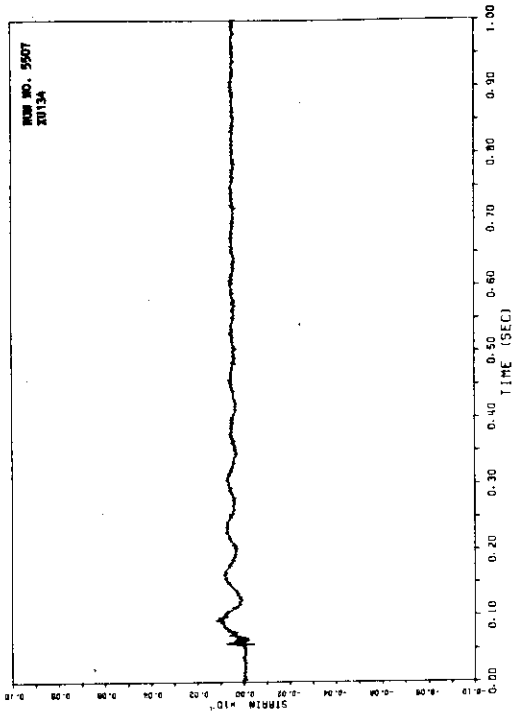

A.282

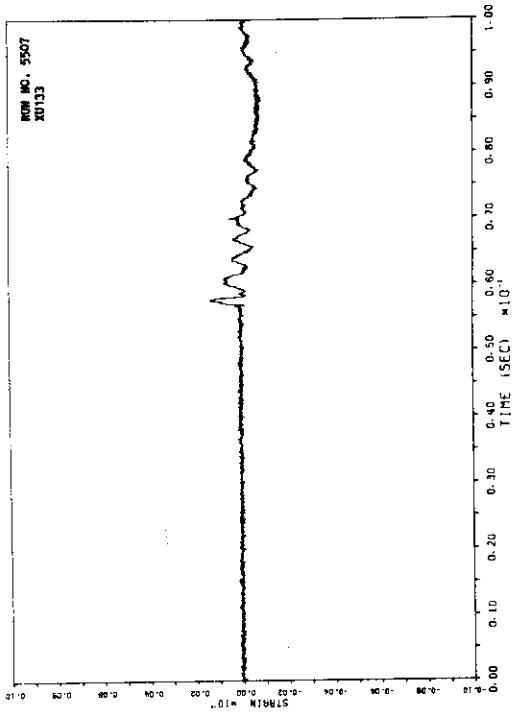

A.279

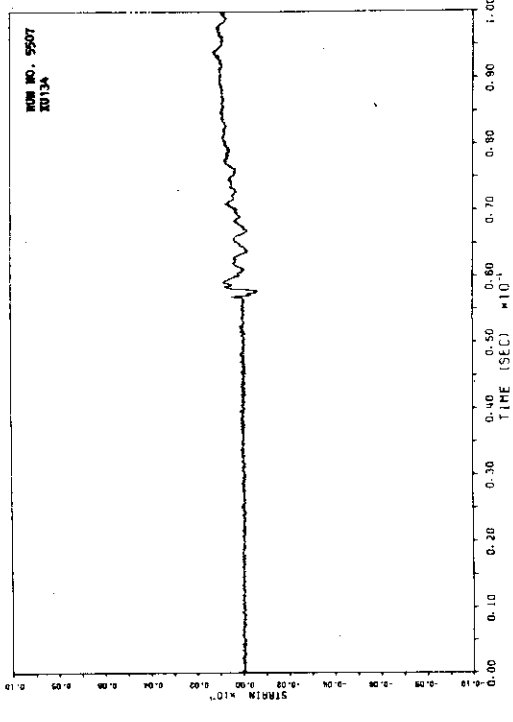

A.281

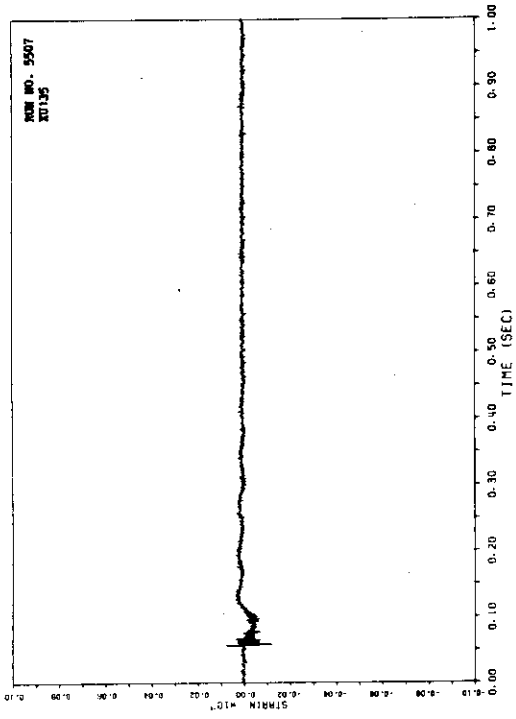

A.284

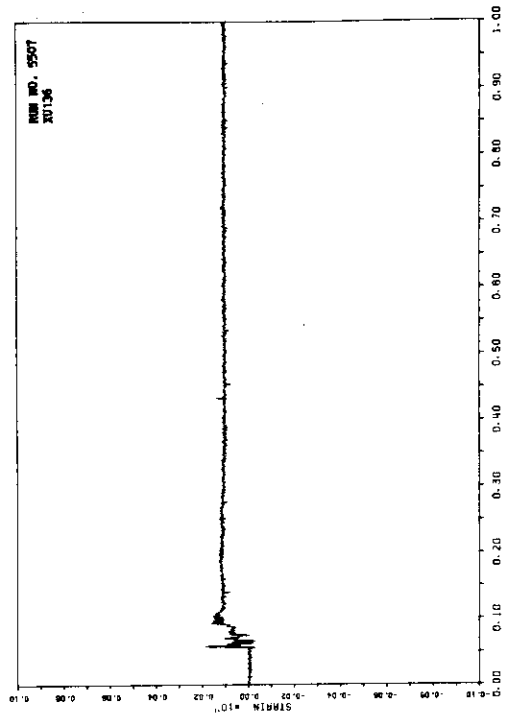

A.286

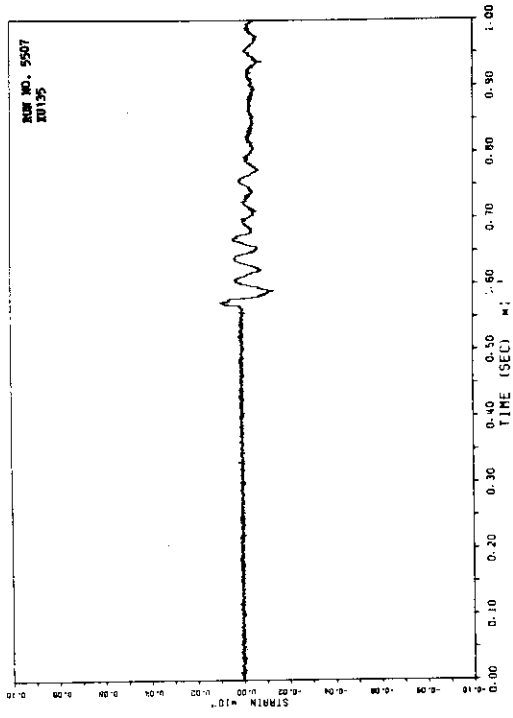

A.283

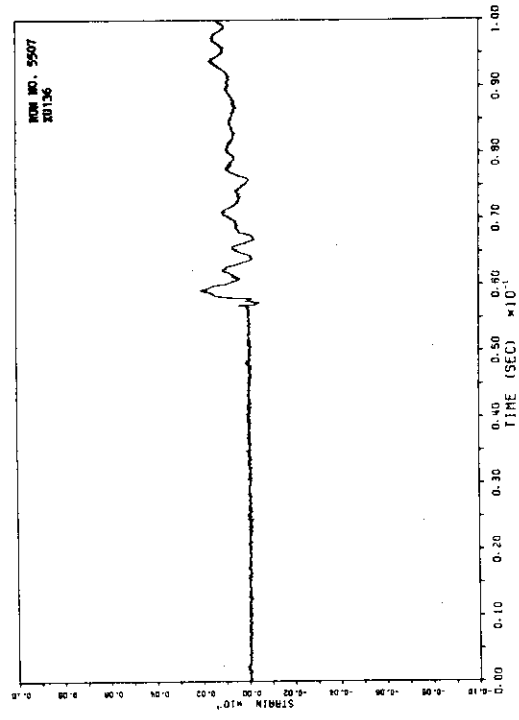

A.285

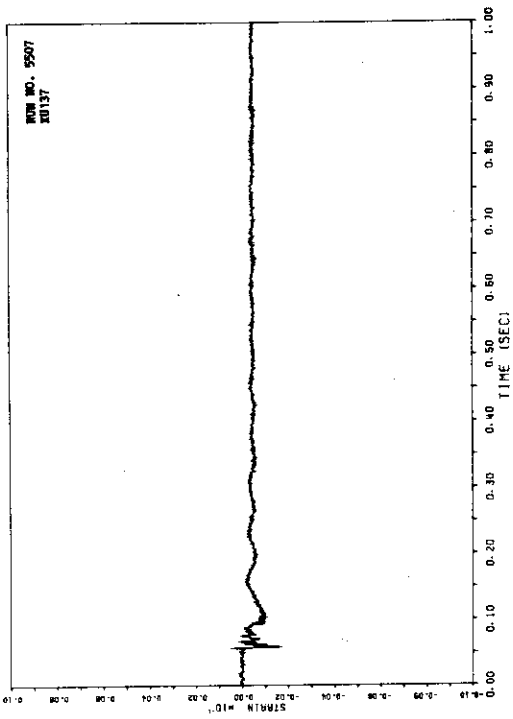

A.288

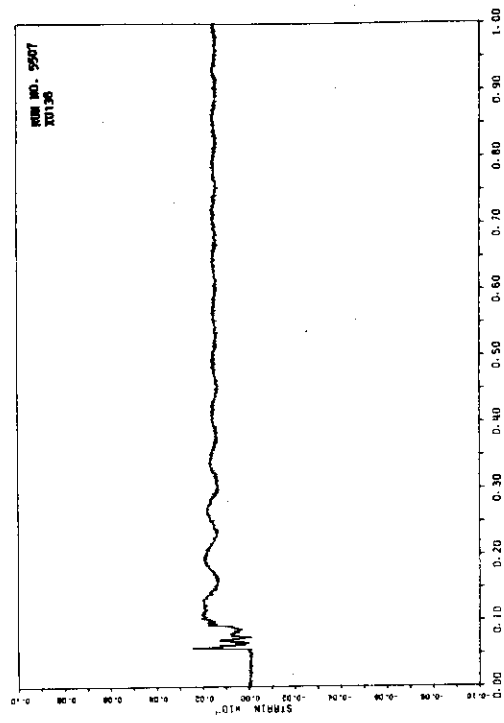

A.290

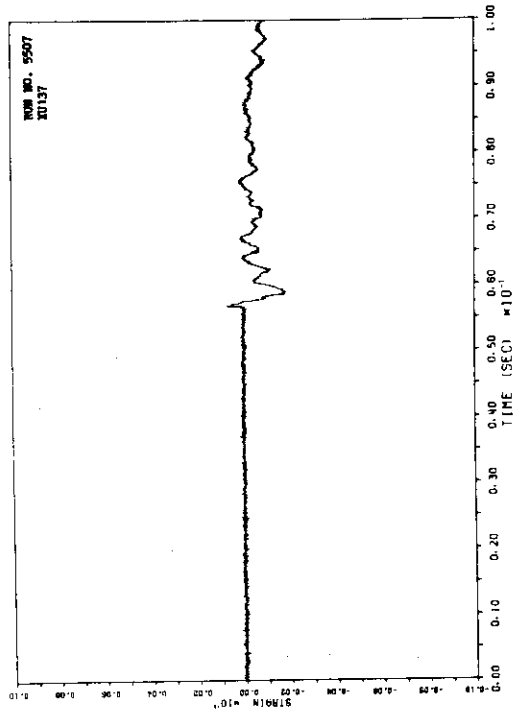

A.287

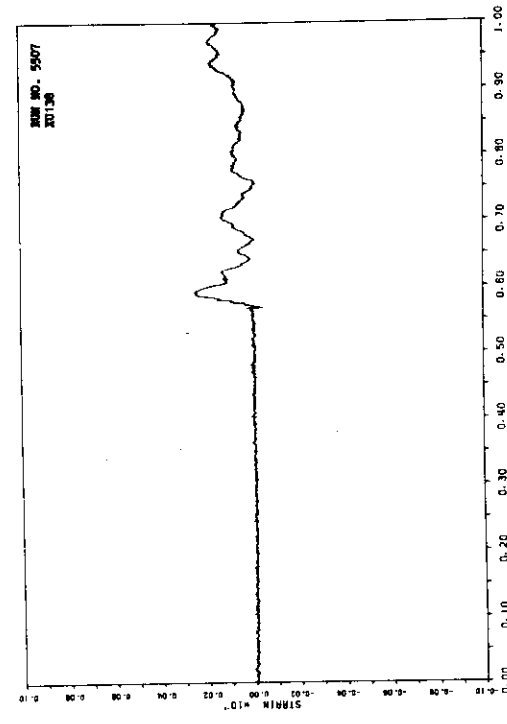

A.289

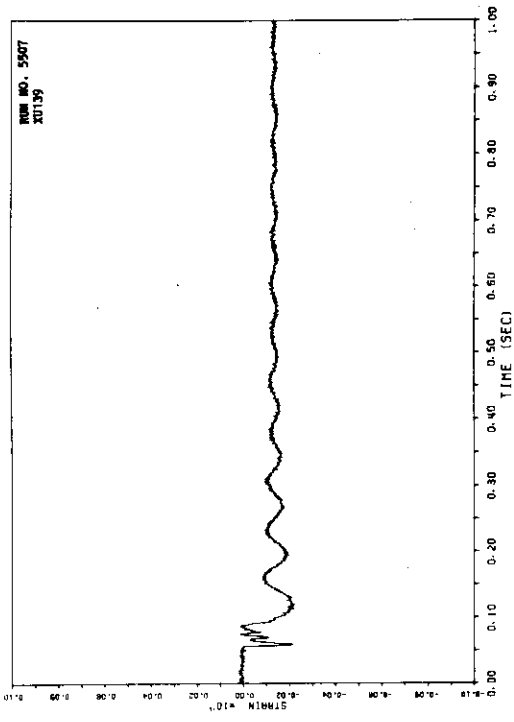

A.292

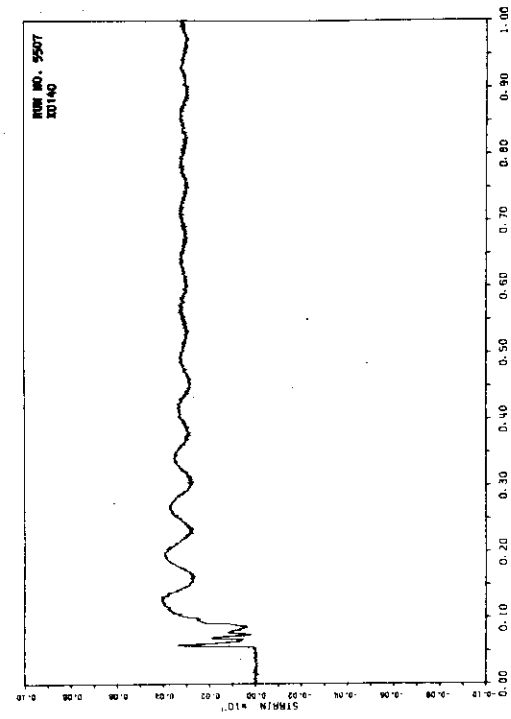

A.294

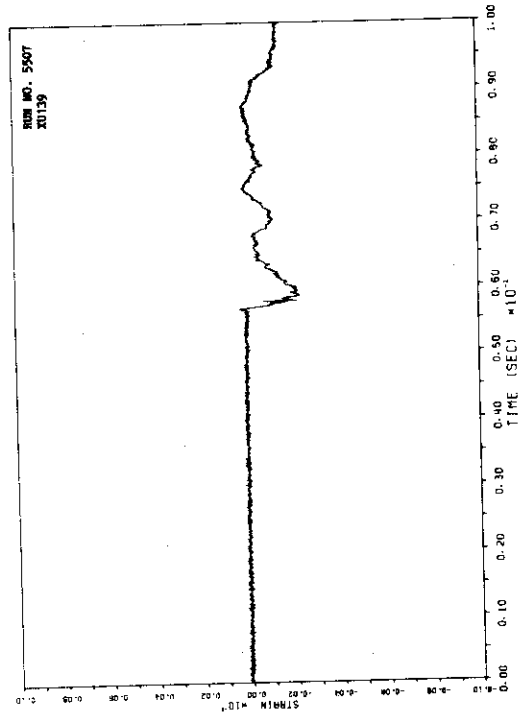

A.291

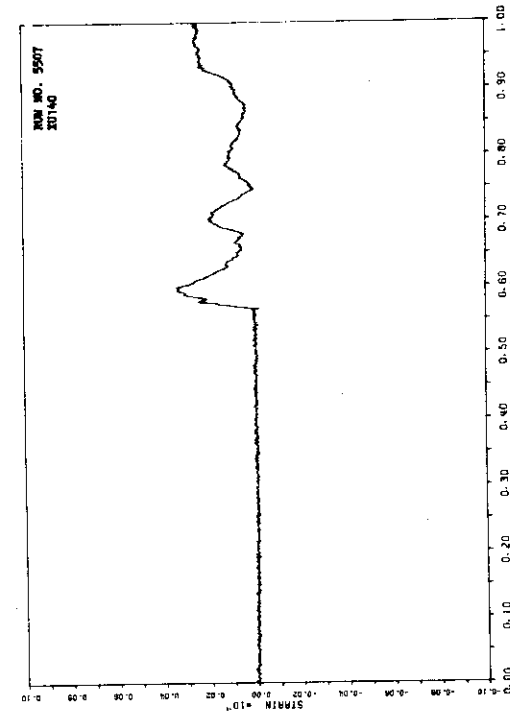

A.293

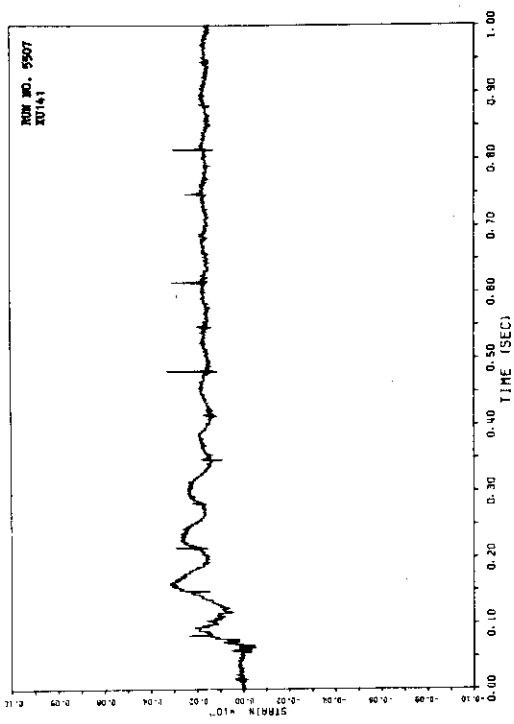

A.296

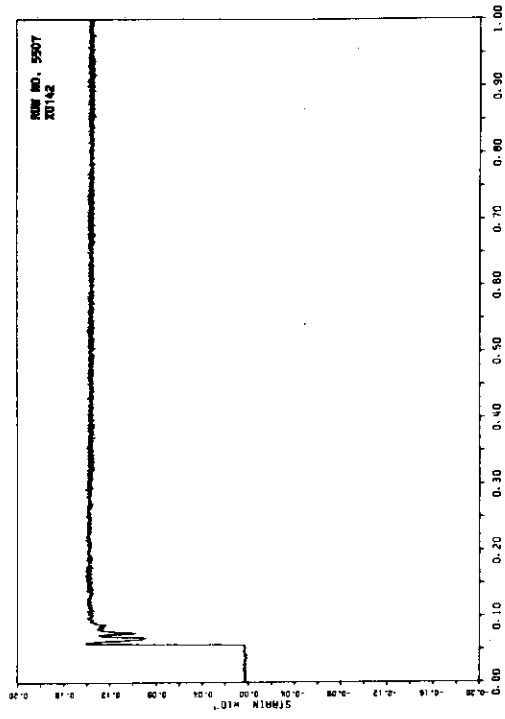

A.298

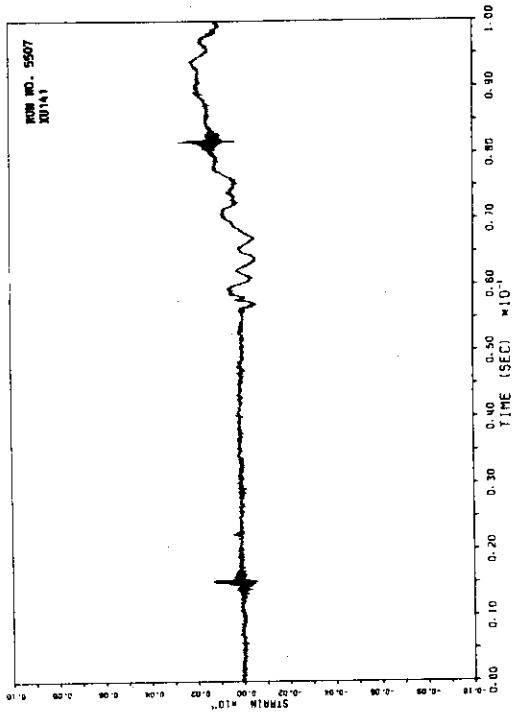

A.295

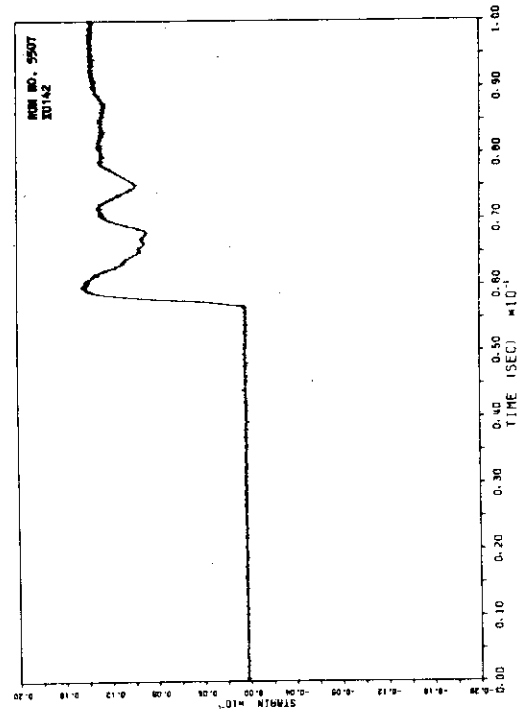

A.297

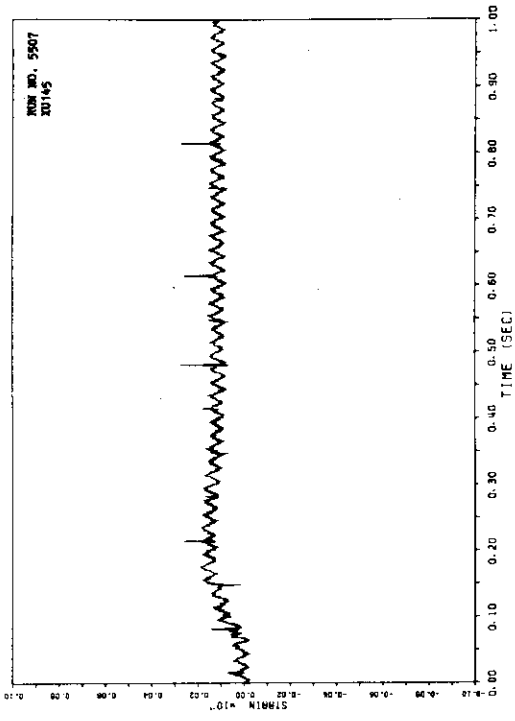

A.300

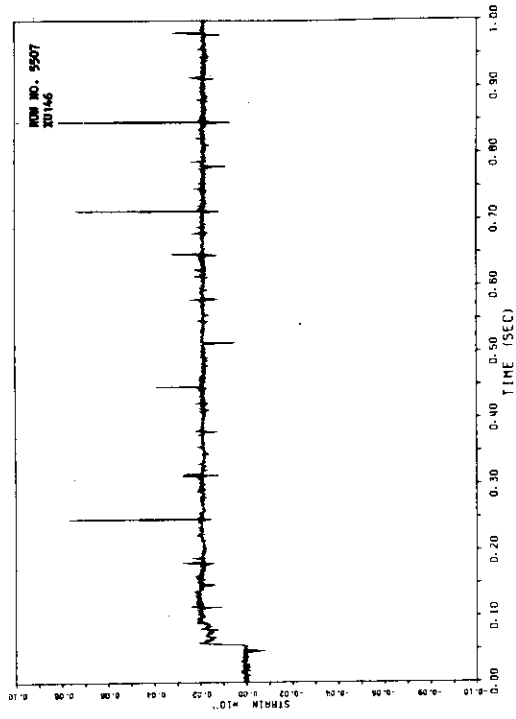

A.302

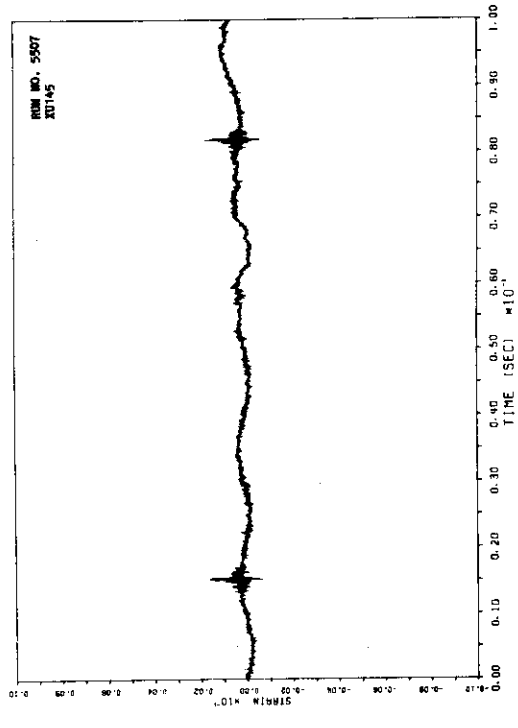

A.299

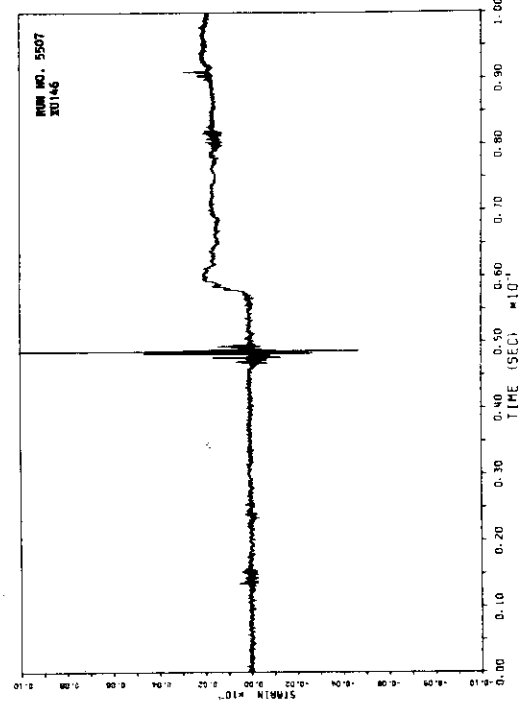

A.301

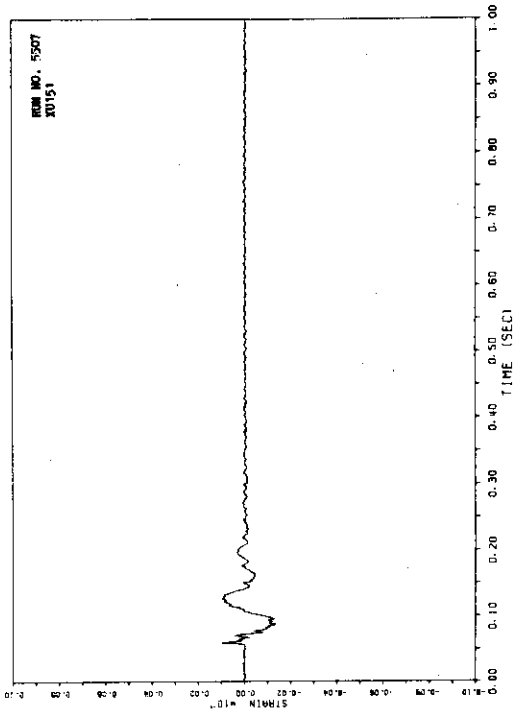

A.304

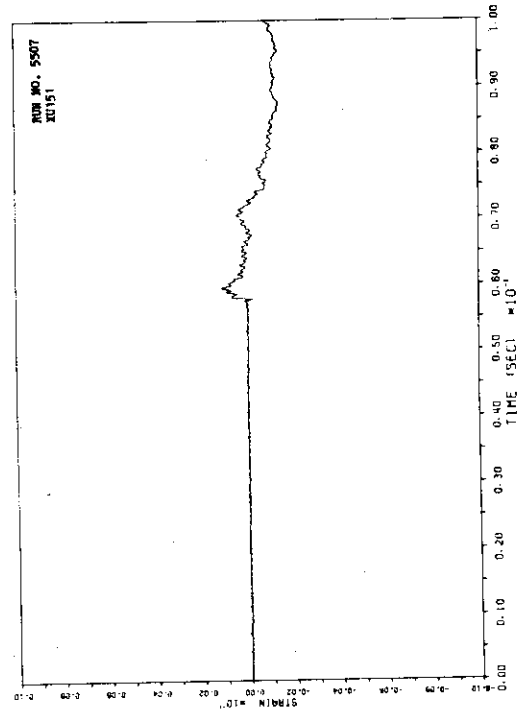

A.303

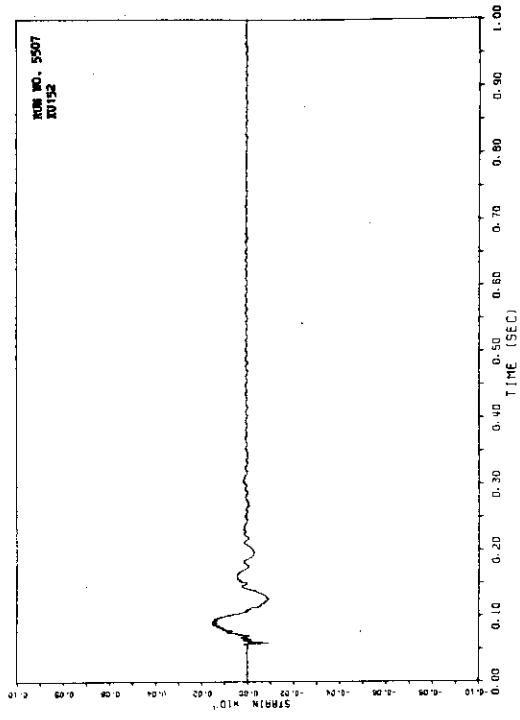

A.306

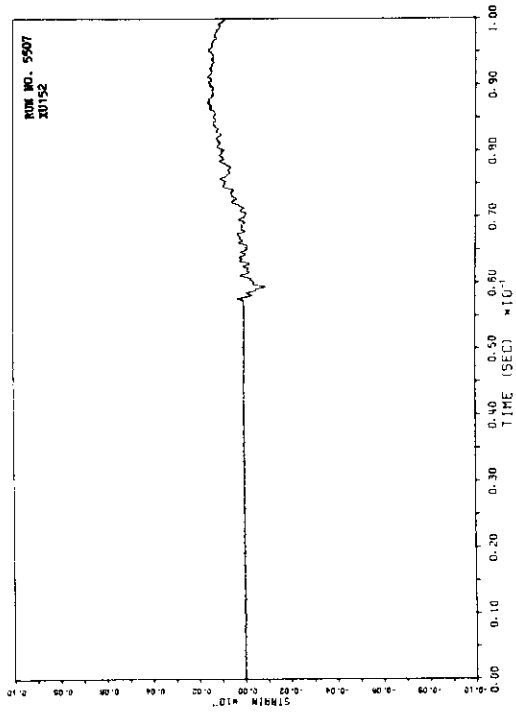

A.305

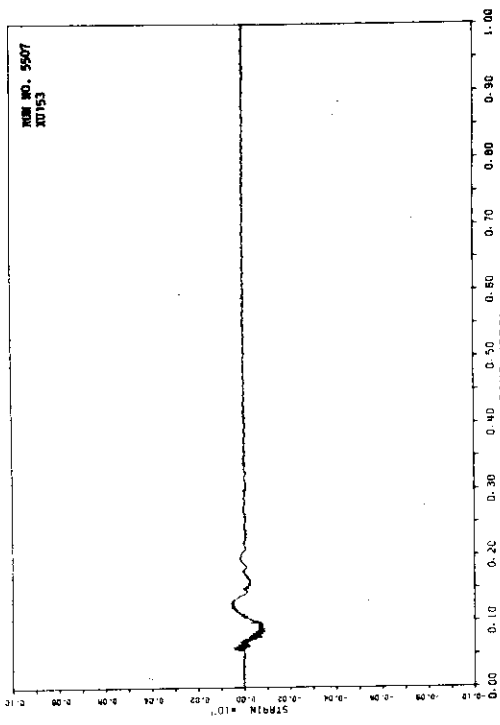

A.308

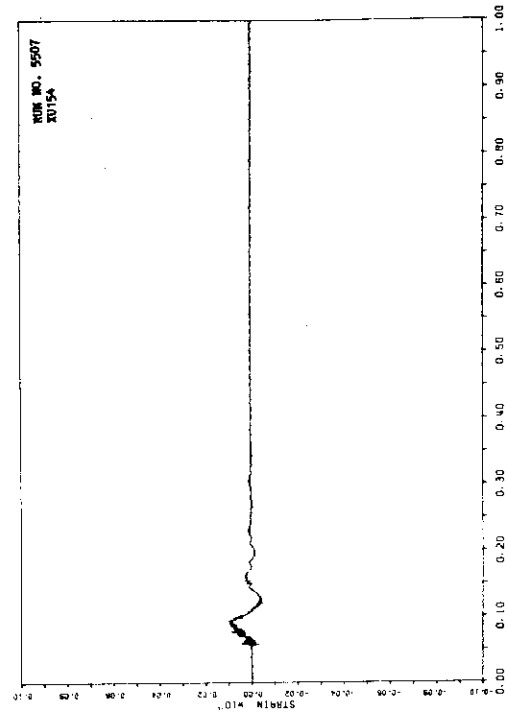

A.310

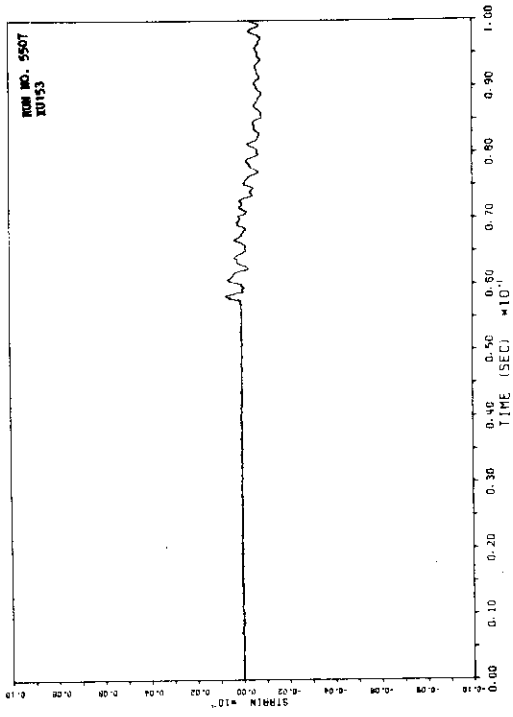

A.307

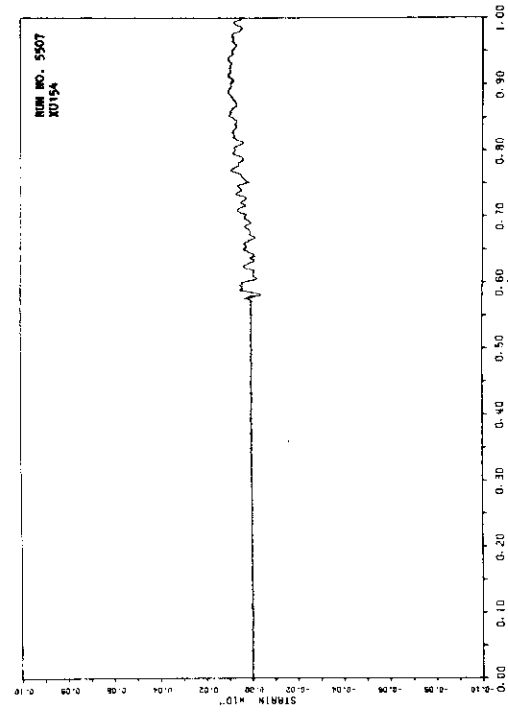

A.309

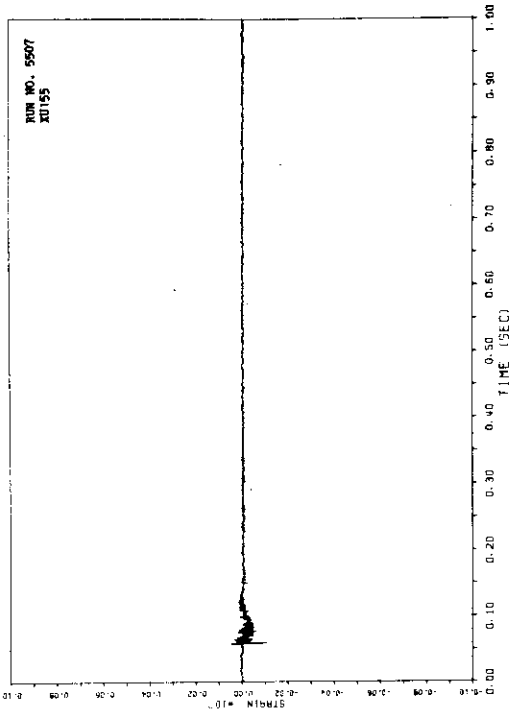

A.312

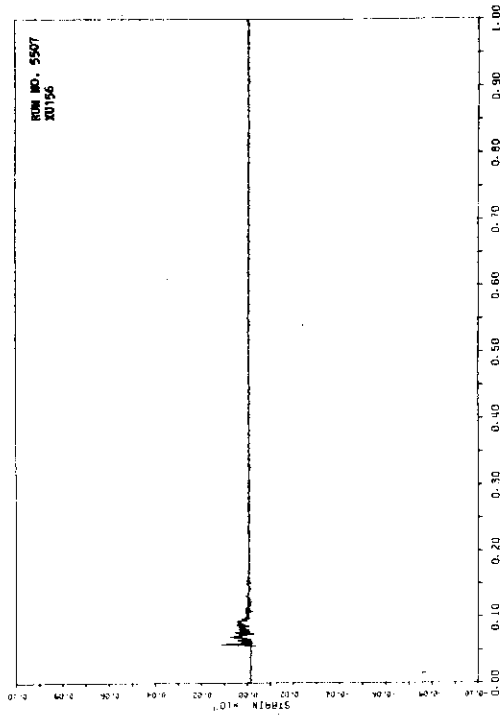

A.314

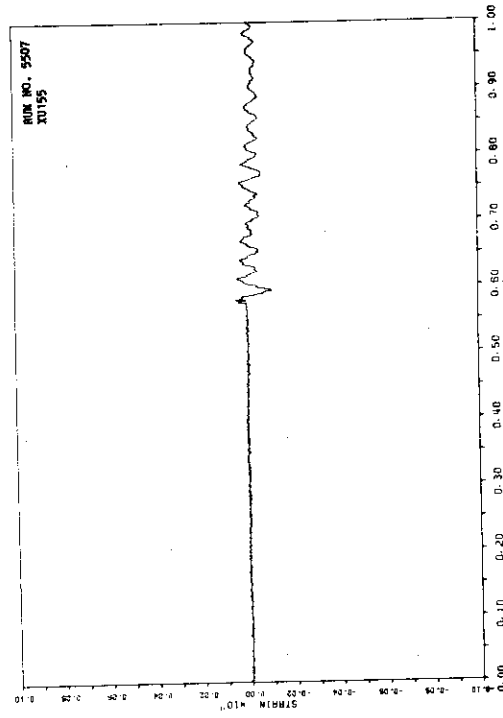

A.311

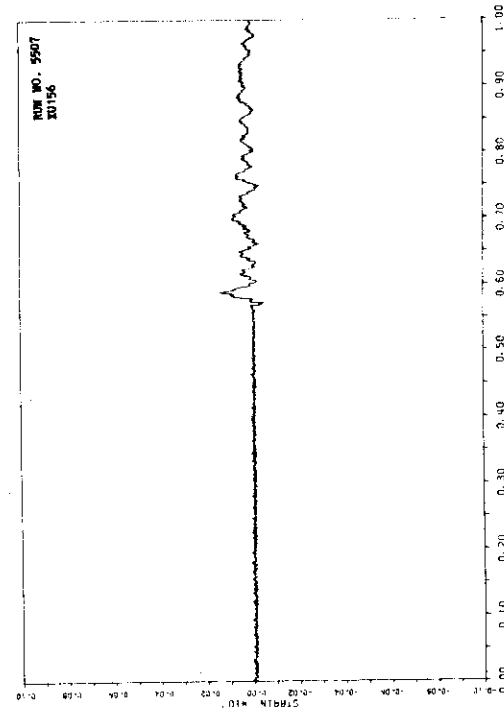

A.313

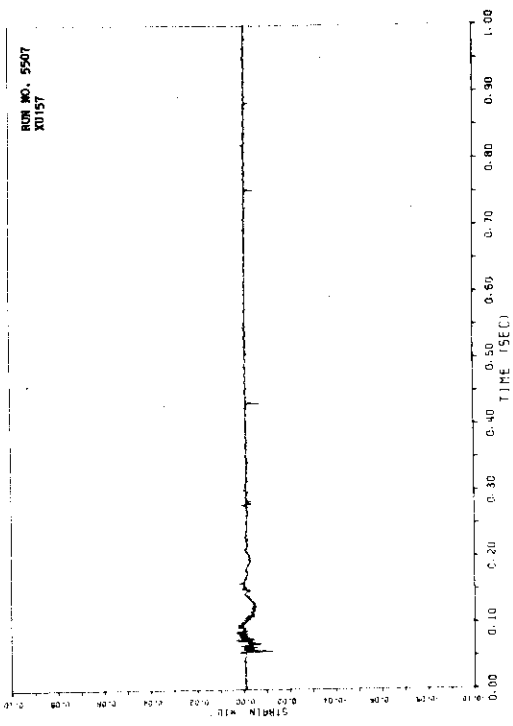

A.316

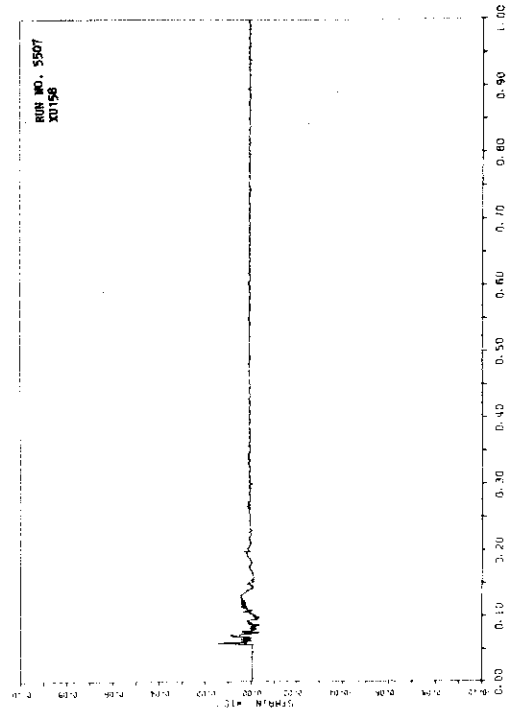

A.318

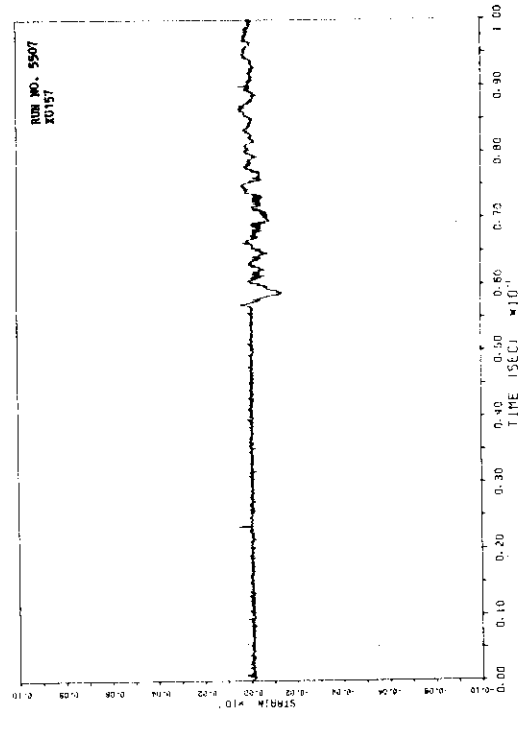

A.315

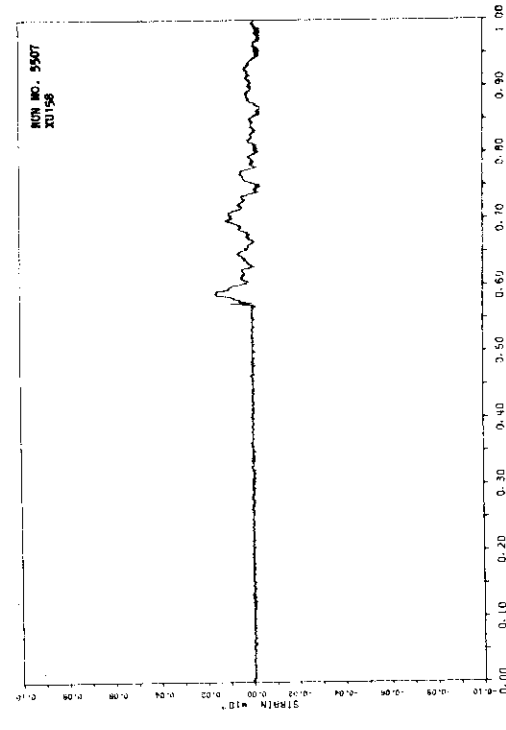

A.317

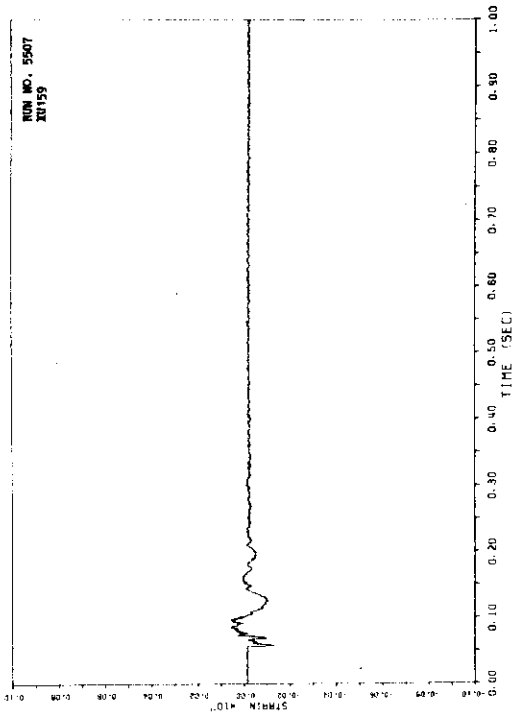

A.320

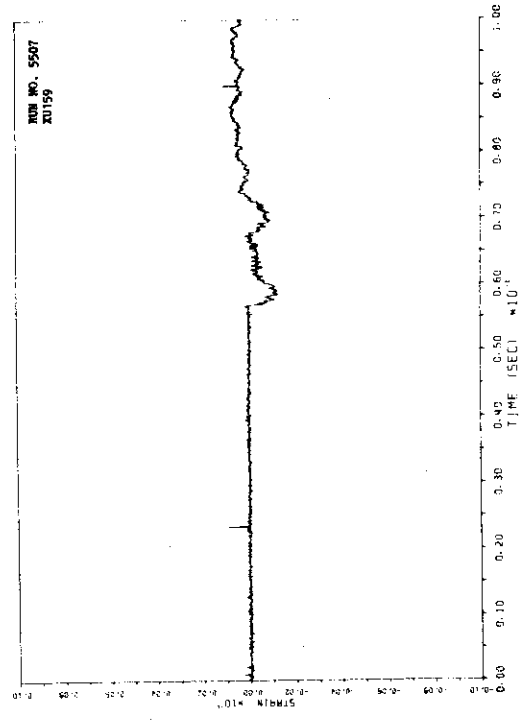

A.319

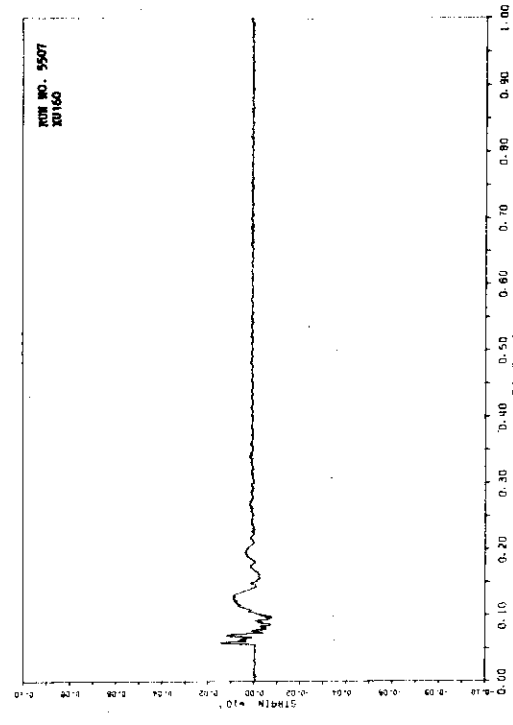

A.322

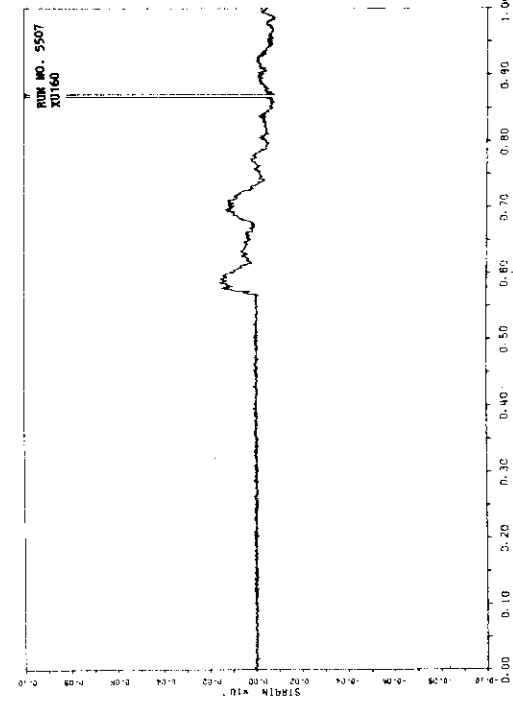

A.321

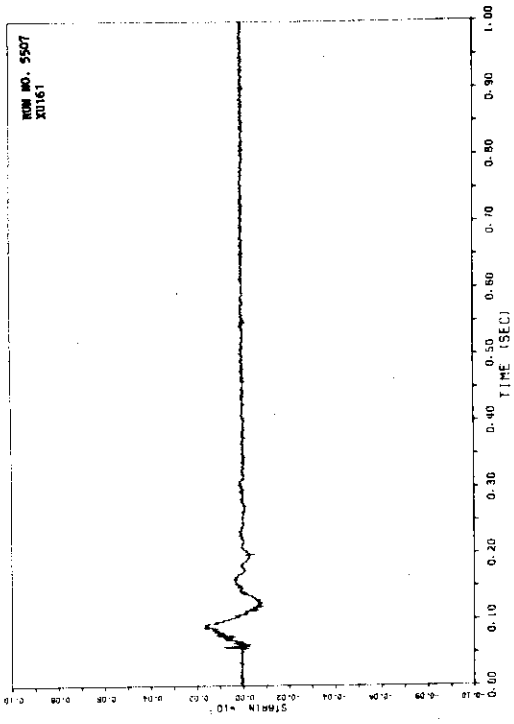

A.324

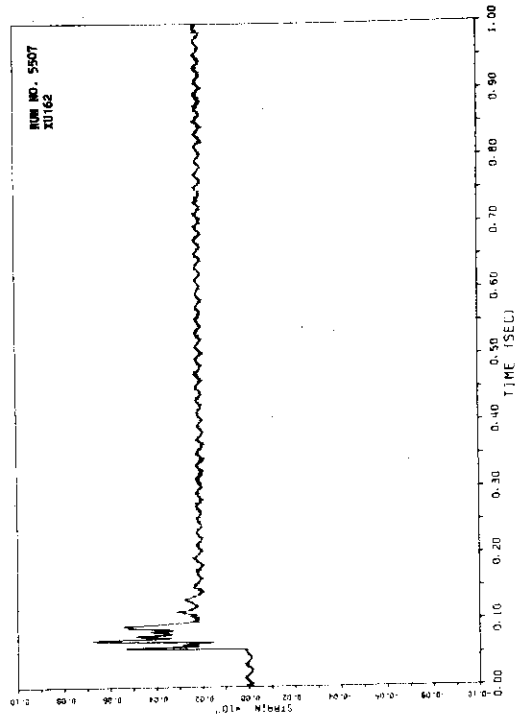

A.326

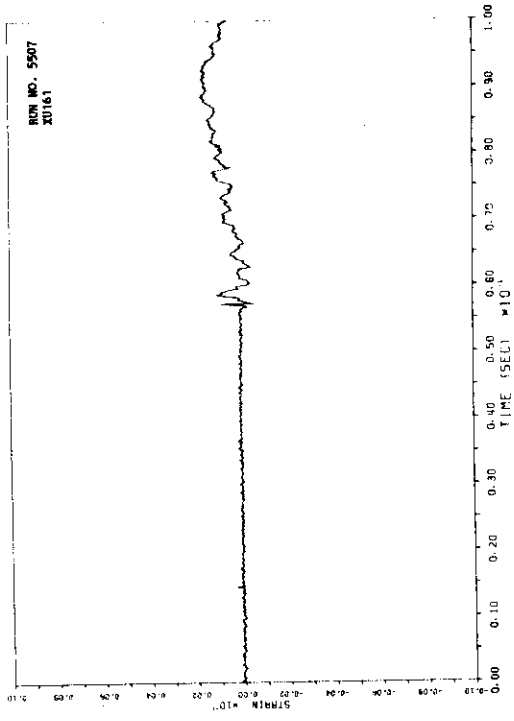

A.323

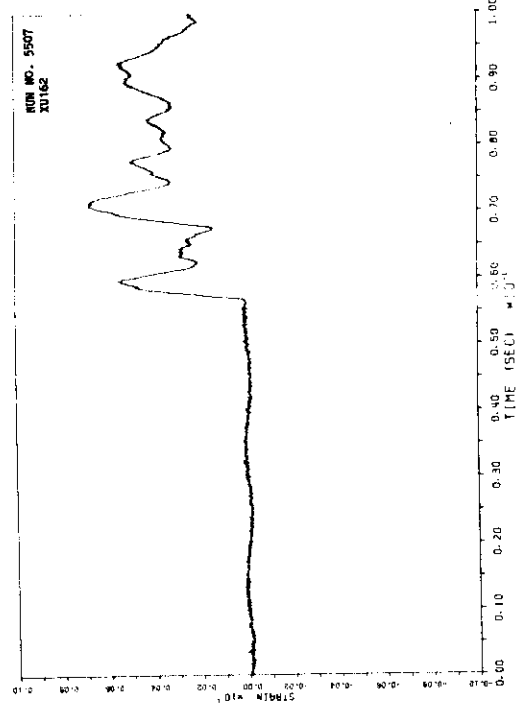

A.325

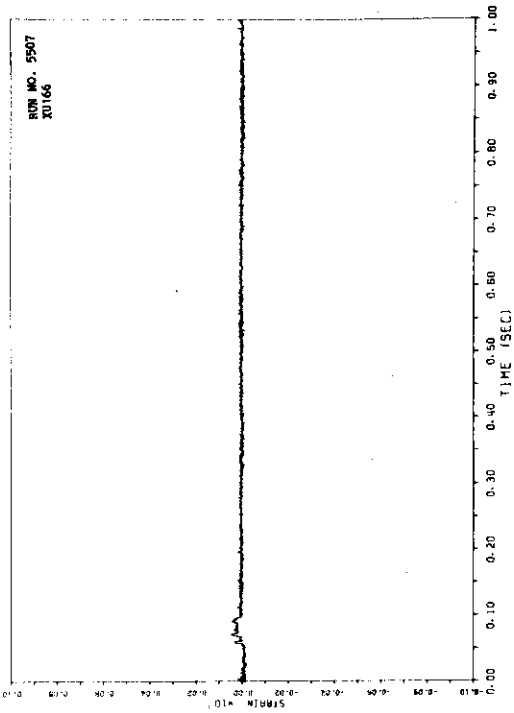

A.328

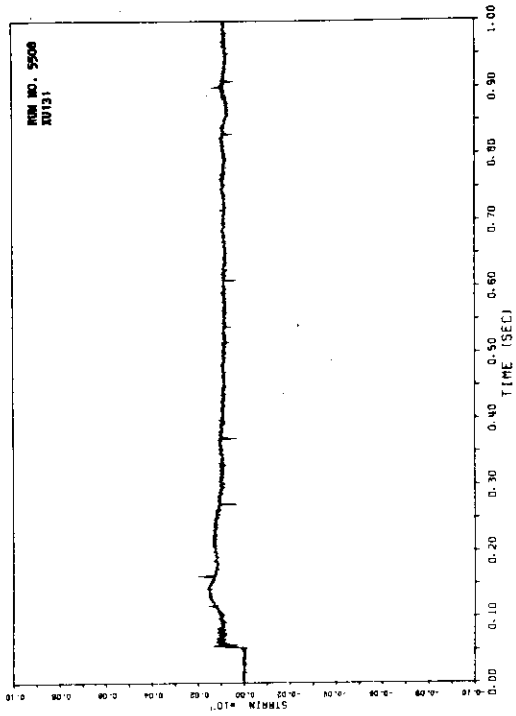

A.330

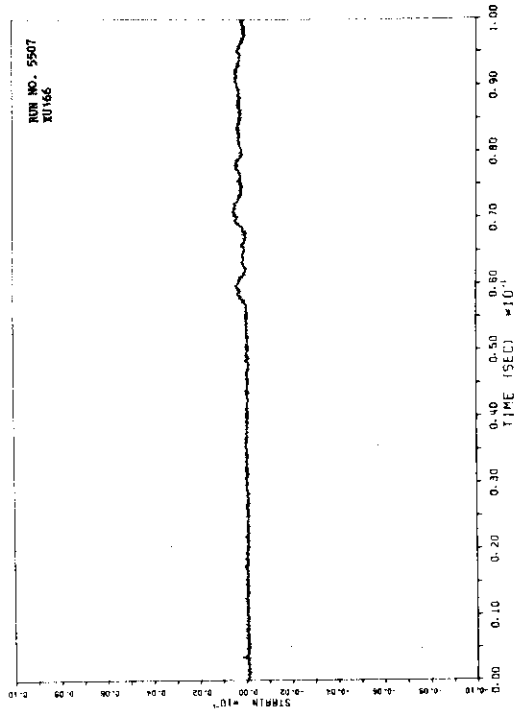

A.327

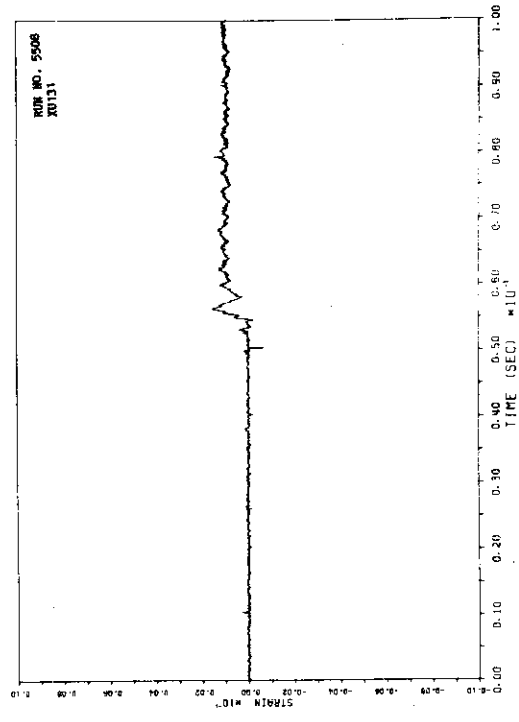

A.329

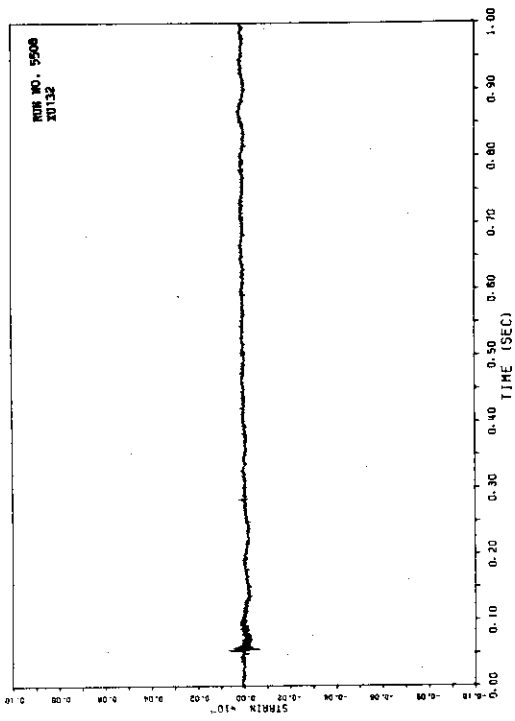

A.332

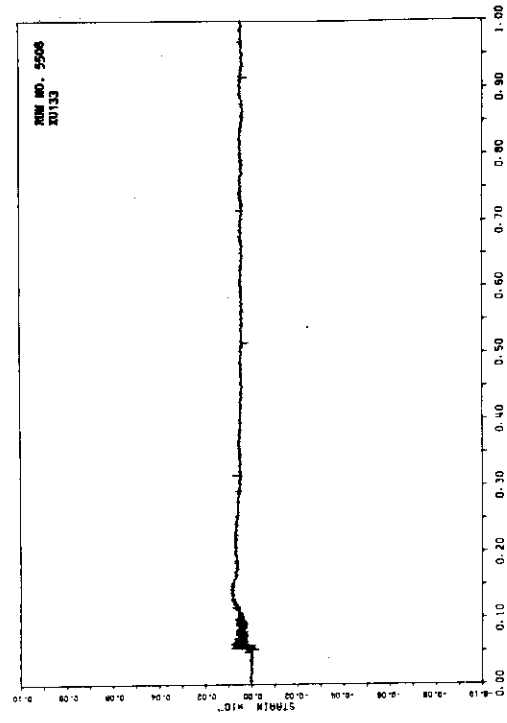

A.334

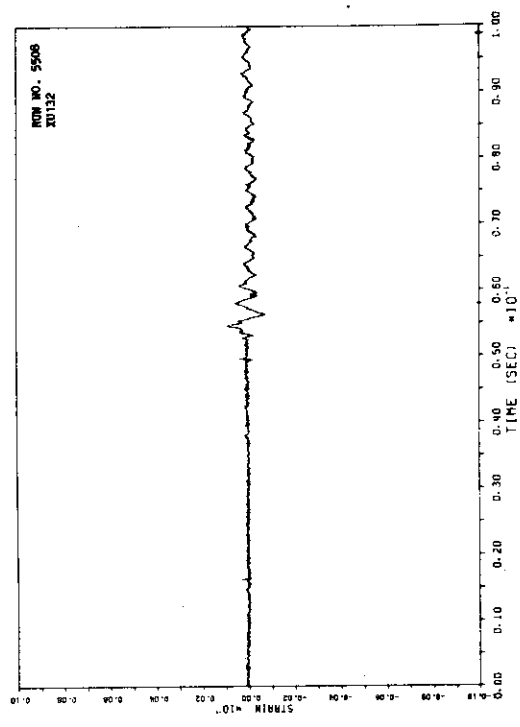

A.331

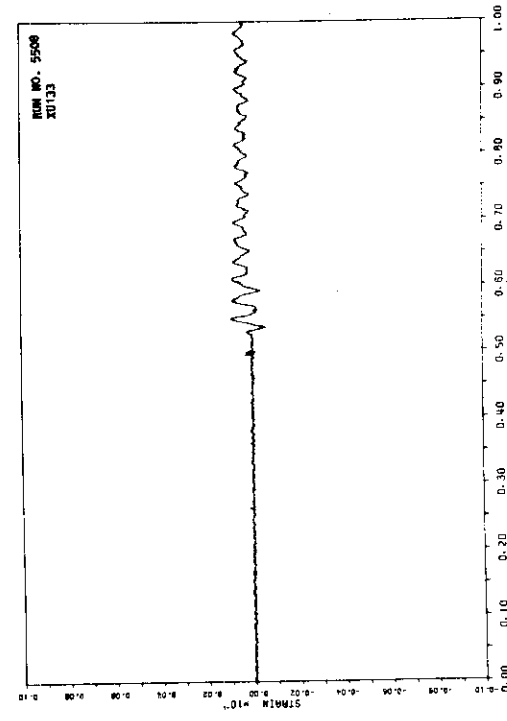

A.333

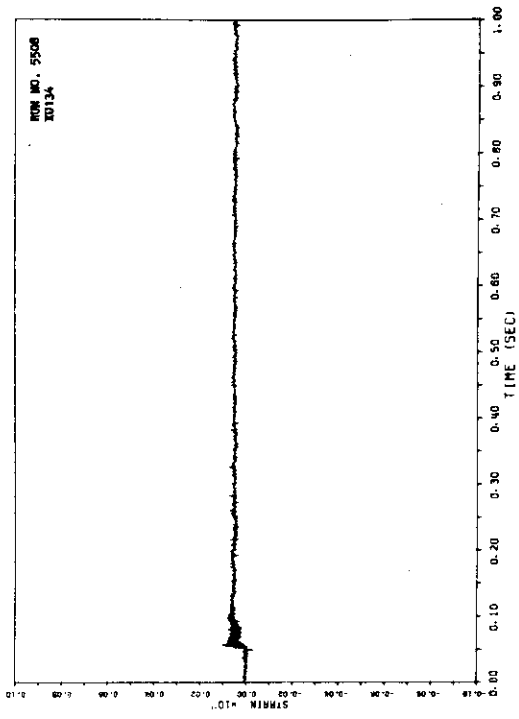

A.336

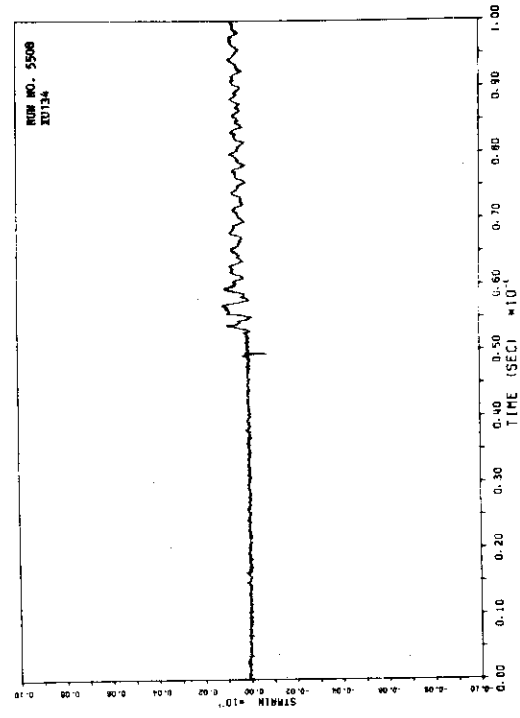

A.335

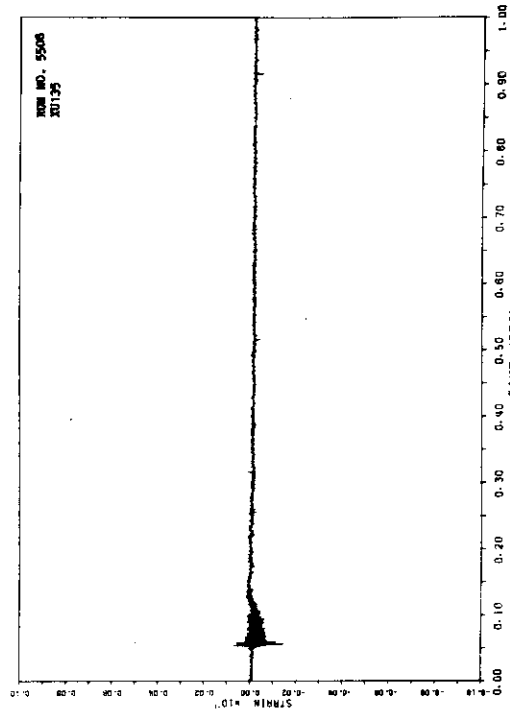

A.338

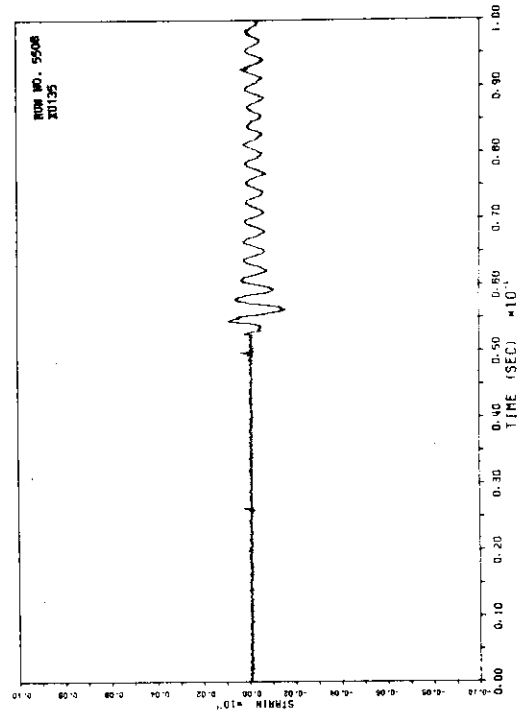

A.337

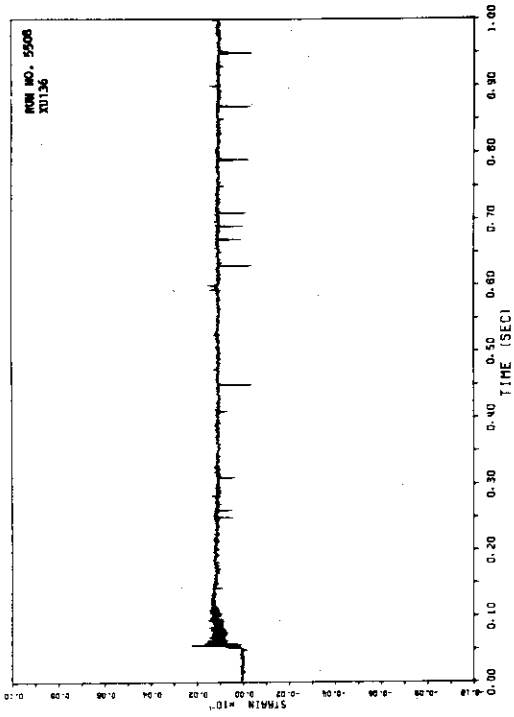

A.340

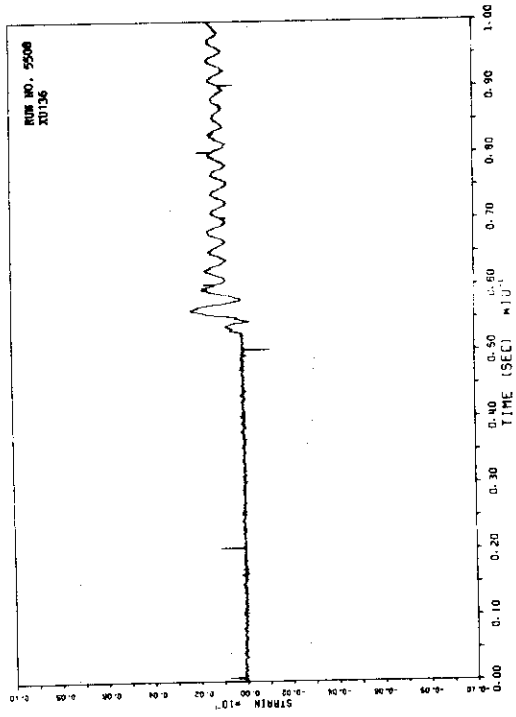

A.339

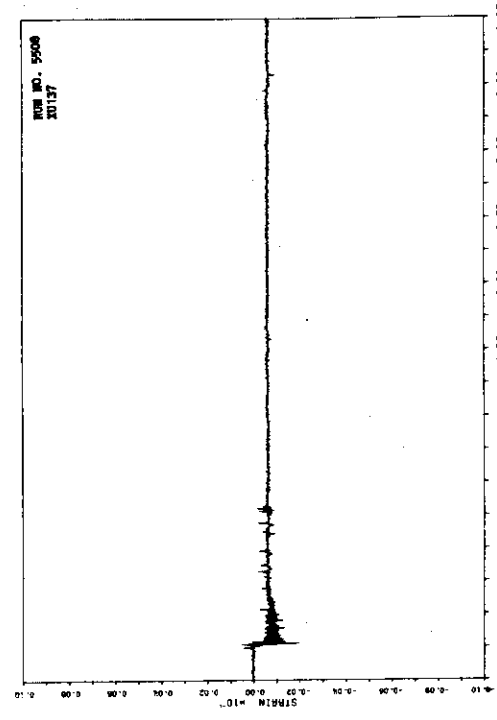

A.342

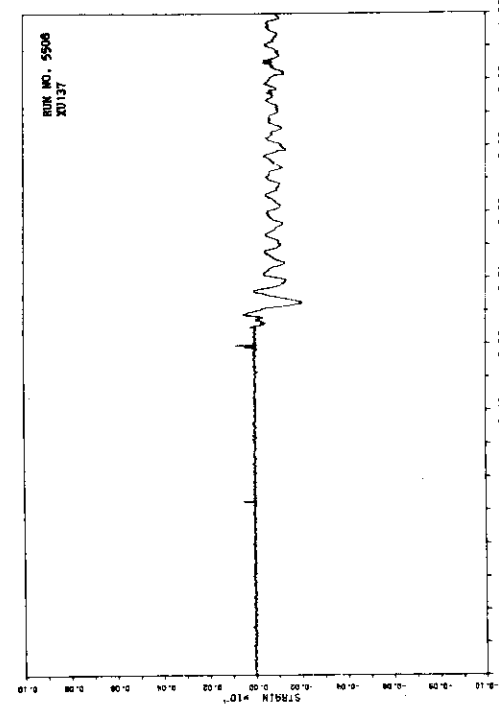

A.341

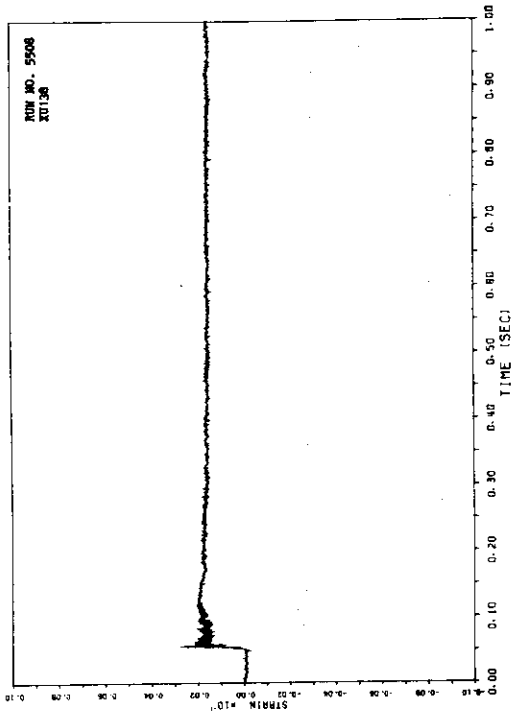

A.344

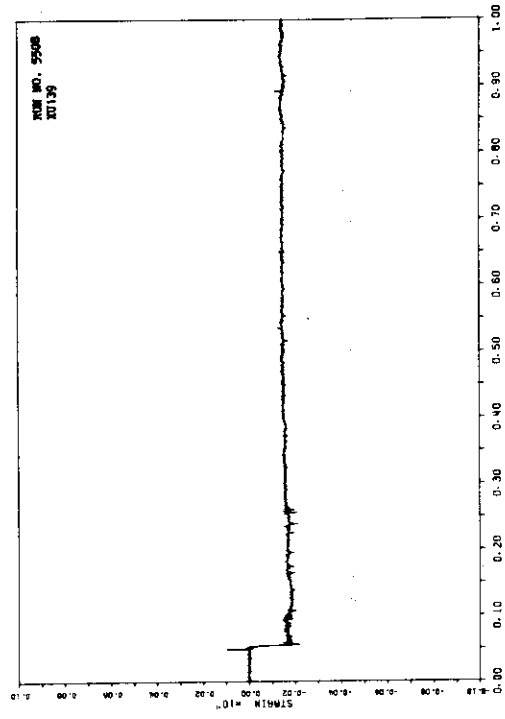

A.346

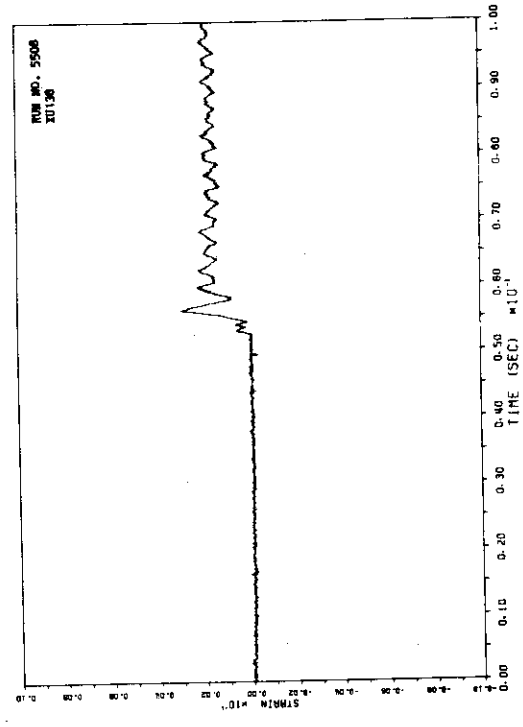

A.343

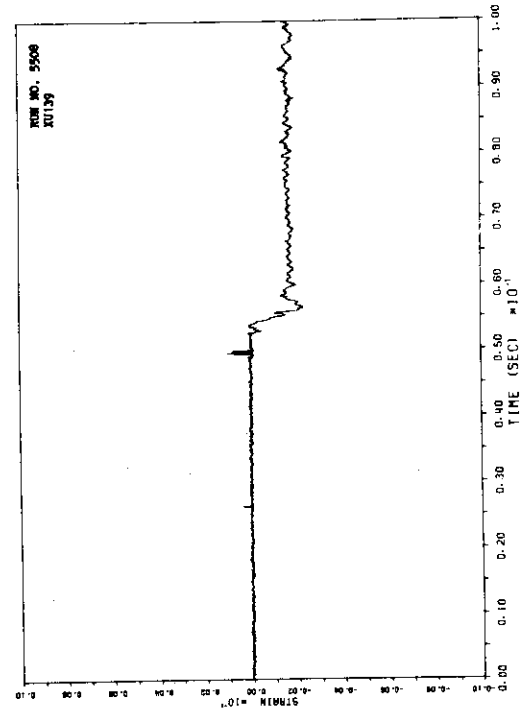

A.345

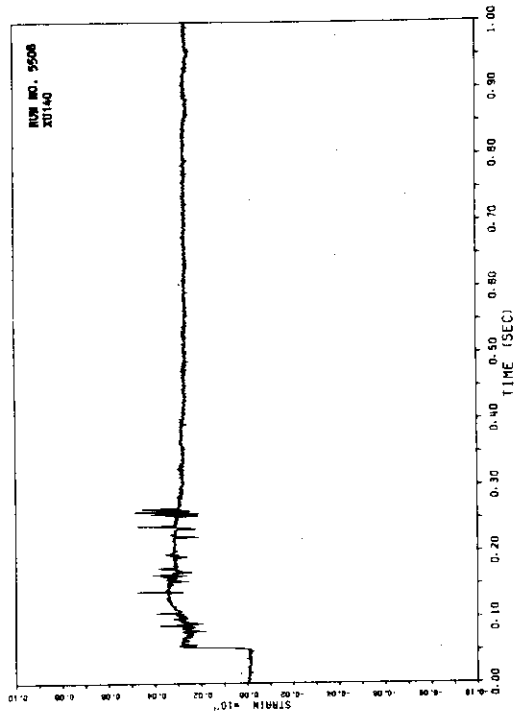

A.348

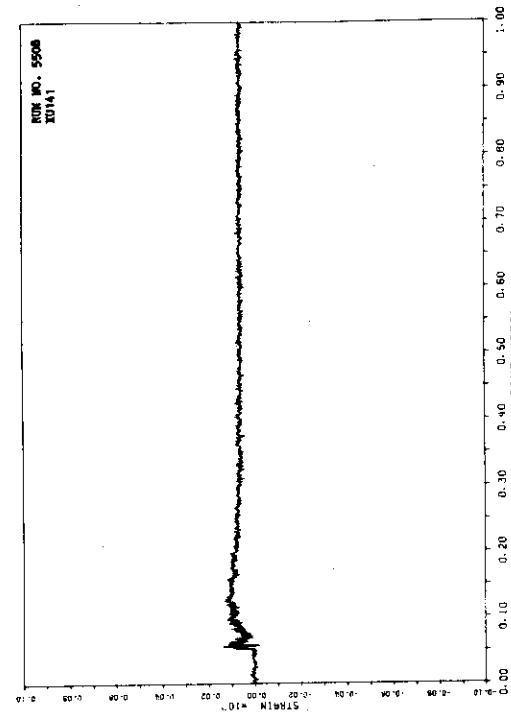

A.350

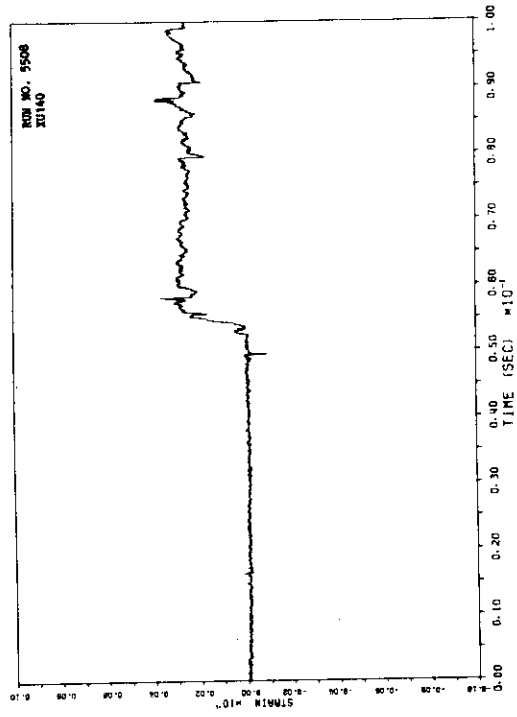

A.347

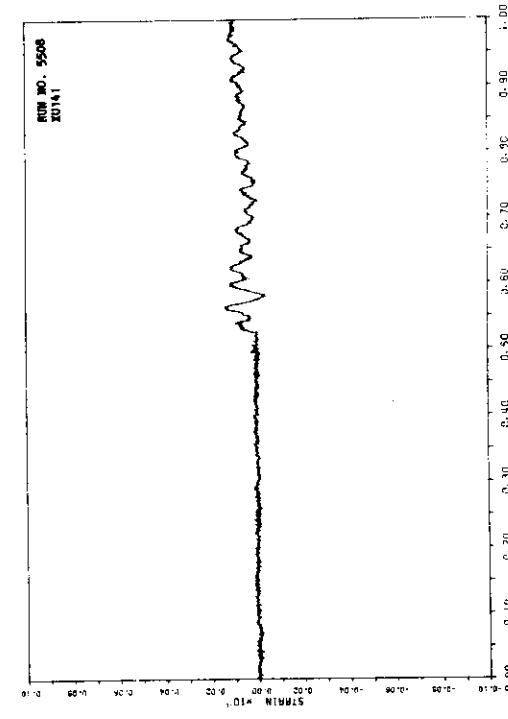

A.349

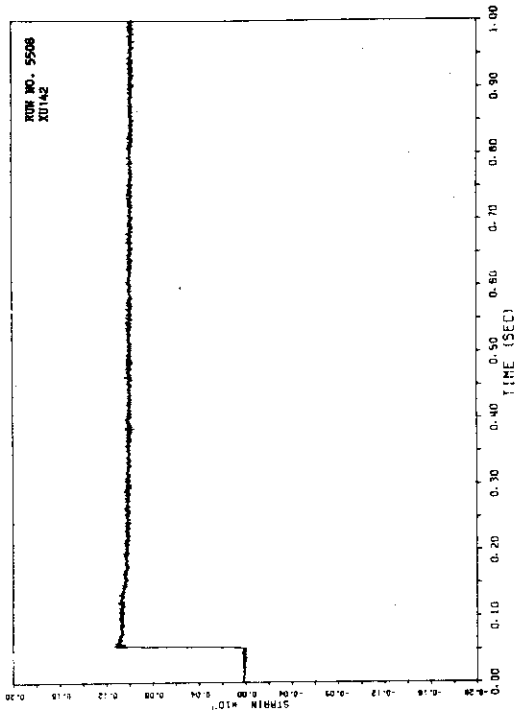

A.352

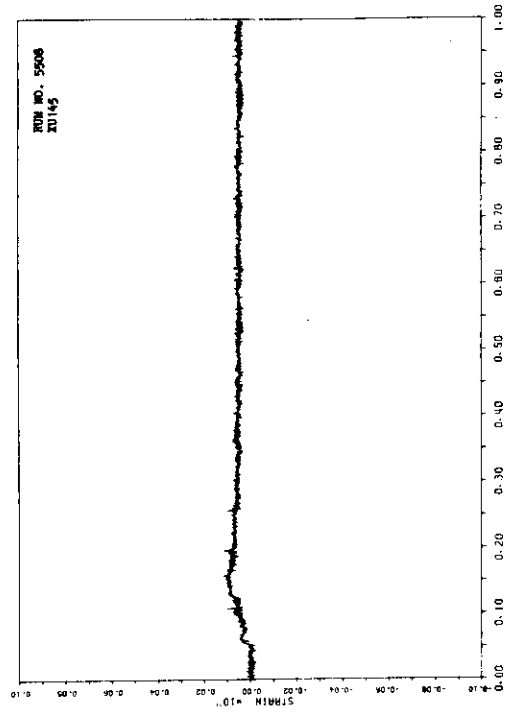

A.354

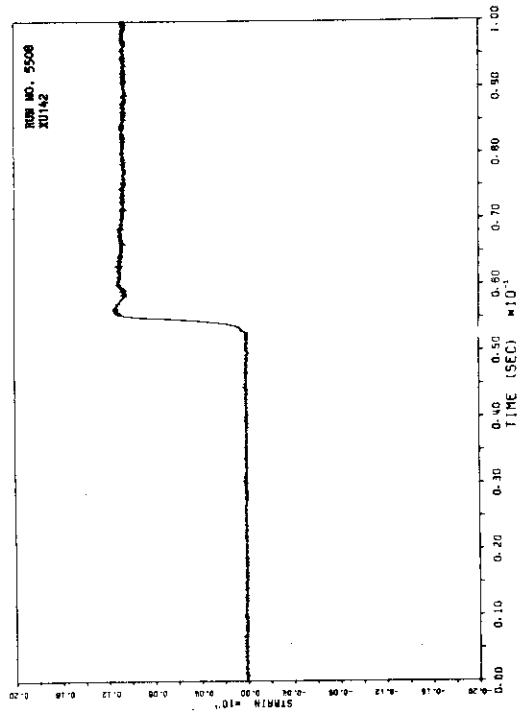

A.351

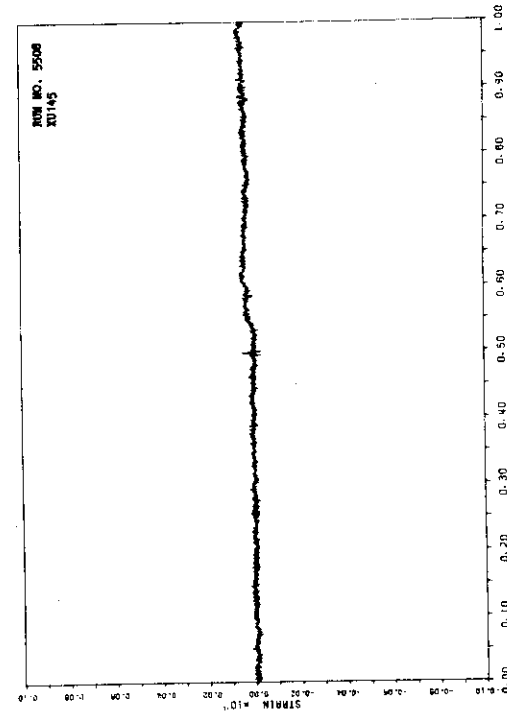

A.353

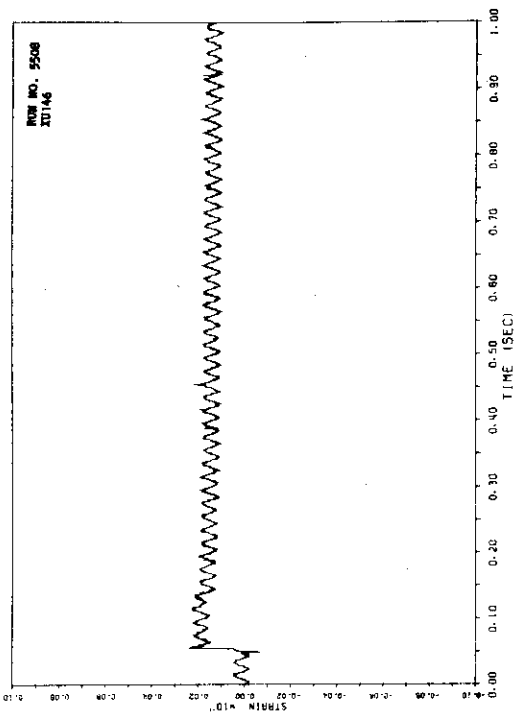

A.356

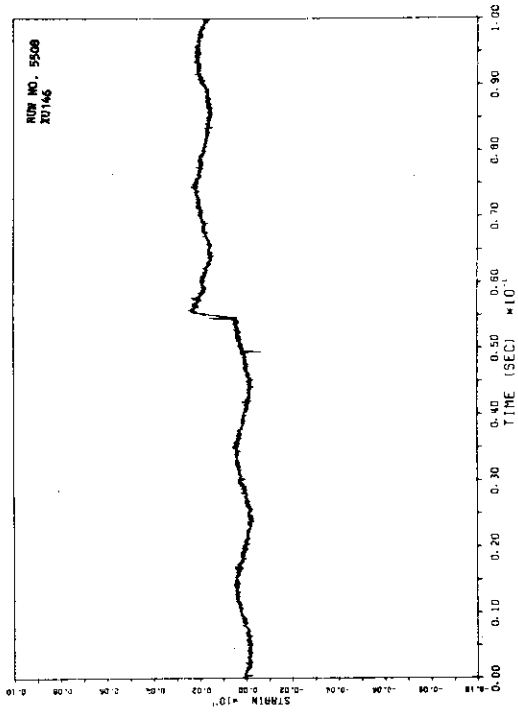

A.355

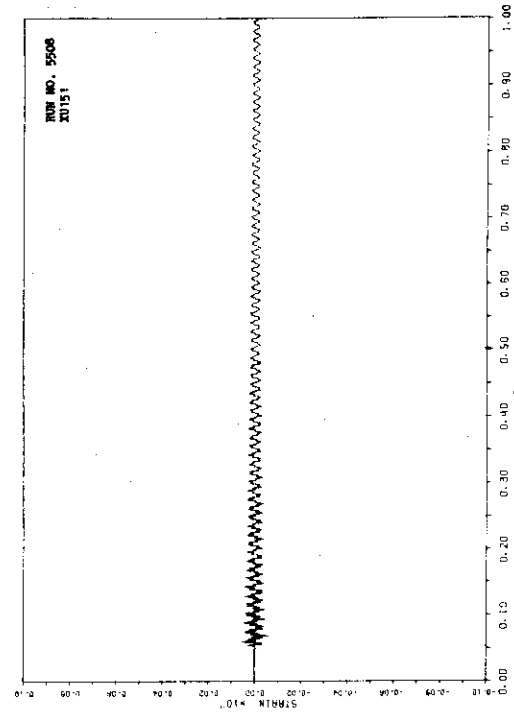

A.358

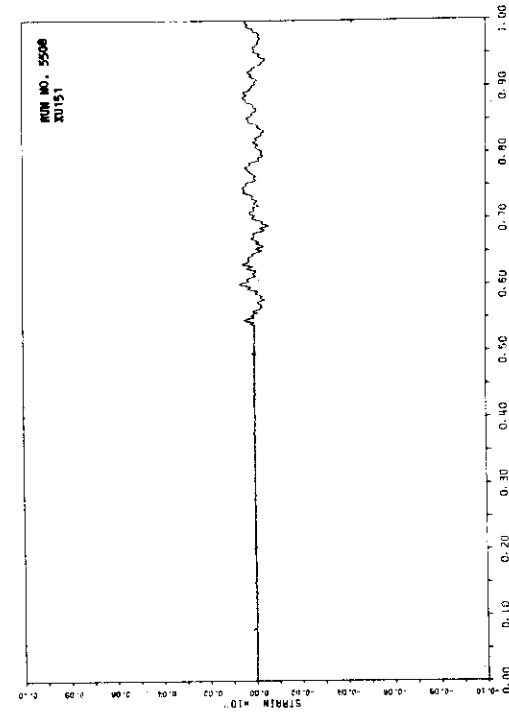

A.357

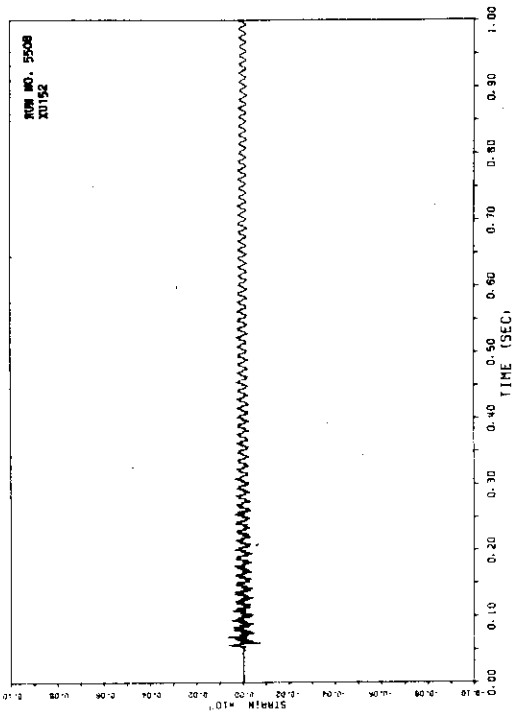

A.360

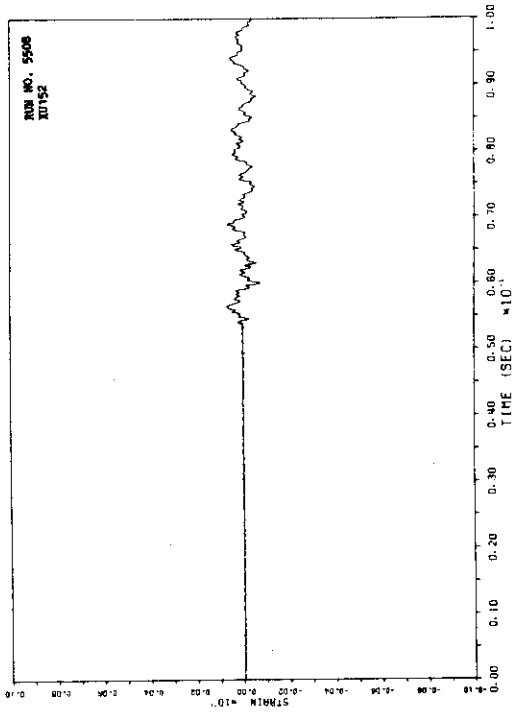

A.359

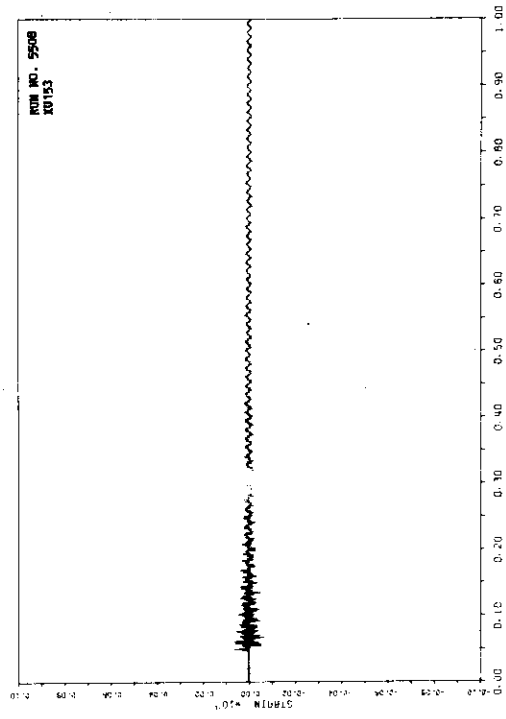

A.362

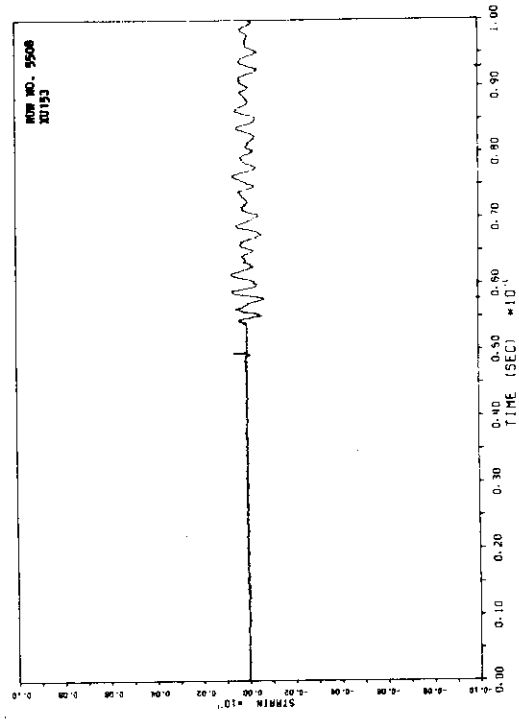

A.361

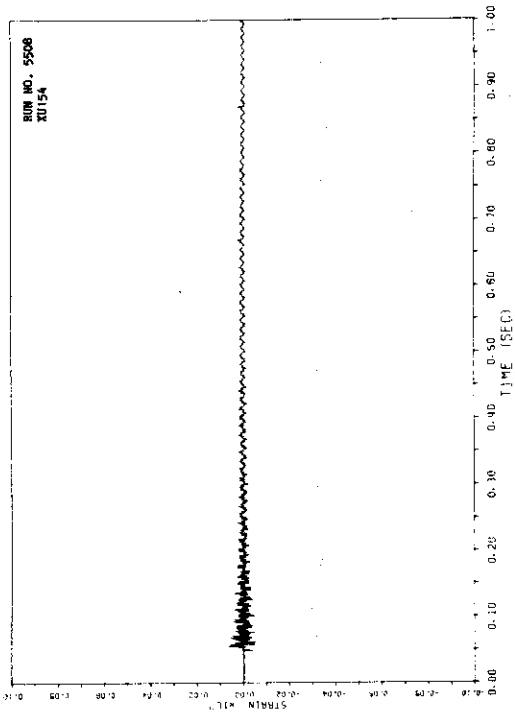

A.364

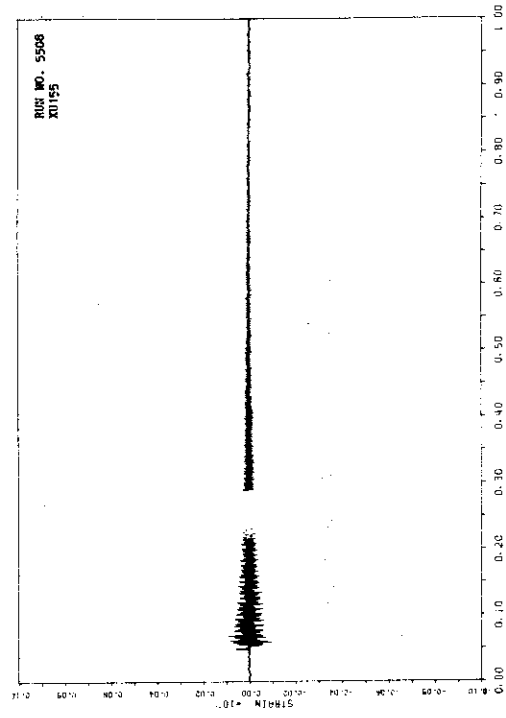

A.366

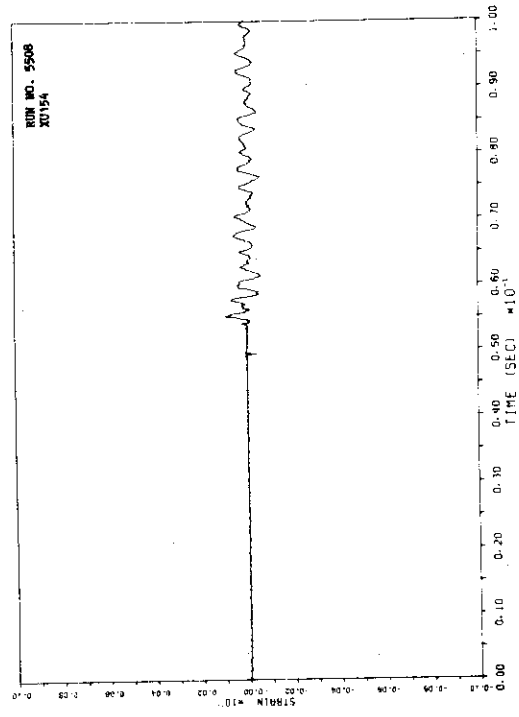

A.363

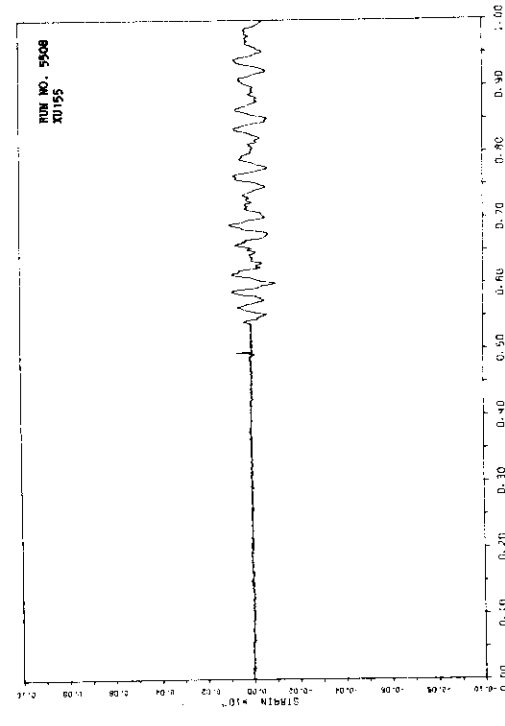

A.365

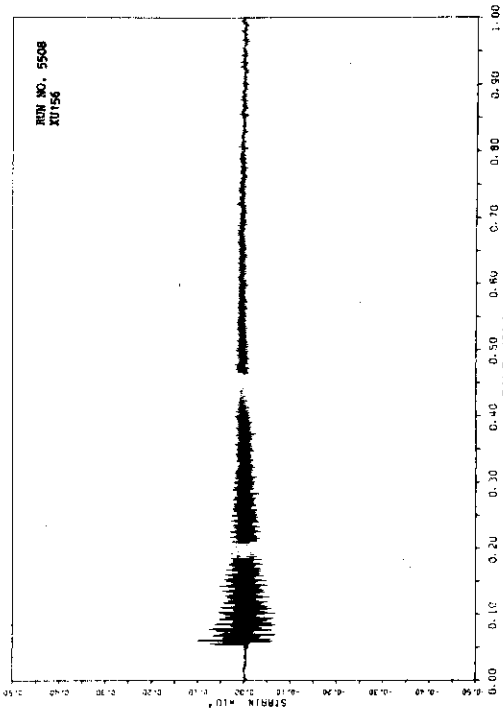

A.368

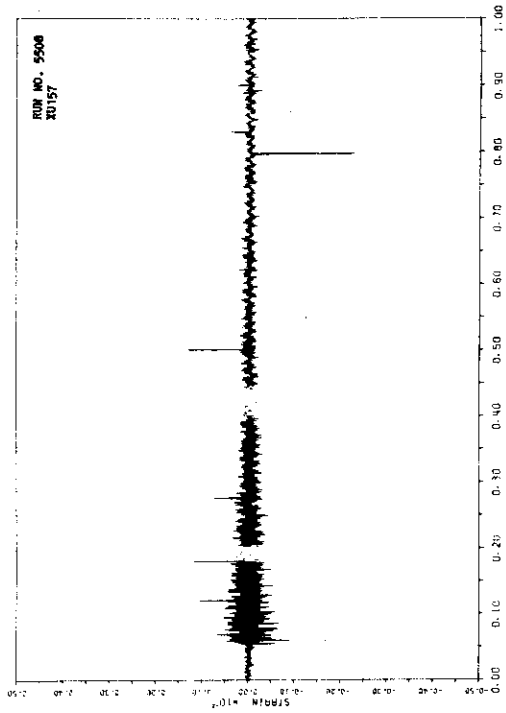

A.370

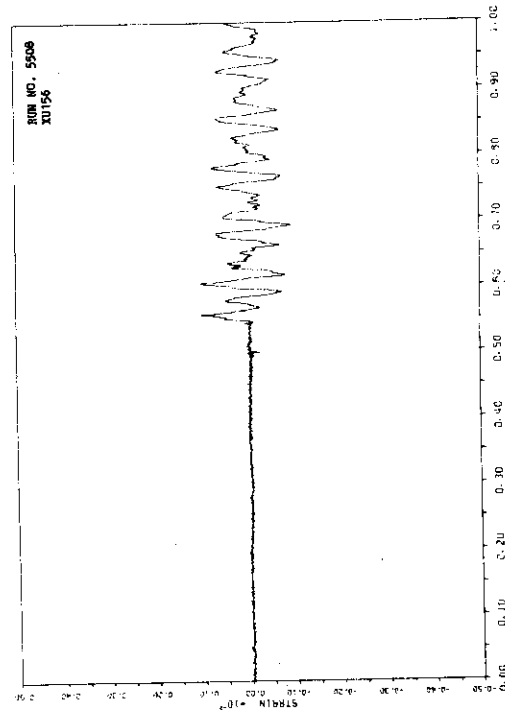

A.367

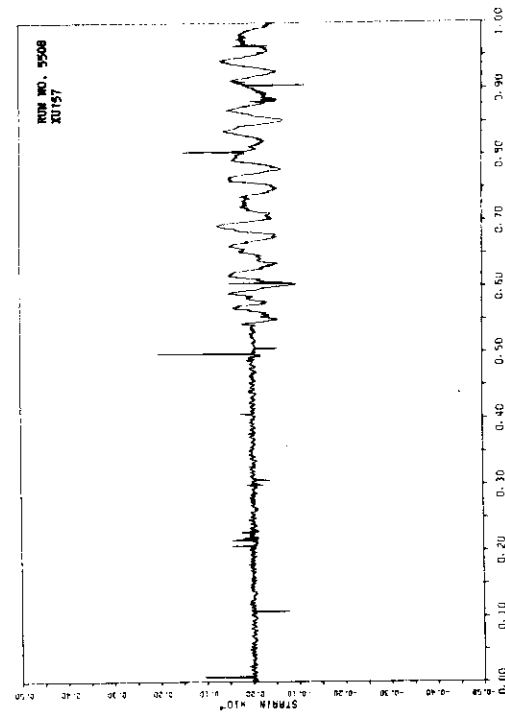

A.369

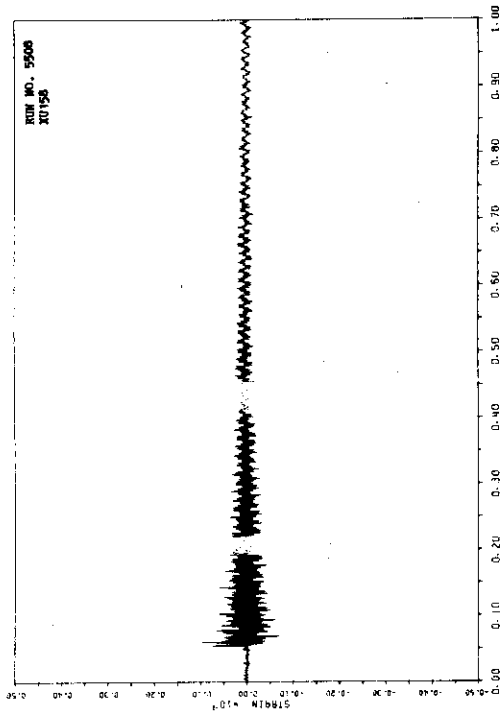

A.372

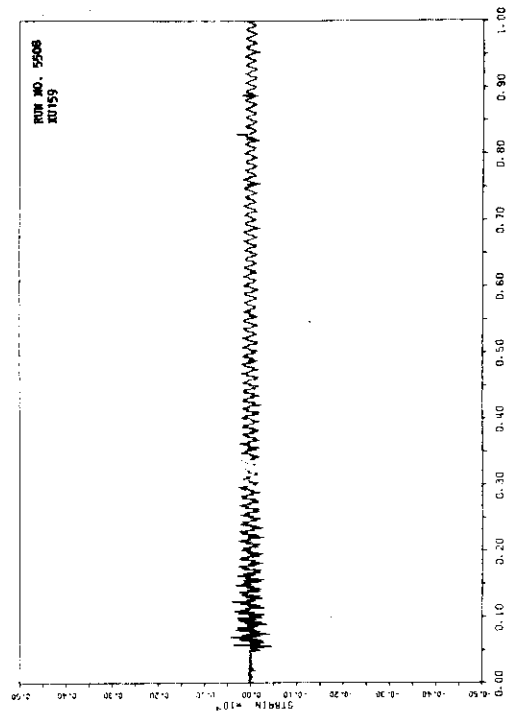

A.374

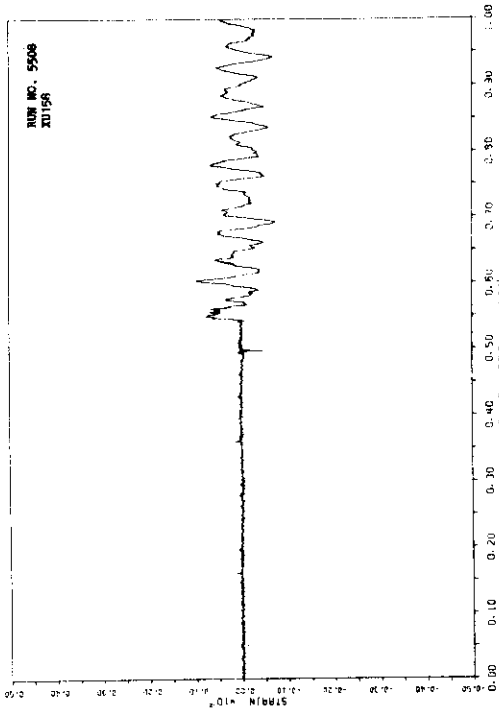

A.371

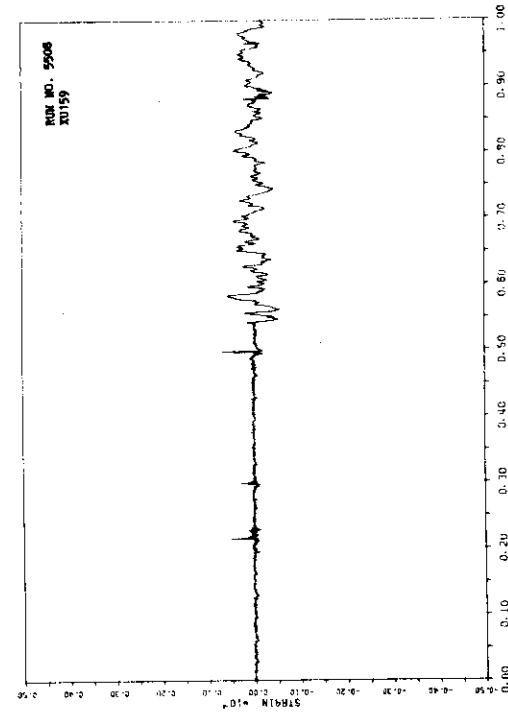

A.373

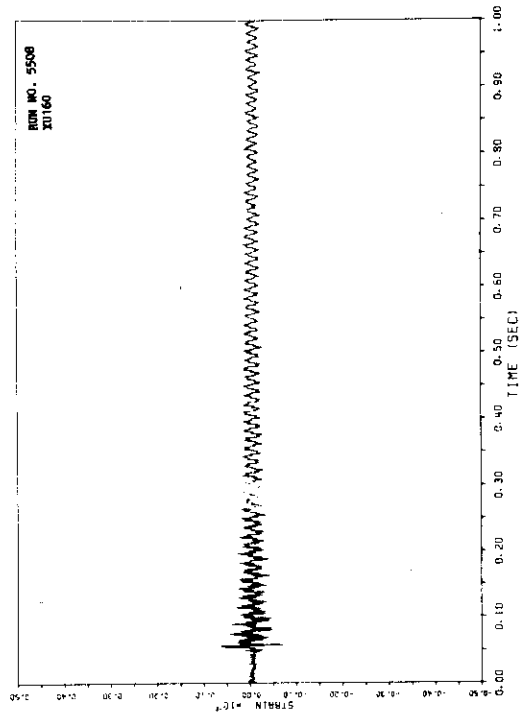

A.376

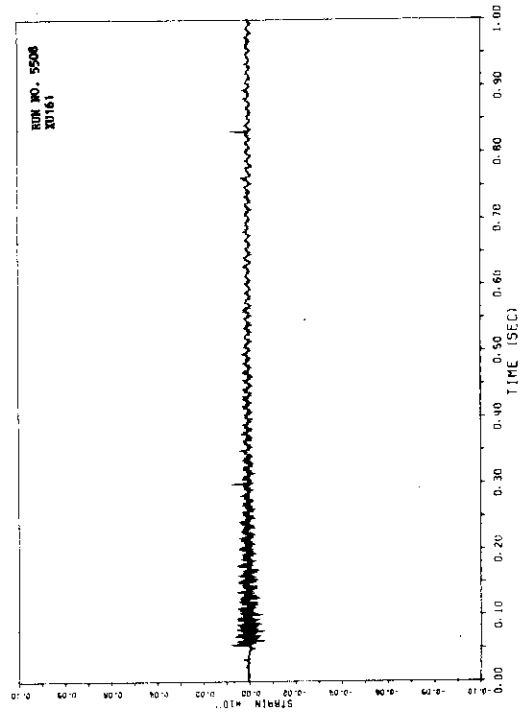

A.378

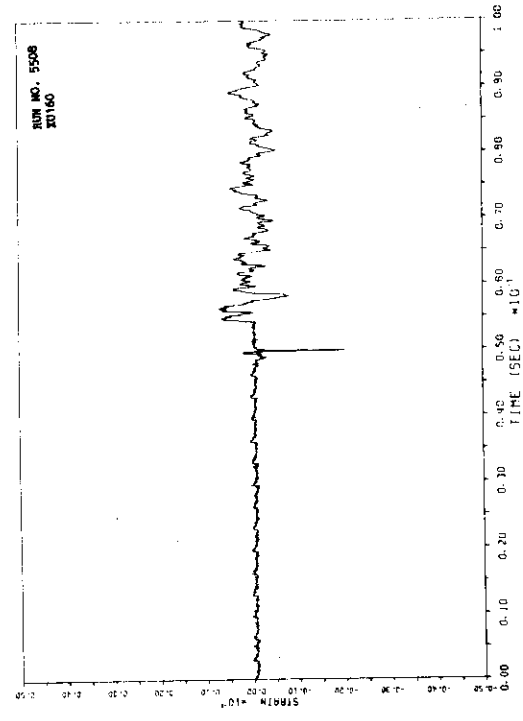

A.375

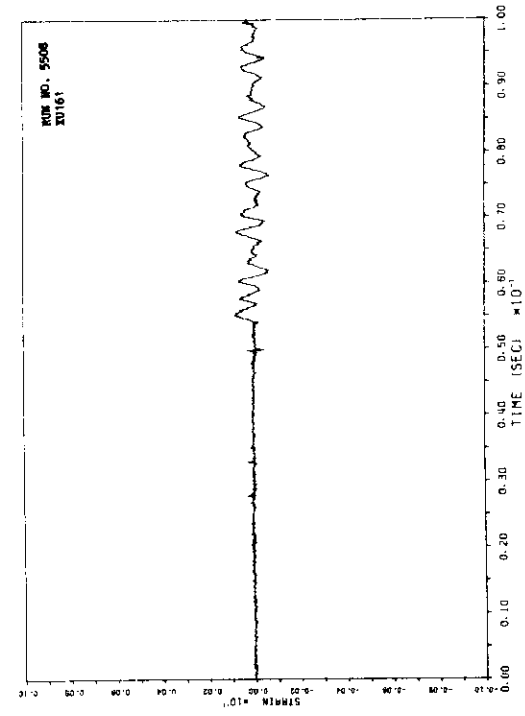

A.377

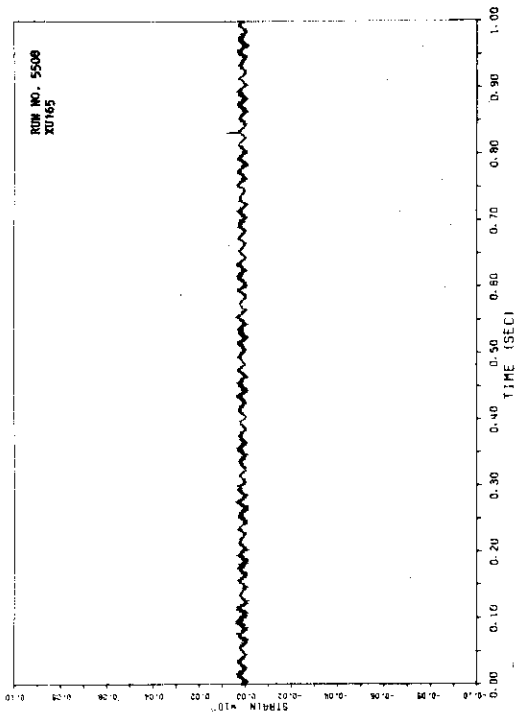

A.380

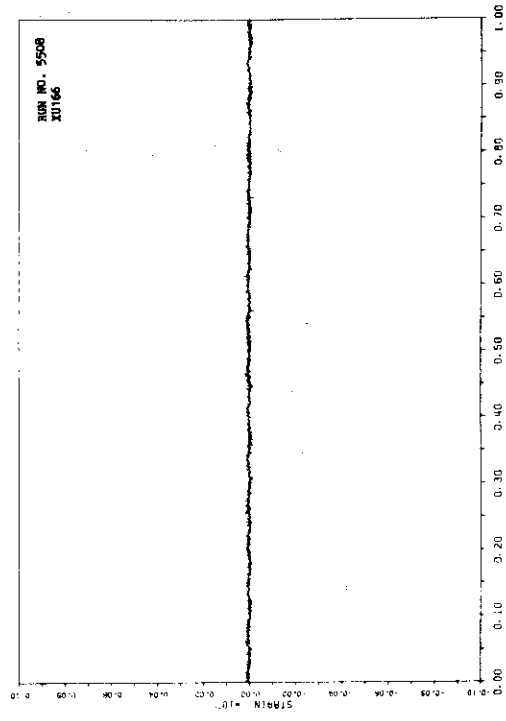

A.382

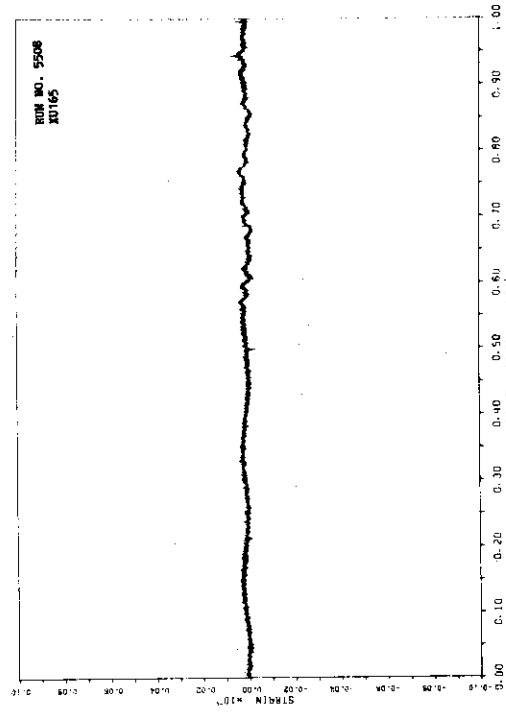

A.379

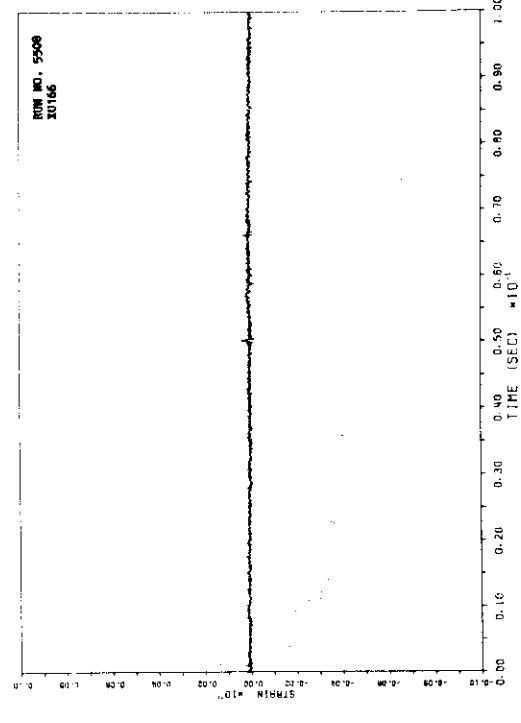

A.381

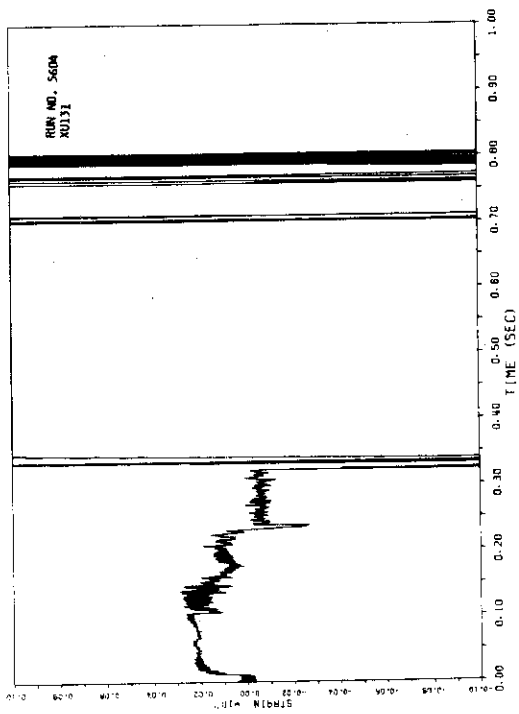

A.384

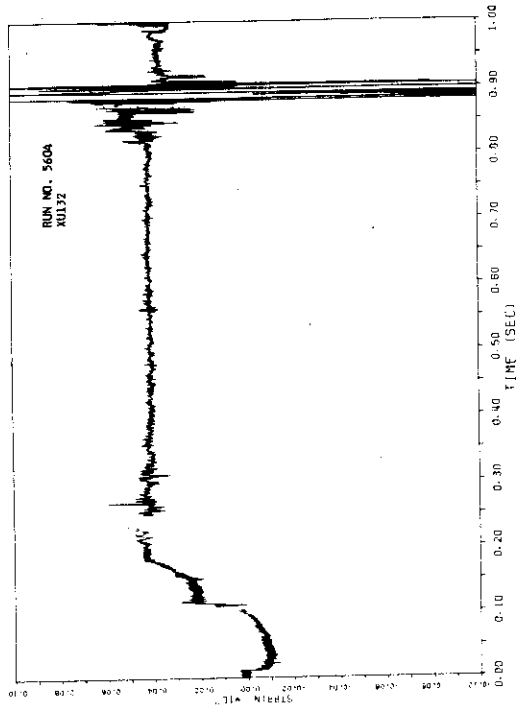

A.386

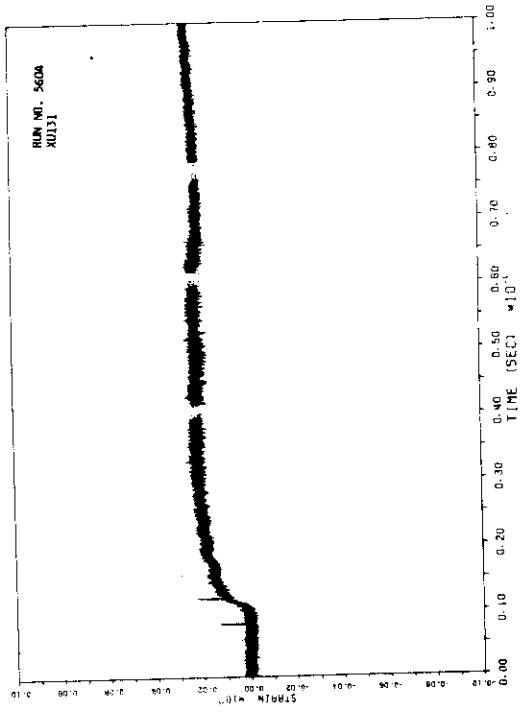

A.383

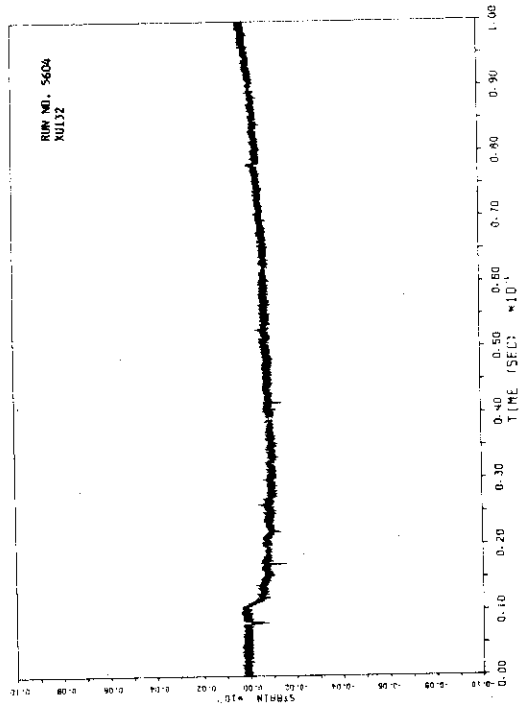

A.385

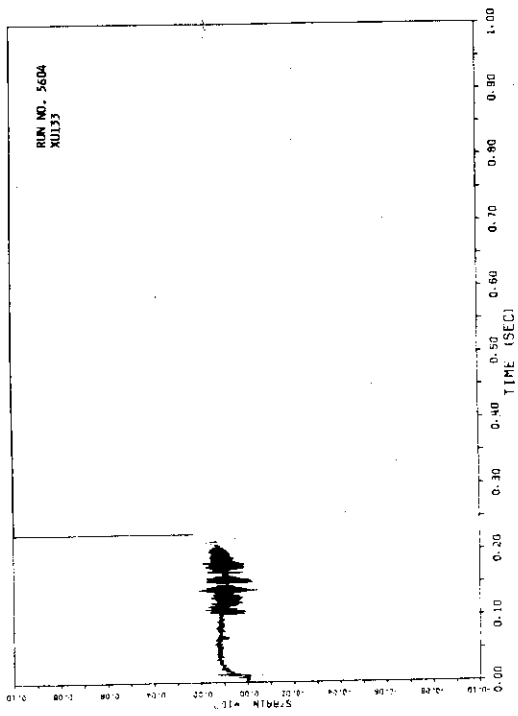

A.388

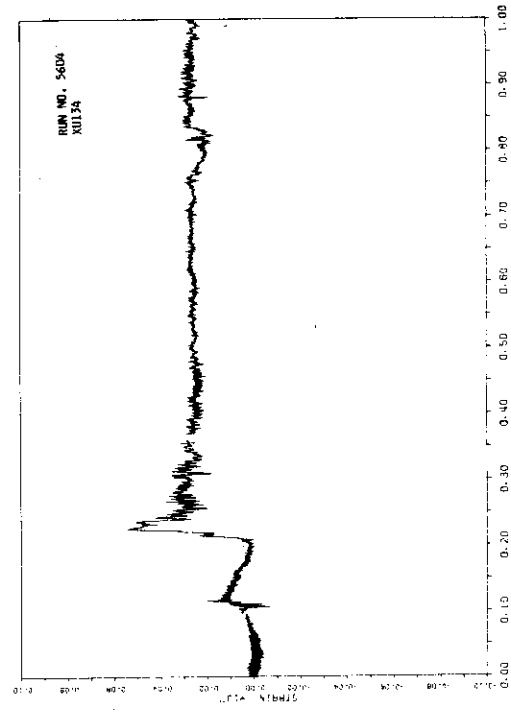

A.390

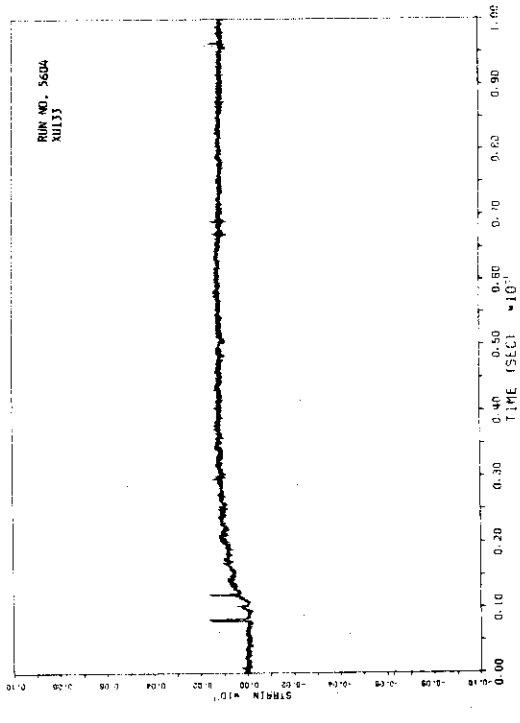

A.387

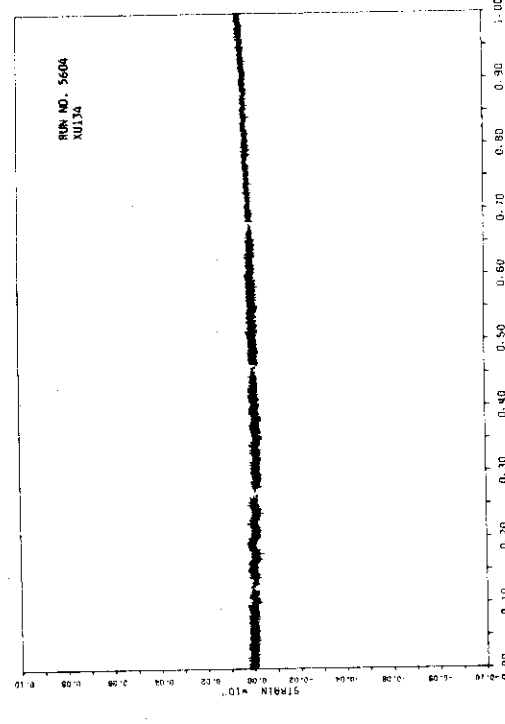

A.389

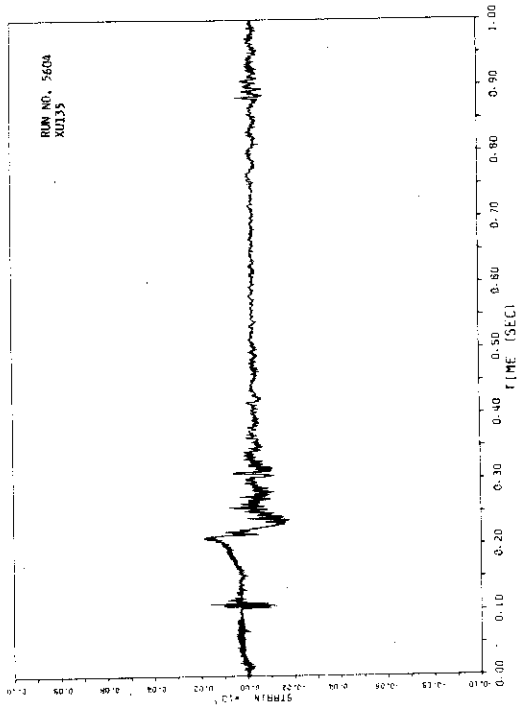

A.392

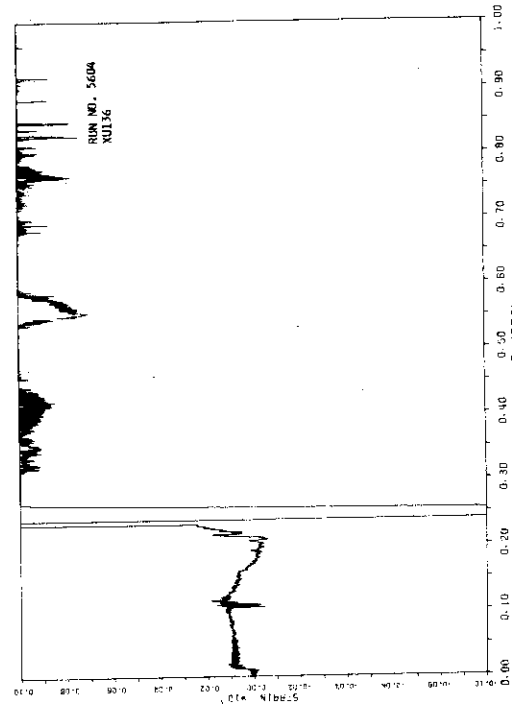

A.394

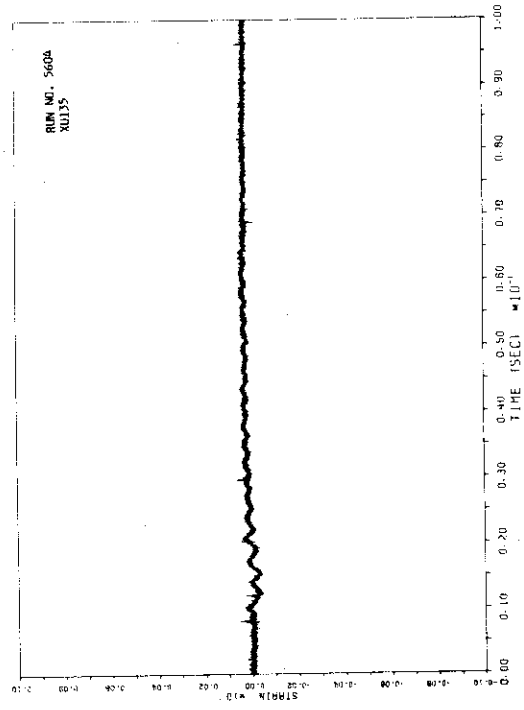

A.391

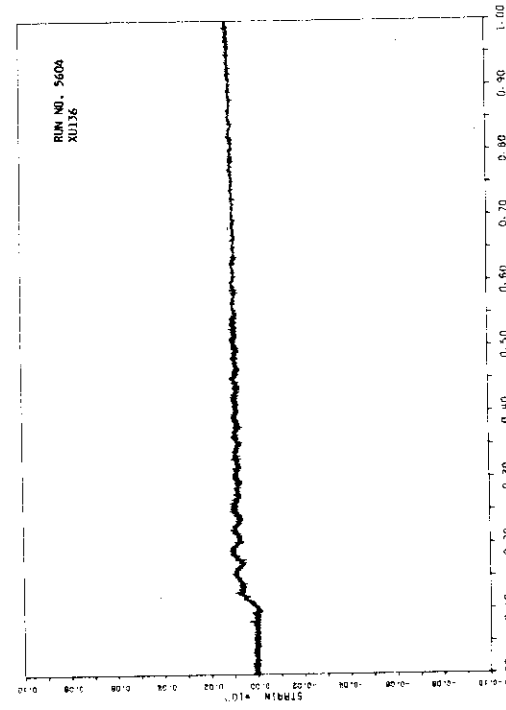

A.393

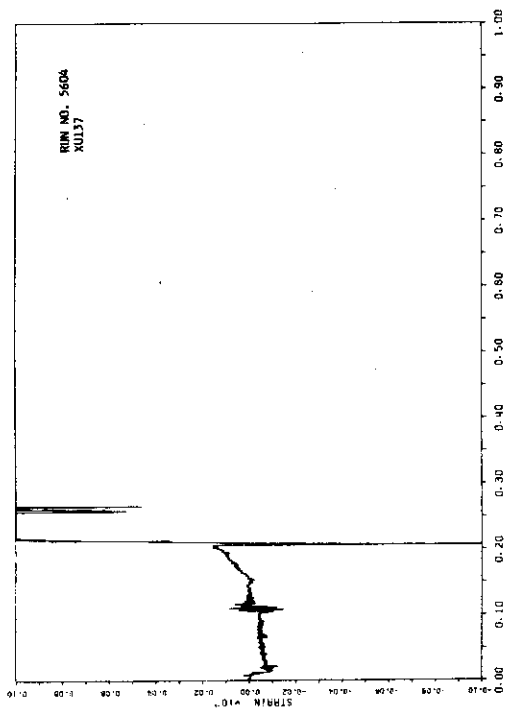

A.396

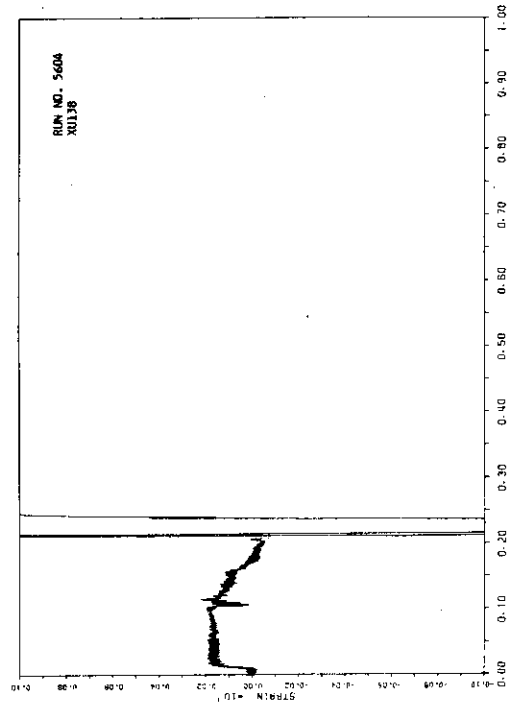

A.398

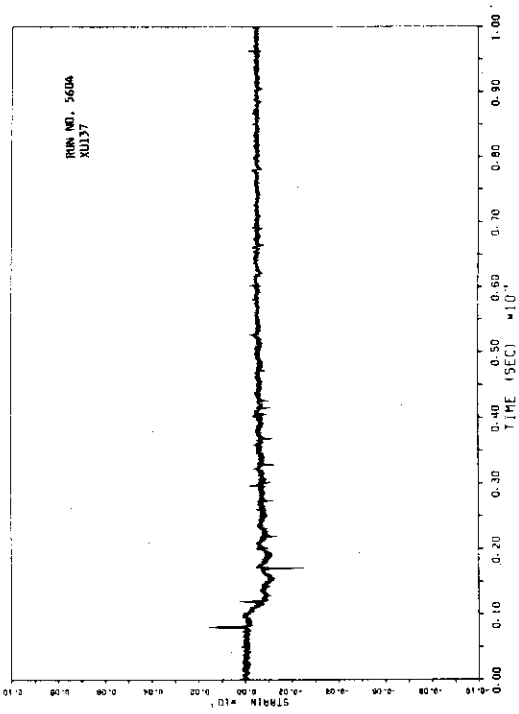

A.395

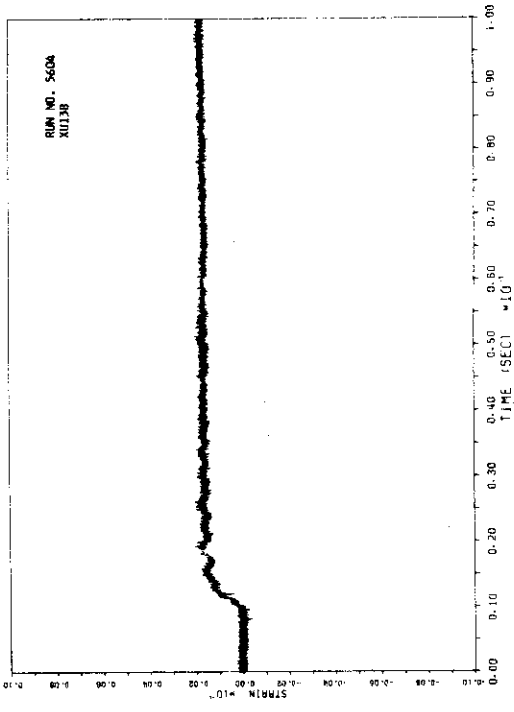

A.397

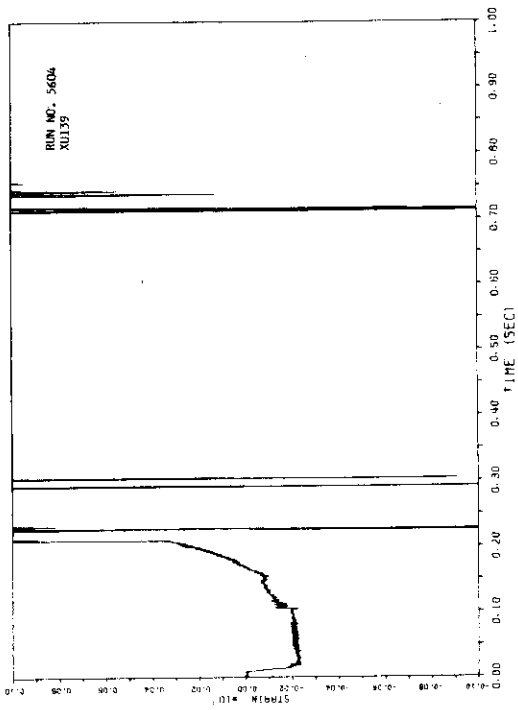

A.400

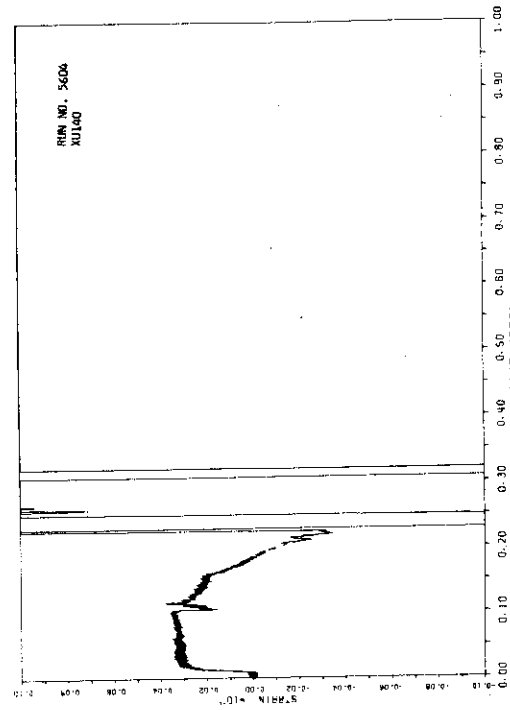

A.402

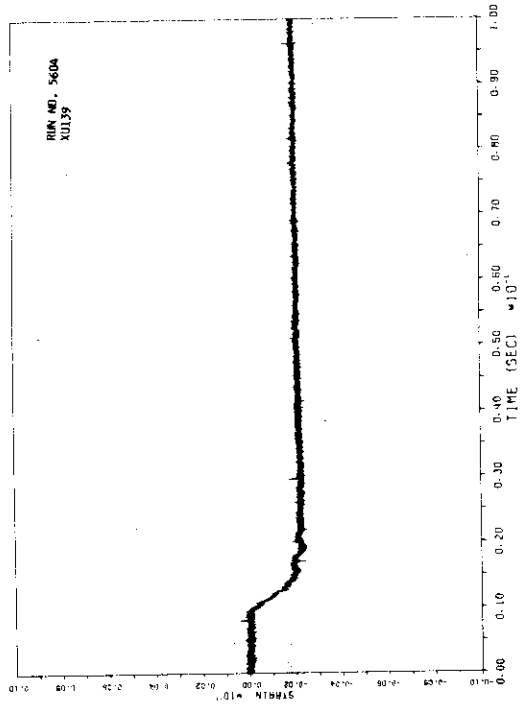

A.399

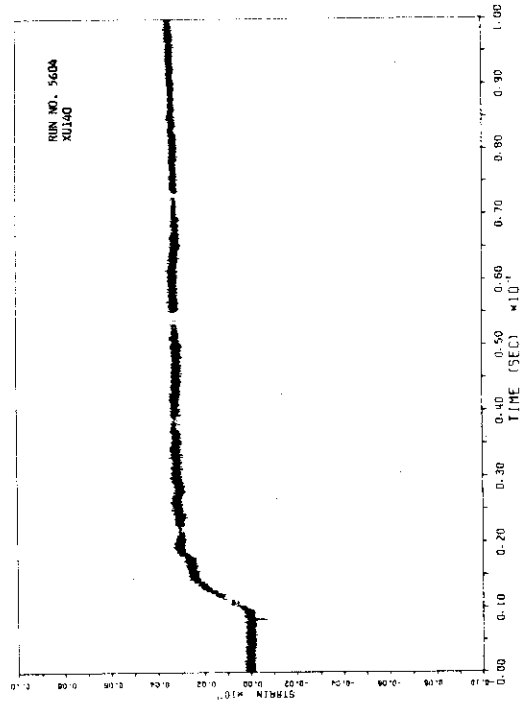

A.401

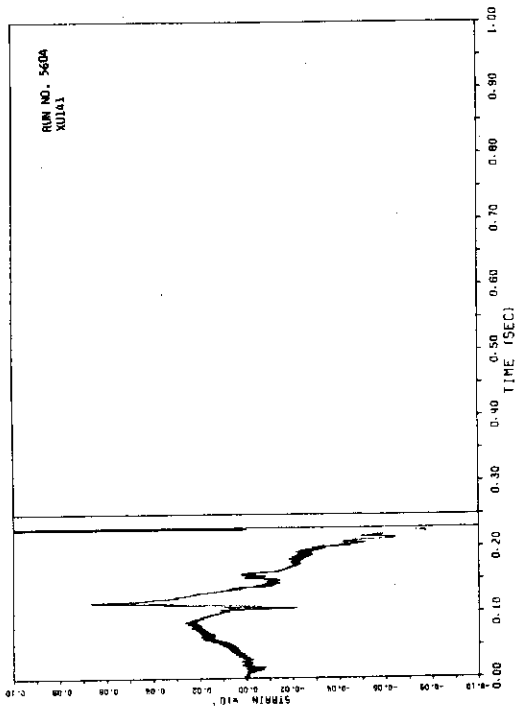

A.404

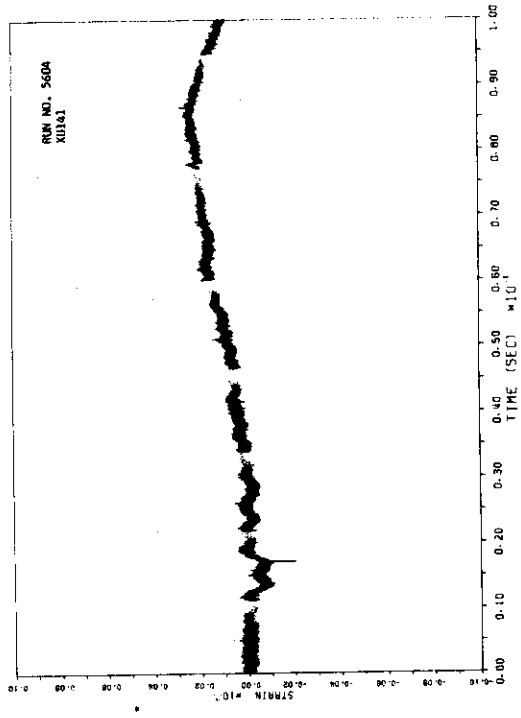

A.403

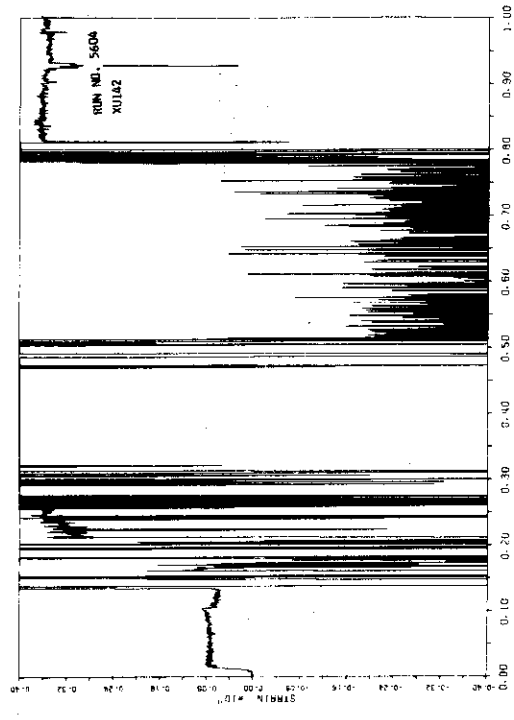

A.406

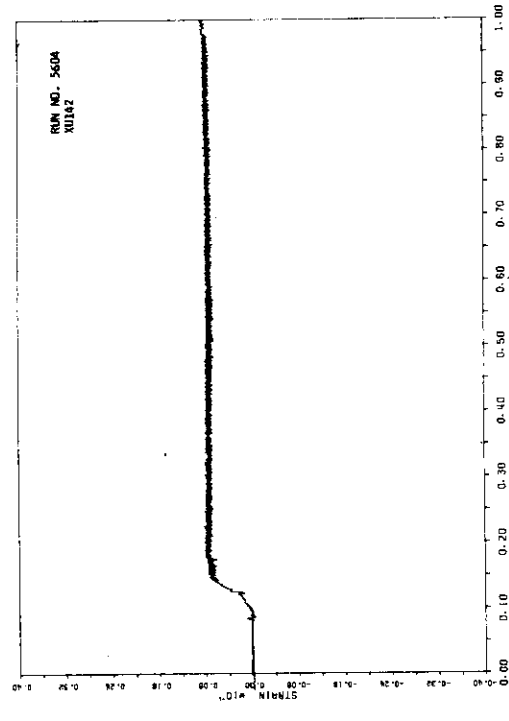

A.405

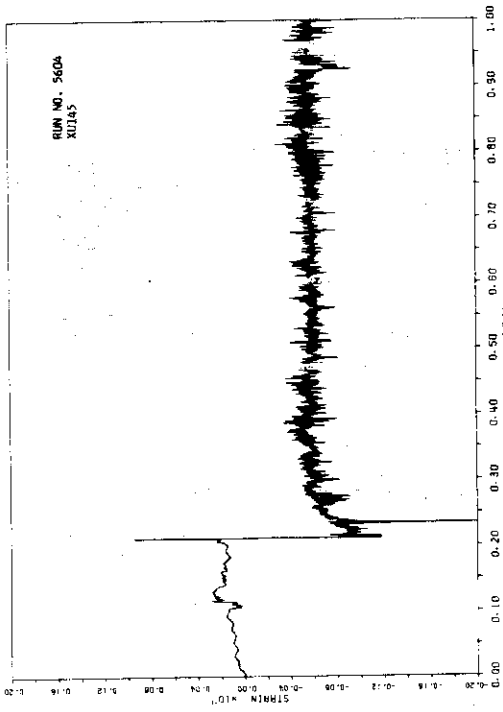

A.408

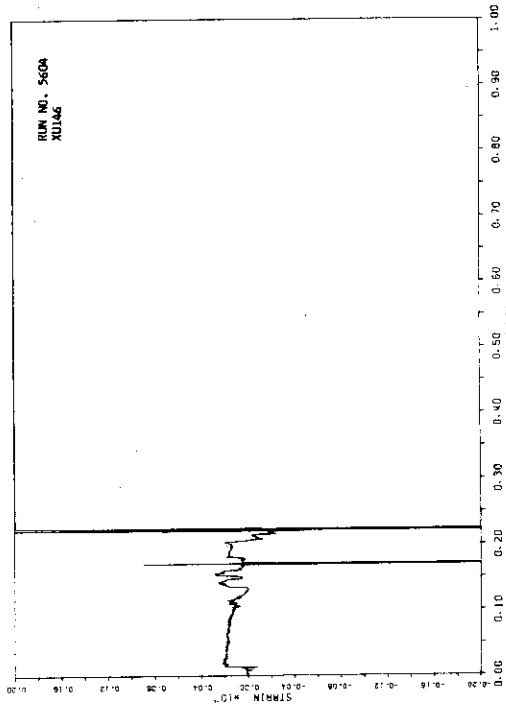

A.410

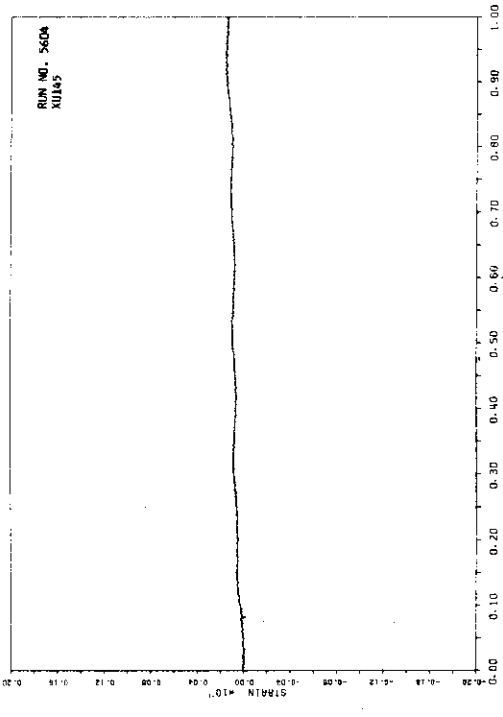

A.407

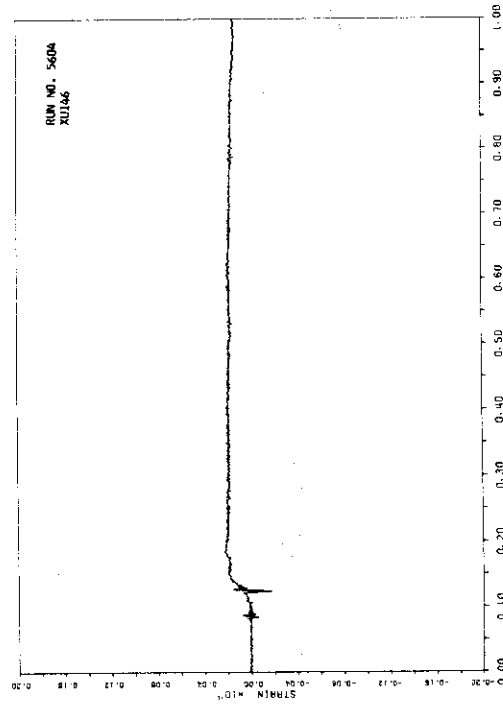

A.409

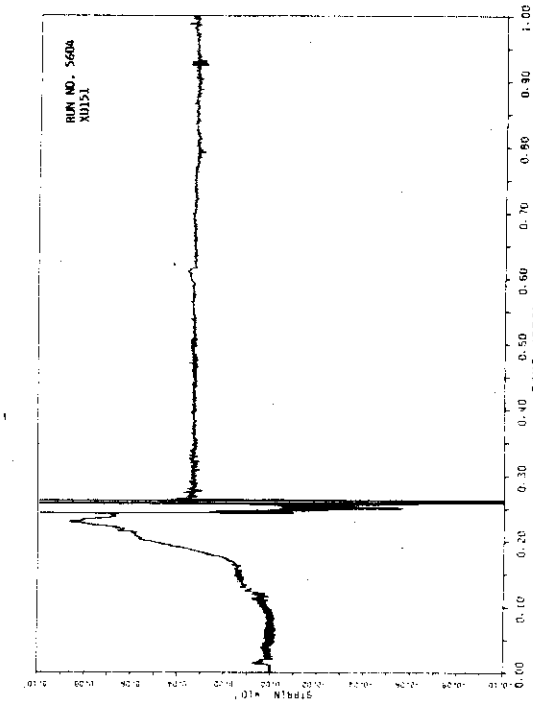

A.412

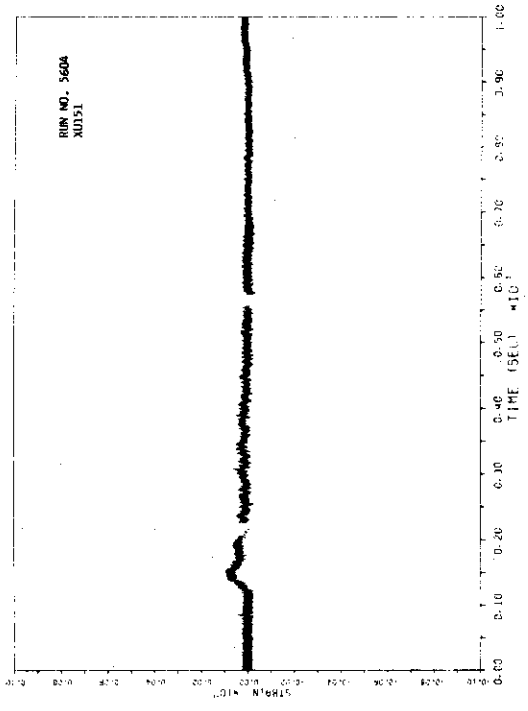

A.411

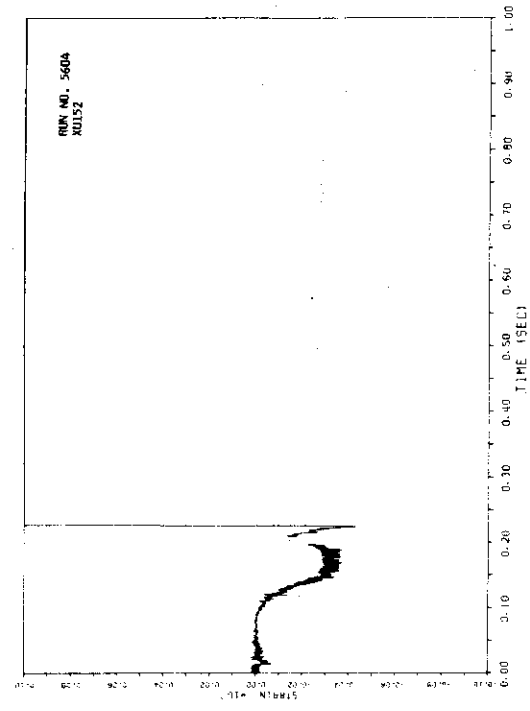

A.414

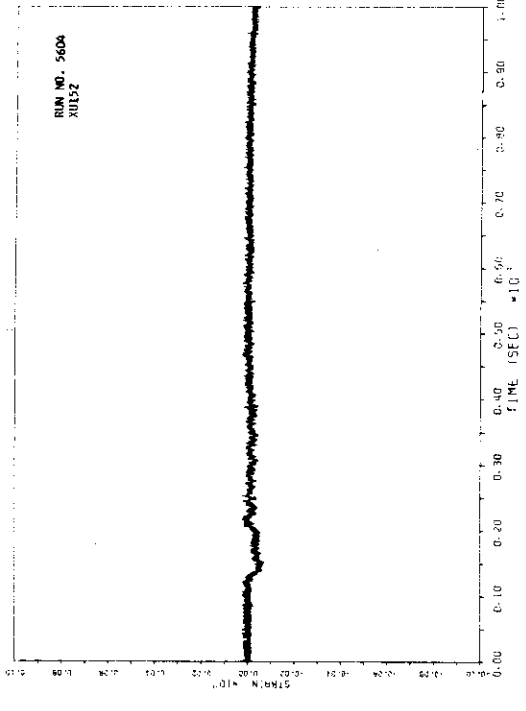

A.413

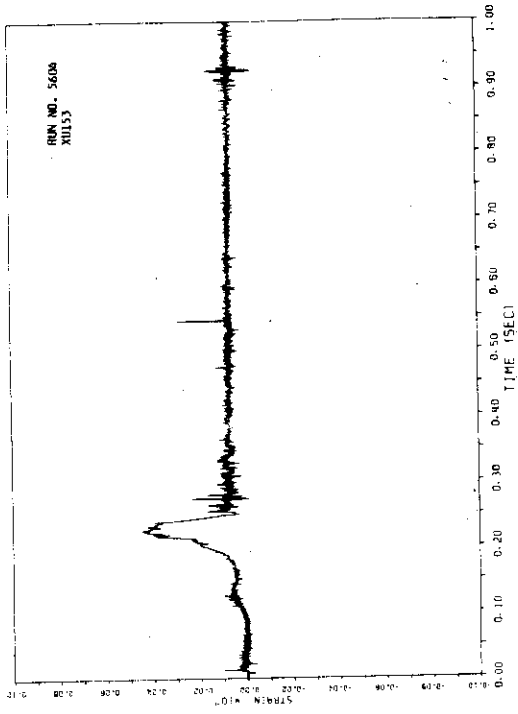

A.416

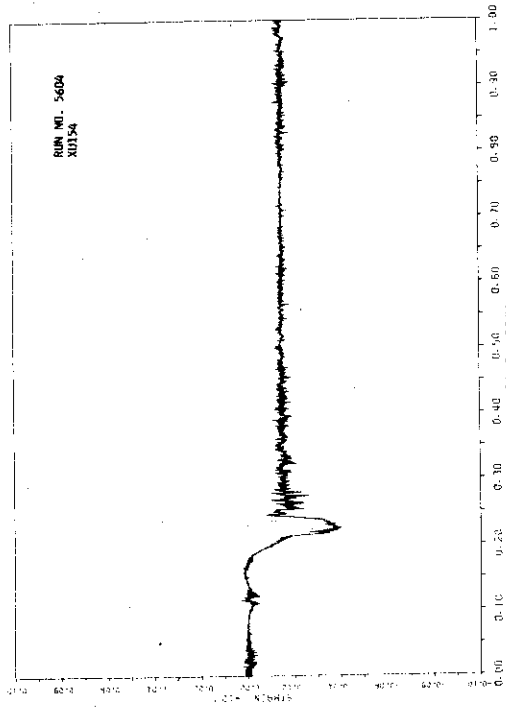

A.418

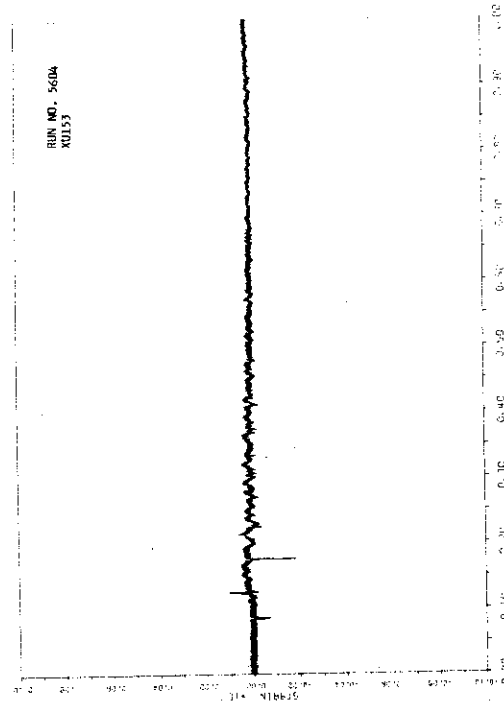

A.415

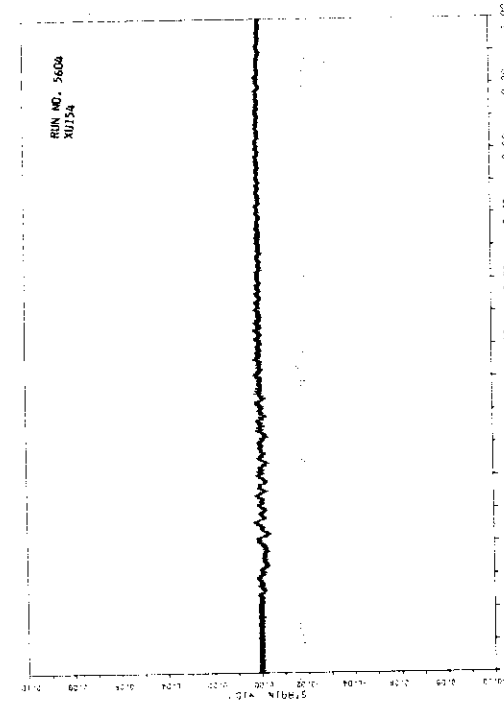

A.417

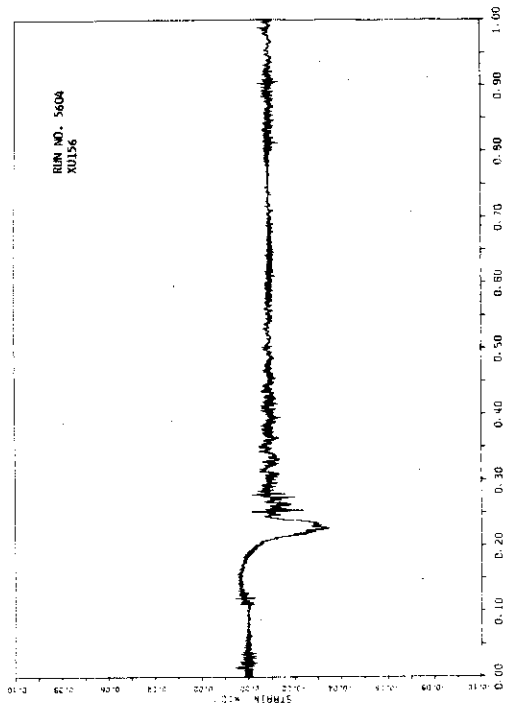

A.420

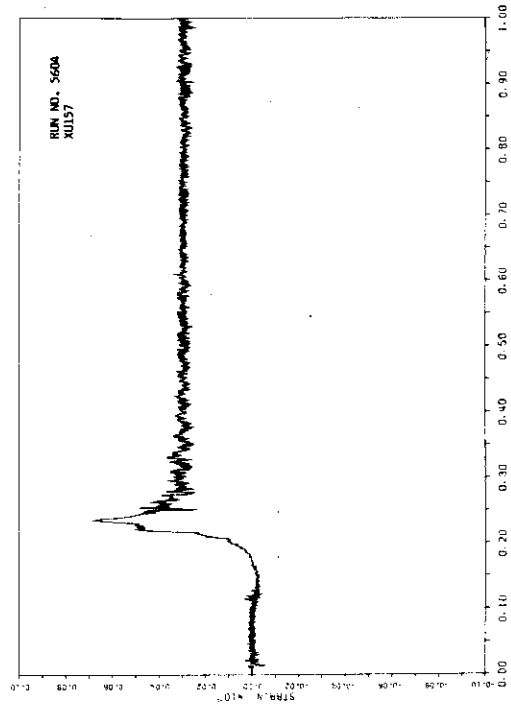

A.422

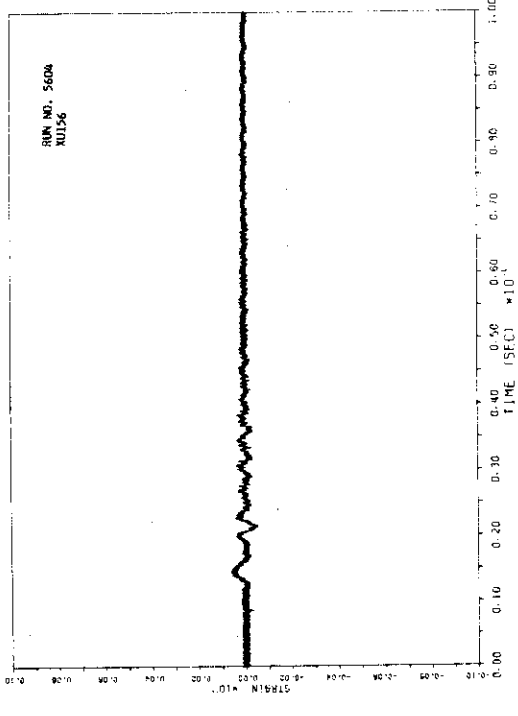

A.419

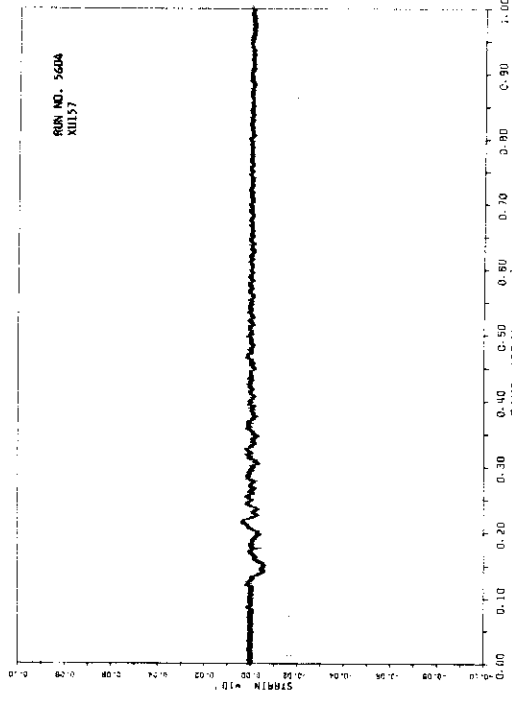

A.421

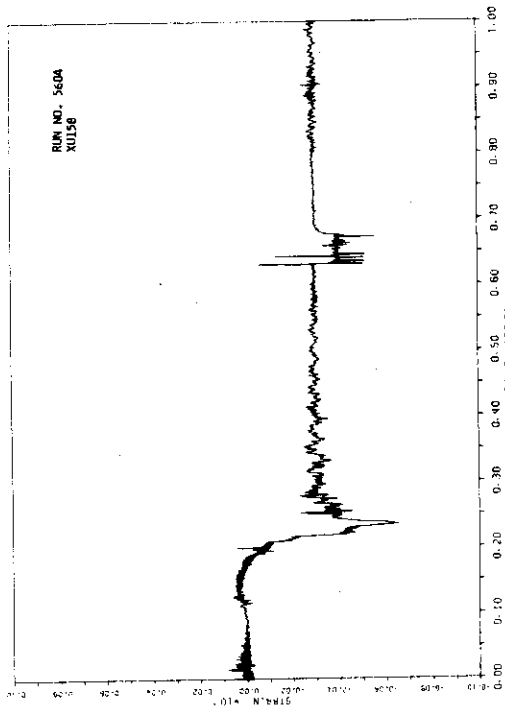

A.424

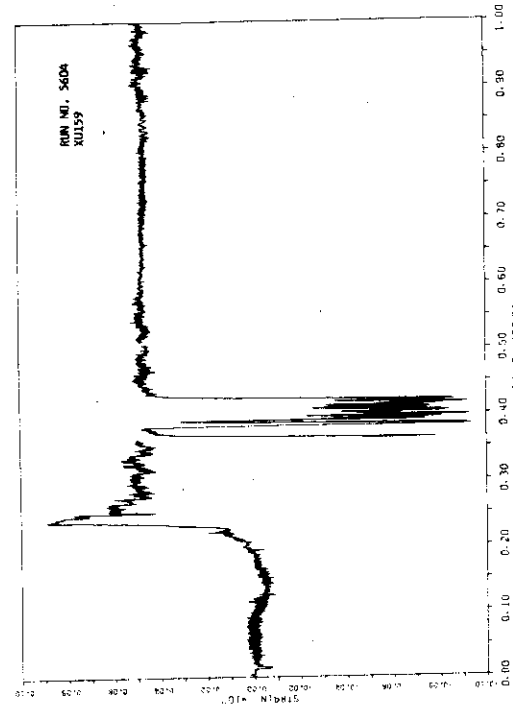

A.426

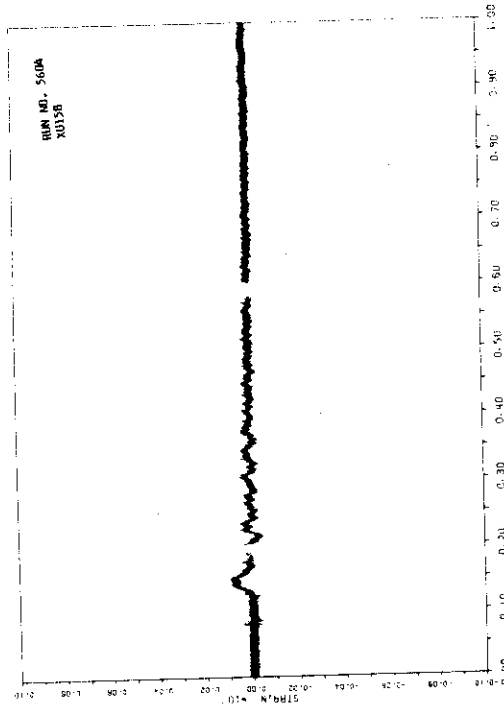

A.423

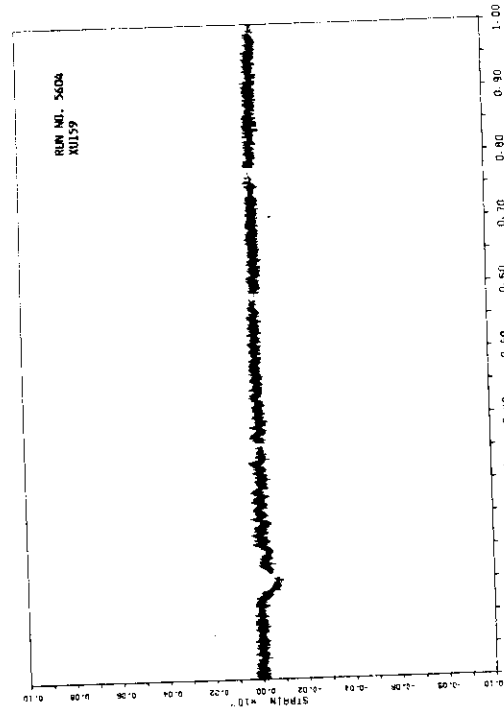

A.425

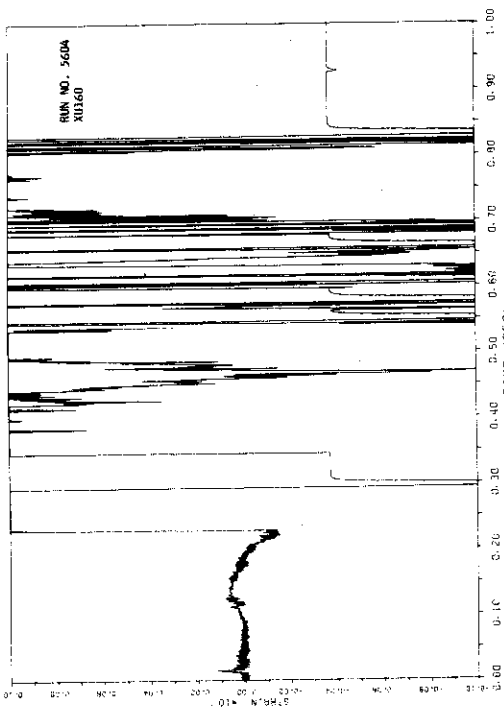

A.428

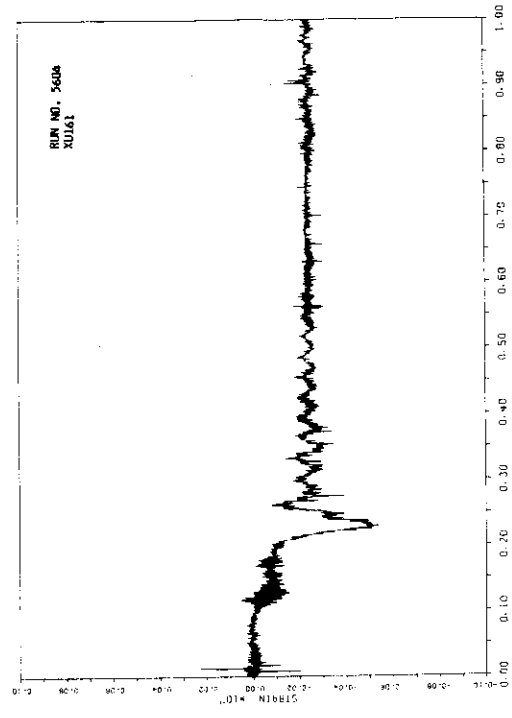

A.430

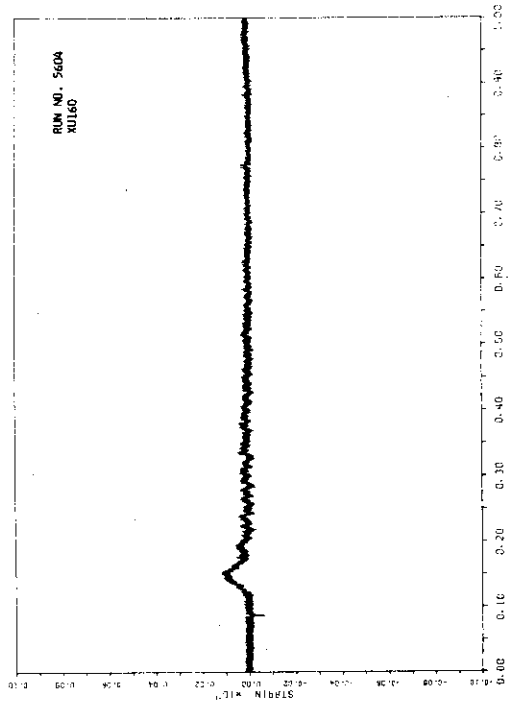

A.427

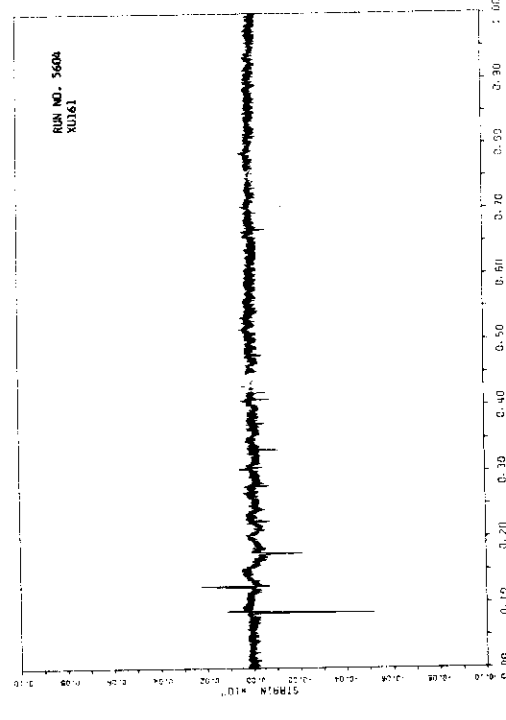

A.429

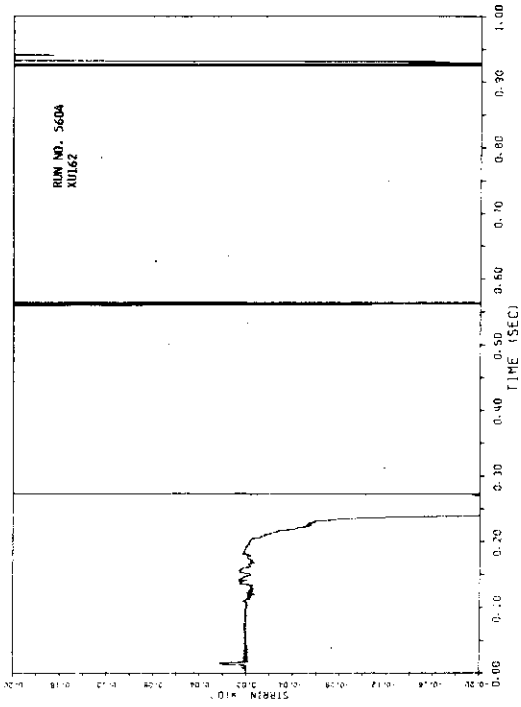

A.432

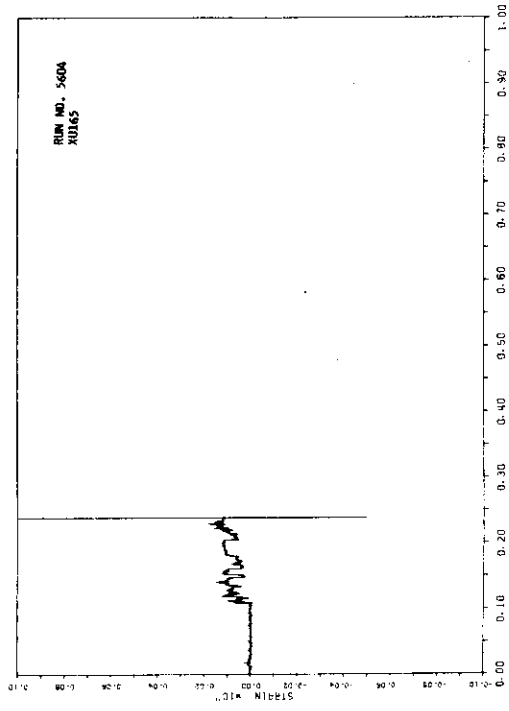

A.434

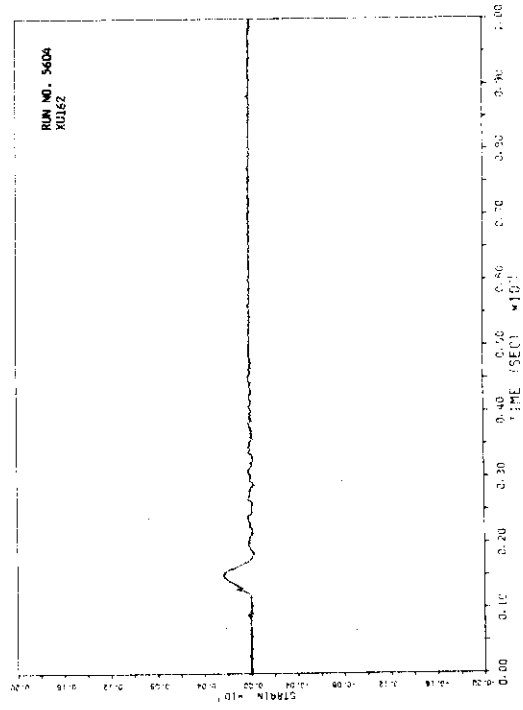

A.431

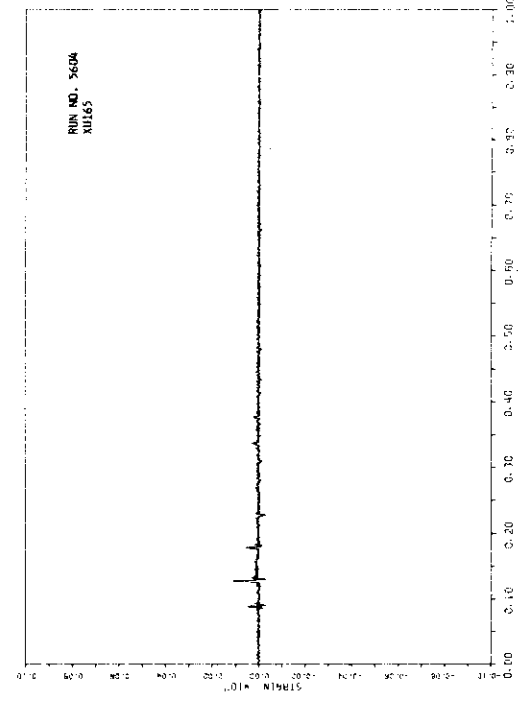

A.433

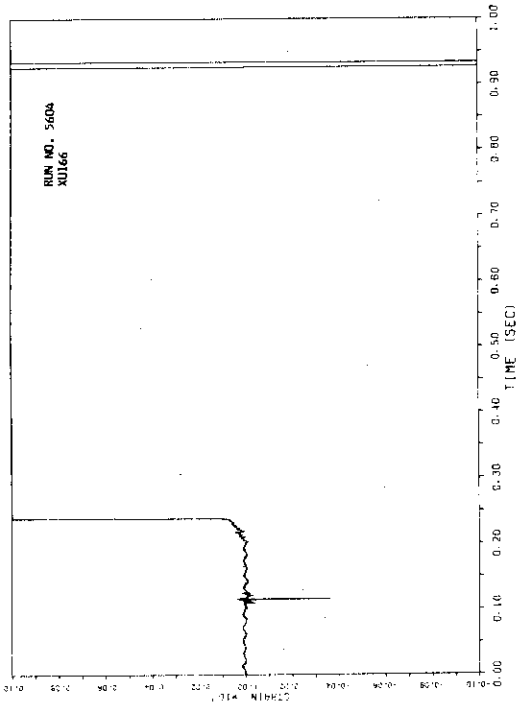

A.436

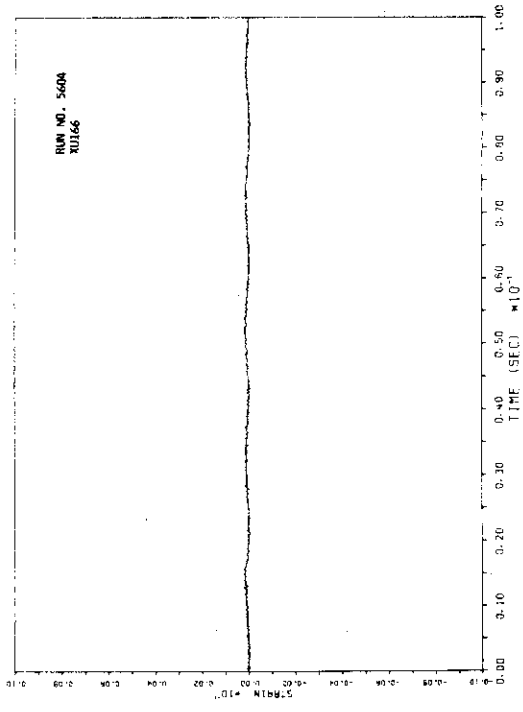

A.435

(f) Reaction forces of the restraints (A.437-A.500)

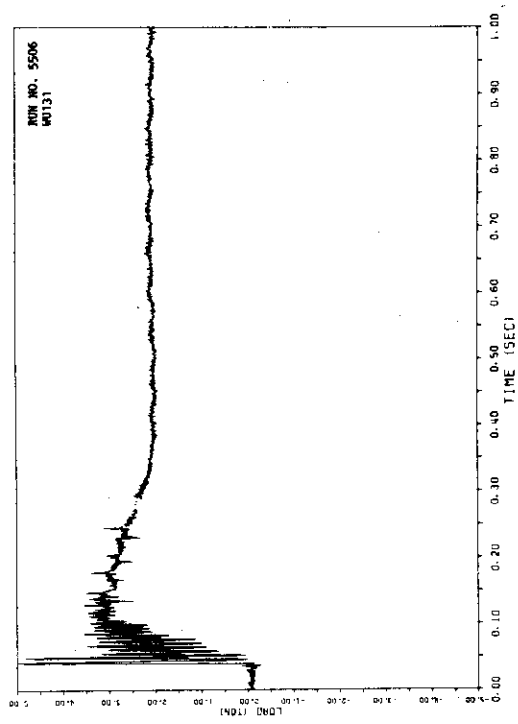

A.438

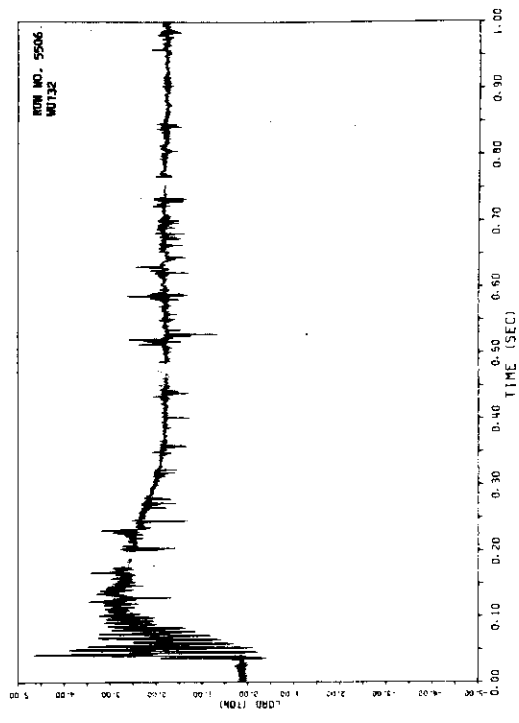

A.440

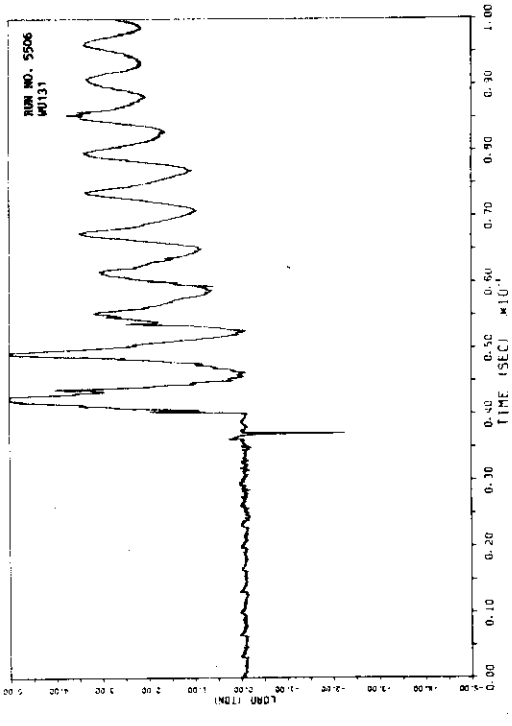

A.437

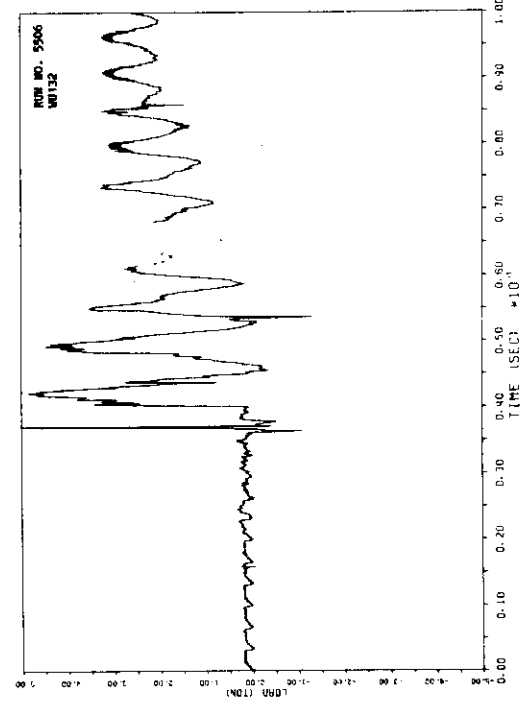

A.439

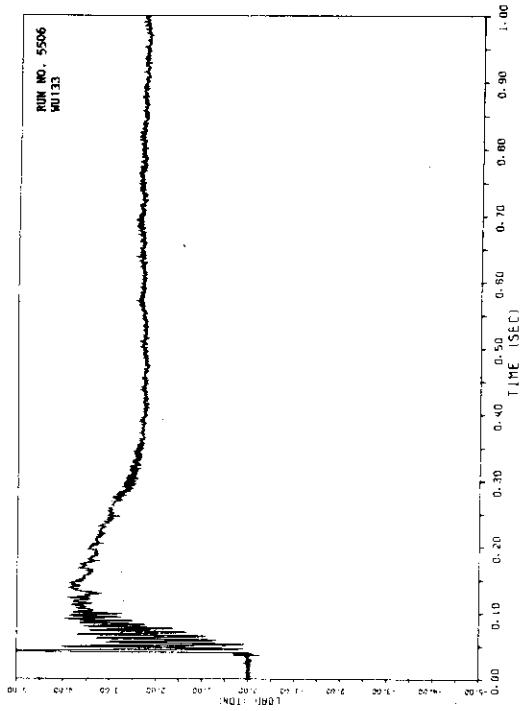

A.442

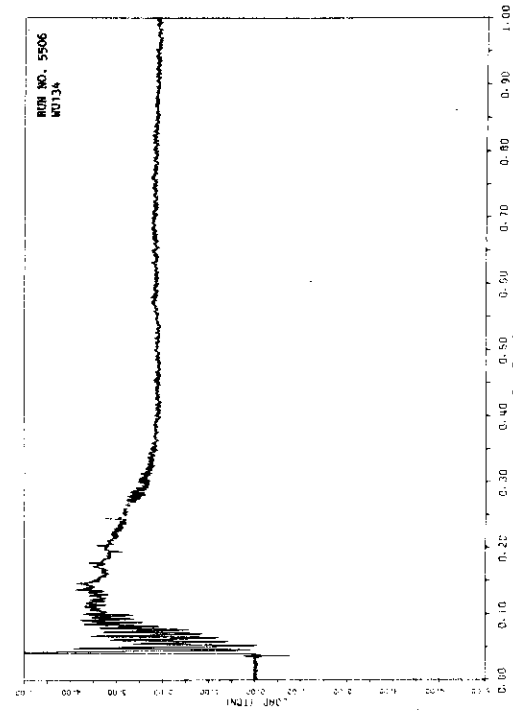

A.444

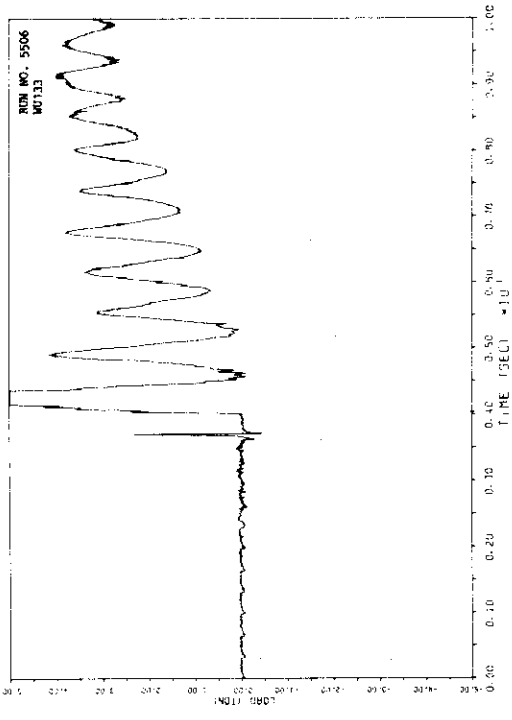

A.441

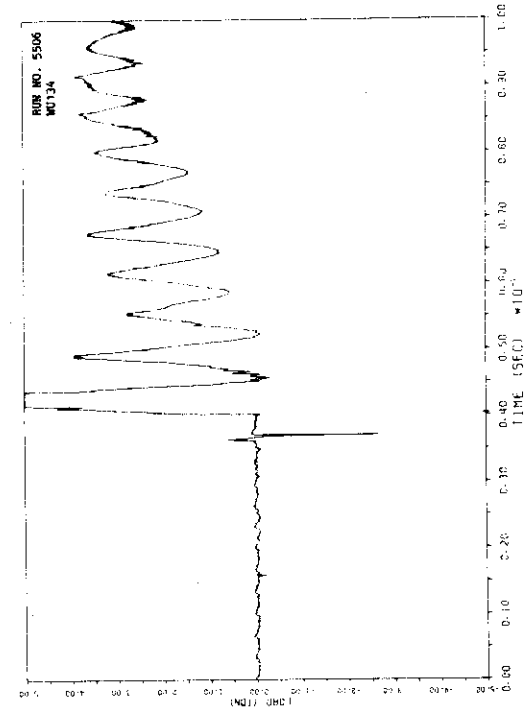

A.443

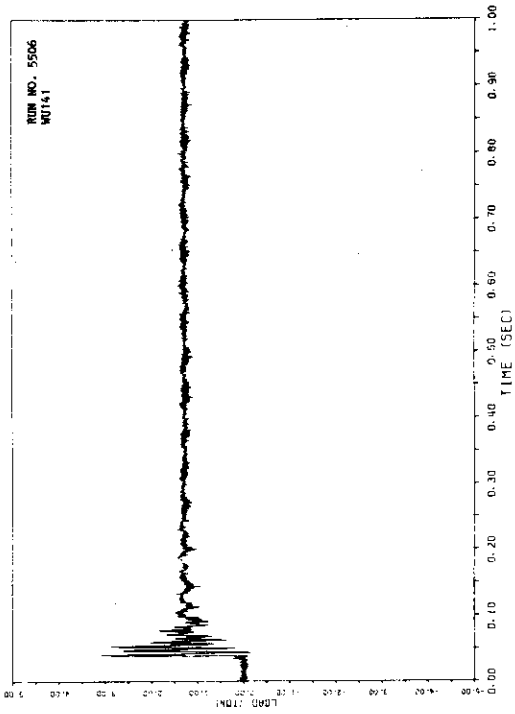

A.446

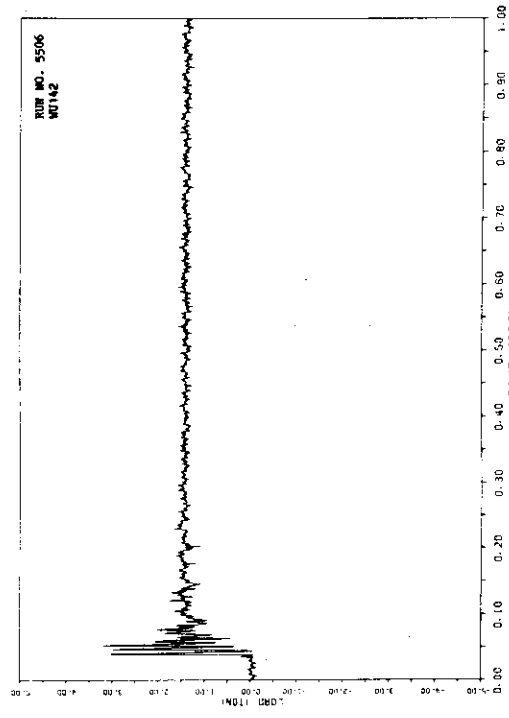

A.448

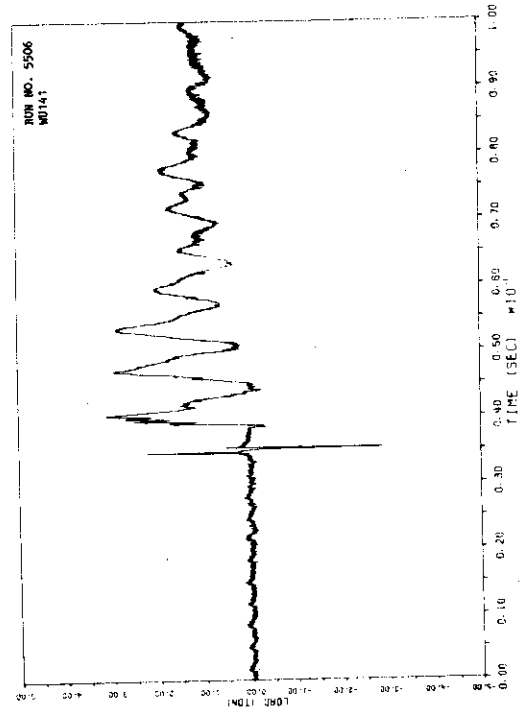

A.445

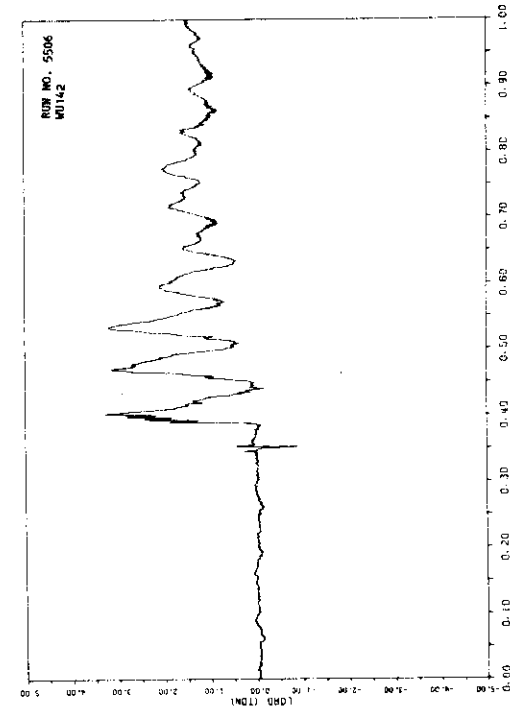

A.447

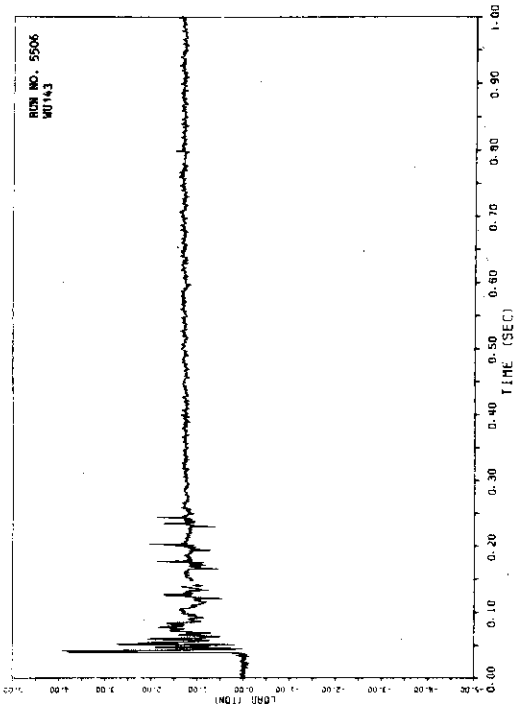

A.450

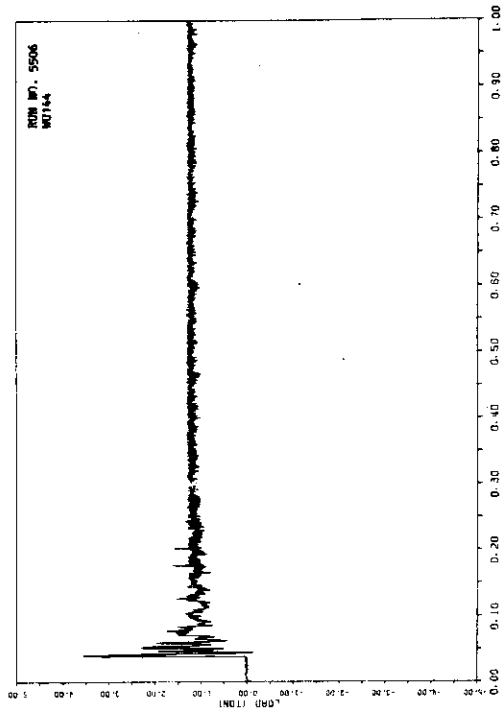

A.452

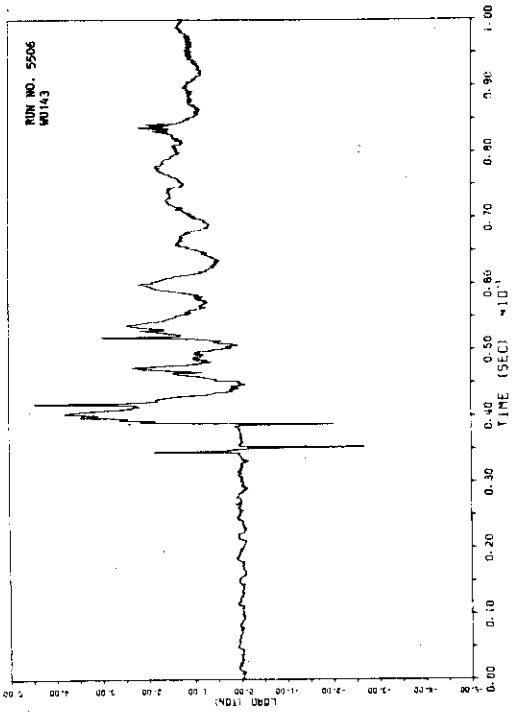

A.449

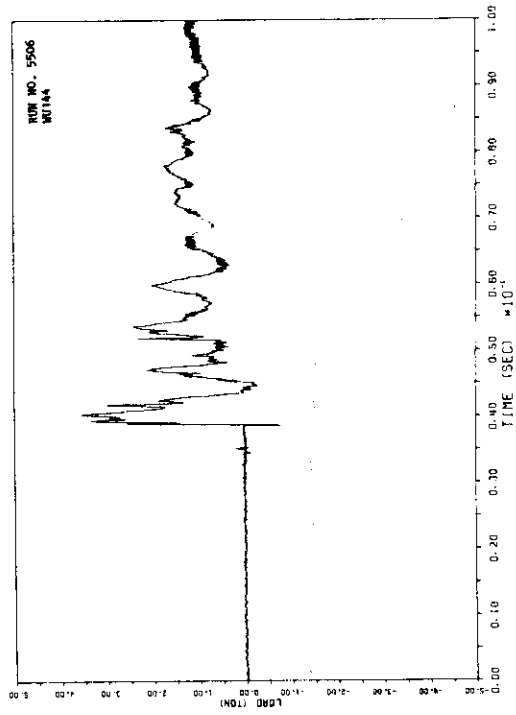

A.451

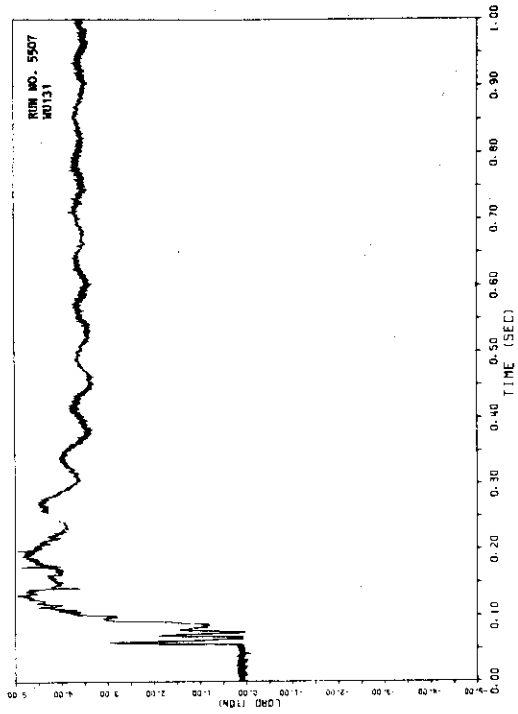

A.454

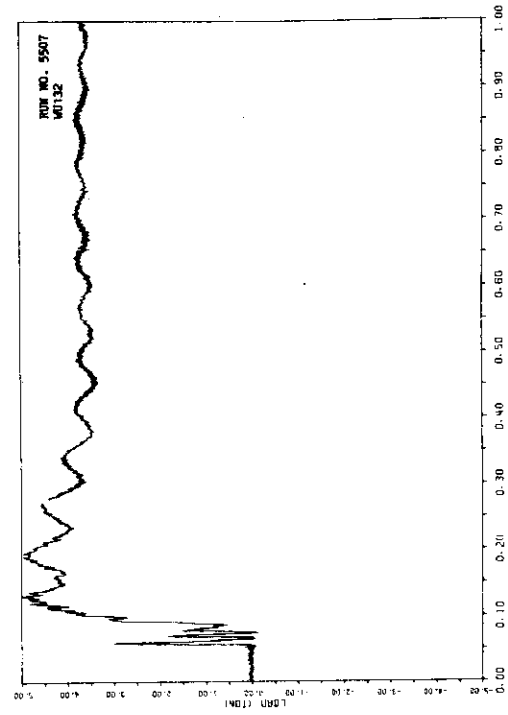

A.456

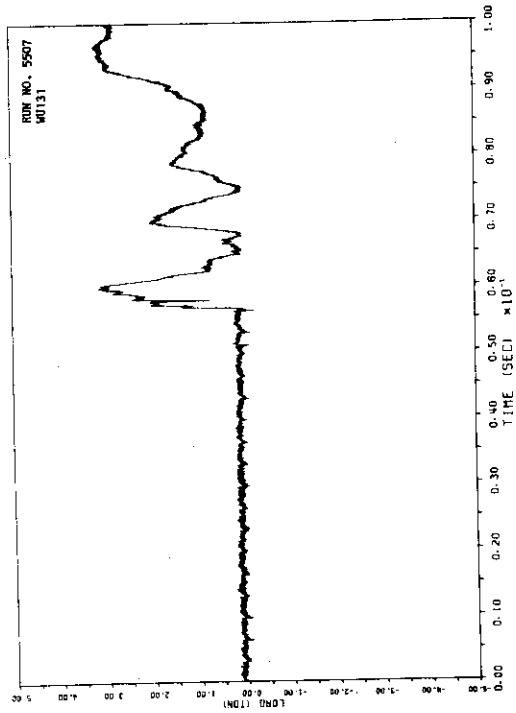

A.453

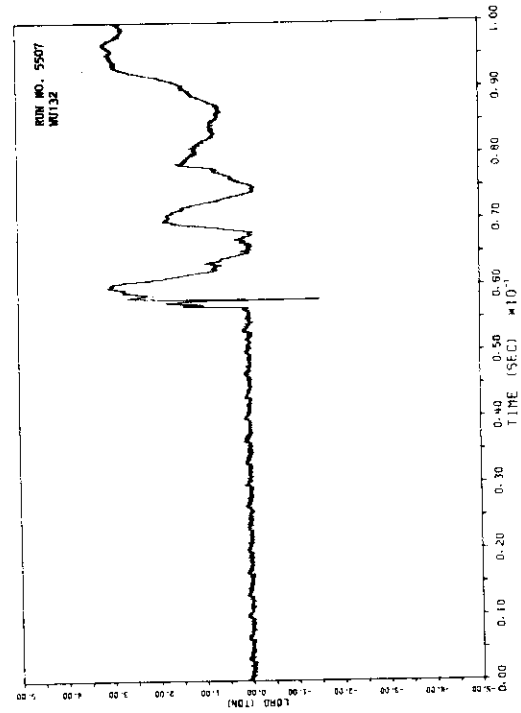

A.455

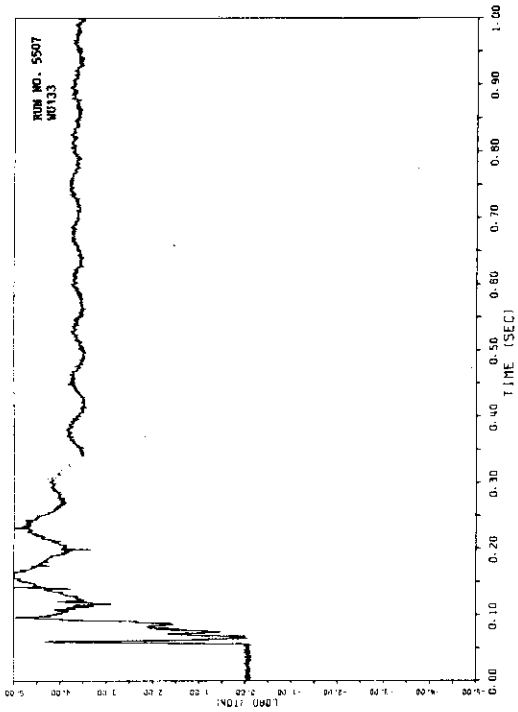

A.458

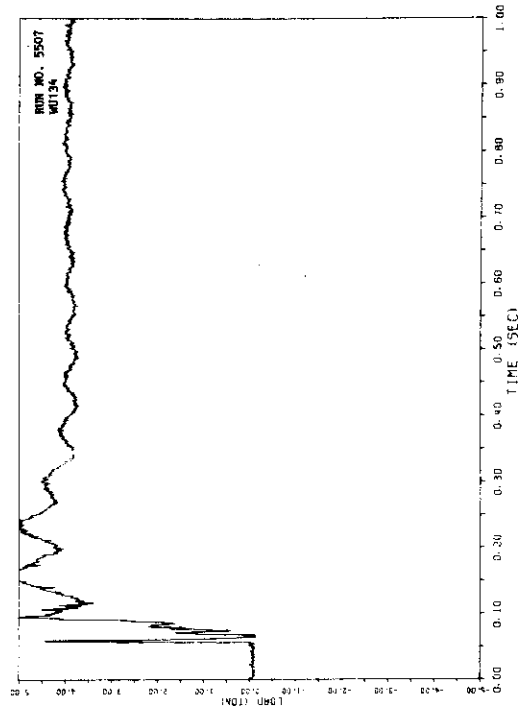

A.460

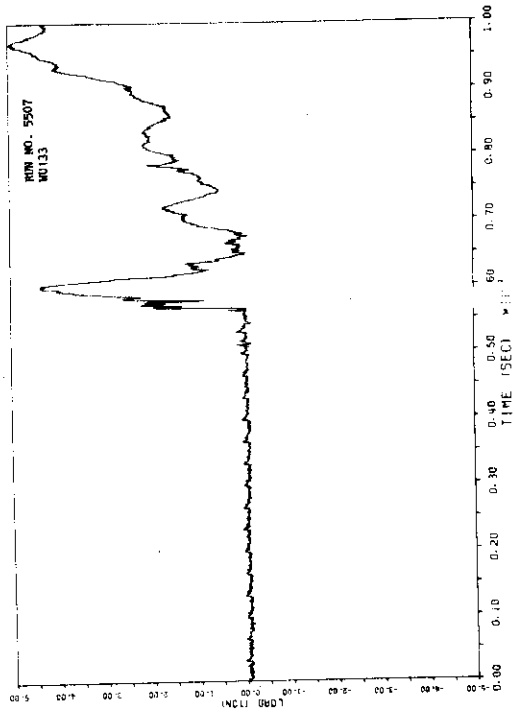

A.457

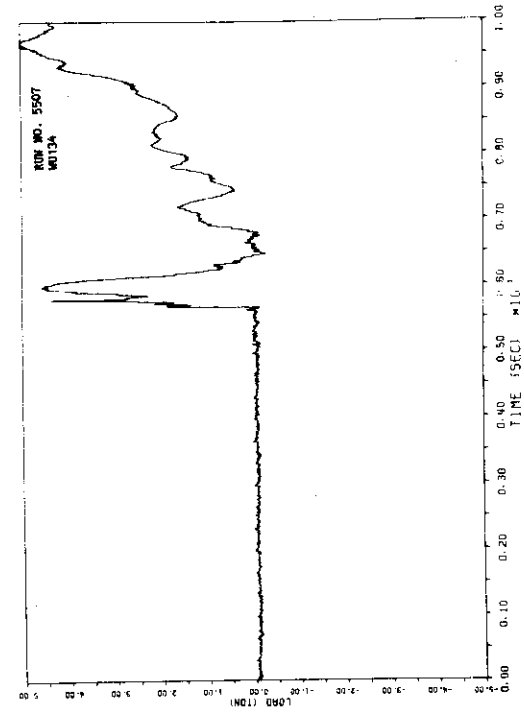

A.459

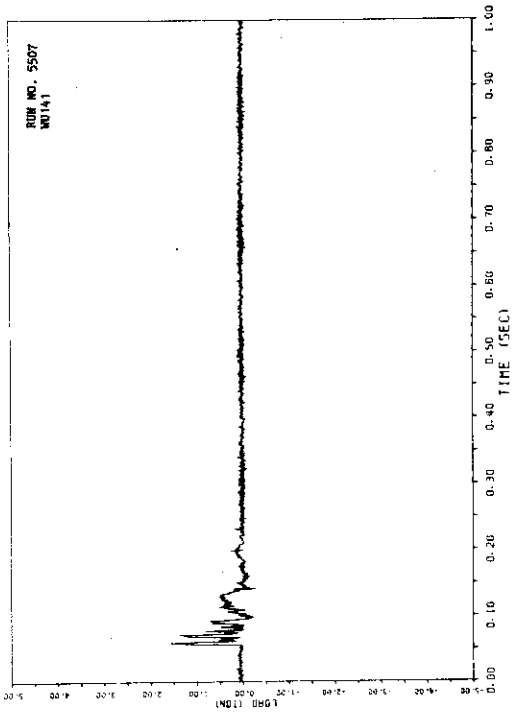

A.462

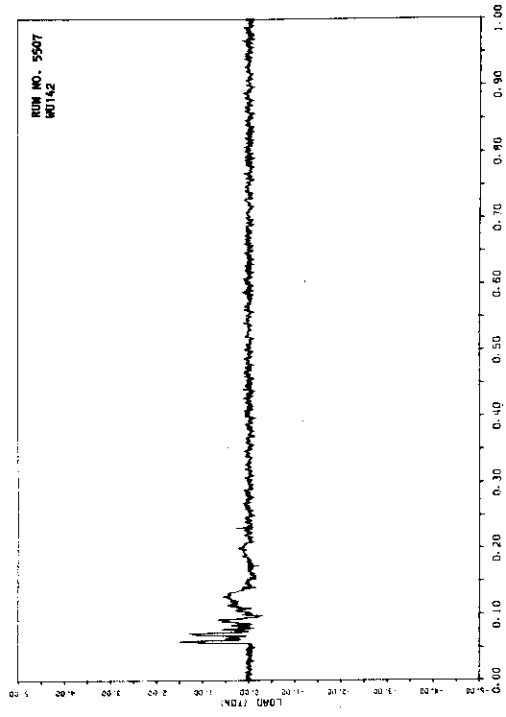

A.464

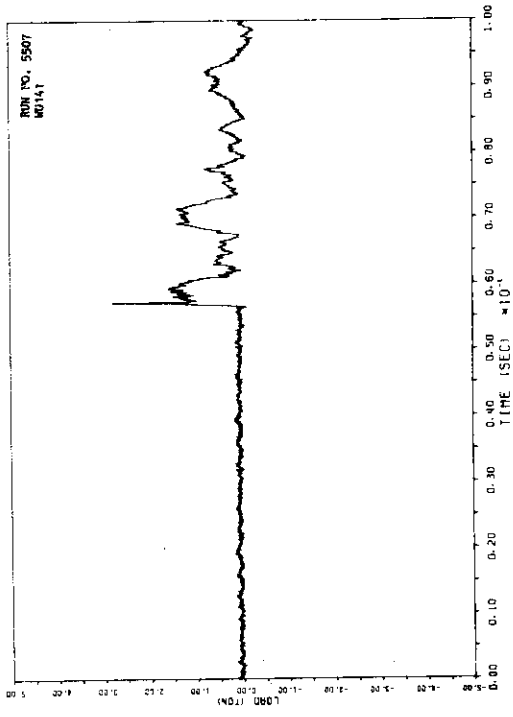

A.461

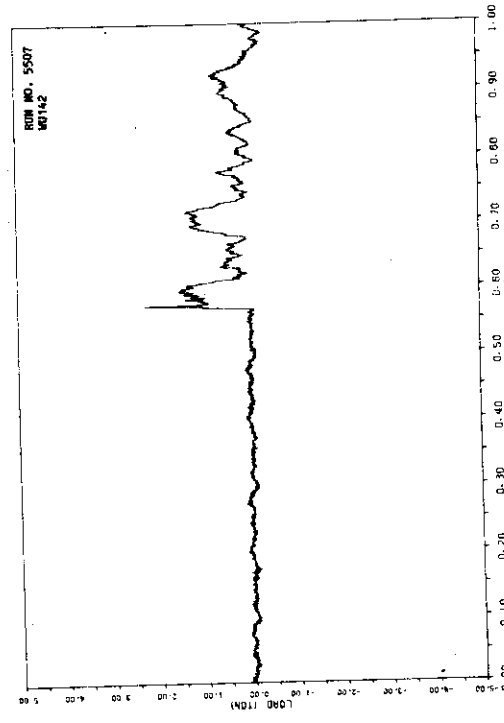

A.463

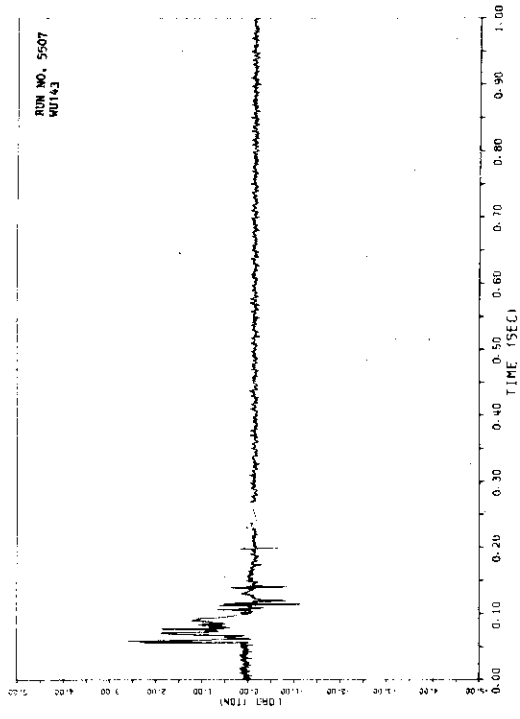

A.466

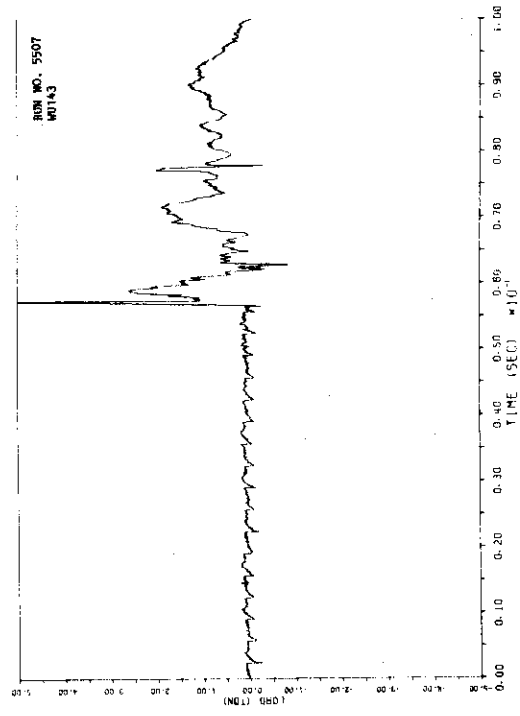

A.465

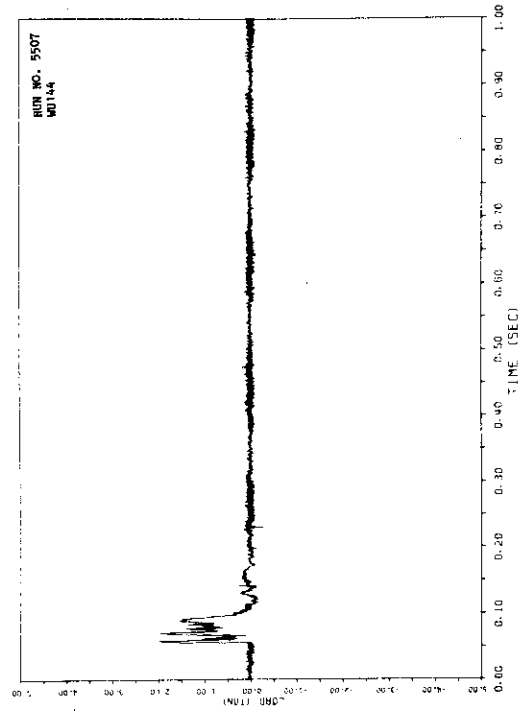

A.468

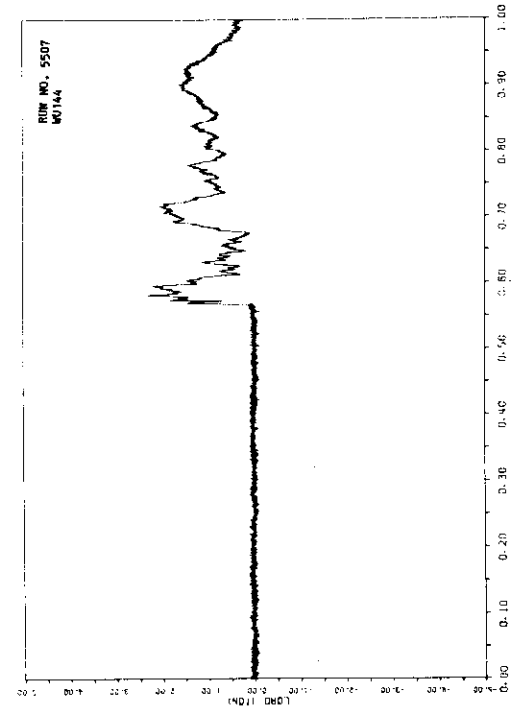

A.467

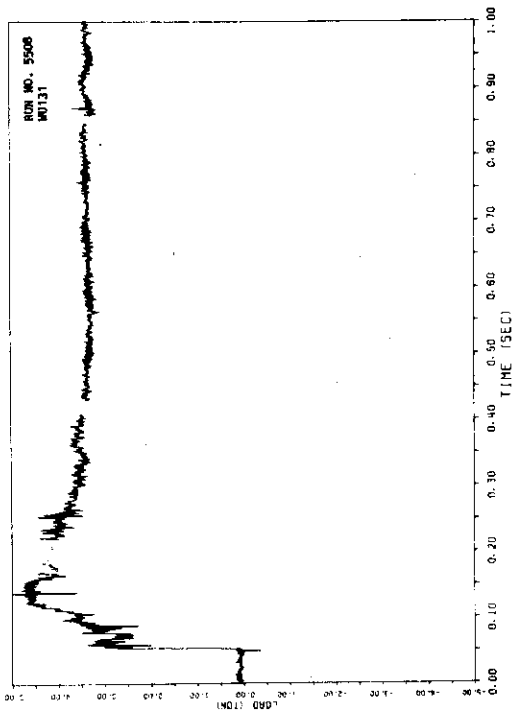

A.470

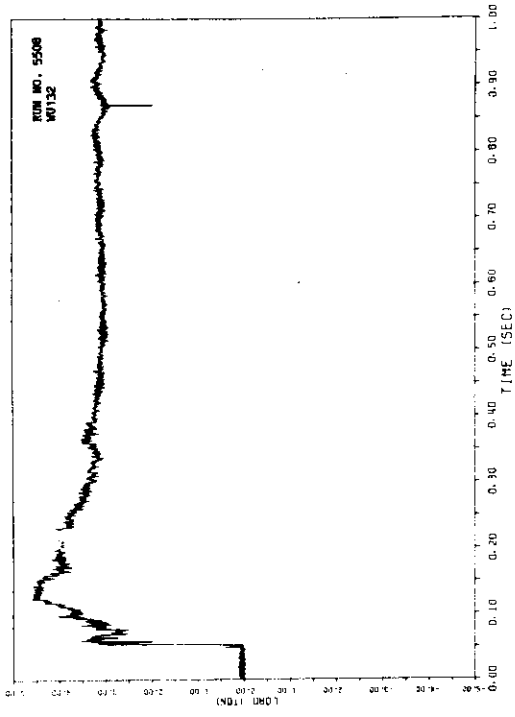

A.472

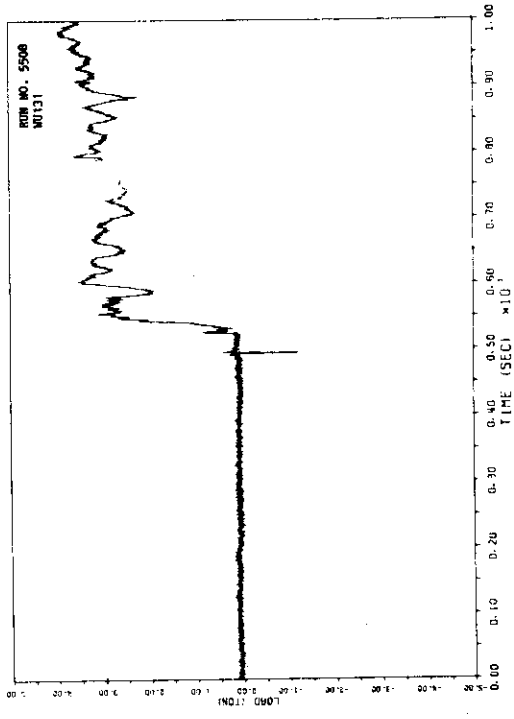

A.469

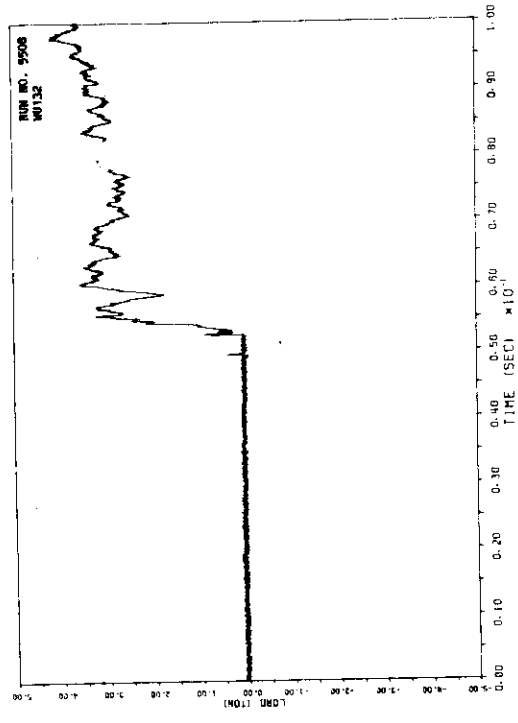

A.471

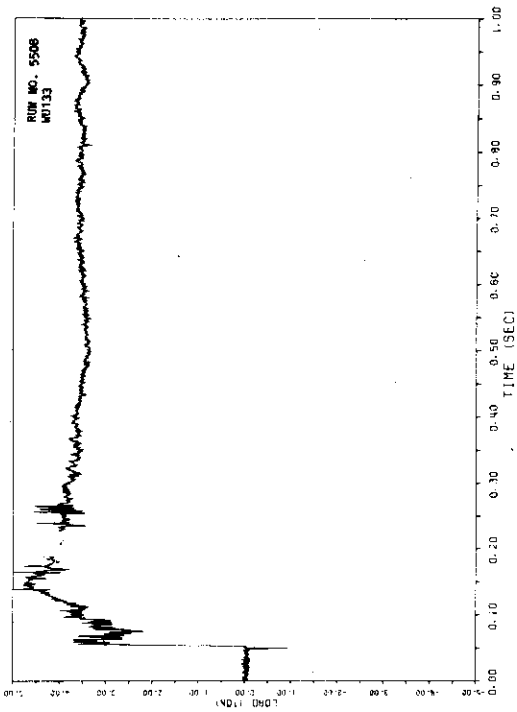

A.474

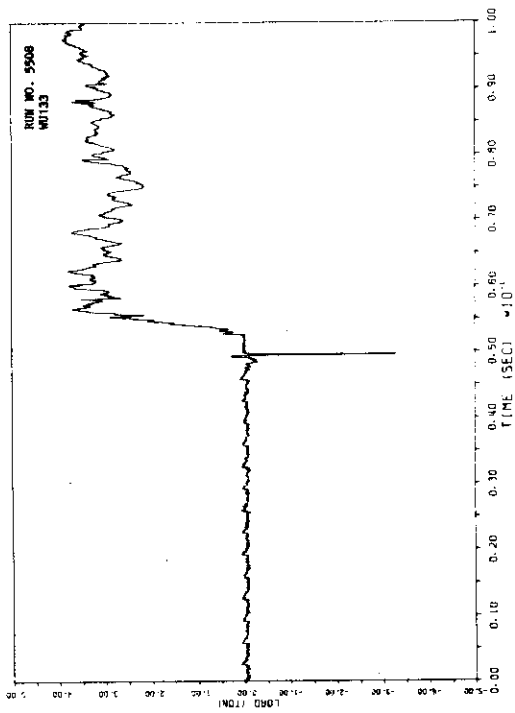

A.473

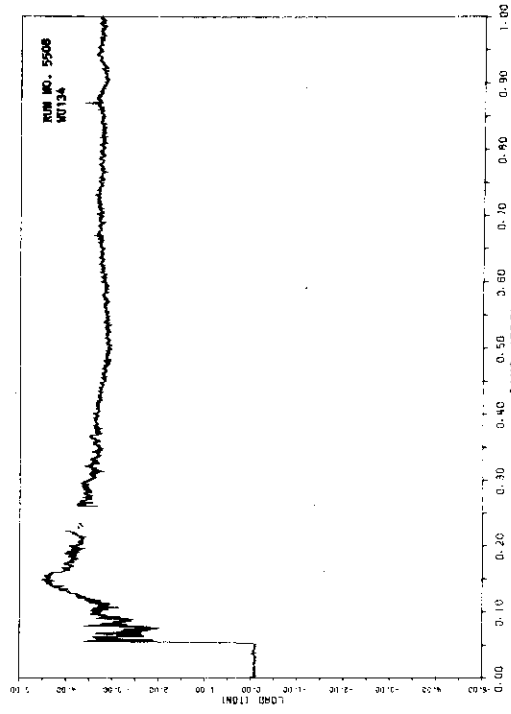

A.476

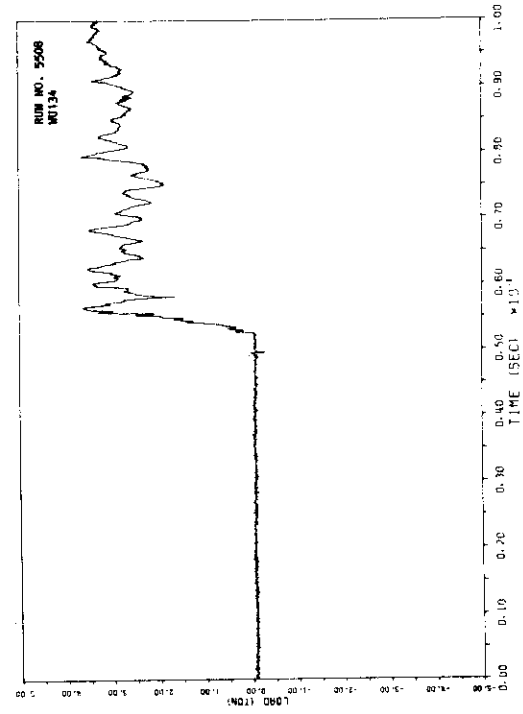

A.475

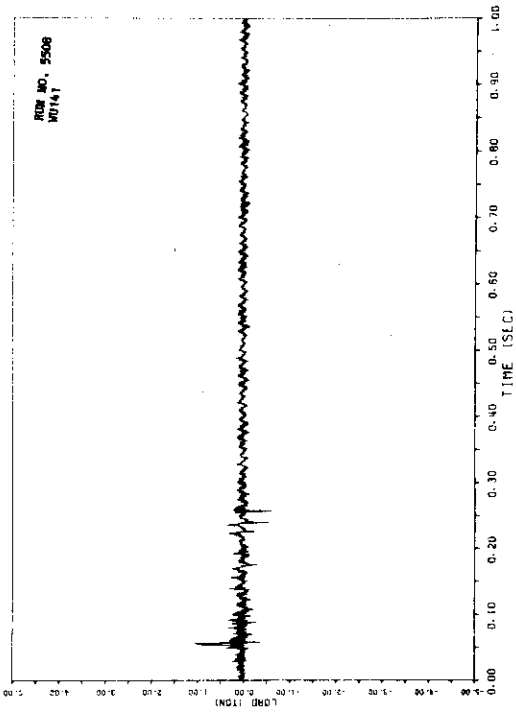

A.478

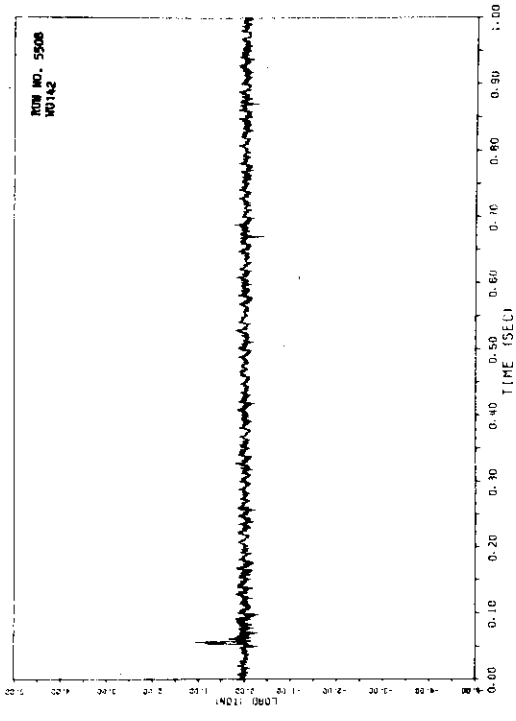

A.480

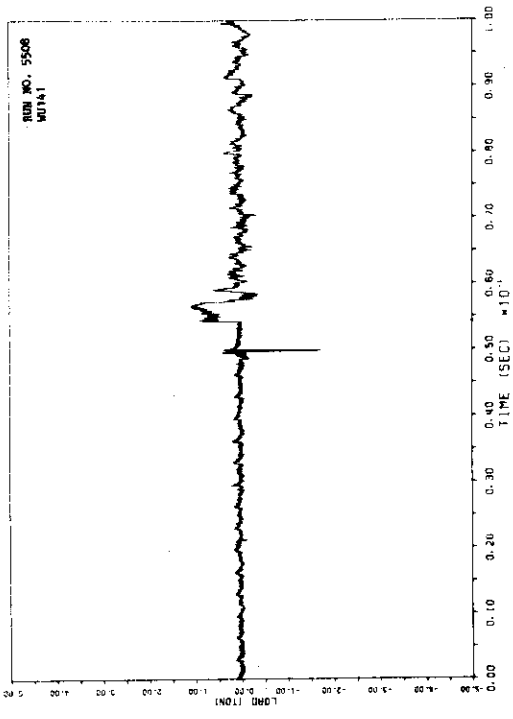

A.477

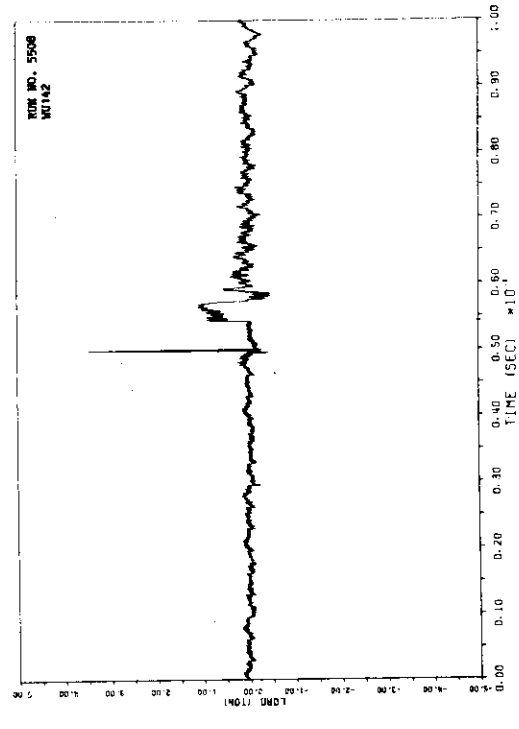

A.479

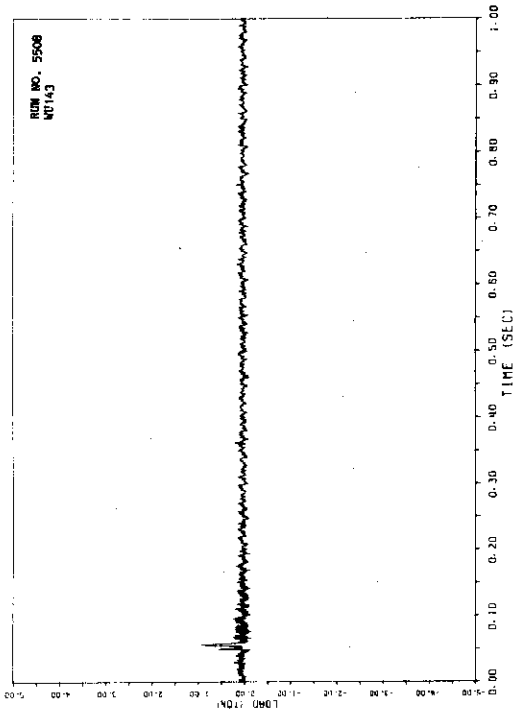

A.482

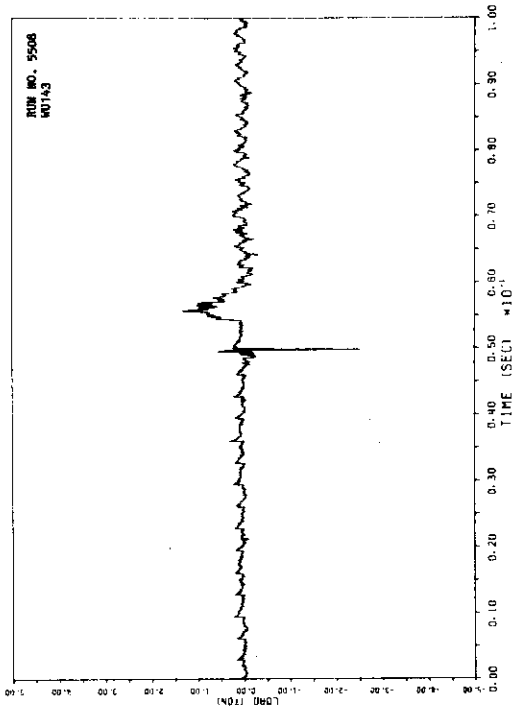

A.481

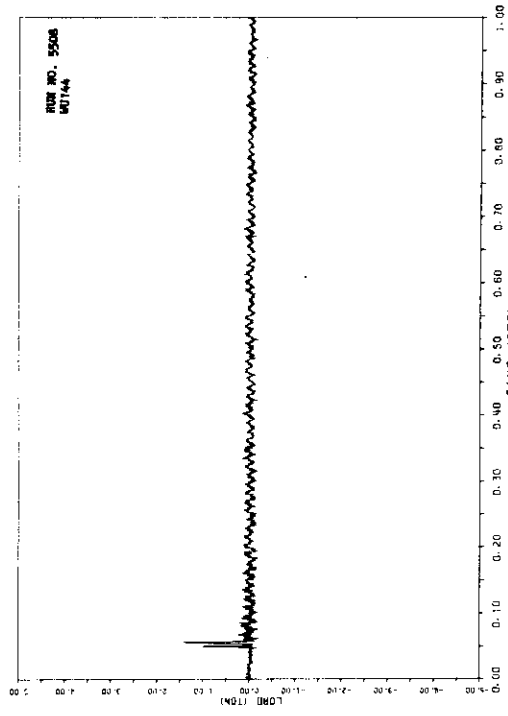

A.484

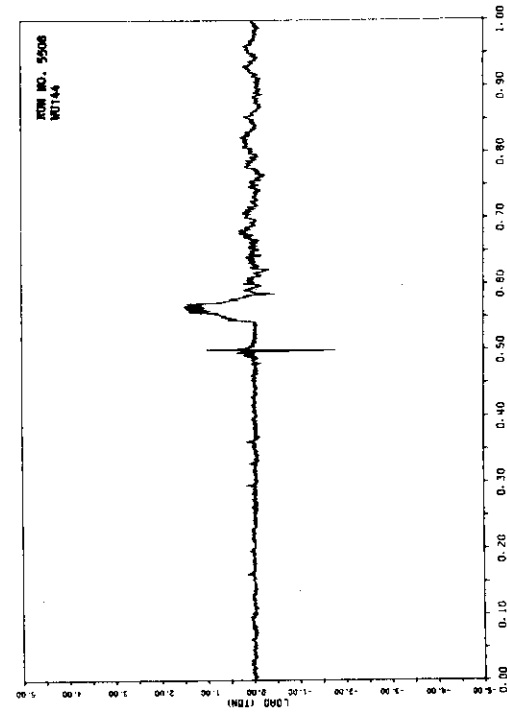

A.483

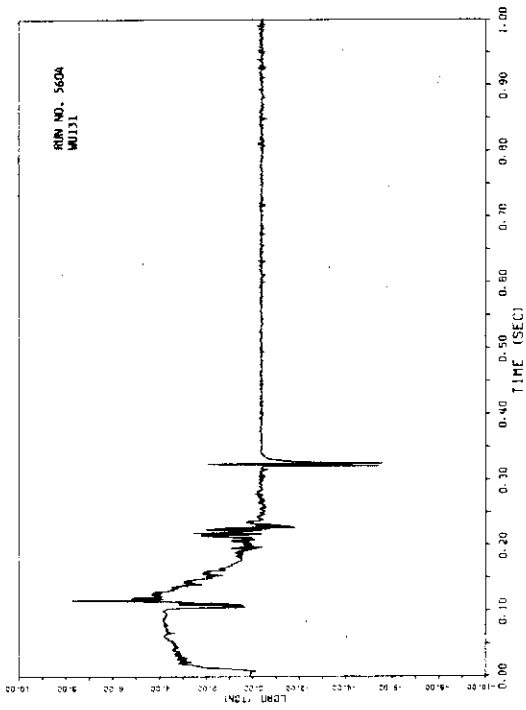

A.486

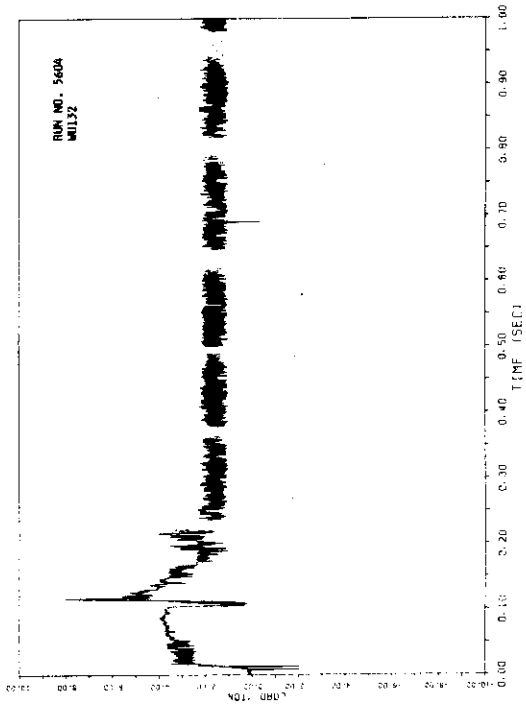

A.488

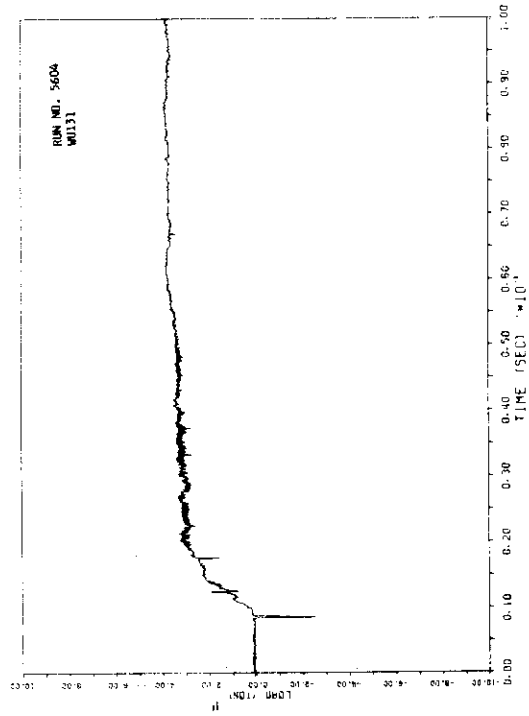

A.485

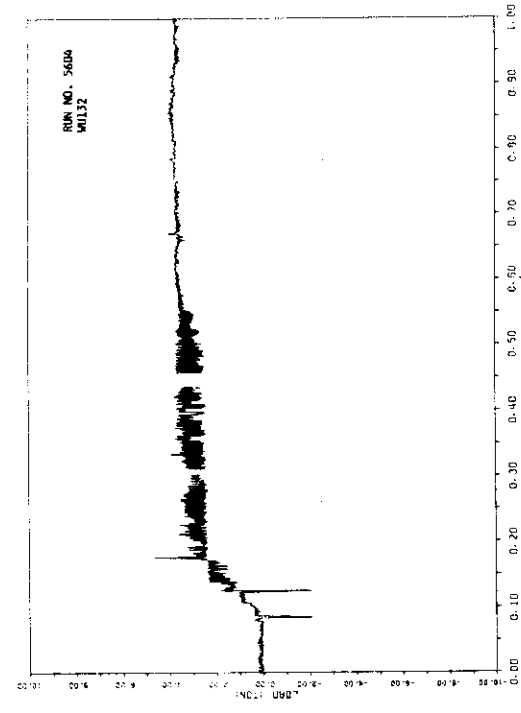

A.487

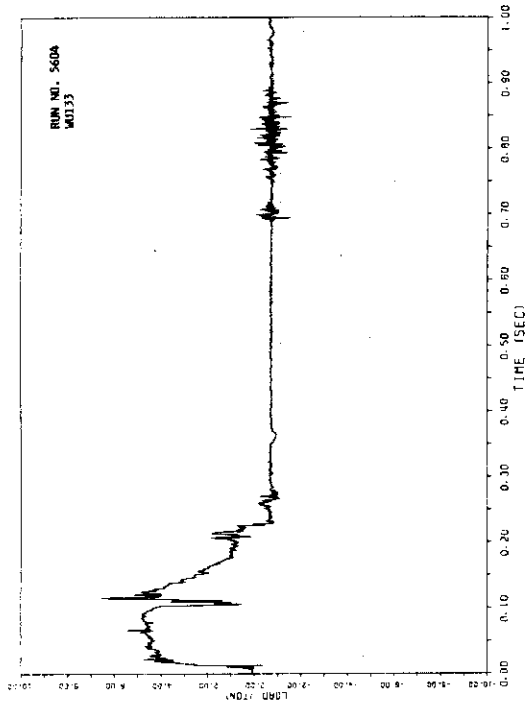

A.490

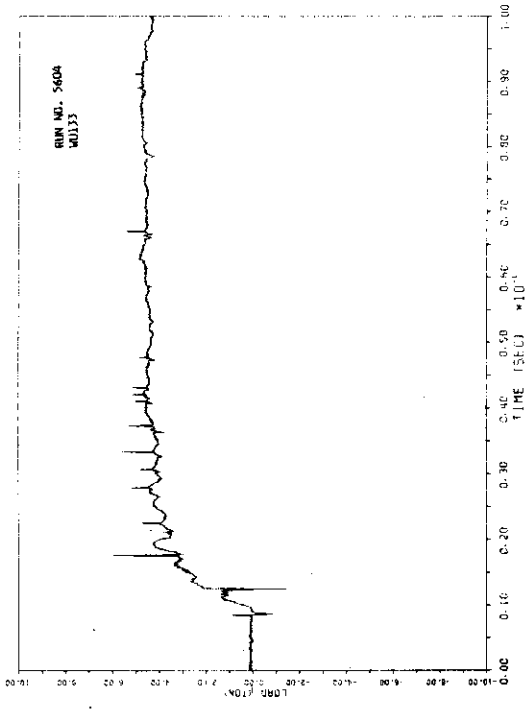

A.489

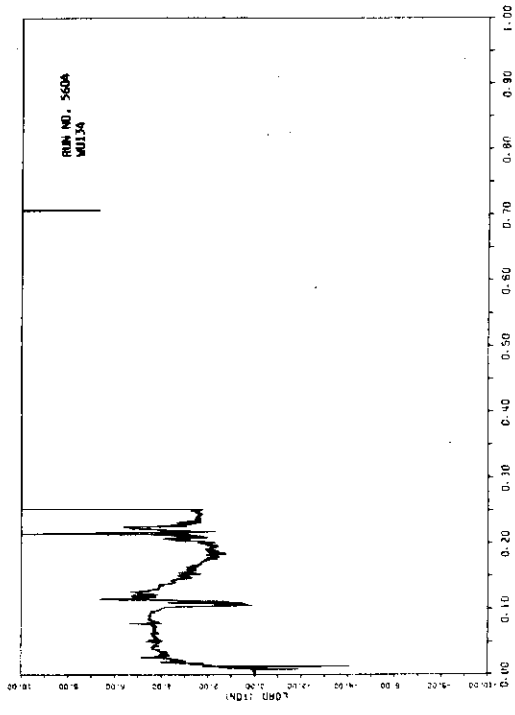

A.492

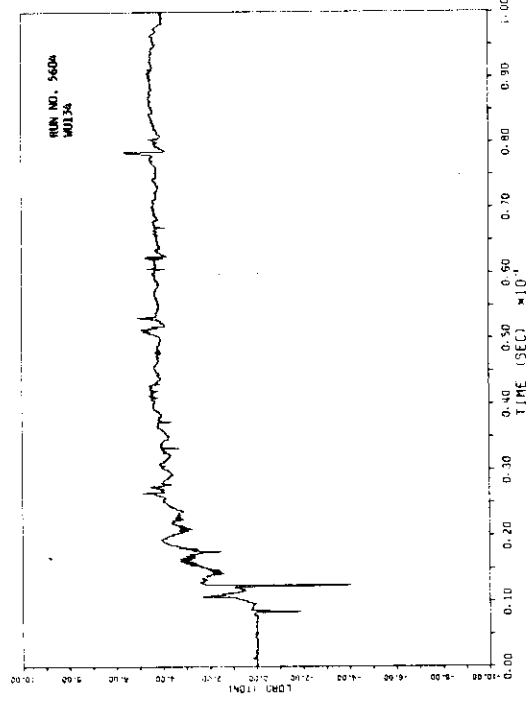

A.491

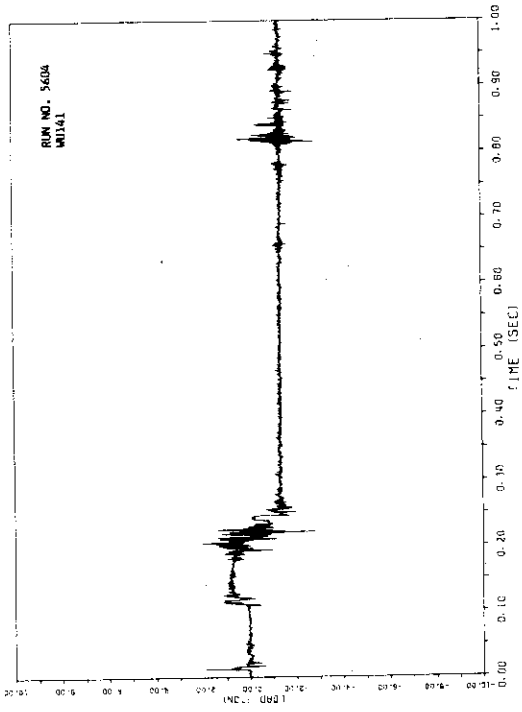

A.494

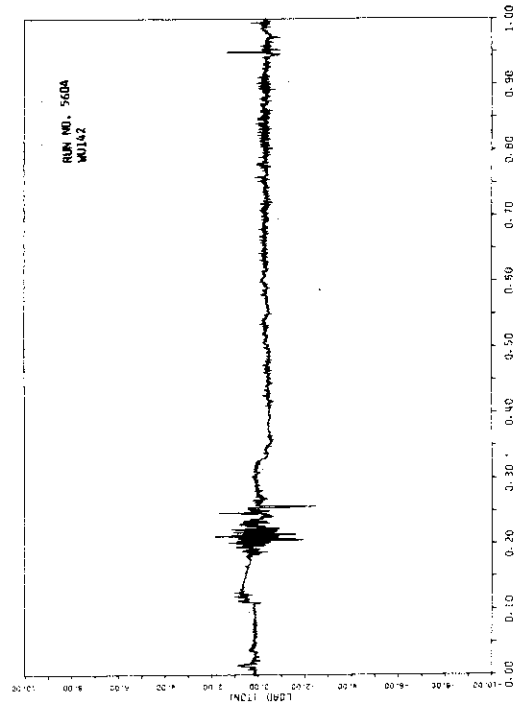

A.496

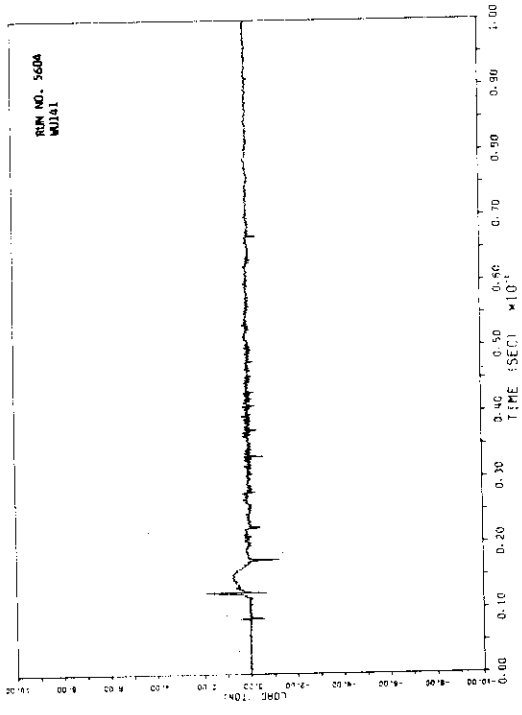

A.493

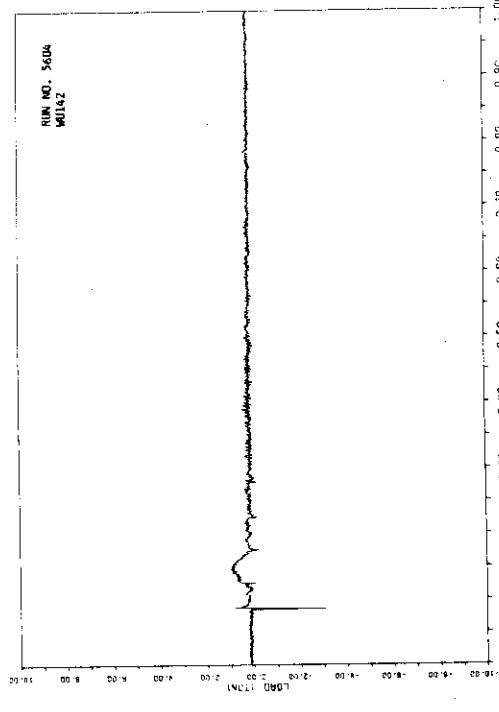

A.495

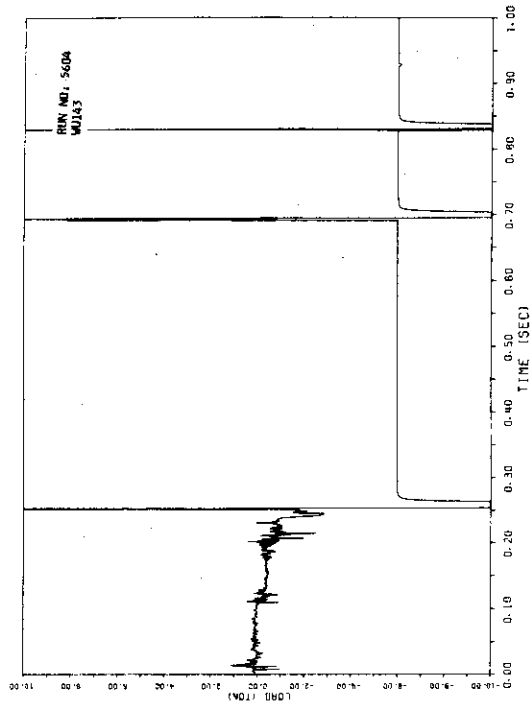

A.498

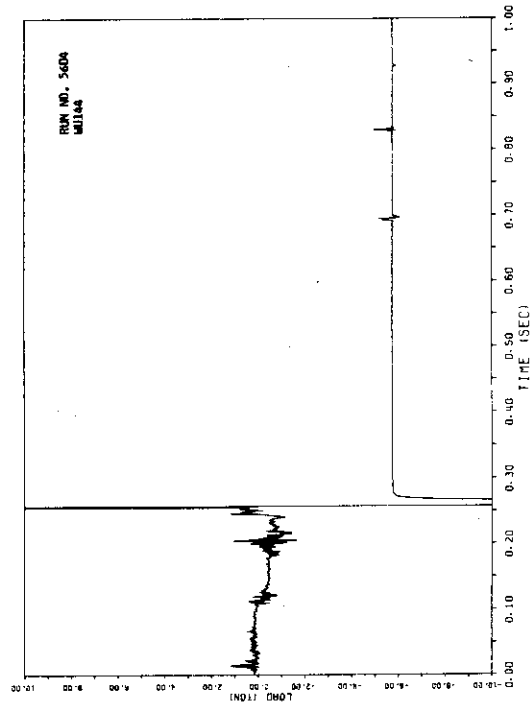

A.500

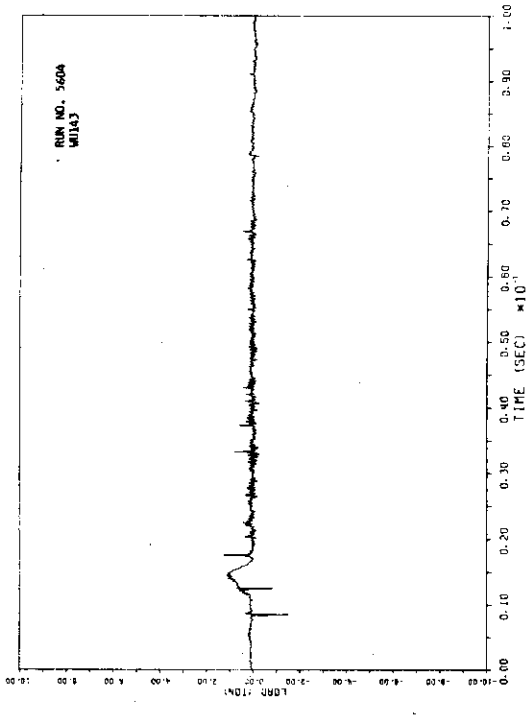

A.497

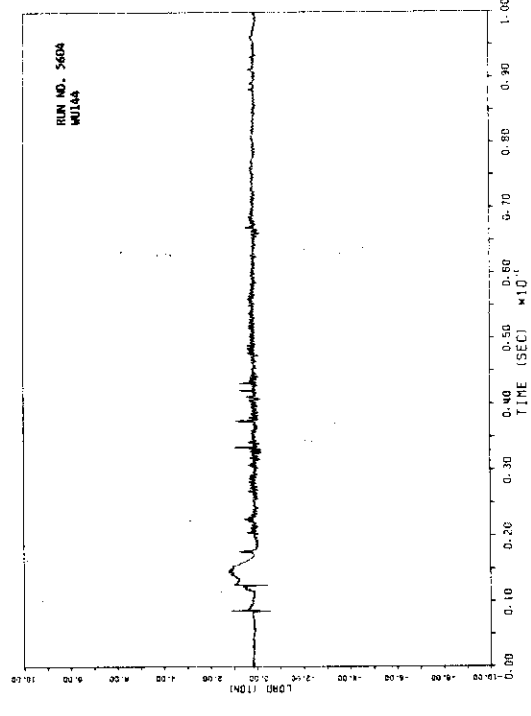

A.499

(g) Accelerations of the test pipe (A.501-A.510)

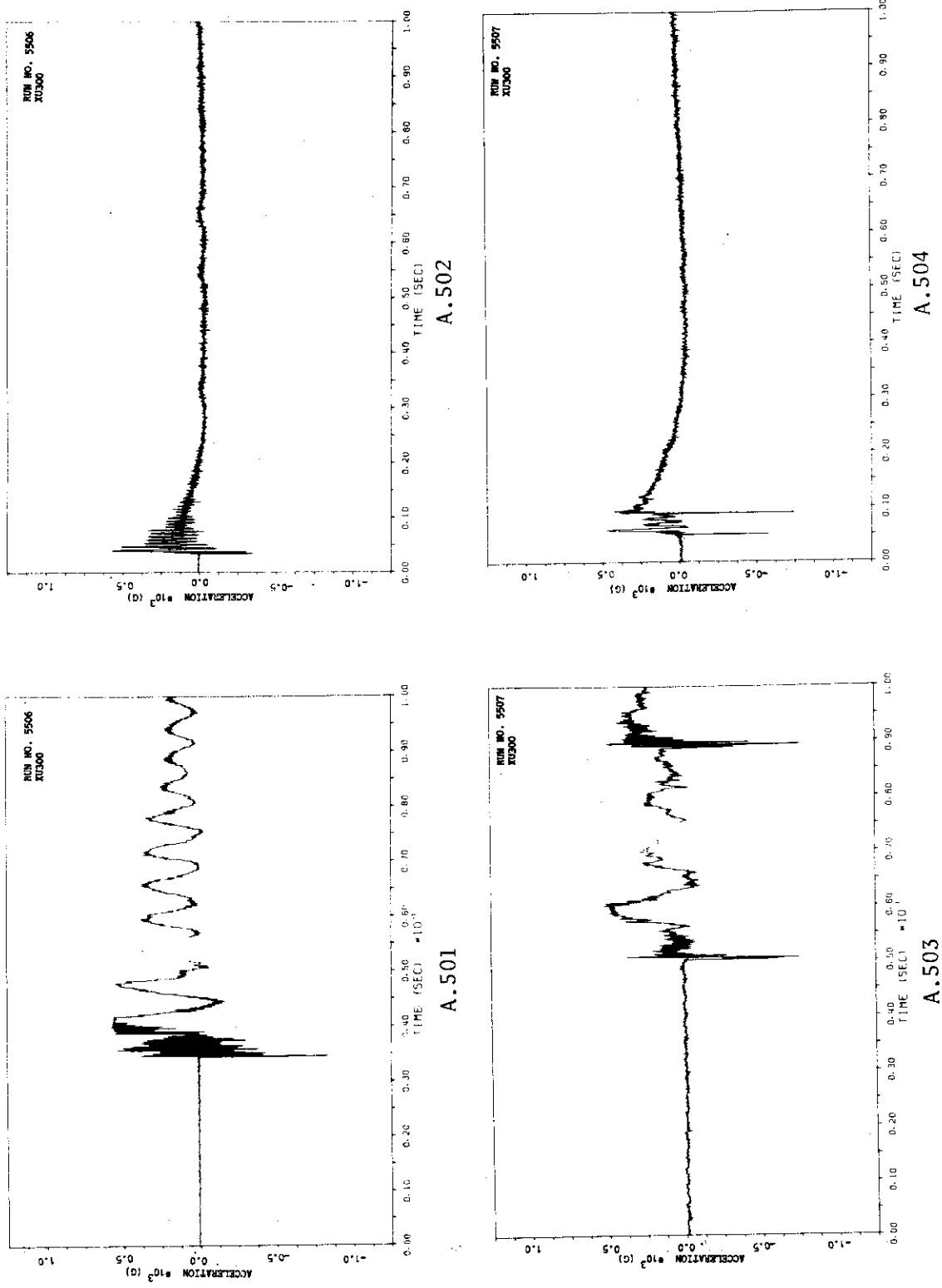

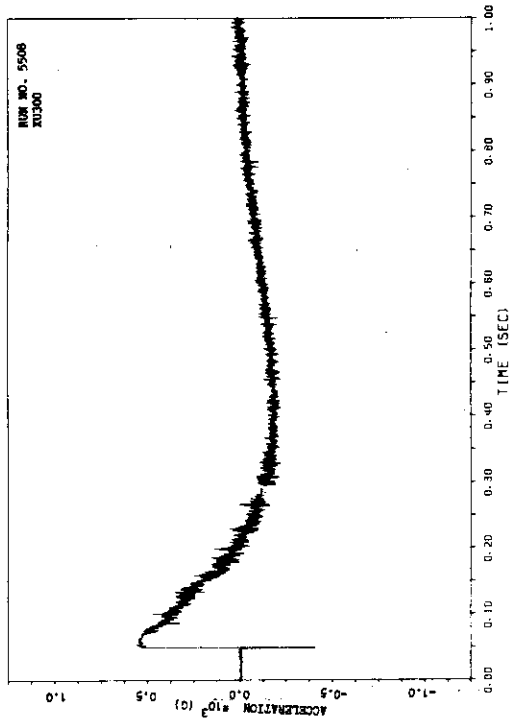

A.506

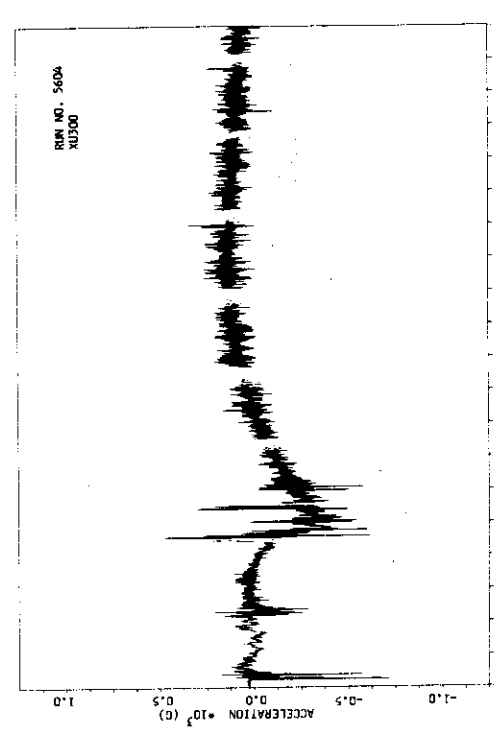

A.508

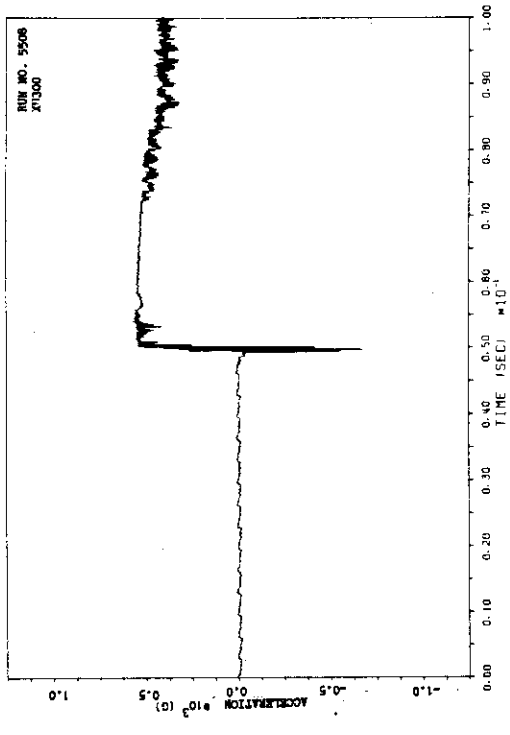

A.505

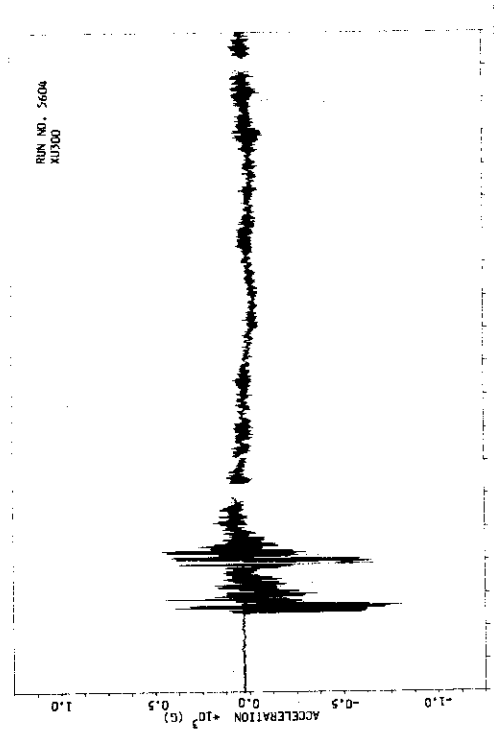

A.507

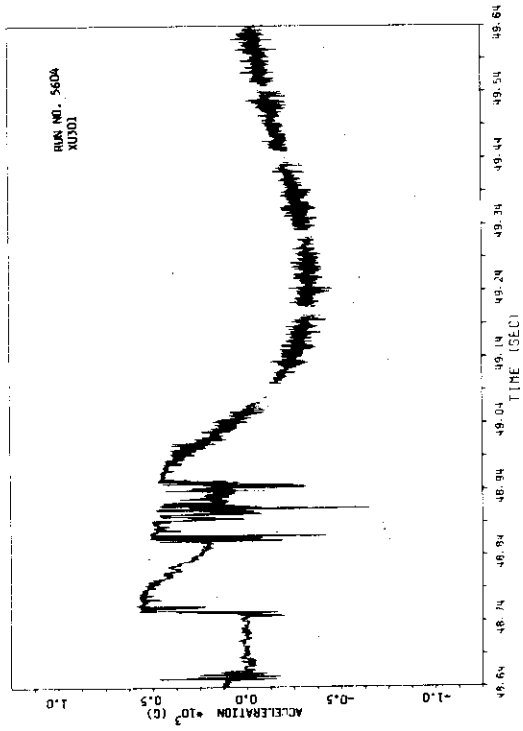
RUN NO. 5604
XU301
ACCELERATION *10³ (G)
TIME (SEC)

A.510

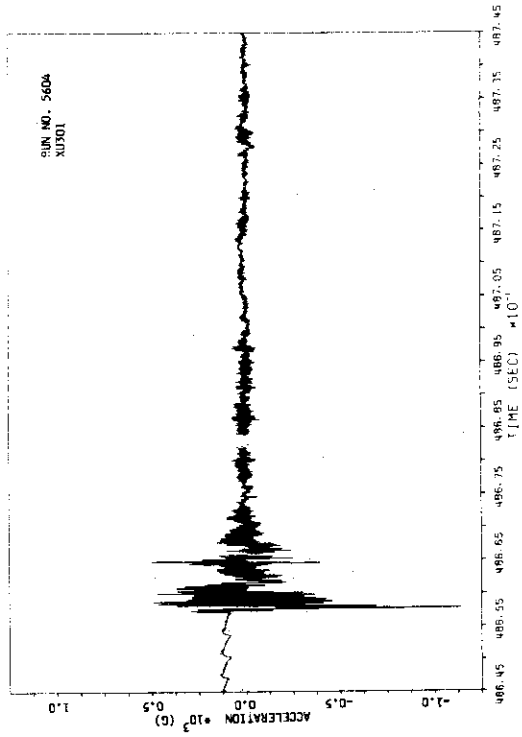
RUN NO. 5604
XU301
ACCELERATION *10³ (G)
TIME (SEC) *10⁻¹

A.509

(h) Strains of the strain gages XU169 and XU170 (A.511,A.512)

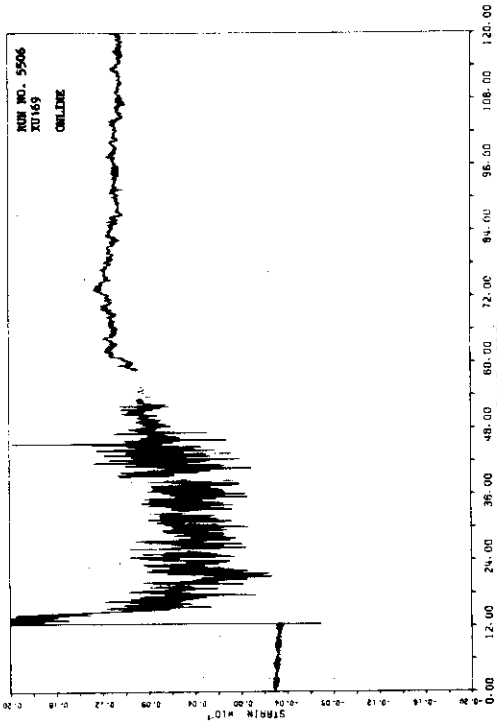

A.511

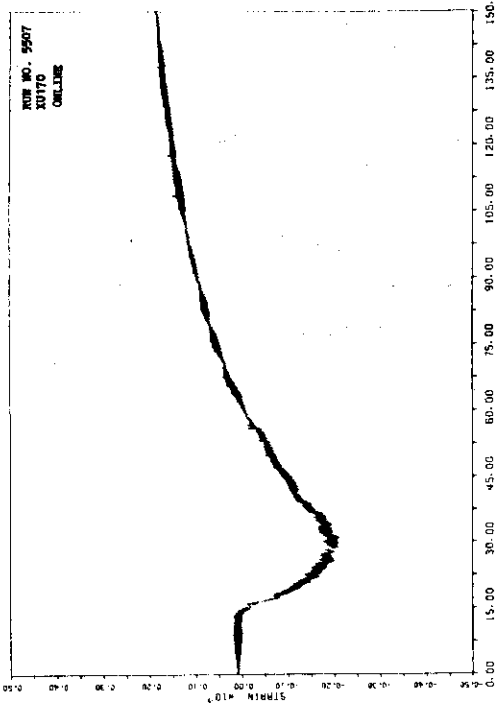

A.512

APPENDIX B RESULTS OF TENSILE TESTS FOR RESTRAINT AND PIPE MATERIALS

B.1 Test specimens

Figure B.1 shows the shape of the test specimens made of the restraint material SS41 mild steel. Test specimen No. 8-1 to 8-3 and 2-1 to 2-3 denote the test specimens made of the bars with the diameter of 38 mm and 32 mm, respectively.

Figure B.2 shows the shape of the test specimens made of the pipe material SUS304 stainless steel. Test specimen No. PR-1 to PR-3 and PH-1 to PH-3 denote the test specimens for room temperature test and high temperature test, respecitvely. Figure B.3 shows another shape of the test specimens made of the pipe material. These test specimens are called RT-1, -2 and HT-1, -2.

B.2 Test Procedure

B.2.1 Restraint material

Tensile tests of the restraint material were performed under room temperature. Strain gages were mounted on the test specimens to obtain stress-strain curves.

B.2.2 Pipe material

Tensile tests of the pipe material were performed both under room temperature and under high temperature. Strain gages were mounted on the test specimens PR-1 to PR-3, PT-1, -2 and HT-1, -2 to obtain stress-strain curves. On the other hand, the displacement of the cross-head of the test machine was recorded to obtain the 0.2% strength and the tensile strength for PH-1 to PH-3.

B.3 Test Results

The stress-strain curves for 8-1 to 8-3, 2-1 to 2-3, RT-1, -2 and HT-1, -2 are given in Figs. B.4 and B.5, respectively. The test results are also summarized in Table B.1.

Table B.1 Results of Tensile Tests

Test Material	Test Specimen No.	Test Temperature (℃)	Yield Stress (MPa)	0.2% Strength (MPa)	Tensile Strength (MPa)	Young Modulus (MPa)
SS-41 38φ (Restraint)	8-1	10	362		462	2.136×10^5
	8-2	10	308		460	2.204×10^5
	8-3	10	305		460	2.089×10^5
SS-41 32φ (Restraint)	2-1	10	382		515	2.126×10^5
	2-2	10	325		510	2.126×10^5
	2-3	10	333		512	2.123×10^5
SUS304 (Pipe)	PR-1	10		303	688	2.070×10^5
	PR-2	10		298	655	2.120×10^5
	PR-3	10		275	626	2.095×10^5
SUS304 (Pipe)	PH-1	325		191	447	
	PH-2	325		197	448	
	PH-3	325		188	448	
SUS304 (Pipe)	RT-1	R.T.		253	631	2.064×10^5
	RT-2	R.T.		248	634	2.172×10^5
SUS304 (Pipe)	HT-1	320		176	445	1.939×10^5
	HT-2	320		164	443	1.933×10^5

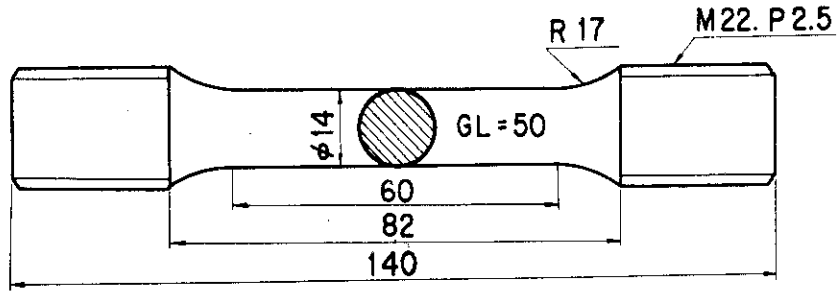

Fig. B.1 Tensile Test Specimen of Restraint Material ----- JIS No.4 Test Specimen (8-1 ∿ 8-3, 2-1 ∿ 2-3)

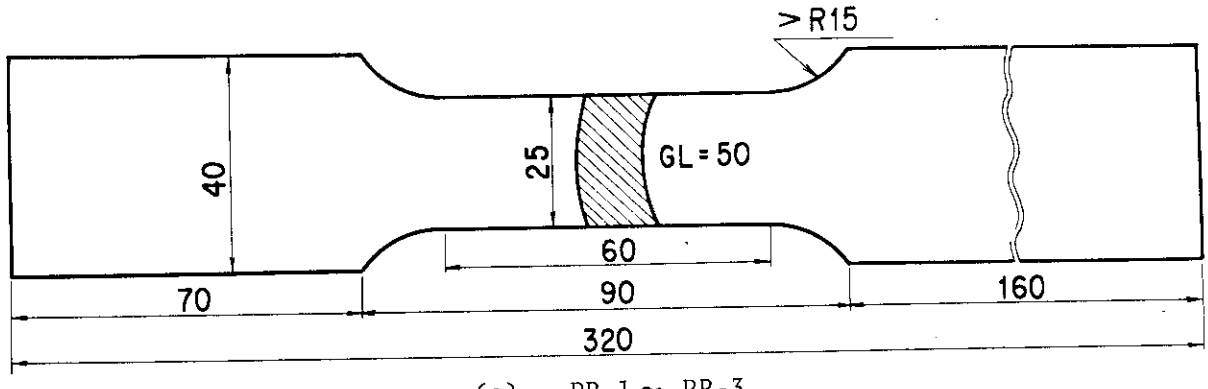

(a) PR-1 ~ PR-3

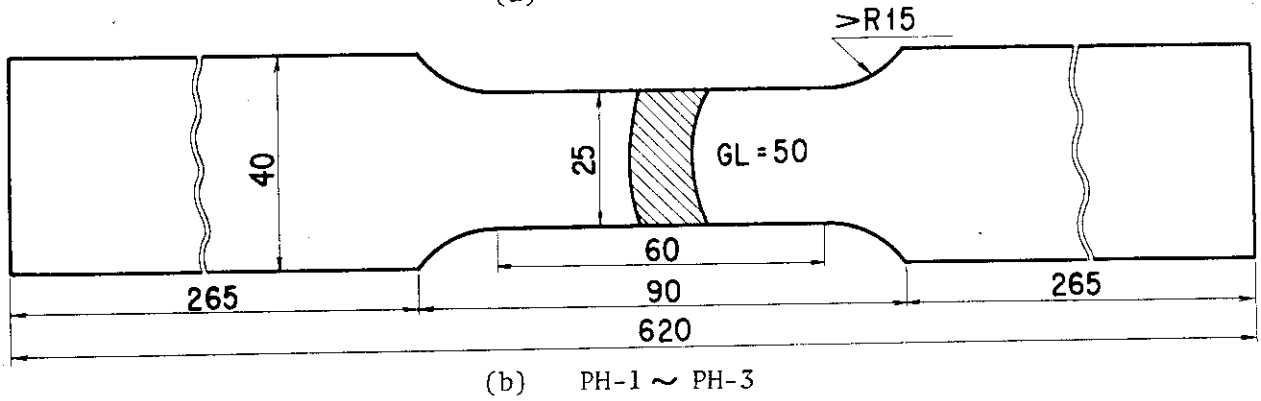

(b) PH-1 ~ PH-3

Fig. B.2 Tensile Test Specimen of Test Pipe ----- JIS No.12-B Test Specimen

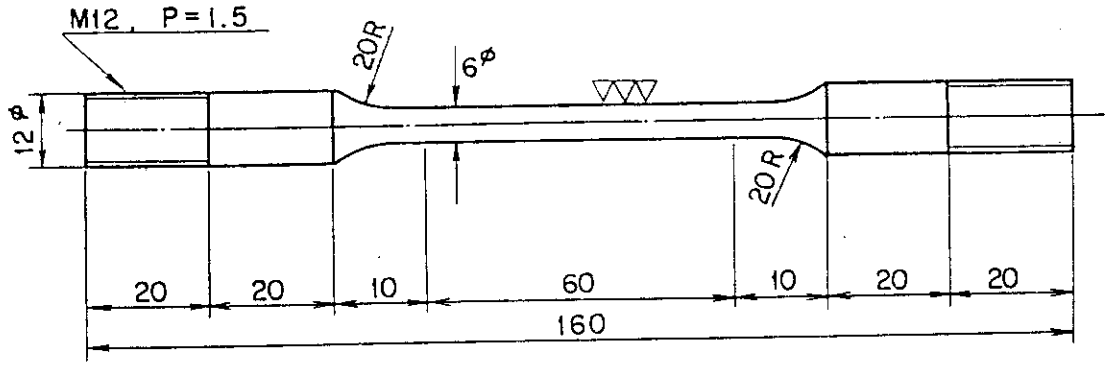

Fig. B.3 Tensile Test Specimen of Test Pipe (RT-1, RT-2, HT-1, HT-2)

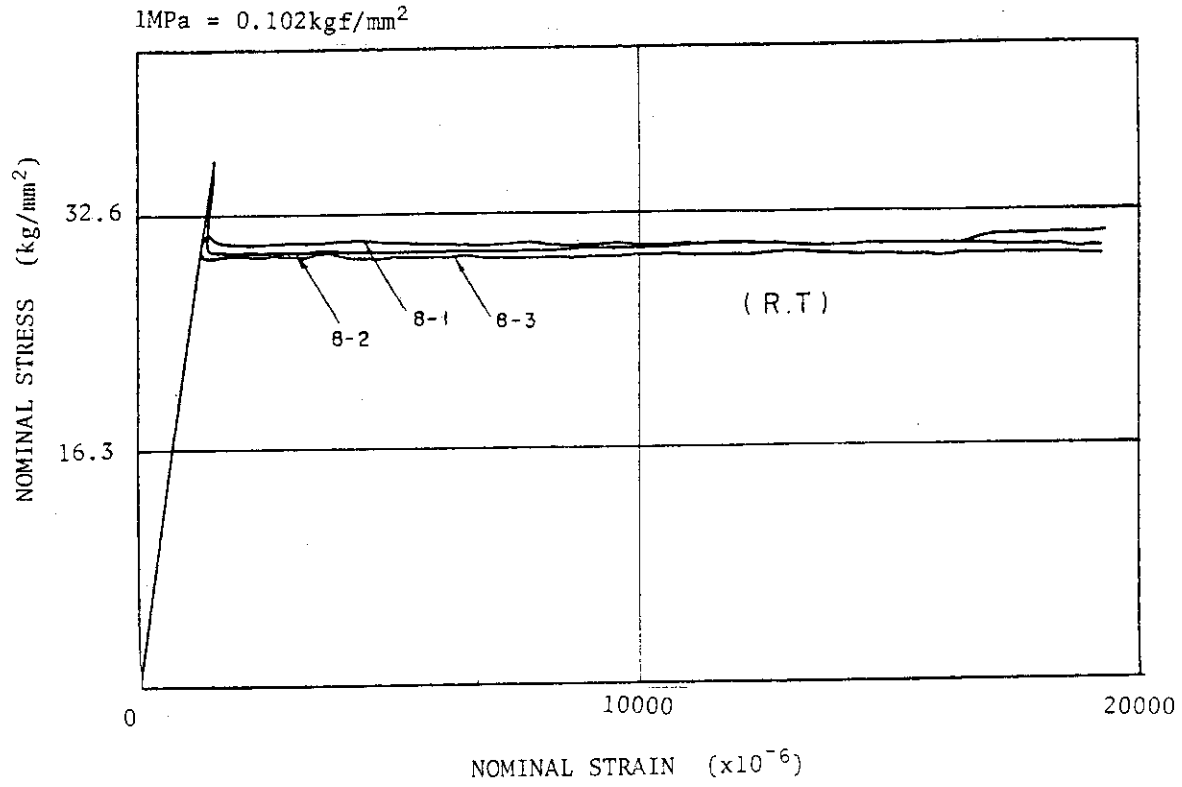

(a) 8-1 ∿ 8-3

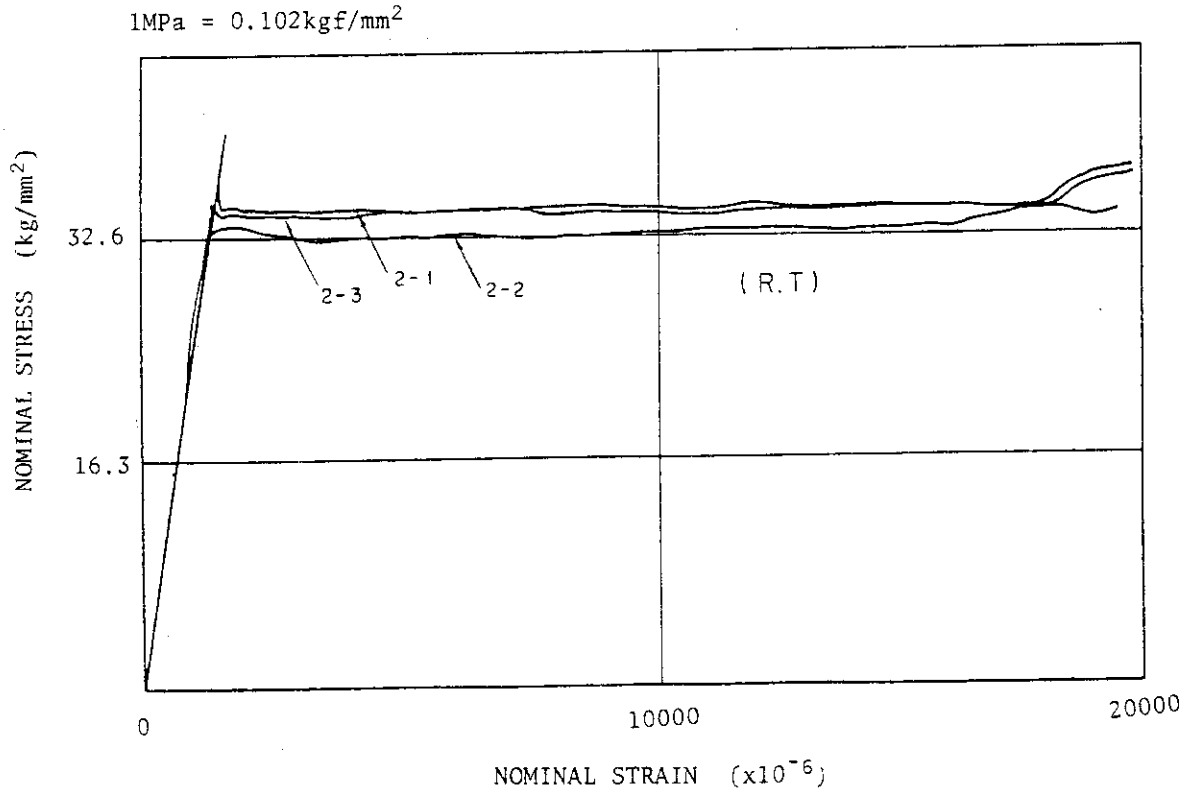

(b) 2-1 ∿ 2-3

Fig. B.4 Stress-Strain Curves of Restraint Material

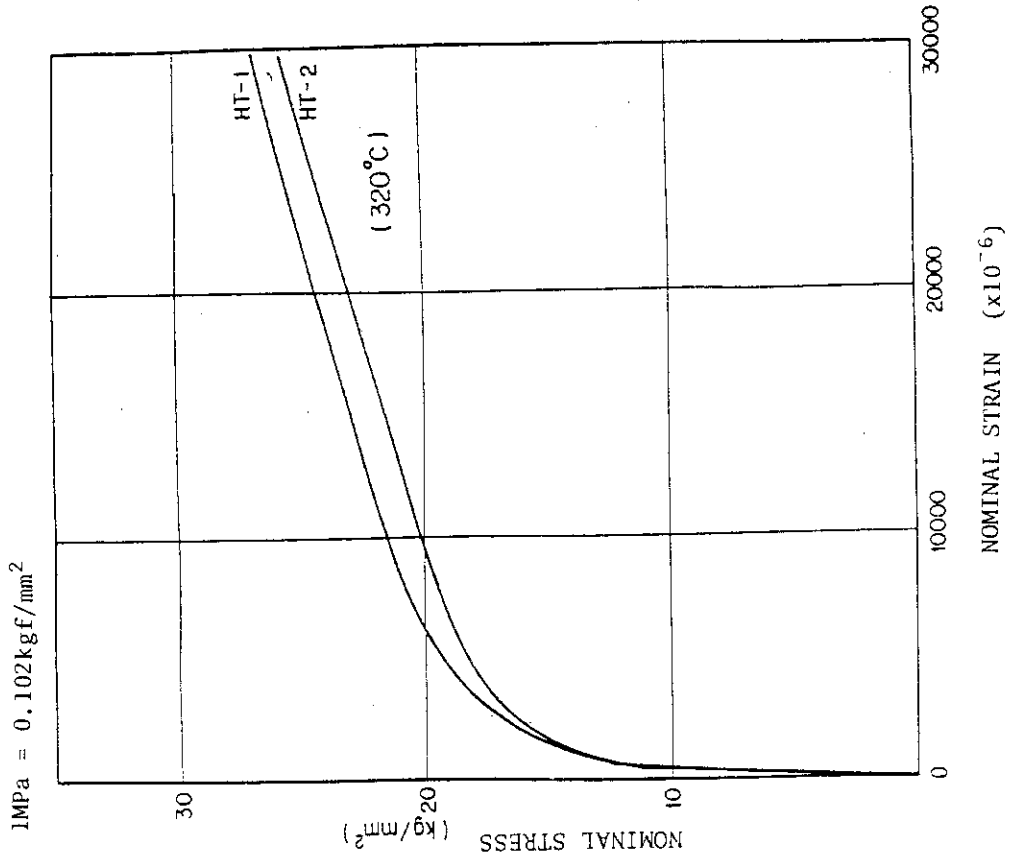

(b) HT-1, HT-2

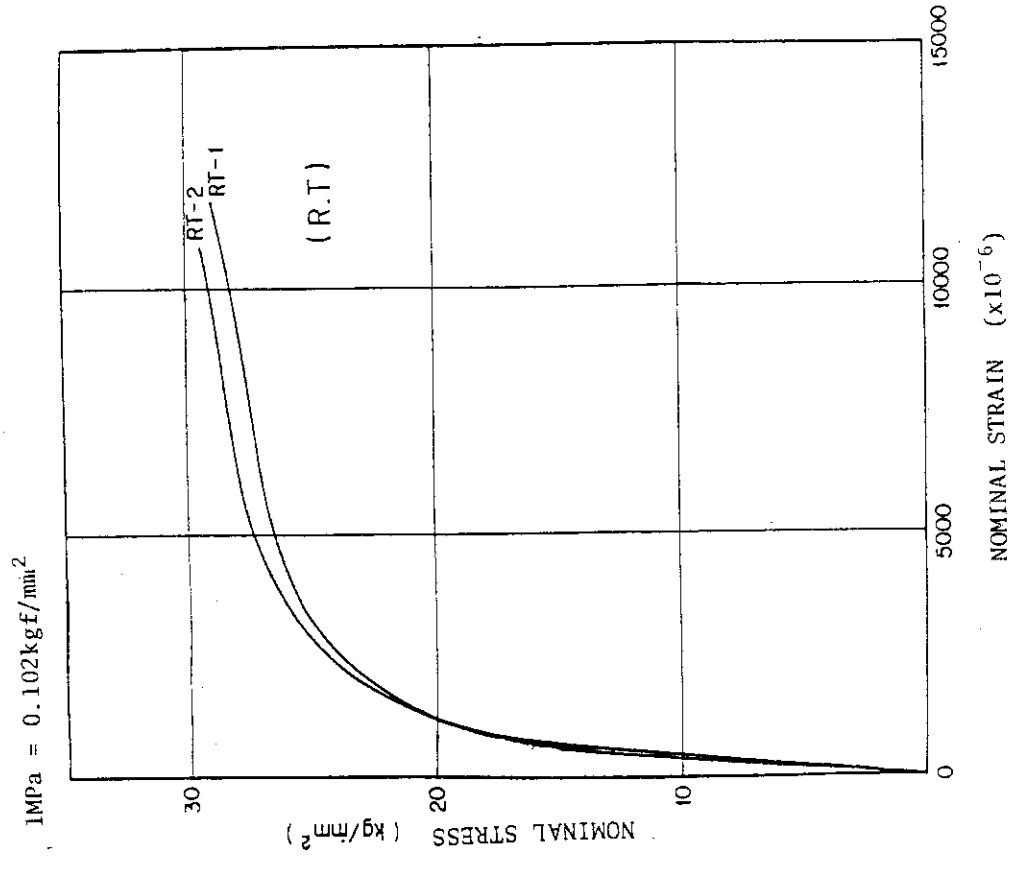

(a) RT-1, RT-2

Fig. B.5 Stress-Strain Curves of Pipe Material